

UNIVERSIDAD AUTONOMA DE MADRID

ESCUELA POLITECNICA SUPERIOR



PROYECTO FIN DE CARRERA

**DISEÑO DE UN ARRAY LINEAL DE PARCHES SOBRE GUÍA
DE SUSTRATO INTEGRADO PARA BANDA KU**

David García Valverde

Julio 2012

DISEÑO DE UN ARRAY LINEAL DE PARCHES SOBRE GUÍA DE SISTRATO INTEGRADO PARA BANDA KU

Autor: David García Valverde

Tutor: Juan Córcoles Ortega

Ponente: José Luis Masa Campos

RFCAS (Grupo de Radiofrecuencia, Circuitos, Antenas y Sistemas)



Dpto. de Tecnología Electrónica y de las Comunicaciones

Escuela Politécnica Superior

Universidad Autónoma de Madrid

Julio de 2012

Resumen

El objetivo de este proyecto es diseñar un sistema radiante formado por un array lineal de parches sobre tecnología de guía de onda impresa (SIW), con polarización lineal dentro de la banda de microondas Ku (16.3 GHz – 17.7 GHz). Para los elementos radiantes de la antena se ha utilizado una estructura de doble parche en tecnología impresa, cuya disposición en el array se ajusta para conformar el diagrama de radiación deseado en el diseño.

Por otra parte, se ha llevado a cabo el diseño de una transición SMA-microstrip-SIW para la alimentación de la antena. Esta transición contará además con asilamiento electromagnético para reducir pérdidas por radiación no deseada.

Finalmente, será combinado el array lineal y la transición diseñada para la integración completa de la antena. Para verificar los resultados obtenidos en las simulaciones, se construirá un prototipo de la antena en el laboratorio de circuitos impresos de la Escuela Politécnica Superior (EPS) de la U.A.M., para su posterior medida en reflexión y diagrama de radiación. Además, se pretende comprobar la viabilidad de construcción de proyectos de esta envergadura en las instalaciones de la EPS con el material y tecnología disponibles.

Palabras Clave

SIW, guía de onda, microstrip, parches, parámetros S, reflexión, adaptación, substrato, constante dieléctrica, pérdidas, línea de acoplo, vía, antena, array lineal, transición, diagrama de radiación, modelo de compensación de acoplos mutuos.

Abstract

The objective of this project is to design a radiant system consistent of a linear patch array over substrate integrate waveguide (SIW), with linear polarization in the microwave band Ku (16.3 GHz – 17.7 GHz). For the radiant elements of the antenna it has been used a double patch structure in printed circuit technology, whose placement in the array is adjusted to conform the desired radiation pattern of the design.

On the other hand, the design of a SMA-microstrip-SIW transition for the feeding of the antenna will be carried out. This transition will have electromagnetic insulation in order to avoid undesired radiation losses.

Finally, the linear array and the transition will be integrated in the complete antenna. In order to verify the obtained results from the simulations, a prototype will be manufactured in laboratory of printed circuits at Escuela Politécnica Superior (EPS) at U.A.M., for its further measurement in reflection and radiation pattern. Moreover, it will be important to verify the construction viability of similar projects in the facilities of EPS, with the available resources and technology.

Key Words

SIW, waveguide, microstrip, patches, S parameters, reflection, adaptation, substrate, dielectric constant, losses, coupling line, via, antenna, linear array, transition, radiation pattern, mutual coupling compensation model.

Agradecimientos

Se cierra una etapa muy importante en mi vida y resulta extremadamente complicado agradecer a tantísima gente el apoyo que me ha dado estos últimos años. Espero no olvidar mencionar a nadie importante y que esto no resulte demasiado largo.

En primer lugar me gustaría darle las gracias a José Luis Masa y Juan Córcoles, tutores y mentores de este proyecto. Gracias por estar ahí cuando me podía el desánimo y no veía el final, por motivarme y espolearme hasta el final; y por vuestra comprensión y paciencia cuando me atascaba y mis circunstancias personales sugerían otra perspectiva. Si ya tenía en alta estima a José Luis como profesor, ahora mucho más después de todo lo que hemos sufrido juntos. Espero que hayáis disfrutado al menos una mínima parte de lo que yo he disfrutado realizando este proyecto con vosotros.

También quiero dar las gracias al resto de profesores del grupo RFCAS. A Jorge, por sus inolvidables clases y por darme ese último empujón para hacer el proyecto en RFCAS; y a Bazil, por hacerme disfrutar enormemente en el laboratorio con innumerables conversaciones de toda índole, haciéndome valorar aún más que la formación de una persona debe ser lo más amplia posible (bendita Wikipedia y Google) y por estar siempre disponible a echarme una mano en lo que necesitase.

Y por supuesto a mis compañeros de laboratorio, aquellos con los que coincidí poco tiempo, y aquellos con los que he echado infinitas horas en el C-107. A Marta, por ser tan dulce y encantadora, y acompañarme a por cafés cuando nadie más quería hacerlo al principio; a Daniel, por olvidar los resquemores a pesar haberle quitado vilmente el ordenador y ser tan buena persona; a Sergio, porque tener un buen humor es contagioso y por ser fuente inagotable de anécdotas; a Pascu, por ser compañero de fatigas en ACAF y las largas tardes de soledad; y por supuesto a Pablo, por ayudarme tantísimo desde el principio al fin de este proyecto y estar siempre ahí para cualquier cosa que necesitase. Gracias por hacer que cada día llegase y me fuese con una sonrisa de la universidad. No hay palabras para agradecer cuánto me ha supuesto vuestra compañía y amistad en los momentos difíciles que he me ha tocado pasar.

Es justo también agradecer a todos los compañeros de clase que he tenido su aportación en mi crecimiento como persona, y el haber hecho tan agradable la convivencia con ellos. Ya sea dando conversación en la biblioteca mientras debatíamos el bajo porcentaje de aprobados en asignaturas de 2º, sufriendo en prácticas en Navidad y hasta el último segundo para conseguir terminar el trabajo, de tertulia futbolística y baloncestística defendiendo al gran capitán o a la Bomba, o acompañándome siempre en las comidas y la cola de los microondas a la vez que contaba anécdotas del Decathlon. Ha sido un verdadero placer pasar estos años a vuestro lado y os deseo lo mejor en el futuro.

Sin embargo hay tres personas a las que debo dar las gracias por duplicado, pues han sido mi mayor apoyo durante estos años. A Mario, por estar siempre disponible para escucharme y darme consejo y apoyo moral; a Jorge, por enseñarme a tomarme las cosas de otra manera y centrarme en lo realmente importante; y a Sergio, por preocuparse y acordarse de mí siempre el primero. Un gran trocito de esto os lo debo a vosotros.

Gracias a todos mis compañeros del baloncesto, Macavis y Centauros; pues gracias a vosotros conseguía desconectar y olvidarme de muchos de mis problemas. Y sobre todo a

Peder, porque sabe lo duro que es esto, y su amistad y cariño durante todos estos años es algo que nunca podré olvidar.

A mis amigos del Erasmus, por haber estado a mi lado en el año más maravilloso de mi vida. A las niñas de Madrid (y adopción) y Valencia; a los Mongoose, Charly, Ale, Chema y Alessandro. Y sobre todo a mi verdadera familia, porque los he querido y quiero tanto que me emociono al escribir de ellos. A Nacho, ese vecino que vivió más tiempo en mi casa que en la suya; a Maurizio, cuyo sentido del deber y sus dotes culinarias me calaron tan hondo; y a Guille, por ser la persona más increíble que he conocido y abrirme los ojos a la vida en muchos aspectos. Vosotros fuisteis mi Erasmus.

A mi familia, por quererme y apoyarme siempre, a pesar de los malos ratos y todas esas pequeñas cosas que nos diferencian.

A aquellos que en cierto modo nos dejaron. A mi abuelo Antonio, mi abuelo del fútbol, que siempre me quiso y disfrutaba recordando mi examen de la puerta del garaje. Y a Luis, por cuidar de nosotros todos los días, y porque siempre querré ser un poco mejor persona para intentar parecerme a él. Siempre os llevaré en el corazón.

Y por último a mis padres y mi hermana. A los que más os debo, menos sé que deciros. Gracias por todos los esfuerzos que habéis realizado a lo largo de todos estos años para permitirme tener una buena formación y educación. Gracias por inculcarme el ser buena persona por encima de todo. Gracias por creer siempre en mí y por haber esperado con paciencia este día. Gracias por ser fuertes por mí cuando yo no he podido serlo. Si por alguien estoy realmente feliz es por vosotros. Finalmente lo conseguí.

Muchísimas gracias de todo corazón, pues sin vosotros no sería nada.

David

ÍNDICE DE CONTENIDOS

1	INTRODUCTION	1
1.1	Project Motivation	1
1.2	Goals.....	1
1.3	Document Structure.....	2
2	STATE OF THE ART.....	3
2.1	Introduction	3
2.2	Principles of Antennas.....	3
2.2.1	Concept of Antenna	3
2.2.2	Types of Antennas	4
2.2.2.1	Wire Antennas.....	5
2.2.2.2	Travelling Wave Antennas.....	5
2.2.2.3	Array Antennas.....	5
2.2.2.4	Aperture Antennas.....	6
2.2.3	Input Impedance.....	6
2.2.4	Scattering Parameters (S Parameters).....	7
2.2.5	Matching.....	8
2.2.6	Standing Wave Ratio (SWR).....	9
2.2.7	Radiation Pattern.....	10
2.2.8	Radiation Intensity, Directivity and Gain	12
2.2.8.1	Radiation Intensity	12
2.2.8.2	Directivity	12
2.2.8.3	Gain	13
2.2.9	Radiation efficiency	13
2.2.10	Polarization.....	13
2.2.11	Bandwidth	15
2.2.12	Radiant elements.....	15
2.2.12.1	Patches	15
2.2.12.2	Slots	18
2.3	Principles of Arrays.....	19
2.3.1	Linear Arrays	20
2.3.2	Planar Arrays.....	21
2.3.3	Phased Arrays	21
2.4	Theory of Waveguides.....	22
2.4.1	Propagation modes.....	22
2.4.2	Waveguide Types.....	23

2.4.2.1	Rectangular waveguide	23
2.4.2.2	Circular waveguide	25
2.4.3	Feeding Systems	26
2.5	Microstrip Line Theory	27
2.5.1	Microstrip Feeding.....	28
2.6	SIW Theory	29
2.6.1	SIW Feeding System.....	31
2.7	Design and Simulation Tools	32
2.7.1	CST Microwave Studio	32
2.7.2	Advanced Design Systems (ADS)	33
2.7.3	Ensemble 1D Array Synthesis	33
2.7.4	Ansoft Ensemble 8.0	34
3	DESIGN OF ANTENNAS	35
3.1	Introduction	35
3.2	General Structure	35
3.3	Waveguide's Characterization	36
3.3.1	Hybrid Modes	37
3.3.1.1	Transverse Resonance Method (TRM)	37
3.3.2	Design Considerations	39
3.4	SIW's Characterization	40
3.5	Design of Linear Array	41
3.5.1	General Characteristics.....	41
3.5.2	Coupling Lines Design	44
3.5.2.1	3-port analysis model.....	44
3.5.2.2	Progressive wave feeding.....	47
3.5.3	Different Linear Array Approaches	48
3.5.4	Coupling model: S_{11} Optimization two-by-two.....	49
3.5.5	S_{11} Optimization vs. Constant Phase Difference Feeding Arrays	51
3.6	Design of Unitary Element	53
3.6.1	Design and Fabrication of the 16 th Element	54
3.6.2	Simulation Results	56
3.7	Linear Array Implementation	57
3.7.1	Radiated Electric Near-Field Compensation Model.....	58
3.7.2	Simulation Results	59
3.7.2.1	S_{11} Parameter	60
3.7.2.2	Radiation Pattern	61
3.7.2.3	Gain	71
3.7.3	Conclusions	71

4	DESIGN OF TRANSITIONS	74
4.1	Introduction	74
4.2	Printed Circuit Feeding Transitions	74
4.2.1	Vertical SMA Connector	74
4.2.2	Horizontal SMA Connector.....	76
4.3	Proposed Transition	76
4.3.1	General Features	76
4.3.2	Simulation Results.....	78
5	INTEGRATION AND RESULTS	81
5.1	Proposed Transition	81
5.2	Union of the Linear Array Antenna	81
5.3	Manufacturing of the Prototype	82
5.3.1	Construction of all Layers.....	82
5.3.2	Mounting of the Upper SIW and Lower Patch Layers	84
5.3.3	Assembly of the SIW.....	85
5.3.4	Mounting of Connector and Transition.....	86
5.3.5	Final Assembly of the Patch Structure	87
5.4	Prototype's Measurements.....	87
5.4.1	S_{11} Parameter	87
5.4.2	Radiation Patterns.....	88
5.5	Comparison and Results.....	91
5.5.1	S_{11} Parameter	91
5.5.2	Radiation Pattern	91
5.5.3	Linear Array Antenna with Uniform Air Gap	92
5.5.4	Efficiency	93
6	CONCLUSIONS AND FUTURE WORK.....	94
6.1	Introduction	94
6.2	Conclusions	94
6.3	Future Work	95
A.	INTRODUCCIÓN.....	I
B.	CONCLUSIONES	III
C.	MANUFACTURING OF PRINTED CIRCUITS.....	VI
D.	MEASUREMENTS WITH NETWORK ANALYZER.....	IX
E.	PLANS	XI
F.	PUBLICATIONS.....	XII
G.	PRESUPUESTO	XXVII
H.	PLIEGO DE CONDICIONES.....	XXVIII

ÍNDICE DE FIGURAS

Figure 2-1: 34 m. aperture antenna in Kashima Space Research Center.....	3
Figure 2-2: Patch wireless antenna for broadband communications	3
Figure 2-3: Antenna’s classification according to its operating frequency	5
Figure 2-4 VHF ground plane antenna	5
Figure 2-5 Yagi antenna.....	5
Figure 2-6 Circular slot antenna for satellite communications in band Ku.....	6
Figure 2-7: Slotted array antenna on substrate integrated waveguide for Ku band	6
Figure 2-8: Conical horn antenna	6
Figure 2-9: Typical structure of a horn antenna.....	6
Figure 2-10: High-gain reflector antenna used for radio, television and data communications ..	6
Figure 2-11: Two-port circuit with incoming and outgoing power waves	7
Figure 2-12: Antenna circuit connected to a generator through a transmission line.....	8
Figure 2-13: Omnidirectional radiation pattern.....	10
Figure 2-14: Directional radiation pattern of a horn antenna	10
Figure 2-15: Polar coordinates (left) and Cartesian coordinates (right) normalized radiation patterns	11
Figure 2-16: Isotropic (left), omnidirectional (center) and directive (right) radiation patterns .	11
Figure 2-17: Polarization ellipse	14
Figure 2-18: Vertical polarization of electric and magnetic field	14
Figure 2-19: Circular polarization of electric field.....	14
Figure 2-20: Axes in elliptical polarization	15
Figure 2-21: Upper view of a microstrip rectangular patch antenna.....	16
Figure 2-22: Side view of microstrip rectangular patch antenna.....	16
Figure 2-23: Field lines in microstrip patch	16
Figure 2-24: Microstrip transmission line feeding	17
Figure 2-25: Coaxial connector feeding	17
Figure 2-26: Aperture coupling feeding	17
Figure 2-27: Undesired surface waves which appear in a too thick substrate	17
Figure 2-28: Diagram of a rectangular slot.....	18
Figure 2-29: Slots cut off a rectangular waveguide.....	18
Figure 2-30: Slot fed with a microstrip line	19
Figure 2-31: Linear slotted array antenna.....	19
Figure 2-32: Planar slotted array antenna	19
Figure 2-33: Conformal slotted array antenna.....	19
Figure 2-34: Linear array of N elements equally separated a distance d	20
Figure 2-35: MxN elements distribution in a planar array.....	21
Figure 2-36: Rectangular waveguide filled with dielectric.....	22
Figure 2-37: TE and TM field lines in rectangular waveguide	23
Figure 2-38: Rectangular waveguide.....	23
Figure 2-39: Attenuation of various modes in a rectangular brass waveguide with a = 2 cm....	24
Figure 2-40: TE and TM modes field lines of the first propagated modes in a rectangular waveguide	25
Figure 2-41: Circular waveguide.....	25
Figure 2-42: Bessel functions of first kind	25
Figure 2-43: Attenuation of various modes in a circular waveguide with a = 2.54 cm.....	26
Figure 2-44: Field lines of first modes propagated in circular waveguides.....	26
Figure 2-45: Chassis type SMA connector	27
Figure 2-46: Positioning of coaxial connector in the waveguide	27
Figure 2-47: General geometry of a microstrip line.....	28

Figure 2-48: Field propagation in a microstrip line	28
Figure 2-49: Vertical coaxial probe feeding of microstrip line	29
Figure 2-50: Horizontal coaxial connector feeding a microstrip line	29
Figure 2-51: Substrate Integrated Waveguide with its characteristic parameters.....	30
Figure 2-52: Width's equivalence of SIW and ordinary waveguide	30
Figure 2-53: Vertical coaxial probe feeding of a SIW	31
Figure 2-54: Microstrip transition to SIW in the same substrate.....	31
Figure 2-55: Mode propagation in rectangular waveguide and in microstrip line	31
Figure 2-56: CST user friendly working interface	32
Figure 2-57: Schematic working environment in ADS.....	33
Figure 2-58: Layout working environment in ADS	33
Figure 2-59: Working environment of Ensemble 1D Array Synthesis.....	34
Figure 2-60: Ansoft Ensemble 8.0 working interface	34
Figure 3-1: Appearance of an antenna designed in CST working environment.....	35
Figure 3-2: Geometry of a waveguide filled with two different substrates.....	37
Figure 3-3: Cross section of a rectangular waveguide and transmission line equivalent for Transverse Resonance Method (TRM).....	38
Figure 3-4: Propagation constant for different dielectric constants in the structure.....	38
Figure 3-5: Modes chart of the designed SIW	40
Figure 3-6: Coupling factor of a coupling line with length 4.55 mm. as a function of its width at central working frequency (17 GHz)	43
Figure 3-7: Example of a coupling line section in conventional waveguide with 3-port model .	45
Figure 3-8: Coupled power as a function of the distance of the via from the line's edge	45
Figure 3-9: Coupling factor after individual design of each element.....	47
Figure 3-10: Progressive wave propagating along the SIW feeding array	47
Figure 3-11: S_{11} parameter comparison for approximately (a) $d = 3\lambda g/4$ and (b) $d = \lambda g$	48
Figure 3-12: Feeding array structure in SIW with 17 ports, fed by a conventional waveguide port.....	49
Figure 3-13: Example of two adjacent coupling line sections when applying compensation model	50
Figure 3-14: SIW feeding array ended in short-circuit, fed by conventional waveguide port	51
Figure 3-15: Reflection coefficient of the two patch structures designed	54
Figure 3-16: Design in CST Microwave Studio of the 16 th element, with the bottom patch plane hidden.....	55
Figure 3-17: Detail of the coupling element (a) and bottom view in the ground plane (b).....	55
Figure 3-18: Top (a) and bottom (b) view of the 16 th element in the prototype, before the insertion of the rivets.....	56
Figure 3-19: S_{11} parameter of the 16 th element in dB (a) and in its Smith chart (b)	56
Figure 3-20: Reflection of the linear array with the feeding array joined with the patch structure	57
Figure 3-21: Theoretical versus simulated radiation pattern at 17 GHz.....	57
Figure 3-22: Cross-polar component of the linear array at 17 GHz for plane $\phi = 90^\circ$	58
Figure 3-23: S_{11} parameter (in dB) of the linear array antenna	60
Figure 3-24: S_{11} parameter (in Smith chart) of the linear array antenna.....	60
Figure 3-25: 3D radiation pattern at 16.3 GHz.....	61
Figure 3-26: Simulated co-polar component of the radiation pattern at 16.3 GHz vs. the theoretical one	61
Figure 3-27: Cross-polar component of the radiation pattern at 16.3 GHz.....	62
Figure 3-28: 3D radiation pattern at 16.5 GHz.....	62
Figure 3-29: Simulated co-polar component of the radiation pattern at 16.5 GHz vs. the theoretical one	63
Figure 3-30: Cross-polar component of the radiation pattern at 16.5 GHz.....	63

Figure 3-31: 3D radiation pattern at 16.8 GHz.....	64
Figure 3-32: Simulated co-polar component of the radiation pattern at 16.8 GHz vs. the theoretical one.....	64
Figure 3-33: Cross-polar component of the radiation pattern at 16.8 GHz.....	65
Figure 3-34: 3D radiation pattern at 17 GHz.....	65
Figure 3-35: Simulated co-polar component of the radiation pattern at 17 GHz vs. the theoretical one.....	66
Figure 3-36: Cross-polar component of the radiation pattern at 17 GHz.....	66
Figure 3-37: 3D radiation pattern at 17.2 GHz.....	67
Figure 3-38: Simulated co-polar component of the radiation pattern at 17.2 GHz vs. the theoretical one.....	67
Figure 3-39: Cross-polar component of the radiation pattern at 17.2 GHz.....	68
Figure 3-40: 3D radiation pattern at 17.5 GHz.....	68
Figure 3-41: Simulated co-polar component of the radiation pattern at 17.5 GHz vs. the theoretical one.....	69
Figure 3-42: Cross-polar component of the radiation pattern at 17.5 GHz.....	69
Figure 3-43: 3D radiation pattern at 17.7 GHz.....	70
Figure 3-44: Simulated co-polar component of the radiation pattern at 17.5 GHz vs. the theoretical one.....	70
Figure 3-45: Cross-polar component of the radiation pattern at 17.7 GHz.....	71
Figure 4-1: Design in CST (a) and prototype fabricated (b) of a vertical SMA transition to SIW back-to-back.....	74
Figure 4-2: S_{11} parameter response of a SMA coaxial connector with a microstrip line.....	75
Figure 4-3: S_{21} parameter response of a SMA coaxial connector with a microstrip line.....	75
Figure 4-4: Horizontal SMA coaxial connector and microstrip line.....	76
Figure 4-5: Scheme of the coaxial-microstrip-SIW transition proposed in [17].....	76
Figure 4-6: Design of the proposed transition in CST Microwave Studio, with and without the upper piece.....	77
Figure 4-7: View of the two metallic pieces of the proposed transition: upper cover (a) and connector fixer (b).....	77
Figure 4-8: Manufactured transition pieces, insulating box (a) and connector fixer (b).....	77
Figure 4-9: Detail of the tapered microstrip line, with an emptying around it and the extension of the SIW's vias.....	78
Figure 4-10: Reflection coefficient in dB (a) and in Smith chart (b) for the transition with connector [18].....	78
Figure 4-11: Transmission coefficient in dB for the transition with connector [18].....	79
Figure 4-12: Reflection coefficient in dB (a) and in Smith chart (b) for the transition with connector [19].....	79
Figure 4-13: Transmission coefficient in dB for the transition with connector [19].....	79
Figure 4-14: Radiation pattern in 3D at 17 GHz for the connector [18].....	80
Figure 4-15: Radiation pattern in 3D at 17 GHz for the connector [19].....	80
Figure 5-1: Linear array antenna with the designed transition, and a detail of coupling line section.....	81
Figure 5-2: Top view of all the layers: upper patch (a), ROHACELL (b), lower patch (c), upper SIW (d) and bottom of lower SIW (e).....	83
Figure 5-3: Bottom view of all the layers: upper patch (a), ROHACELL (b), lower patch (c), upper SIW (d) and top of lower SIW (e).....	83
Figure 5-4: Top view of the lower patch layer.....	84
Figure 5-5: Detailed view of the lower patches of the 14 th , 15 th and 16 th elements (from left to right), which include the three different patch structures designed.....	84
Figure 5-6: Top view of the upper SIW layer (a), bottom view with the coupling lines (b) and detail of the coupling lines from 11 th to 16 th element.....	84

Figure 5-7: Mounted and soldered patches to the coupling vias	85
Figure 5-8: Riveting process (a) and SIW completely riveted before soldering (b)	85
Figure 5-9: Bottom view of the riveted SIW.....	86
Figure 5-10: Top view of mounted and soldered SIW.....	86
Figure 5-11: Mounted and soldered connector in the SIW	86
Figure 5-12: Soldered connector (a) and fully mounted transition (b).....	87
Figure 5-13: Antenna completely assembled with fiber glass piece for later measurement in anechoic chamber	87
Figure 5-14: Measured S_{11} parameter (in dB)	88
Figure 5-15: Measured co-polar and cross-polar components versus the air gap co-polar component at 16.3 GHz	88
Figure 5-16: Measured co-polar and cross-polar components versus the air gap co-polar component at 16.7 GHz	89
Figure 5-17: Measured co-polar and cross-polar components versus the air gap co-polar component at 17 GHz	89
Figure 5-18: Measured co-polar and cross-polar components versus the air gap co-polar component at 17.3 GHz	90
Figure 5-19: Measured co-polar and cross-polar components versus the air gap co-polar component at 17.7 GHz	90
Figure 5-20: Measured reflection coefficient (a) versus reflection response of the linear array with air gap (b).....	92
Figure C-1: Diagram of the software design process involved in the manufacturing of the prototype	VII
Figure D-1: Network analyzer E5071C property of EPS	IX
Figure D-2: Coaxial cables used for measurements with VNA, property of EPS.....	IX
Figure D-3: Content of the calibration kit 85052D de Agilent Technologies, property of EPS	X
Figure E-1: Top view of the transition section with all the important concerning parameters...	XI
Figure E-2: Plans of the fixer metallic piece of the proposed transition.....	XII
Figure E-3: Plans of the insulating metallic piece of the proposed transition	XII

ÍNDICE DE TABLAS

Table 2-1: Frequency bands	4
Table 2-2: Microwave Frequency Bands	4
Table 2-3: Two-port circuit S parameters description	8
Table 2-4: Field regions of an antenna.....	10
Table 3-1: Summary table of SIW and equivalent waveguide parameters.....	41
Table 3-2: Amplitude and coupling coefficients for a linear array of 16 elements with Taylor -26 dB distribution and 2% power loss	42
Table 3-3: Coupling factors for single via element with different substrate configurations	43
Table 3-4: Amplitude and coupling coefficients for a linear array of 16 elements with uniform distribution and 2% power loss.....	44
Table 3-5: Obtained amplitude for the coupling coefficients and line's dimensions for each element	46
Table 3-6: Comparison of the line's dimensions before and after the reflection optimization process	50
Table 3-7: Amplitude and coupling coefficients for a linear array of 16 elements with uniform distribution with no power loss	52
Table 3-8: Amplitude and phase difference of the coupling coefficients, for S_{11} optimization and constant phase difference SIW feeding arrays	52
Table 3-9: Summary table of patch structure parameters.....	54
Table 3-10: Comparison of different parameters of the linear array, before and after applying the radiated electric near-field compensation model.....	59
Table 3-11: Maximum gain values of the radiation at different frequencies	71
Table 3-12: Summary table of the parameters of the initial linear array	73
Table 3-13: Summary table of the parameters of the final linear array, after applying the near-field compensating model	73
Table 5-1: Measured maximum gain	93
Table 5-2: Measured and simulated gain and efficiency of the antenna	93
Table E-1: Values of the parameters of the transition section	XI

1 INTRODUCTION

In this document it is described the engineering project consistent of a linear patch array over substrate integrated waveguide, which operates in the Ku band (12.4 – 18 GHz).

1.1 Project Motivation

With the continuous emergence of new technologies and its improvement, it is of the outmost importance to adapt the existent structures and devices to them. These motivations can be caused by several factors, such as antenna's size, cost, adaptation to the environment, etc. In the end, the objective is to provide to users a quality service and communication as wide as possible, so new solutions must be sought and developed.

For many applications, the single element antennas are unable to meet the requirements of radiation pattern or gain. Combining several of these single element antennas in arrays, it is possible to obtain new solutions through the combined effect of all the antennas.

Finally, the printed circuit technology is acquiring more and more importance each day; as it enables the possibility of manufacturing high gain antennas with lower costs and smaller dimensions than the conventional technology can offer.

For all these reasons, in this Career Final Project (CFP) the design of a completely new linear array antenna will be developed. Through the combination of a patch structure for the radiating elements and coupling lines inside a waveguide for their feeding, the linear array will be characterized. Moreover, the waveguide will be implemented in substrate integrated waveguide (SIW), in order to reduce costs, simplify the manufacturing procedure and verify the usefulness of this technology.

1.2 Goals

The objective of this project is the design and characterization of a linear array antenna implemented over printed circuit technology for Ku band. The concrete objectives of this project are the following:

1. Design of the radiant elements with optimal reflection, consistent of coupling lines and patches; and their further characterization.
2. Design of the linear array on substrate integrated waveguide (SIW) technology, implementing the elements previously mentioned.
3. Design and characterization of transitions that can effectively feed the antenna and at the same time maintain good levels of matching with the antenna.

1. Introduction

4. Integration of the linear array and the designed transitions for further construction and measurement.

1.3 Document Structure

The documentation of this project is structured as follows:

- **Chapter 1: Introduction**

This chapter presents the motivation, objectives and structure of this document.

- **Chapter 2: State of the Art**

In this chapter it is exposed the state of the art of array antennas, printed circuit technologies and SIW, among others.

- **Chapter 3: Design of Antennas**

There are three differentiated parts in this chapter:

- Design of the array in SIW with the coupling lines that feed the patches.
- Design of the different unitary patch elements.
- Design of antennas with certain directivity and linear polarization characteristics, and their simulation results.

- **Chapter 4: Design of Transitions**

Different feeding transitions are described in this chapter, considering that they must be feasible and offer good matching levels.

- **Chapter 5: Integration and Results**

In this chapter the combination of the linear arrays and transitions is presented, as well as the results from the measurements of the manufactured antenna.

- **Chapter 6: Conclusions and Future Work**

This final chapter summarizes the main achievements of the project, discusses the results obtained from the design and manufacturing process; and finally suggests possible improvements and future lines of work.

2 STATE OF THE ART

2.1 Introduction

This chapter will introduce basic concepts of antennas and arrays, as well as a brief introduction to the theory of waveguides, SIW and microstrip used in the design of this project. Finally, the specific tools used for design and simulation of the different designs will be described.

2.2 Principles of Antennas

2.2.1 Concept of Antenna

An antenna is a device designed for transmitting and receiving electromagnetic waves from free space, which matches the output of the transmitter or the input of the receiver to the medium. A good antenna will be characterized by a good radiating efficiency, a good matching between the antenna and the transmission line that feeds it and an appropriate radiation pattern.



Figure 2-1: 34 m. aperture antenna in Kashima Space Research Center



Figure 2-2: Patch wireless antenna for broadband communications

According to the wavelength and the antenna's dimensions, the antennas can be classified among different groups. If the dimensions are smaller than the wavelength, the antennas are named elemental; if the dimensions are of the order of half a wavelength, they are called resonant; and if the size is much bigger than a wavelength they are denominated directive.

2. State of the Art

Standard Frequency Bands

The frequency bands are the intervals of the electromagnetic spectrum assigned for different kinds of communications. Depending on the frequency/wavelength, they would be more suitable for a given application or another.

Acronym	Name	Wavelength	Frequency Range	Applications
VLF	Very Low Frequency	30.000 m. to 10.000 m.	10 KHz to 30 KHz	Navigation, sonar
LF	Low Frequency	10.000 m. to 1.000 m.	30 KHz to 300 KHz	Radio beacons, Navigational aids
MF	Medium Frequency	1.000 m. to 100 m.	300 KHz to 3 MHz	AM broadcasting, maritime radio, direction finding
HF	High Frequency	100 m. to 10 m.	3 MHz to 30 MHz	Telephone, telegraph, amateur radio, citizen's band, ship-to-coast and ship-to-aircraft comm.
VHF	Very High Frequency	10 m. to 1 m.	30 MHz to 300 MHz	Television, FM broadcasting, air traffic control, police, taxi mobile radio
UHF	Ultra High Frequency	1 m. to 10 cm.	300 MHz to 3 GHz	Television, satellite communication, radiosonde, surveillance radar
SHF	Super High Frequency	10 cm. to 1 cm.	3 GHz to 30 GHz	Airborne radar, microwave links, carrier land mobile communications, satellite communication
EHF	Extremely High Frequency	1 cm. to 1 mm.	30 GHz to 300 GHz	Radar, experimental

Table 2-1: Frequency bands

Band	Frequency Range	Wavelength
L	(1 -2) GHz	(30 – 15) cm.
S	(2 -4) GHz	(15 – 7.5) cm.
C	(4 -8) GHz	(7.5 – 3.75) cm.
X	(8 -12.4) GHz	(3.75 – 2.42) cm.
Ku	(12.4 -18) GHz	(2.42 – 1.66) cm.
K	(18 -26.5) GHz	(1.66 – 1.11) cm.
Ka	(26.5 -40) GHz	(11.1 – 7.5) mm.
mm	(40 -300) GHz	(7.5 – 1) mm.

Table 2-2: Microwave Frequency Bands

2.2.2 Types of Antennas

There are several types of antennas according to the way they radiate. From the classic classification described in [1] and [2]:

2. State of the Art

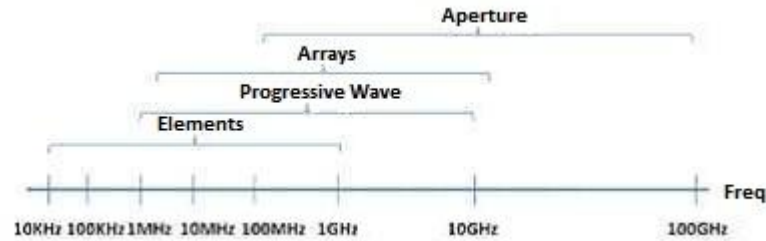


Figure 2-3: Antenna's classification according to its operating frequency

2.2.2.1 Wire Antennas

Antennas in this group are built with conductor tubes with a very small diameter in comparison with wavelength. Some of the most popular antennas of this type are monopoles, dipoles, spiral and helical antennas.



Figure 2-4 VHF ground plane antenna

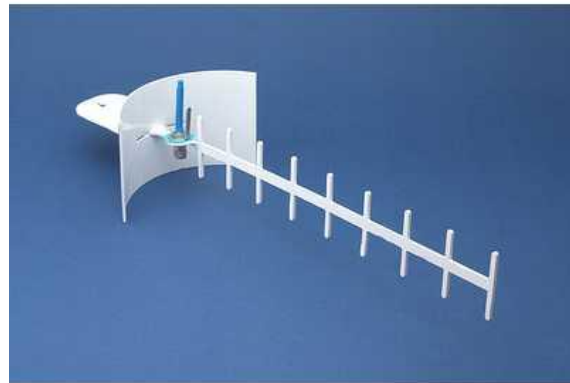


Figure 2-5 Yagi antenna

2.2.2.2 Travelling Wave Antennas

Usually constructed with conductor tubes electrically long and terminated in matched loads.

2.2.2.3 Array Antennas

The array antennas are made of identical (or very similar) antennas, so the radiation pattern of each individual antenna ends up forming the radiation pattern of a single antenna, if the radiating elements are arranged properly in the array. This is particularly useful if the radiation pattern needs to be modified in order to use the antenna's design for a different application. Different radiation patterns can be achieved if the feeding amplitude and phase of each element is modified.

2. State of the Art



Figure 2-6 Circular slot antenna for satellite communications in band Ku

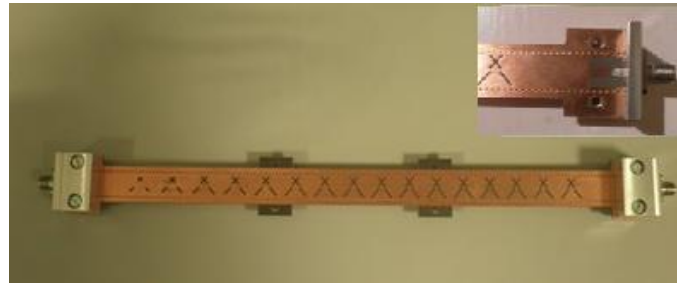


Figure 2-7: Slotted array antenna on substrate integrated waveguide for Ku band

2.2.2.4 Aperture Antennas

Part of the structure of these antennas is an opening or a surface, through which electromagnetic waves flow in the medium if the antenna is working as a transmitter. If the antenna operates as a receiver, the waves are collected via the aperture. Aperture antennas are capable of focusing the electromagnetic beam into a concrete direction. Some examples of antennas belonging to this group are horns used in microwave range, and reflectors for ground-to-ground or satellite communications.



Figure 2-8: Conical horn antenna

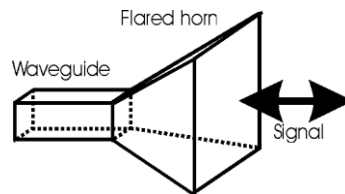


Figure 2-9: Typical structure of a horn antenna



Figure 2-10: High-gain reflector antenna used for radio, television and data communications

2.2.3 Input Impedance

The input impedance of an antenna is defined as the relation between the voltage and the current at its terminals [2]. This impedance is composed of real part $R_A(\omega)$ known as resistance, and imaginary part $X_A(\omega)$ called reactance, both of dependent of frequency.

$$Z_A = R_A(\omega) + j \cdot X_A(\omega) \quad (2.1)$$

The real part of the antenna can be defined in two terms considering the radiation resistance R_r , and the resistance associated to ohmic losses R_L :

$$R_r = \frac{2P_{rad}}{|I_A|^2} \quad (2.2)$$

$$R_L = \frac{2(P_{in} - P_{rad})}{|I_A|^2} \quad (2.3)$$

2. State of the Art

Therefore, the dissipated power of the antenna can be separated into radiative power of the antenna (P_r) and power dissipated into heat (P_L) as it follows:

$$P_r = \frac{1}{2} |I_A|^2 R_r \quad (2.4) \qquad P_L = \frac{1}{2} |I_A|^2 R_L \quad (2.5)$$

Where I_A is the current at the input terminals of the antenna.

2.2.4 Scattering Parameters (S Parameters)

All of the microwave circuits can be characterized as a two-port network, where the first port is the physical input port of the circuit and the second is the output terminal. Antennas are not an exception, and port one would be the physical input with a typical value of 50 Ω , and the other would be the physical radiation port.



Figure 2-11: Two-port circuit with incoming and outgoing power waves

Working with microwave circuits, it is possible to characterize them by several relations between voltage and current at its terminals; establishing impedance matrix Z or admittance matrix Y . These parameters are obtained considering open circuits or short-circuit at each terminal. However, this is difficult to achieve when working at high frequencies. Better results can be obtained relating the incident voltage waves in each port with the reflected ones in every port, through the scattering matrix.

With the S parameters there is no need of further consideration, as they are valid at all frequencies. Based on the power levels existing at the ports, new voltage incident wave a_n and reflected wave b_n , both normalized to the reference impedance of the corresponding port. The direction of each one of the waves is seen in Figure 2-11.

In the case of a two-port circuit, the existent relation between the incident and reflected waves is set through four S parameters defined as follows:

$$\begin{aligned} b_1 &= S_{11} \cdot a_1 + S_{12} \cdot a_2 \\ b_2 &= S_{21} \cdot a_1 + S_{22} \cdot a_2 \end{aligned} \quad (2.6)$$

For calculating the scattering parameter S_{ji} it is necessary to have each port ended with a load of the same characteristic impedance of the port, with the exception of port i where there would be a generator which will provide the incident wave a_i .

$$S_{ji} = \left(\frac{b_j}{a_i} \right)_{a_k \neq 0 (\forall k \neq i)} \quad (2.7)$$

2. State of the Art

For the two-port circuit, the meaning of each S parameter is described in the following table:

Parameter	Coefficient	Description	Formula
S_{11}	Input reflection	Power reflected in port 1 when fed with an incident wave in port 1	$S_{11} = \left. \frac{b_1}{a_1} \right _{a_2=0}$
S_{12}	Transmission or inverse gain	Power that reaches port 2 when the circuit is fed from port 2	$S_{12} = \left. \frac{b_1}{a_2} \right _{a_1=0}$
S_{21}	Transmission or direct gain	Power that reaches port 2 when the circuit is fed from port 1	$S_{21} = \left. \frac{b_2}{a_1} \right _{a_2=0}$
S_{22}	Output reflection	Power reflected in port 2 when fed with an incident wave in port 2	$S_{22} = \left. \frac{b_2}{a_2} \right _{a_1=0}$

Table 2-3: Two-port circuit S parameters description

Some other interesting parameters can be defined from the previous S parameters, which will be particularly useful when working with power values:

- $|S_{ii}|^2 = \frac{\text{Reflected power in port } i}{\text{Available power at port } i}$
- Input return loss (dB): $-20 \cdot \log_{10}|S_{ii}|$
- $|S_{ji}|^2 = \frac{\text{Transmitted power to port } j}{\text{Available power at port } i}$
- Insertion loss (dB): $-20 \cdot \log_{10}|S_{ji}|$

2.2.5 Matching

For its proper functioning, the antenna must be connected to the transmitter or the receiver by a transmission line.

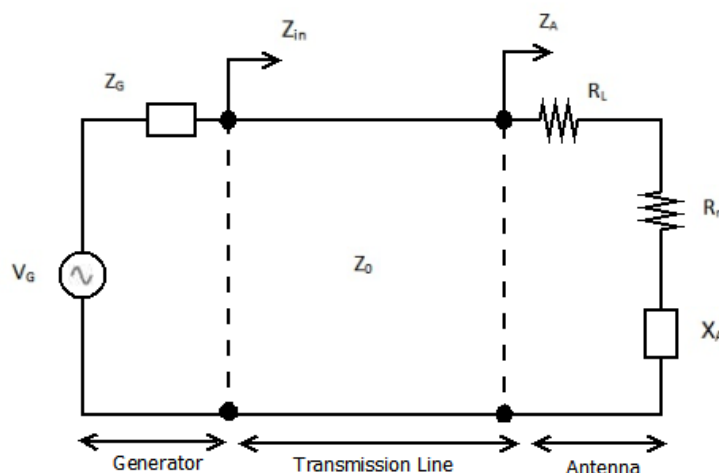


Figure 2-12: Antenna circuit connected to a generator through a transmission line

Connecting the antenna to a circuit implies going from the characteristic impedance of the antenna to the one seen on the circuit. As it has been stated in the previous paragraph, parameter S_{11} represents the power reflected at the port and consequently gives a hint of how

2. State of the Art

much power is transmitted to the antenna's port. Parameter S_{11} can be defined according to the impedances of both the antenna and the transmission line connected to it:

$$S_{11} = \Gamma = \frac{Z_A - Z_0}{Z_0 + Z_A} \quad (2.8)$$

Where Z_0 is the characteristic impedance of the transmission line and Z_A is the input impedance of the antenna seen in Figure 2-12:

$$Z_A = (R_L + R_r) + j \cdot X_A \quad (2.9)$$

Similarly, the input impedance looking into the terminated transmission line from the generator end is $Z_{in} = R_{in} + jX_{in}$, and the input current defined as I . Thus, the input power of the network P_{in} and the reflection coefficient seen looking into the generator Γ_G can be defined as:

$$P_{in} = \frac{1}{2} |I|^2 R_{in} \quad (2.10)$$

$$\Gamma_G = \frac{Z_G - Z_0}{Z_G + Z_0} \quad (2.11)$$

It can be proved that the maximum power will be transferred to the transmission line when $Z_G = Z_{in}^*$, i.e. conjugated matching. However, the fulfillment of this condition does not assure that there would be no reflection at the antenna terminals ($S_{11} = \Gamma = 0$). It is important to note that both situations will be only achievable simultaneously if both Z_G and Z_0 are real.

So finally, the power available at the entrance when there is matching between the feeding network and the transmission line will be:

$$P_{in} = \frac{1}{2} \left| \frac{V_G}{Z_{in}^* + Z_{in}} \right|^2 \cdot R_{in} = \frac{1}{8} \frac{|V_G|^2}{R_G} \quad (2.12)$$

2.2.6 Standing Wave Ratio (SWR)

When there is no matching between the transmission line and the load, a reflected voltage wave appears and consequently a standing wave where the magnitude of the voltage wave is not constant. The measure of this mismatch of a line is called standing wave ratio (SWR), and is defined as:

$$SWR = \frac{V_{\max}}{V_{\min}} = \frac{1 + |\Gamma|}{1 - |\Gamma|} \quad (2.13)$$

As it has been seen in equation (2.8), $|\Gamma| = S_{11}$, so SWR is a good indicator of how mismatched is the antenna to the transmitter, i.e. how much power is transmitted to the load. From (upper formula), SWR is a real number such that $1 < SWR < \infty$, where the case of $SWR = 1$ implies a perfectly matched load ($S_{11} = 0$).

2. State of the Art

2.2.7 Radiation Pattern

A radiation pattern is a graphical representation of the radiation properties of an antenna, which varies with the space coordinates.

Depending on the distance to the antenna, the far-field is defined into different regions. If the distance from the antenna is r , D is the maximum dimension of the antenna and λ is the working wavelength; supposing that $r \gg D$ and $r \gg \lambda$, the different regions cases where $D \gg \lambda$ can be summarized as follows:

Region	Distance form antenna (r)
Reactive near field	0 to $0.62\sqrt{D^3/\lambda}$
Radiating near field	$0.62\sqrt{D^3/\lambda}$ to $2D^2/\lambda$
Far field	$2D^2/\lambda$ to ∞

Table 2-4: Field regions of an antenna

The radiation pattern can be represented either on a 3D plane or different cutting planes depending on the varying angle; but all of them are usually normalized to the maximum value. The most common representation system is the spherical coordinate one, defined by three magnitudes: radius r , polar angle θ and azimuthal angle ϕ .

For the cutting plane representation, the most important ones are the E and the H planes. E plane represents the electrical field in the maximum radiation direction, whereas H field is the magnetic field in the same direction. Both planes are perpendicular to each other and to the direction of propagation.

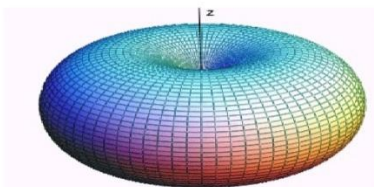


Figure 2-13: Omnidirectional radiation pattern

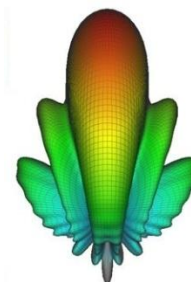


Figure 2-14: Directional radiation pattern of a horn antenna

When representing radiation patterns in 2D, both polar and Cartesian coordinates are used. Polar coordinates are more appropriate for viewing how waves propagate in the medium, showing a clearer power distribution in all directions. On the other hand, Cartesian representation shows a better comparison of main and side lobes level, as well as nulls. In

2. State of the Art

Cartesian representation one angle is fixed (typically at 0° or 90°) and the other angle is swept and represented in abscise axis; while power density is shown in the vertical axis.

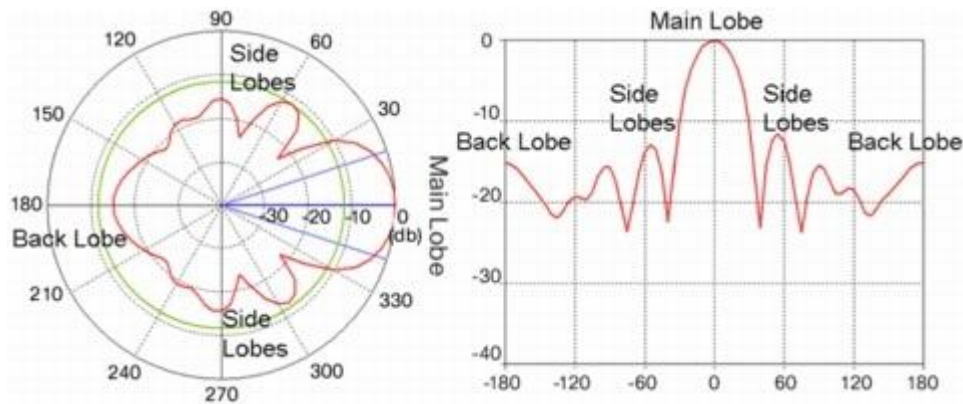


Figure 2-15: Polar coordinates (left) and Cartesian coordinates (right) normalized radiation patterns

According to the service provided by the antenna and the radiation directivity of it, the radiation pattern can be classified as follows:

- Isotropic: The same power density is radiated in every spatial direction.
- Omnidirectional: The radiation pattern has revolution symmetry around an axis.
- Directive: The maximum power radiated is focused on a determined direction.

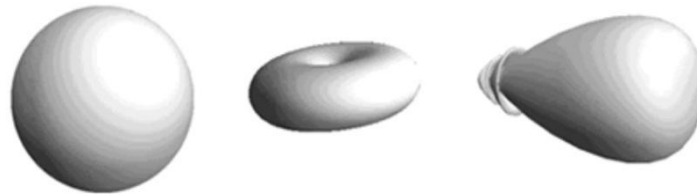


Figure 2-16: Isotropic (left), omnidirectional (center) and directive (right) radiation patterns

In a radiation pattern, the most important parameters are the following:

- Direction of propagation: Direction of maximum radiation.
- Main lobe: Region of the radiation pattern delimited by weaker radiation regions. It aims the direction of propagation.
- Minor lobe: Any lobe other than the main one. Minor lobes are composed of side lobes and back lobes (directly opposite the main lobe).
- Secondary lobe: The two adjacent lobes to the main one with the highest relative amplitude.
- Side lobe level (SLL): Relation in dB between the maximum value of the main lobe and the maximum amplitude value of the side lobes.
- Beamwidth at -3 dB: Angular width of the half power radiated within a certain cut through the main lobe where most of the power is radiated. Defined by the two points of the main lobe 3 dB below its maximum value.

2. State of the Art

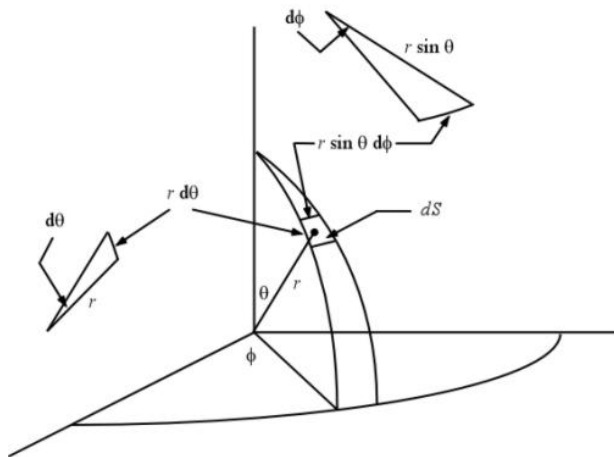
2.2.8 Radiation Intensity, Directivity and Gain

2.2.8.1 Radiation Intensity

Radiation intensity is the power radiated in a given direction per unit solid angle (steradian), and it is an indicator of how an antenna can radiate in a determined direction. Radiation intensity is the radiated density power (W_{rad}) by square of distance (r), and it is independent of distance [2]. It can be expressed as:

$$U(\theta, \phi) = \frac{\langle S(r, \theta, \phi) \rangle dS}{d\Omega} = r^2 \langle S(r, \theta, \phi) \rangle \quad (2.14)$$

Where the differentials are defined as follows:



$$d\Omega = \frac{dS}{r^2} = \sin \theta d\theta d\phi \quad (2.15)$$

$$dS = r^2 \sin \theta d\theta d\phi \quad (2.16)$$

The radiation intensity of an isotropic source is constant over all space, at a value of U_{ave} . Then:

$$P = \iint U_{ave} \cdot d\Omega = 4\pi U_{ave} \quad (2.17)$$

If the radiating source is nonisotropic, the radiation intensity is not constant throughout space, but an average power per steradian can be defined as:

$$U_{ave} = \frac{1}{4\pi} \iint U(\theta, \phi) \cdot d\Omega = \frac{P_{rad}}{4\pi} \quad (2.18)$$

2.2.8.2 Directivity

The directivity of an antenna is the ability to concentrate energy in one direction in preference to radiation in other directions. It is defined as the relation between the radiation intensity of the antenna in each direction and an isotropic antenna which radiates the same power:

$$D(\theta, \phi) = \frac{U(\theta, \phi)}{U_{ave}} = 4\pi \frac{U(\theta, \phi)}{P_{rad}} \quad (2.19)$$

2. State of the Art

As directivity is usually quoted without reference of a direction, maximum directivity is usually intended. Maximum directivity is the value of directivity in the direction of propagation. Thus, maximum directivity follows from (2.19) as:

$$D_{\max} = \frac{U_{\max}}{U_{\text{ave}}} = \frac{4\pi \cdot U_{\max}}{P_{\text{rad}}} \quad (2.20)$$

2.2.8.3 Gain

Gain is defined as the relation, in each spatial direction, between the radiation intensity of the antenna and an isotropic antenna with the same incoming power P_{inc} than the antenna under study.

$$G(\theta, \phi) = \frac{4\pi \cdot U(\theta, \phi)}{P_{\text{in}}} \quad (2.21)$$

Thus, gain can be expressed as a function of θ and ϕ and can be given as a value in a specific direction. If no direction is specified by any θ or ϕ , it is assumed to be the maximum gain:

$$G = \frac{4\pi \cdot U_{\max}}{P_{\text{in}}} \quad (2.22)$$

2.2.9 Radiation efficiency

It is important to note how efficient an antenna radiates and characterize its performance. For this reason the radiation efficiency is defined as the relation between the radiated power P_{rad} and the input power P_{in} :

$$\eta_{\text{rad}} = \frac{P_{\text{rad}}}{P_{\text{in}}} \quad (2.23)$$

From radiation efficiency, there is a relation between gain and directivity as follows:

$$G(\theta, \phi) = \eta_{\text{rad}} \frac{4\pi \cdot U(\theta, \phi)}{P_{\text{in}}} = \eta_{\text{rad}} \frac{U(\theta, \phi)}{U_{\text{ave}}} = \eta_{\text{rad}} \cdot D(\theta, \phi) \quad (2.24)$$

2.2.10 Polarization

The polarization on an antenna is the polarization of the wave radiated by the antenna when transmitting. The phase front (surface of constant phase) of a wave radiated can be considered planar over small observation regions, so this wave is referred as a *plane wave*. The polarization of a plane wave is how its electric field varies with time at a fixed observation point, in the propagation direction. As time progresses, the electric field oscillates back and forth along a vertical line; resulting in a general polarization ellipse.

2. State of the Art

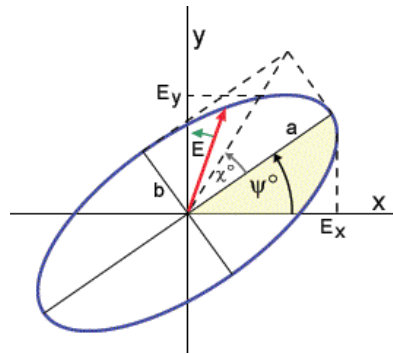


Figure 2-17: Polarization ellipse

Although the general case describes an ellipse of the electric field variation, there are some important special cases of it:

- Linear polarization: The electric field vector moves back and forth along line, so the traced figure is a segment. The linear polarization can be either vertical or horizontal.

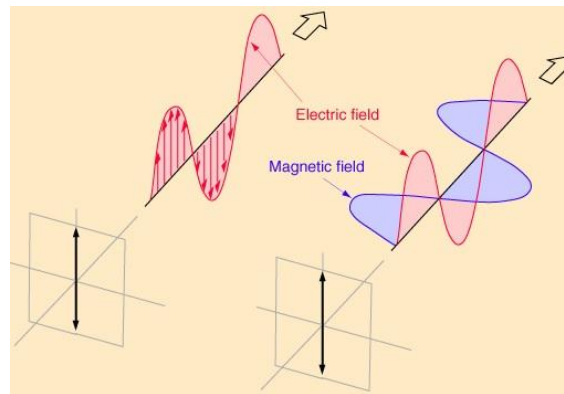


Figure 2-18: Vertical polarization of electric and magnetic field

- Circular polarization: The electric field vector is constant in length but rotates around in a circular path. If the rotation of the vector is clockwise, the wave is *left-hand polarized*. On the other hand, if the rotation is counterclockwise, the plane wave is *right-hand polarized*.

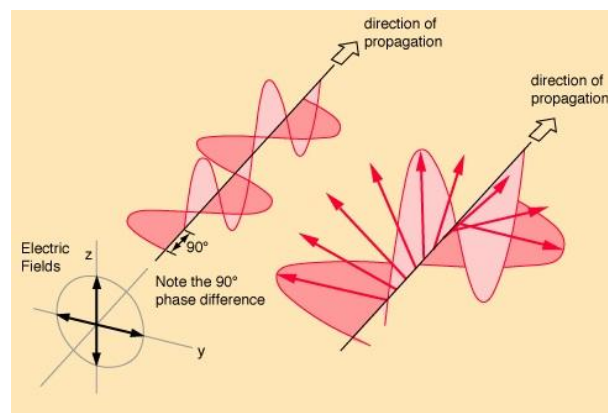


Figure 2-19: Circular polarization of electric field

2. State of the Art

In order to know the type of polarization of the plane wave, the parameter *axial ratio* (*AR*) is defined. The axial ratio is the relation between the major axis electric field component to that along the minor axis.

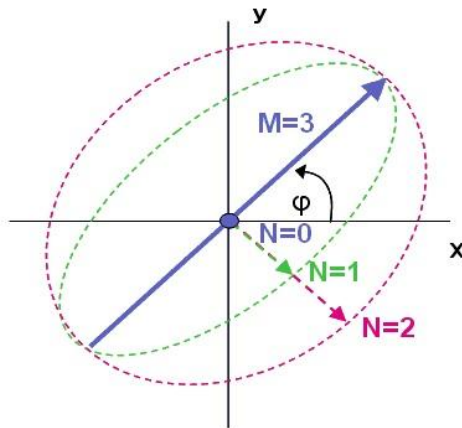


Figure 2-20: Axes in elliptical polarization

$$AR = \frac{M}{N} \Rightarrow 1 \leq |AR| \leq \infty$$

- If $AR = \infty \rightarrow$ Linear polarization
- If $AR = 1 \rightarrow$ Circular polarization
- For $1 < |AR| < \infty \rightarrow$ Elliptical Polarization

2.2.11 Bandwidth

Antennas are designed to work in certain frequency bands, as it is impossible for them to function correctly all over the electromagnetic spectrum due to their finite geometry. The bandwidth of an antenna is the frequency range where the antenna works with some determined characteristics. It is defined as the relation (percentage) between the frequency ranges where it operates in:

$$BW_{\%} = \frac{f_{\max} - f_{\min}}{f_c} \cdot 100 \quad (2.25)$$

Where f_c is the central frequency of the frequency functioning range.

2.2.12 Radiant elements

The radiant elements of an antenna can have multiple designs or configurations. In printed circuit antennas, a portion of the metallization layer is responsible for radiation. Among all, two elements can be highlighted [3]: patches and slots.

2.2.12.1 Patches

In printed circuit technology, microstrip lines are not designed for dissipating too much power in radiated field. However, it is impossible to prevent this behavior, so to not waste this power it appears the idea of *microstrip antennas*.

The simplest microstrip antenna is composed by two parallels conductors separated by a thin dielectric substrate, being the lower conductor the ground plane. If the upper conductor is a patch, and its dimensions are an appreciable fraction of a wavelength; the device becomes a microstrip antenna. According to the desired way of radiating the power, the dimensions of the patch will be chosen.

2. State of the Art

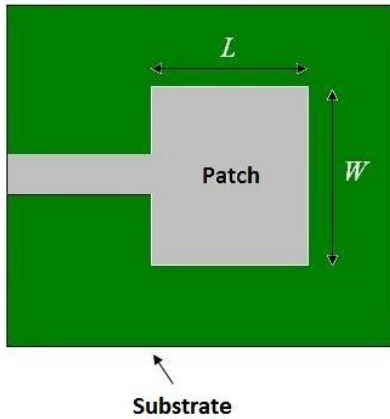


Figure 2-21: Upper view of a microstrip rectangular patch antenna

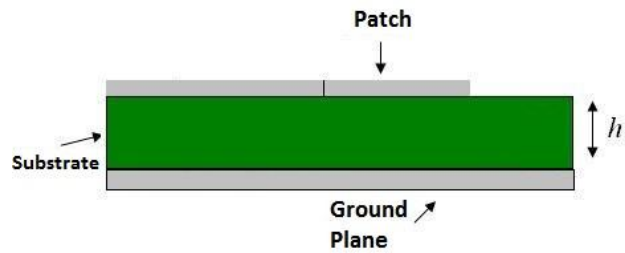


Figure 2-22: Side view of microstrip rectangular patch antenna

Patches can be found in several forms, such as square, rectangular, circular; or even less common shapes such as triangular or elliptical.

The principles of functioning of a patch depend on its equivalence to two slots of dimensions $L \times W$ in the rectangular patch, where radiation appears in the discontinuities and open circuits of the structure when its size is comparable to the wavelength. Radiated fields in the laterals of the patch are cancelled by each other. The fundamental mode propagated is a quasi-TEM, which is mainly confined within the dielectric.



Figure 2-23: Field lines in microstrip patch

The height of the dielectric is an important feature in the design of a patch. If the thickness of the substrate is electrically thin ($0.003\lambda < h < 0.05\lambda$), leakages and surface waves are minimized, resulting in a better behavior of the patch.

Patch antennas can be used in arrays with series or parallel feeding. One of the problems of these types of antennas is that their bandwidth is very narrow, and the radiation characteristics not so good. However, patch antennas are rather small and light, so they are easily adaptable to microwave circuits. Furthermore, as they can be put together to form simple arrays; antennas with better characteristics can be designed from single element microstrip patch antennas.

Feeding:

Patch antennas can be fed in many different ways:

- Through a **transmission line** in the same plane as the patch.
- Through a **coaxial cable** or **probe** feed.
- By **indirect coupling** in a multiple layer structure.

2. State of the Art

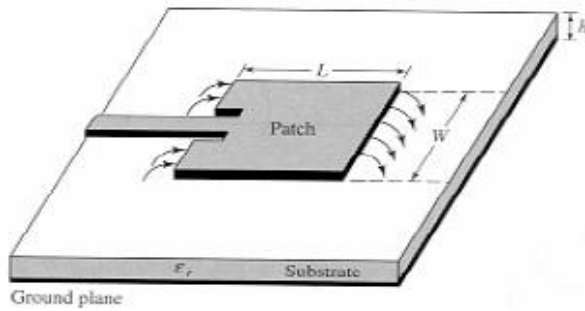


Figure 2-24: Microstrip transmission line feeding

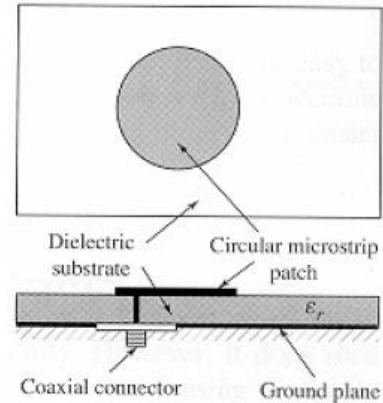


Figure 2-25: Coaxial connector feeding

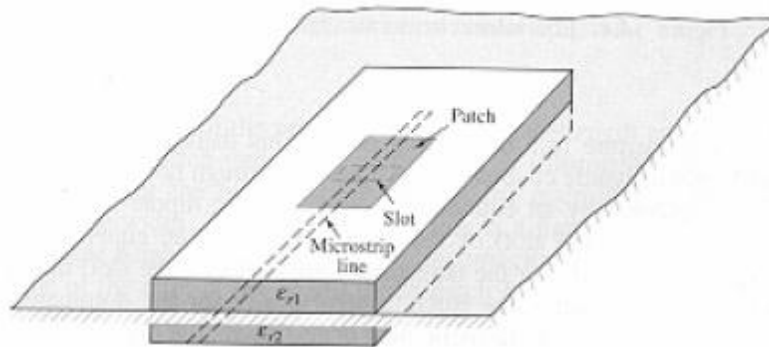


Figure 2-26: Aperture coupling feeding

When designing the whole microstrip antenna, it is of the outmost importance to design the feeding at the same time. In the case of vertical feeding with coaxial cable, the impedance of the patch is modified depending on the location of the inner conductor soldering, i.e. in the center of the patch (supposed in any form) or closer to one of the edges. The same way, with the determined insertion of the transmission line in the patch structure, the patch's impedance varies. The appropriate value of this impedance is crucial to achieve a good matching and avoid undesired reflection waves.

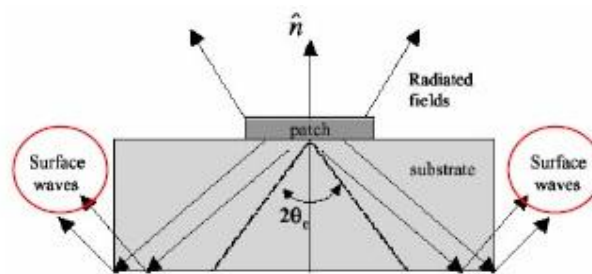


Figure 2-27: Undesired surface waves which appear in a too thick substrate

It is interesting to note that there are some structures that can improve the general behavior of patch antennas. While enlarging the dimensions of the structure (thicker dielectric with lower dielectric constant ϵ_r) increases efficiency and bandwidth; it also increases losses due to surface waves, resulting in higher level of SLL and less power in the radiation pattern. An alternative to this method is using multilayer structures, with different substrates and patch's dimensions in each layer. This way, more resonances are added and a wider bandwidth can be obtained.

2. State of the Art

2.2.12.2 Slots

Slots are apertures made in a ground plane, where one of the dimensions is small in comparison to the other to obtain a resonance (the longest should be slightly shorter than $\lambda/2$). Radiation escapes through them, and they are the equivalent to a dipole of the same length.

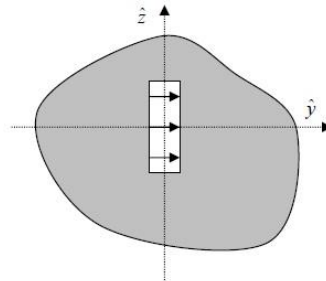


Figure 2-28: Diagram of a rectangular slot

Slots can be fed in different ways, as it happened with patches

- **Waveguide:** Slots are cut in the walls of the waveguide, interrupting the flow of currents and coupling power that will be radiated to the exterior of the waveguide. The more perpendicular the largest dimension of the slot is to the current density lines in the conductor wall, the more power will the slot couple. As it is seen in Figure 2-29, the positioning of the slots will result in a stronger or weaker resonance of the slot, and consequently more or less power coupled. Since the maximum power is coupled if the slot is oriented in the z axis for the vertical walls or x axis direction for the horizontal walls, rotating the slots will decrease the power radiated through them. This is, for example, how the radiated power of each element can be adjusted to obtain the desired radiation pattern of a slotted array.

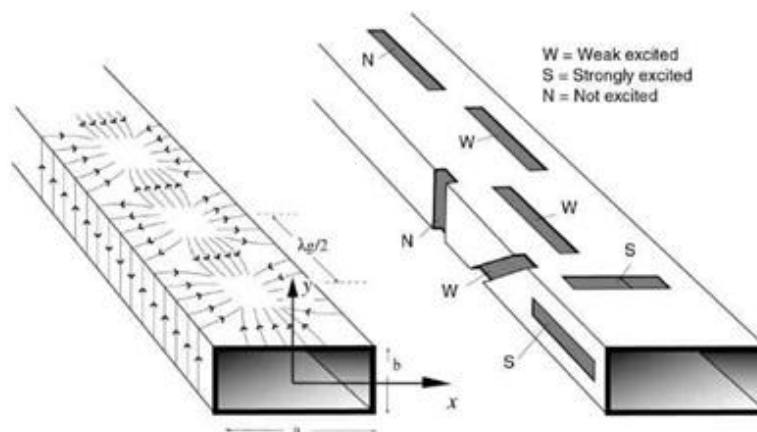


Figure 2-29: Slots cut off a rectangular waveguide

- **Microstrip line:** The slot is placed in the ground plane, and the microstrip line has an open circuit at a distance of $\lambda/4$ from the slot.

2. State of the Art

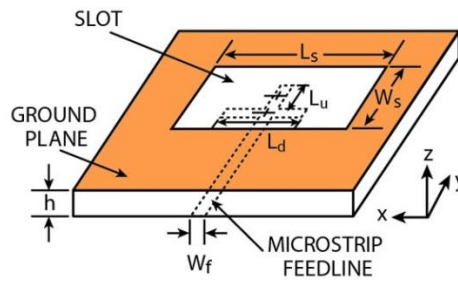


Figure 2-30: Slot fed with a microstrip line

2.3 Principles of Arrays

Sometimes, the radiation pattern on an antenna is very wide, that is it has a low gain. Some applications demand higher gain radiation patterns with higher directivity. Single element antennas could achieve these characteristics if the dimensions were very large, but the configuration of several smaller antennas arranged in space and interconnected can produce a very similar effect. This configuration of radiating elements is referred as an *array antenna*.

Arrays offer several advantages over single element antennas. Apart from higher directivity and gain, arrays can be more easily adjusted to non-planar surfaces, such as cars or airplanes; or electronic scanning of the main beam by changing the phase of the exciting currents. On the drawbacks, arrays require more complex feeding systems for the smaller antennas than a single element; and coupling among the different elements appears making it more difficult to adjust the feeding signals for each element. According to the spatial distribution of the elements, different characteristics can be obtained:



Figure 2-31: Linear slotted array antenna

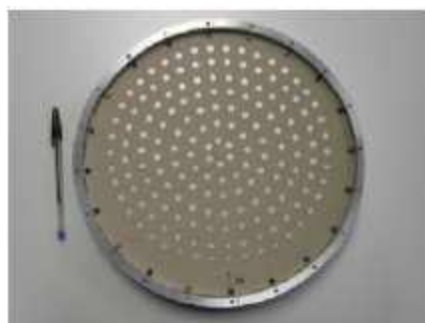


Figure 2-32: Planar slotted array antenna



Figure 2-33: Conformal slotted array antenna

2. State of the Art

An array is defined by certain parameters: position vector \vec{r}_i , feeding currents I_i and the radiation pattern of the unitary element in the coordinate center $\vec{E}_e(\theta, \phi)$:

$$\vec{E}_i(\theta, \phi) = \vec{E}_e(\theta, \phi) \frac{I_i}{I_o} e^{jk_0 \vec{r}_i \cdot \hat{r}} \quad (2.26)$$

Therefore, the total radiated field by the array will be the summation of the radiated fields of each individual element calculated separately:

$$\vec{E}_A(\theta, \phi) = \sum_i \vec{E}_e(\theta, \phi) = \vec{E}_e(\theta, \phi) \sum_{i=1}^N A_i e^{jk_0 \vec{r}_i \cdot \hat{r}} = \vec{E}_e(\theta, \phi) F_A(\theta, \phi) \quad (2.27)$$

Where $F_A(\theta, \phi)$ is known as the *Array Factor*.

The polarization of the radiated field depends only on the unitary element, and in large arrays the array factor varies faster in phase than the radiation pattern of the element, so the radiation pattern of the array can be approximated by $F_A(\theta, \phi)$.

If the radiation pattern must be very directive, the electromagnetic fields need to constructively interfere in the desired propagation direction. This can be achieved with the appropriate adjustment of some parameters, which will then characterize the different types of arrays:

- Geometric position of the elements in the array.
- Relative position of the elements in the array.
- Feeding amplitude of each element.
- Feeding phase of each element.
- Radiation pattern of the radiant element.

2.3.1 Linear Arrays

In linear arrays the elements are positioned along a straight line. Depending on the distance between the elements, two kinds of linear arrays can be distinguished: equally spaced and non-equally spaced.

The equally spaced linear array represents the simplest configuration, as the ' N ' elements are arranged along the z axis and each one separated a distance ' d ' from the adjacent ones.

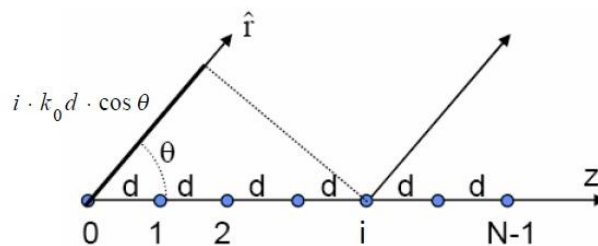


Figure 2-34: Linear array of N elements equally separated a distance d

2. State of the Art

In this case, the array factor of the linear array is defined as follows:

$$\left. \begin{aligned} \vec{r}_i = i \cdot d \cdot \hat{z} \rightarrow \hat{z} \cdot \vec{r}_i = i \cdot d \cdot \cos\theta \\ A_i = a_i \cdot e^{j\alpha_i} \end{aligned} \right\} F_A(\theta, \phi) = \sum_{i=0}^{N-1} A_i \cdot e^{j \cdot k_0 \cdot r \cdot \vec{r}_i} = \sum_{i=0}^{N-1} a_i \cdot e^{j(i \cdot k_0 \cdot d \cdot \cos\theta + \alpha_i)} \quad (2.28)$$

The most commonly used excitation distributions for linear arrays are the following:

- Progressive phase: $A_i = a_i \cdot e^{j(i \cdot \alpha)}$
- Uniformly excited in amplitude and phase: $A_i = 1 \quad \forall i$
- Uniformly excited in amplitude and progressive phase: $A_i = e^{j(i \cdot \alpha)}$
- Symmetric amplitude and decreasing from the center to the edges.

2.3.2 Planar Arrays

Planar arrays have the elements disposed in a rectangular grid of $M \times N$ elements arranged in plane XY . In comparison to linear arrays, planar arrays are more versatile as radiation patterns that aim in any direction can be obtained. Most of the times, elements are separated a fixed distance d_x in X axis and a fixed distance d_y in Y axis. The array factor of a planar array is:

$$F_A(\theta, \phi) = \sum_{m=1}^{M-1} \sum_{n=1}^{N-1} A_{mn} \cdot e^{j \cdot k_0 \cdot \vec{r} \cdot \vec{r}_{mn}} = \sum_{m=1}^{M-1} \sum_{n=1}^{N-1} A_{mn} \cdot e^{j \cdot m \cdot k_0 \cdot d_x \cdot \sin\theta \cdot \cos\phi} \cdot e^{j \cdot n \cdot k_0 \cdot d_y \cdot \sin\theta \cdot \sin\phi} \quad (2.29)$$

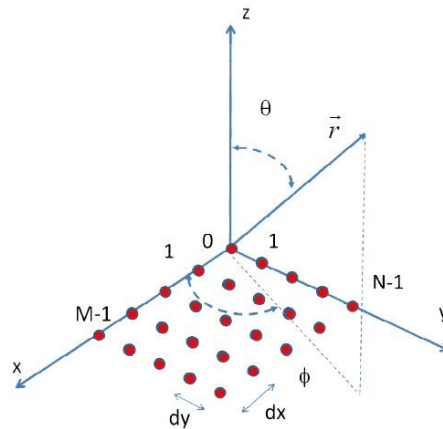


Figure 2-35: $M \times N$ elements distribution in a planar array

2.3.3 Phased Arrays

When feeding a linear or planar array with uniform amplitudes, the radiation pattern must be controlled and adjusted with the phase of the elements. If the progressive phase is varied in a linear array, it is possible to sweep a whole plane ϕ , whereas in a planar array varying α_x and α_y result in a complete scan of space. This kind of arrays are known as *phased arrays* or *scanning arrays*.

2. State of the Art

In these cases, the array factor can be seen as a linear array in direction x , whose unitary element is the array factor in y (or vice versa). In both cases, the array factors F_{Ax} and F_{Ay} are designed independently as follows:

$$\left. \begin{aligned} A_{mn} &= a_m \cdot e^{jm\alpha_x} \cdot a_n \cdot e^{jn\alpha_y} \\ \psi_x &= k_0 \cdot d_x \cdot \sin\theta \cdot \cos\phi + \alpha_x \\ \psi_y &= k_0 \cdot d_y \cdot \sin\theta \cdot \sin\phi + \alpha_y \end{aligned} \right\} F_A(\psi_x, \psi_y) = \sum_{m=0}^{M-1} a_m \cdot e^{j\cdot m \cdot \psi_x} \sum_{n=0}^{N-1} a_n \cdot e^{j\cdot n \cdot \psi_y} = F_{Ax}(\psi_x) F_{Ay}(\psi_y) \quad (2.30)$$

2.4 Theory of Waveguides

A waveguide is a physical element with the ability to propagate electromagnetic waves by confining them inside its structure. Transmitting through a waveguide reduces the energy losses caused by dissipation, making them very useful for high frequency applications such as those of microwave spectrum range. A waveguide consists of a single closed conductor and a dielectric inside it.

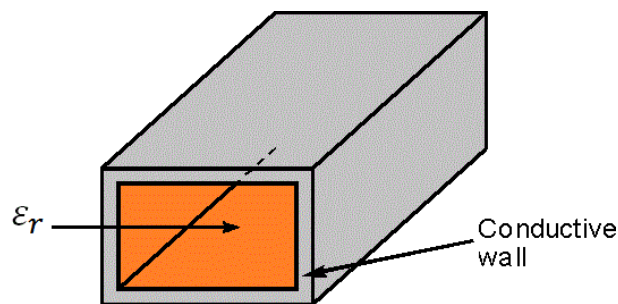


Figure 2-36: Rectangular waveguide filled with dielectric

Although many microwave systems have migrated to other technologies with easier implantation such as planar transmission lines (microstrip lines or striplines), there is still need of waveguides in high-power applications, millimeter wave systems or precision test applications.

2.4.1 Propagation modes

There are different modes which propagate along a transmission media, such as waveguides. From the general solutions to Maxwell's equations as described in [4] and [5], the different modes can be classified depending on their electric and magnetic field components.

- Transverse electromagnetic (TEM): Both electric and magnetic longitudinal field components are null ($E_z = H_z = 0$).
- Transverse electric (TE): Characterized for having a null electric longitudinal field component ($E_z = 0$).
- Transverse magnetic (TM): Characterized for having a null magnetic longitudinal field component ($H_z = 0$).
- Hybrid modes: There are no null components in the electric or magnetic field.

In waveguides there is only one conductor, closed and continuous, so only TE and TM modes can be propagated in the structure. TEM modes propagate in media with two

2. State of the Art

differentiated conductors, such as dielectric substrates with two metallic layers; and hybrid modes appear mainly in optic fiber.

Modes propagate in a waveguide if the cutoff frequency of the mode is lower to the frequency at which the waveguide operates. The first mode that propagates in the waveguide is called *fundamental mode*. Modes with a higher cutoff frequency than the waveguide's are known as *evanescent modes*, and they attenuate so quickly inside the waveguide that they are not considered to have propagated. The first mode that it is not propagated in the waveguide is called *superior mode*. According to the number of modes propagated in the waveguide, they can be classified as follows:

- Monomode: Only one mode propagates.
- Multimode: Several modes propagate through the waveguide.

In waveguides there is an important parameter called monomode bandwidth ($BW_{monomode}$). It defines the range of frequencies where the waveguide propagates only one mode, i.e. the lower frequency would be the cutoff frequency of the fundamental mode and the higher frequency of the range the cutoff frequency of the superior mode.

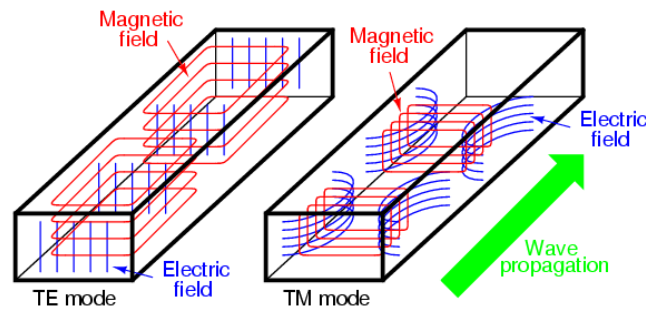


Figure 2-37: TE and TM field lines in rectangular waveguide

2.4.2 Waveguide Types

Since waveguides are only composed of a closed conductor and a dielectric in its interior, multiple designs and shapes can form a waveguide. It is possible to find elliptical or triangular waveguides, as well as with arbitrary shapes. However, the most commonly used are the rectangular and the circular waveguide. A complete mathematical analysis and electromagnetic concepts are thoroughly explained in [4].

2.4.2.1 Rectangular waveguide

In these waveguides the standard convention is to have the longest side of the waveguide along the x -axis, so that $a > b$.

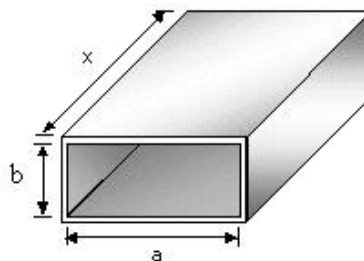


Figure 2-38: Rectangular waveguide

2. State of the Art

The rectangular waveguide can propagate TE and TM modes, but not TEM waves as it has been stated before. The cutoff frequencies of these modes are calculated according to the following expression:

$$f_{c_{mn}} = \frac{c}{2} \sqrt{\left(\frac{m}{a}\right)^2 + \left(\frac{n}{b}\right)^2}; \text{ where } c = \frac{c_0}{\sqrt{\epsilon_r}} \quad (2.31)$$

$$\text{for: } \begin{cases} TE_{mn}: m, n \geq 0 \\ TM_{mn}: m, n \geq 1 \end{cases}$$

The wavelength expression for each propagated mode in the waveguide is the following one:

$$\lambda_{g_{mn}} = \frac{\lambda}{\sqrt{1 - \left(\frac{f_{c_{mn}}}{f_0}\right)^2}}; \text{ where } \lambda = \frac{\lambda_0}{\sqrt{\epsilon_r}} \quad (2.32)$$

Therefore, at a given operating frequency f , only those modes which satisfy $f_c < f$ will propagate, an equivalently $\lambda_g > \lambda$.

Mode representation:

Attenuation due to dielectric and conductor losses varies with frequency. In the following figures it is shown the attenuation behavior (dB/m) versus frequency for a rectangular waveguide, where $a > b$ and the fundamental mode is the TE_{10} . Also, a brief resume of some of the electric and magnetic fields for some modes.

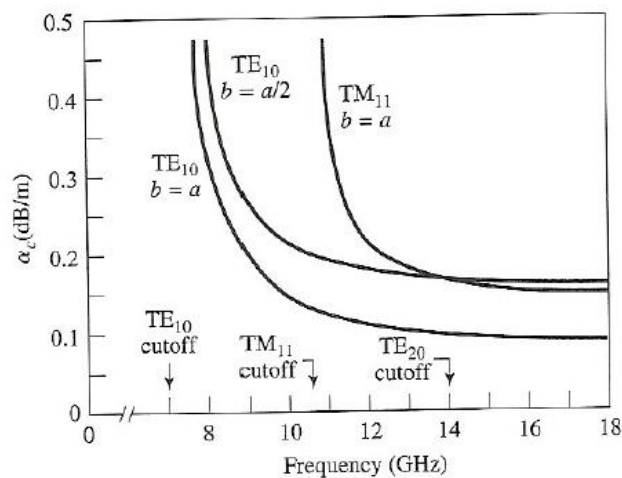


Figure 2-39: Attenuation of various modes in a rectangular brass waveguide with $a = 2$ cm.

2. State of the Art

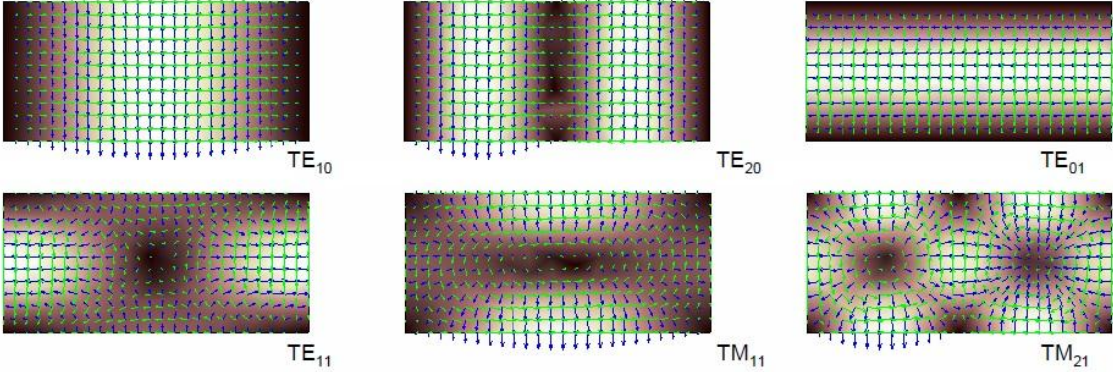


Figure 2-40: TE and TM modes field lines of the first propagated modes in a rectangular waveguide

2.4.2.2 Circular waveguide

A hollow metal tube (filled or not with dielectric) with a circular cross section can also support TE and TM modes. In the next figure it is represented the schematic diagram of a circular waveguide:

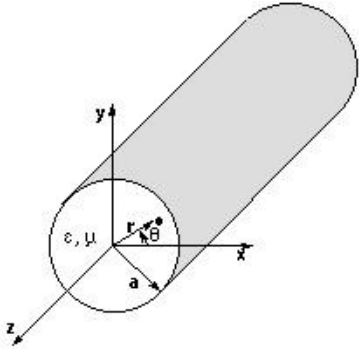


Figure 2-41: Circular waveguide

The only dimension which differentiates one circular waveguide from another is the radius 'a' of the cross section. The cutoff frequencies of the circular waveguide modes can be calculated from the following expressions:

$$TE \text{ modes: } f_{c_{mn}} = \frac{p_{mn}}{2\pi a \sqrt{\mu\epsilon}} \quad (2.33)$$

$$TM \text{ modes: } f_{c_{mn}} = \frac{p'_{mn}}{2\pi a \sqrt{\mu\epsilon}} \quad (2.34)$$

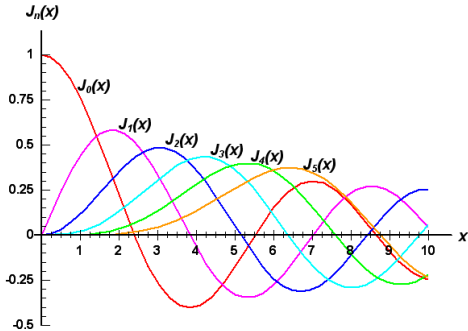


Figure 2-42: Bessel functions of first kind

Where p_{nm} and p'_{nm} are the root solutions to the Bessel functions.

2. State of the Art

Mode representation:

In the same way as before, the next figure illustrates the attenuation of the waveguide (dB/m) versus frequency for various modes of propagation.

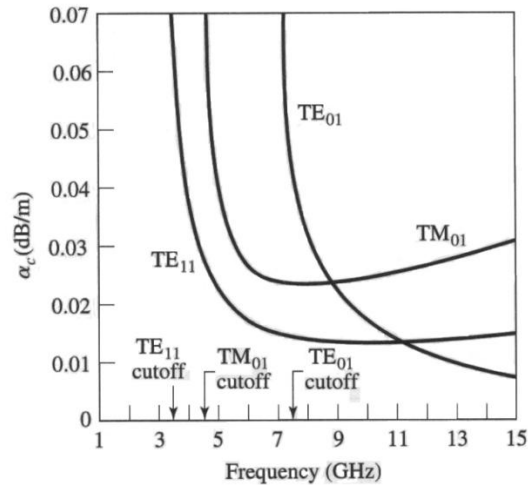


Figure 2-43: Attenuation of various modes in a circular waveguide with $a = 2.54$ cm.

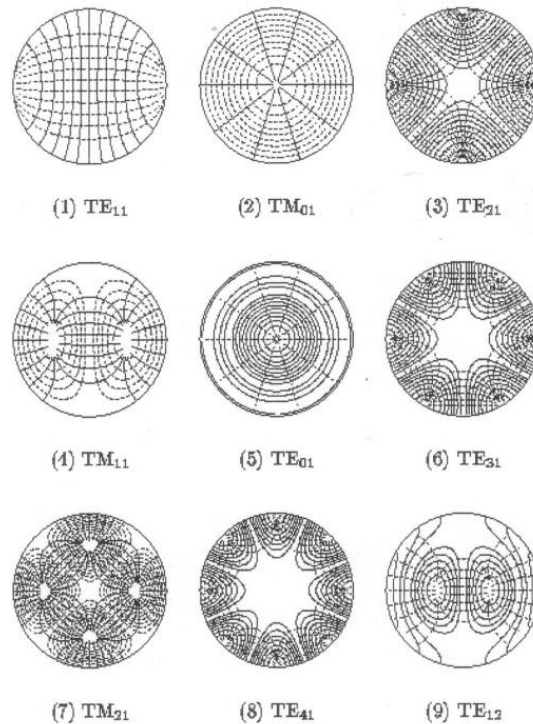


Figure 2-44: Field lines of first modes propagated in circular waveguides

2.4.3 Feeding Systems

The most common way of feeding a waveguide is using a coaxial connector inserted perpendicularly in any conductor wall of the waveguide. The exterior conductor of the connector is connected to the exterior part of the waveguide's conductor, while the inner conductor of the connector is used as a monopole antenna to excite a given mode in the waveguide.

2. State of the Art

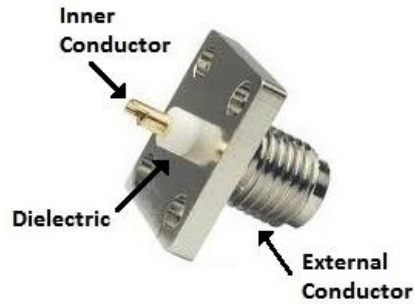


Figure 2-45: Chassis type SMA connector

The position and length of the inner conductor is very important to achieve the best matching at the working frequency f_0 . In the following image it is shown how the connector should be positioned to properly feed a waveguide:

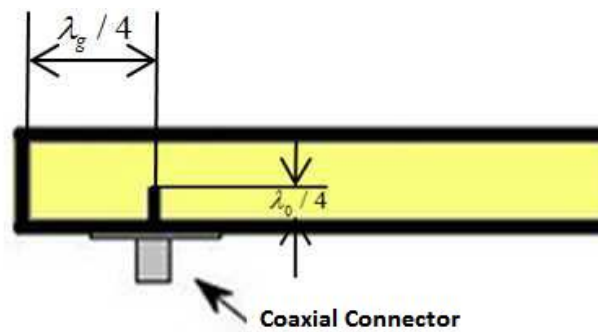


Figure 2-46: Positioning of coaxial connector in the waveguide

In first place, the inner conductor should be placed at a distance $\lambda_g/4$ from the end of the waveguide in the propagation direction axis z . This is important to avoid undesired reflection waves that would increase the reflection coefficient, and therefore the SWR of the feeding system. Considering the length of the inner conductor, it should be approximately $\lambda_0/4$ (typically a little bit less). However, as the inner conductor is located inside the waveguide, it will propagate at λ_g associated to λ_0 .

2.5 Microstrip Line Theory

Microstrip lines are one of the most popular types of planar transmission lines, as they are easily fabricated and integrated in other passive or active microwave circuits. The microstrip line consists of a conductor of width W printed on a thin, grounded dielectric substrate. The geometry of a microstrip line is presented in the next figures:

2. State of the Art

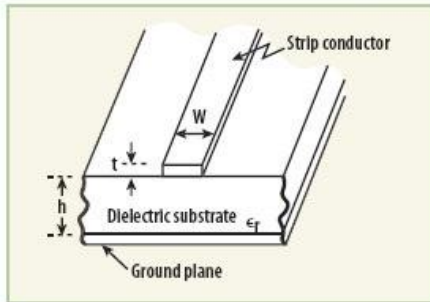


Figure 2-47: General geometry of a microstrip line

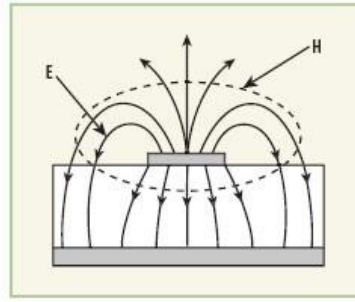


Figure 2-48: Field propagation in a microstrip line

Microstrip technology is much cheaper than metallic waveguide technology, as it is fabricated in low cost printed circuit substrates (PCB). Nevertheless, microstrip lines cannot handle as much power as waveguides do; and they usually have more losses associated to the structure.

Since microstrip lines have two differentiated conductors, TE and TM cannot be propagated through this structure. Moreover, unlike stripline, microstrip's field lines are not fully confined within a dielectric region. Some fraction of this field lines are radiated in the air region above the microstrip. This is the reason why microstrip lines do not propagate pure TEM modes, and instead it propagates quasi-TEM modes.

The same way the presence of air and dielectric influences the propagation of quasi-TEM modes, it also affects the dielectric constant of the whole structure. Now the effective dielectric constant $\epsilon_{r_{eff}}$ is calculated as follows:

$$\epsilon_{r_{eff}} = \begin{cases} \frac{\epsilon_r + 1}{2} + \frac{\epsilon_r - 1}{2} \cdot \left[\left(1 + \frac{12h}{W} \right)^{-0.5} + 0.04 \left(1 - \frac{W}{h} \right)^2 \right]; & \frac{W}{h} < 1 \\ \frac{\epsilon_r + 1}{2} + \frac{\epsilon_r - 1}{2} \cdot \left(1 + \frac{12h}{W} \right)^{-0.5}; & \frac{W}{h} > 1 \end{cases} \quad (2.35)$$

Thus, from the result above the wavelength of the microstrip is:

$$\lambda_{\mu strip} = \frac{\lambda_0}{\sqrt{\epsilon_{r_{eff}}}} \quad (2.36)$$

2.5.1 Microstrip Feeding

Microstrip lines are most commonly fed with coaxial connector, and the feeding can be done with the vertical insertion of the connector in the substrate or horizontal soldering.

- Vertical coaxial probe: This connection method is very similar to the one applied in waveguides. The external conductor of the connector is connected to the ground plane, while the inner conductor is inserted in the substrate until it reaches the microstrip line in the top conductor layer.

2. State of the Art

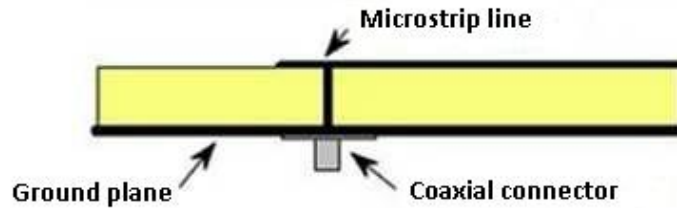


Figure 2-49: Vertical coaxial probe feeding of microstrip line

In this case the positioning of the inner connector is also very important. Its location outer or inner in the microstrip line will determine the entrance impedance, and consequently how well matched is the circuit at that point.

- Horizontal coaxial: To feed the microstrip line with a horizontal coaxial, the external conductor of the connector must be connected to the ground plane, and the inner conductor placed over the microstrip line for the later soldering. This method is very simple, although the inner conductor is unprotected and this can lead to more losses and unexpected radiation at high frequency applications.

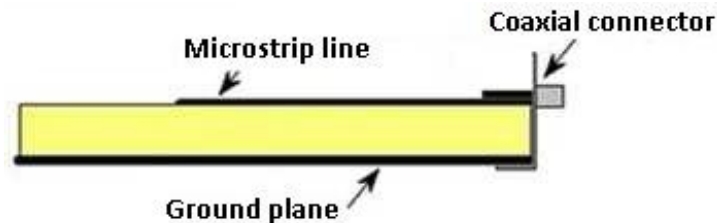


Figure 2-50: Horizontal coaxial connector feeding a microstrip line

2.6 SIW Theory

In the late 1990s appeared a new technology known as SIW (Substrate Integrated Waveguide). This technology integrates the structure of a waveguide in a dielectric substrate, using printed technology as in microstrip lines.

Conventional waveguides are built with metal bars, and result in heavy devices making it difficult to integrate in microwave circuits. However, SIW combines both the advantages of propagation and losses characteristic of waveguides and the low weight and cost of printed substrate technologies. This way some of the disadvantages of the waveguides are eliminated and it is easier to adapt these structures in modern microwave circuits.

SIW consists of drilled holes in the substrate, which are later metallized and join the lower ground plane with the upper metallic plane, confining the signals within the structure. In the following figure it is illustrated the structure of a SIW.

2. State of the Art

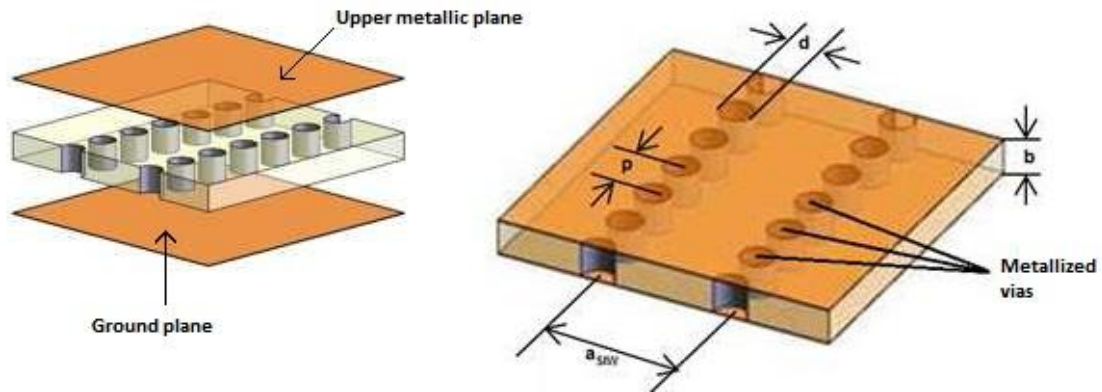


Figure 2-51: Substrate Integrated Waveguide with its characteristic parameters

The via holes have two important parameters of design: the diameter ' d ' and the period of the vias ' p ' or distance between two consecutive holes. These two parameters need to fulfill some restrictions, which have been thoroughly studied in [6]; in order to not incur in too much leakage losses or undesired waveguide behavior.

In relation to the other two parameters shown in Figure 2-51, ' a_{SIW} ' and ' b ', there are also some considerations to take into account. The height b is most of the times restricted to the substrate characteristics (substrates are often fabricated under certain standard dimensions); and will only be adjustable by stacking different substrates. On the contrary, parameter a_{SIW} follows some rules to convert the width of the conventional waveguide into the required width of the equivalent SIW; as this dimension cannot be directly applied to it. A very extensive study is described in [7], where the final formulation establishes the relation between both widths with a 1% error as follows:

$$\xi_1 = 1.0198 + \frac{0.3465}{\frac{a}{p} - 1.0684} \quad (2.37)$$

$$\xi_2 = -0.1183 + \frac{1.2729}{\frac{a}{p} - 1.2010} \quad (2.39)$$

$$\xi_3 = 1.0082 - \frac{0.9163}{\frac{a}{p} + 0.2152} \quad (2.40)$$

$$\bar{a} = \xi_1 + \frac{\xi_2}{\frac{p}{d} + \frac{(\xi_1 + \xi_2 - \xi_3)}{(\xi_3 - \xi_1)}} \quad (2.38)$$

$$a_{RWG} = a_{SIW} \cdot \bar{a} \quad (2.41)$$

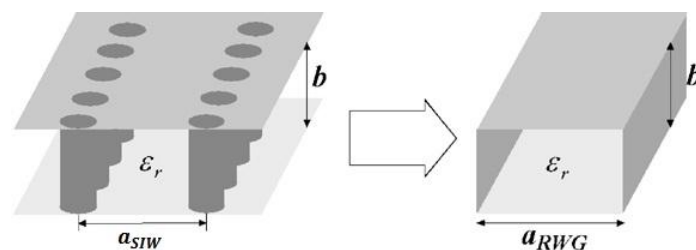


Figure 2-52: Width's equivalence of SIW and ordinary waveguide

2. State of the Art

Considering all these requirements, it is important to note that SIWs were originally conceived for high frequency designs. The reason for this is that at lower frequencies the SIW's dimensions would be very similar to the conventional waveguide, so they would have the same disadvantages as the ordinary waveguides.

2.6.1 SIW Feeding System

SIW can be considered as a particular case of waveguide, so all of the feeding methods mentioned in 2.4.3 can be also applied to it. However, feeding the SIW with a microstrip line is particularly useful as they both share printed technology fabrication.

- Vertical coaxial probe: The same way as it was reported in 2.4.3, SIWs can be fed with a vertical coaxial connector. The external connector is soldered to the lower ground plane, and the inner connector is inserted through the dielectric. The distance from the short circuit of the SIW to the inner connector must be $\lambda_g/4$, in order to avoid undesired reflections.

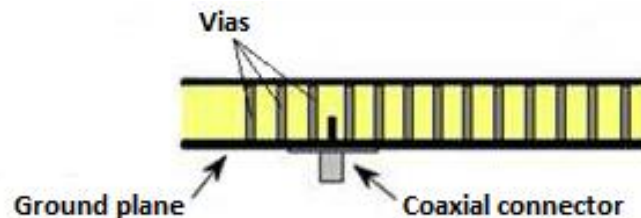


Figure 2-53: Vertical coaxial probe feeding of a SIW

- Microstrip line: Microstrip lines and SIW are fabricated with printed circuit technology, so it is reasonable to try to construct the feeding system of a SIW with microstrip line, and connect both structures with a taper. This method is well studied in [8].

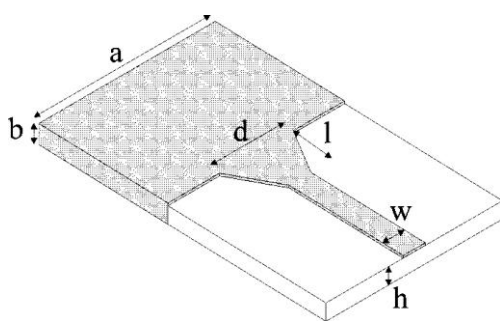


Figure 2-54: Microstrip transition to SIW in the same substrate

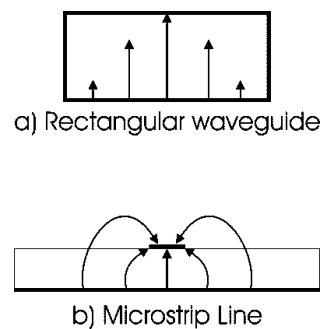


Figure 2-55: Mode propagation in rectangular waveguide and in microstrip line

From Figure 2-55, it can be seen that microstrip line is well suited for exciting the waveguide, and the taper structure will transform the quasi-TEM of the microstrip line into the TE₁₀ fundamental mode of the waveguide; as both electric fields are approximately oriented in the same direction. From the classical waveguide theory, the width of the waveguide is designed to obtain the wanted fundamental mode cutoff frequency. Depending on the substrate's dielectric constant and thickness, the impedance of the microstrip line will be set

2. State of the Art

by adjusting its width, in order to guarantee signal transmission and minimize radiation from the line. The tapered section will be designed so both structures would be matched as well as possible, adjusting the length l and the width d of the taper.

2.7 Design and Simulation Tools



2.7.1 CST Microwave Studio

CST Microwave Studio is a specialized tool for electromagnetic 3D simulations with high frequency components. The version used in group RFCAS at U.A.M. is 2010, and this software has been the main design tool of this PFC.

The program provides a fast and complete analysis for several devices such as antennas, filters, couplers and multilayer structures; all of them designed by 3D drawing. In addition, CST offers users great flexibility through a wide range of different applications and solver technologies. It also enables to import and export CAD files, which is something particularly useful to save time in the construction procedure of the prototypes and final designs.

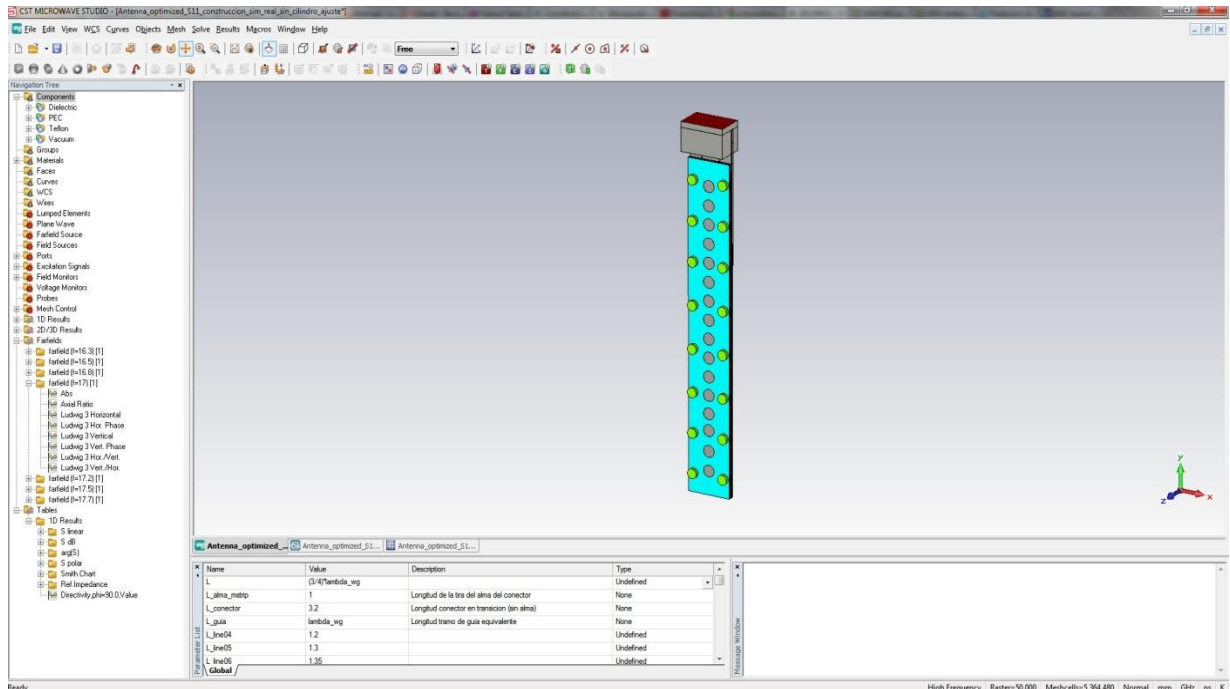


Figure 2-56: CST user friendly working interface

2. State of the Art

2.7.2 Advanced Design Systems (ADS)



Advanced Design Systems (ADS) is a program for circuit and electromagnetic simulation very useful for the vast majority of telecommunications devices, such as amplifiers, transmission lines, resonators, oscillators, etc. This software was created by Agilent Technologies and the version available and used for this PFC at U.A.M. is the 2008.

The key factor of this software is the great precision achieved in the simulations thanks to extensive libraries. Moreover, apart from working with circuits and the results from the simulations, it is possible to implement layouts and see how the physical circuit will be. ADS also enables to import and export files such as CAD or TOUCHSTONE, which are indispensable for the generation of Gerber files (kind of files required for the printed circuit fabrication machine).

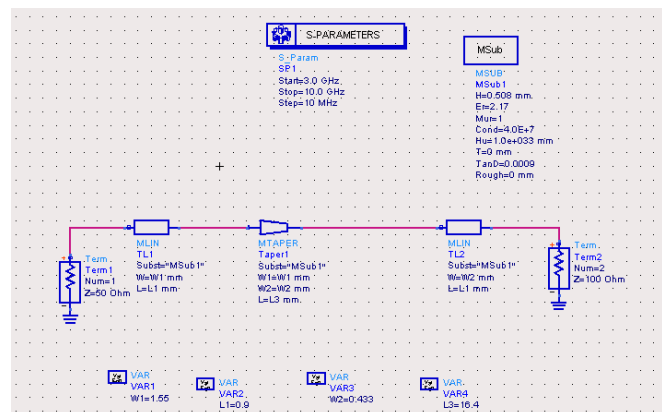


Figure 2-57: Schematic working environment in ADS

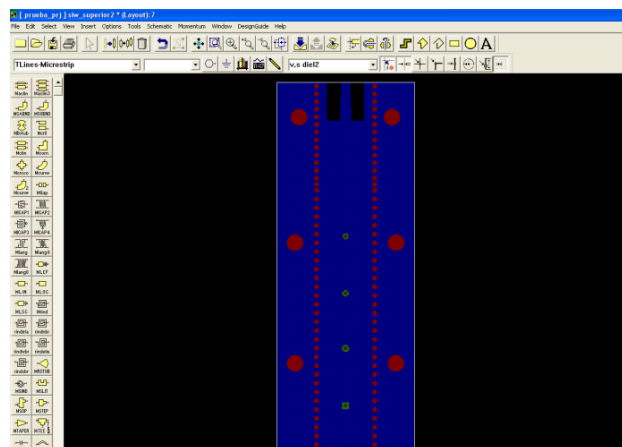


Figure 2-58: Layout working environment in ADS

2.7.3 Ensemble 1D Array Synthesis

Software Ensemble 1D Array Synthesis is a very simple program that provides a very fast approximation of linear array modeling.

2. State of the Art

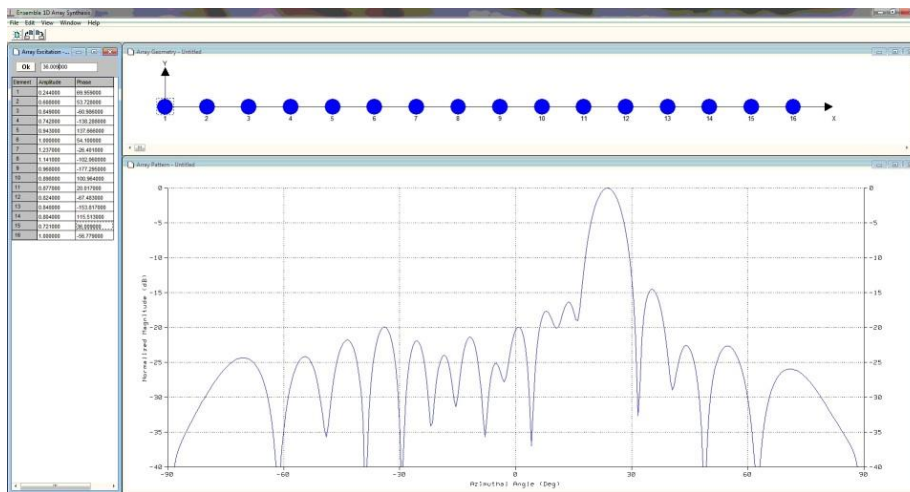


Figure 2-59: Working environment of Ensemble 1D Array Synthesis

This program shows the normalized radiation pattern of the array, given the number of elements that forms the array and the amplitude and phase of each one, according to the desired feeding distribution.

2.7.4 Ansoft Ensemble 8.0

Although Ansoft Ensemble 8.0 is an old version of newer developed electromagnetic simulation software, it has become very handy to run short simulation which would have lasted much more time in other programs like CST Microwave Studio.

Providing that this software assumes some approximations to shorten the simulation time, the results obtained are not very accurate. However, it was used to carry out the first steps of the double patch structure design, whose results were later taken to CST Microwave Studio for further and meticulous design. In spite of not being very user friendly and the results not so reliable, the program had some usefulness for this PFC in the radiant element design.

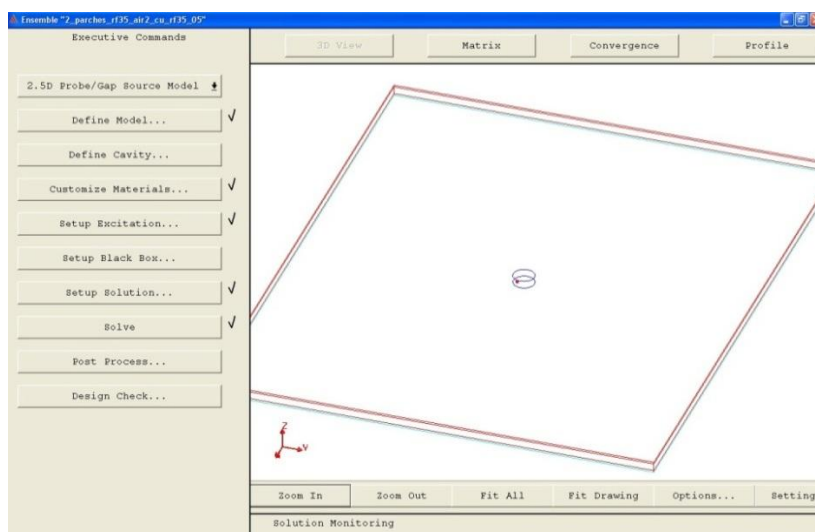


Figure 2-60: Ansoft Ensemble 8.0 working interface

3 DESIGN OF ANTENNAS

3.1 Introduction

In this chapter, the model of antenna developed in this Career Final Project (CFP) will be explained. In first place, a brief description of the different steps required to design and the general structure of the antenna will be introduced. Afterwards, there will be an approach of the design of two of the main parts of the antenna: the feeding linear array and the radiant element. Both parts will be described in detail, leaving their integration in the complete antenna to be explained in further chapters.

3.2 General Structure

The design carried out in this CFP will consist of a linear array of patches over a waveguide constructed on SIW technology with linear polarization. The proposed antenna works in the frequency range from 16.3 GHz to 17.7 GHz, belonging to the Ku frequency band as stated in Table 2-2. The SIW provides the feeding system to the patches array through a series of coupling lines, which transfer the signal power to each one of the radiant elements. The radiant elements have been designed separately from the SIW, and later integrated in the whole structure for the final adjustment. The direction of propagation of the progressive wave is along Y axis, and the measurements of the radiation pattern will be made in the plane YZ or $\phi=90^\circ$.

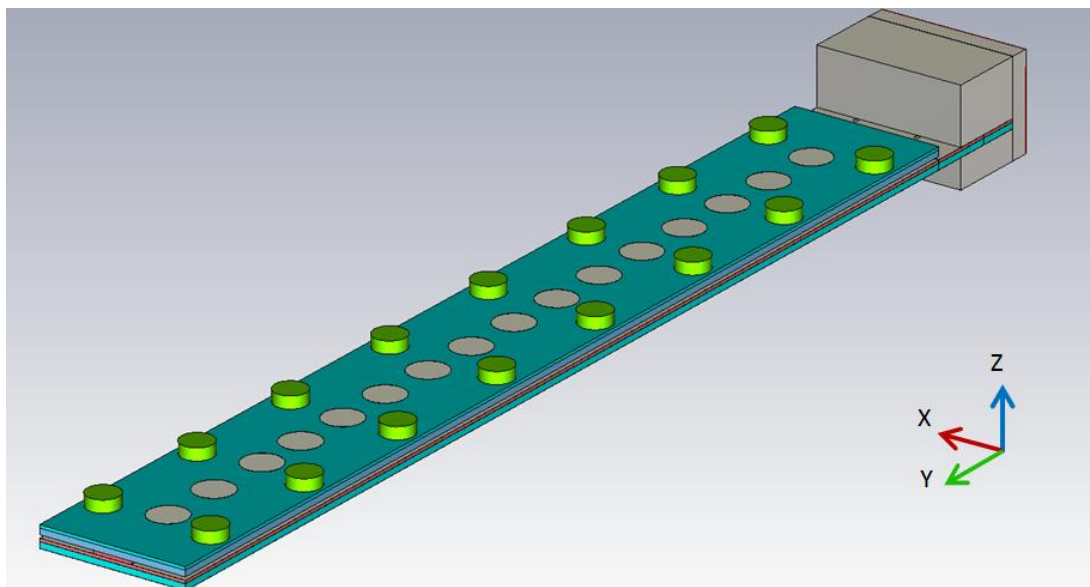


Figure 3-1: Appearance of an antenna designed in CST working environment

3. Design of Antennas

The procedure followed to design the antenna records the following steps:

- Characterization of the waveguide which supports the patches' feeding system.
- Design of the SIW structure and study of the available coupling for different dielectric configurations.
- Design of the coupling lines for each element from the results obtained above.
- Design of radiant elements, completely separated from the SIW array.
- Integration of the radiant elements in the SIW structure.
- Study of coupling model that will compensate the undesired coupling effects among the elements of the linear array.

Later on, several transitions have been designed to feed the antenna, most of them based on previous works realized in group RFCAS. It was of the outmost importance to achieve the best possible matching at the entrance with the transition designed, because in other case the later measurements would not give the real parameters of the antenna.

Substrates Configuration

As one of this project's goals was (is) to compare the antenna with another very similar previously designed in group RFCAS, the substrate election was made according to the thickness chosen in that previous CFP. The final set of substrates used in this CFP is the following:

- **TLY-5A 0400 CH/CH**: Substrate of 1.016 mm. of thickness, covered with a 0.018 mm. copper layer both up and down. The dielectric constant of this substrate is $\epsilon_r=2.17$ and its loss tangent is approximately $\tan\delta=0.001$ at the working frequency 17 GHz. [9]. It was used for the lower part of the SIW.
- **TLY-5A 0200 CH/CH**: Substrate of 0.508 mm of thickness and the same characteristics as the one mentioned immediately above. It was the substrate used for the upper patches' layer.
- **RF-35 0200 CH/CH**: Substrate of 0.508 mm of thickness and two copper layers of 0.018 mm. like the substrate from series TLY-5A. The dielectric constant of this substrate is $\epsilon_r=3.5$ and its loss tangent is approximately $\tan\delta=0.0029$ at 17 GHz. [10]. It was used for the upper part of the SIW and the lower patches' layer.

3.3 Waveguide's Characterization

When designing waveguide structures, it is necessary to settle its parameters according to the waveguide's working frequency band. The design parameters available in waveguides are width " a ", height " b " and the inside dielectric with dielectric constant " ϵ_r ". In rectangular waveguides, width is bigger than height ($a > b$), so the fundamental mode propagated in the waveguide is TE_{10} . In the SIWs designed in this project, height b is much lower than width a . If it were not this way, the fundamental mode propagated would be TE_{01} .

When a waveguide is filled with a uniform dielectric, the coupling line structure does not work as it should. With the introduction of two different dielectric constants, the propagated fundamental mode changes from a pure TE_{10} to the so called **hybrid modes**.

3. Design of Antennas

3.3.1 Hybrid Modes

For some waveguide configurations, such as the concerning SIW, where waveguides are partially filled or combine different materials; TE^z or TM^z modes cannot satisfy the boundary conditions of the structure. Therefore, modes propagated in these structures (or solutions of the wave equation) are combinations of TE^z and TM^z . These modes are referred to as **hybrid modes** or **longitudinal section magnetic (LSM)** modes. In the particular case of Figure 3-2, which is the same as the SIW, the modes are LSM to a direction that is perpendicular to the interface. Thus, the solutions are modes TE^y or LSM^y .

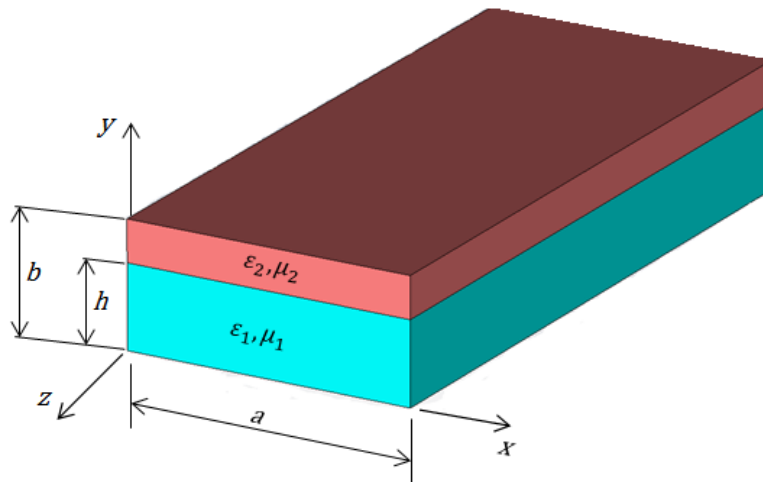


Figure 3-2: Geometry of a waveguide filled with two different substrates

LSM^y modes, just as for other modes, can be derived from the usual field expressions as seen in [11]. However, it is different the direction of propagation of the real mode propagated in the SIW (which is along z axis) to the axial component of the field of the LSM^y mode (which is y , perpendicular to the separation interface of the dielectrics). With this hybrid mode, the E_z field component is not null. Thanks to this, inside the SIW there is a double coupling action: the via couples power from the E_y field component (similar to the regular TE_{10} mode), whereas the lines disposed longitudinally along the SIW couple the E_z field component generated by the LSM^y mode. All the power is transmitted to the double patch structure by the vias. As a result of this, the cutoff frequency of the LSM^y mode is within the range given by ϵ_{r_1} and ϵ_{r_2} :

$$\frac{1}{2a\sqrt{\mu_2\epsilon_{r_2}}} \leq f_{c_{LSM10}} \leq \frac{1}{2a\sqrt{\mu_1\epsilon_{r_1}}} \quad (3.1)$$

This will be a value between the two cutoff frequencies determined by the different dielectric constants of each substrate.

3.3.1.1 Transverse Resonance Method (TRM)

In order to find the propagation constant in composite waveguide structures, the **transverse resonance method (TRM)** is used [11]. By using this method, the cross section of a waveguide is represented as a two-dimensional transmission line system. The fields in this structure must satisfy the transverse electric equation; and it will yield to expressions for the propagation constants of the waveguide.

3. Design of Antennas

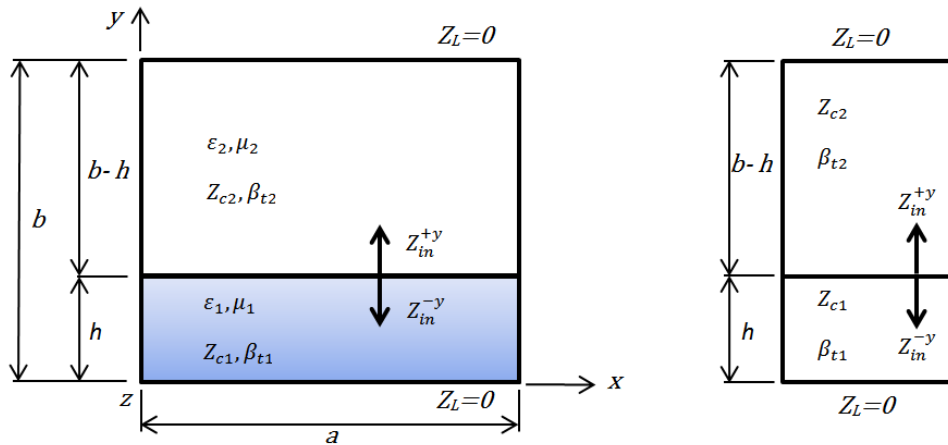


Figure 3-3: Cross section of a rectangular waveguide and transmission line equivalent for Transverse Resonance Method (TRM)

Regarding that each transmission line is considered shorted at its load, and each one with its characteristic impedance and propagation constant. From the procedure described in [11], the value of LSM_{10}^y mode cutoff frequency and the effective dielectric constant is found:

$$f_{c_{LSM_{10}^y}} = 9.419 \text{ GHz}$$

$$\epsilon_{r_{eff}} = 2.486$$

Once the effective dielectric constant is obtained, the propagation constant of the structure at 17 GHz can be calculated:

$$\beta_z = 467.33 \text{ (1/m)}$$

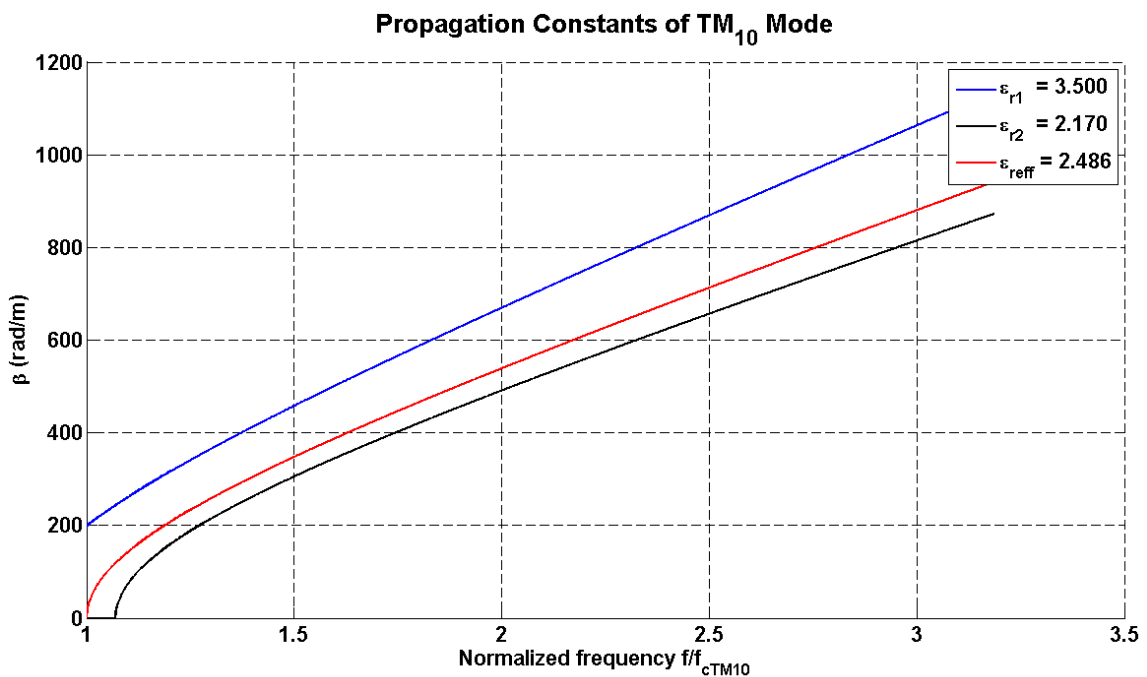


Figure 3-4: Propagation constant for different dielectric constants in the structure

3. Design of Antennas

In Figure 3-4 it is presented the propagation constants as if the structure were only filled with dielectric of $\epsilon_r = 3.5$, $\epsilon_r = 2.17$ or $\epsilon_{r_{eff}} = 2.486$, normalized at the cutoff frequency of the hybrid structure. It can be seen that the effective propagation constant and its cutoff frequency for mode LSM^y_{10} are between the other two.

3.3.2 Design Considerations

Due to its special configuration, the dielectric constant of the SIW structure has the contribution of both dielectrics involved in its configuration (RF-35 with $\epsilon_r=3.5$ and TLY-5A with $\epsilon_r=2.17$). For designing the dimensions and the cutoff frequency of the fundamental and superior mode, it can be considered that there is a waveguide full of dielectric with the effective dielectric constant calculated in the previous subsection for the configuration with two substrates. Moreover, the LSM^y mode generated can be approximated by a TE_{10} mode propagated in a waveguide with a dielectric with $\epsilon_{r_{eff}}$.

In the case of $b > a$, from (reference to equation), the cutoff frequency of the fundamental mode would be:

$$f_{c_{TE_{01}}} = \frac{c_0}{2\sqrt{\epsilon_r}} \sqrt{\left(\frac{1}{b}\right)^2} = \frac{c_0}{2 \cdot b \sqrt{\epsilon_{r_{eff}}}} = \frac{3 \cdot 10^{11}}{3.048 \sqrt{\epsilon_{r_{eff}}}} \Rightarrow f_{c_{TE_{01}}} = 62.43 \text{ GHz}$$

This cutoff frequency does not belong to the frequency range where the antenna is being designed (16.3 GHz – 17.7 GHz). Therefore, in these rectangular SIWs width "a" must be bigger than height "b" in order to propagate mode TE_{10} as the fundamental mode.

The choice of width "a" should be made so that the superior mode has a margin of at least 1 GHz over the cutoff frequency of the fundamental mode. This way it is guaranteed that the superior mode will be considerably attenuated; and so on the SIW will act as a monomode waveguide. Furthermore, as height "b" is significantly smaller than width "a", the superior mode of the SIW is TE_{20} . From (2.31):

$$f_{c_{TE_{10}}} = \frac{c_0}{2\sqrt{\epsilon_r}} \sqrt{\left(\frac{1}{a}\right)^2} = \frac{c_0}{2 \cdot a \sqrt{\epsilon_r}} \quad (3.2)$$

$$f_{c_{TE_{20}}} = \frac{c_0}{2\sqrt{\epsilon_r}} \sqrt{\left(\frac{2}{a}\right)^2} = \frac{c_0}{a \sqrt{\epsilon_r}} \quad (3.3)$$

To fulfill all these requirements, it has been chosen a width "a" of 10.1 mm. With this dimension and the equivalent dielectric constant of the SIW, the cutoff frequencies of the fundamental mode and the superior mode are:

$$f_{c_{TE_{10}}} = \frac{c_0}{2a \sqrt{\epsilon_{r_{eff}}}} = 9.42 \text{ GHz}$$

$$f_{c_{TE_{20}}} = \frac{c_0}{a \sqrt{\epsilon_{r_{eff}}}} = 18.84 \text{ GHz}$$

3. Design of Antennas

However, the cutoff frequencies of the next modes have to be checked to guarantee that mode TE₂₀ is the superior mode:

$$f_{cTE_{30}} = \frac{3c_0}{2a\sqrt{\epsilon_{r_{eff}}}} = 28.26 \text{ GHz} \qquad f_{cTE_{01}} = \frac{c_0}{2b\sqrt{\epsilon_{r_{eff}}}} = 62.43 \text{ GHz}$$

$$f_{c_{TM_{11}}^{TE_{11}}} = \frac{c_0}{2\sqrt{\epsilon_r}} \sqrt{\left(\frac{1}{a}\right)^2 + \left(\frac{1}{b}\right)^2} = 63.13 \text{ GHz}$$

Now it can be confirmed that for dimensions $a = 10.1 \text{ mm}$. and $b = 1.542 \text{ mm}$. (considering the air gap between both dielectrics), and $\epsilon_r=2.486$; the fundamental mode propagated is TE₁₀ and the superior mode is TE₂₀. It can be stated that the cutoff frequency of mode TE₁₀ is much lower than the start of the working frequency band, so the fundamental mode will be well defined inside the SIW. The modes chart of the SIW is the following one:

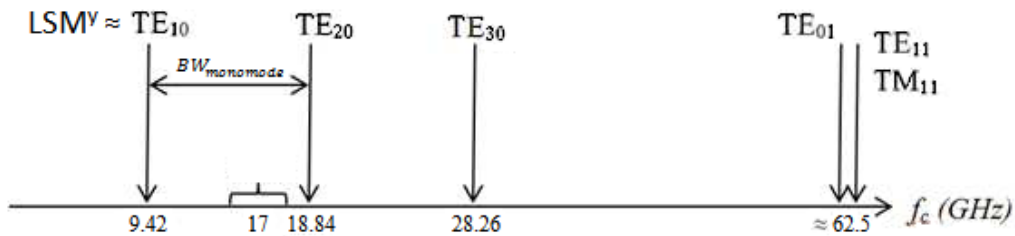


Figure 3-5: Modes chart of the designed SIW

The wavelength of the wave propagated in the waveguide, associated to the fundamental mode is:

$$\lambda_{gTE_{10}} = \frac{\lambda_0/\sqrt{\epsilon_{r_{eff}}}}{\sqrt{1 - \left(\frac{f_{cTE_{10}}}{f_0}\right)^2}} = 13.44 \text{ mm.}$$

Where f_0 and λ_0 are respectively the working frequency and wavelength at it, and $f_{cTE_{10}}$ the cutoff frequency of the fundamental mode.

3.4 SIW's Characterization

Once the waveguide is characterized by its dimensions and mode propagation, the equivalent SIW will be designed from the specifications described in the previous point. Given conventional waveguide width $a=10.1$, the equivalent SIW's width can be calculated from the formulas exposed in 2.6. Nevertheless, the diameter of the vias and the separation among them influences this calculation.

Choosing an appropriate diameter and separation depends on many factors. In this CFP there has been used vias with a diameter $d = 0.8 \text{ mm}$. and periodicity $p = 1.6 \text{ mm} = 2 \cdot d$. The first and main limiting factor for choosing these values is that, in the laboratory of printed

3. Design of Antennas

circuits at E.P.S. in U.A.M., there are only available three different kinds of rivets. The available external diameters of them are 0.6, 0.8 and 1.2 mm, whose data sheets can be consulted in [12]. These two parameters follow the design formulas described in [7], and offer a good characterization of the SIW while not over-placing too many vias in the structure. From the literature studied, these two values are similar to the ones most commonly used in SIW's designs. As there are not very strong restrictions about them, it is understood that the chosen values are as valid as the ones found in the different papers.

From the chosen values of waveguide's width, diameter of the vias and periodicity among them; and making use of (2.41):

$$a_{SIW} = 10.6 \text{ mm.}$$

This measurement is defined between centers of the vias that form the SIW. Consequently, there is a little less usable space than the value a_{SIW} calculated. The effective place left for internal designs in the SIW is $a_{SIW} - d = 9.8 \text{ mm}$. From now on, this parameter will be considered as $a_{SIW_{int}}$.

A summary table with all the important design values described in the last two subsections is presented as follows:

a (mm.)	10.1
b (mm.)	1.548
ϵ_r	2.57
$TLY - 5A \tan\delta$ ($f = 17 \text{ GHz}$)	0.0011
$RF - 35 \tan\delta$ ($f = 17 \text{ GHz}$)	0.0029
$f_{c_{TE_{10}}}$ (GHz)	9.35
$f_{c_{TE_{20}}}$ (GHz)	18.7
λ_g (mm.)	13.18
d (mm.)	0.8
p (mm.)	1.6
a_{SIW} (mm.)	10.6
$a_{SIW_{int}}$ (mm.)	9.8

Table 3-1: Summary table of SIW and equivalent waveguide parameters

3.5 Design of Linear Array

3.5.1 General Characteristics

The first step when designing a linear array is to decide what kind of array it is going to be used. As it was mentioned before, one of the objectives of this CFP is to compare this work with other CFPs previously made in group RFCAS. For this reason, it has been decided that the array would have **16 elements**.

Afterwards, a decision about the feeding distribution of the elements has to be made. The previous CFP's antenna was fed with a current that had a Taylor distribution of -26 dB with 2% of residual power (which is wasted and not radiated). However, it was necessary to check that it is possible to achieve the coupling coefficients required for each element given this

3. Design of Antennas

distribution. The Taylor distribution coefficients are presented in the following table and the formulation required for obtaining the coupling coefficients in dBs seen in [13], as well as the parameters defined:

$$|s_k| = \frac{P_{rad,k}}{P_{in,k}} = \frac{F_k^2(x_k)}{\frac{\sum_{i=1}^M F_i^2(x_i)}{1-t} - \sum_{i=1}^{k-1} F_i^2(x_i)} \quad (3.4)$$

$$s_{k(dB)} = 10 \cdot \log_{10}(s_k) \quad (3.5)$$

- s_k : Coupling coefficient of each ' k ' element of the array.
- $P_{rad,k}$: Power radiated by each ' k ' element of the array.
- $P_{in,k}$: Input individual power of each ' k ' element of the array.
- F_k : Feeding coefficient of each ' k ' element of the array.
- M : Number of elements in the array.
- t : Percentage of residual lost power not coupled in the antenna

Element (k)	Feeding Function (F_k)	Coupling Coefficient S_k (dB)
1	0.151021	-25.3061
2	0.278881	-19.9657
3	0.426329	-16.2351
4	0.581392	-13.4361
5	0.729932	-11.2583
6	0.857394	-9.5225
7	0.950702	-8.1112
8	1	-6.9433
9	1	-5.9626
10	0.950702	-5.1328
11	0.857394	-4.4392
12	0.729932	-3.9002
13	0.581392	-3.6044
14	0.426329	-3.8111
15	0.278881	-5.1632
16	0.151021	-8.9134

Table 3-2: Amplitude and coupling coefficients for a linear array of 16 elements with Taylor -26 dB distribution and 2% power loss

From the primary stages of design, it was proved that it was only possible to obtain some variation range of coupling when the difference between the dielectric constant of both substrates was significant. At first it was considered the option of using substrates of $\epsilon_r=3.5$ and $\epsilon_r=2.5$, or even just one type of substrate. However, the variation was very little and it was mandatory to change the configuration to a set of substrates with bigger difference of dielectric constants previously described in 3.2 and explained in 3.3.2.

With the substrates appropriately chosen, the next step was to check if the needed coupling coefficients could be obtained. After some simulations in CST, it was stated that reaching the highest values of coupling was reasonably easy with the coupling line structure (which will be thoroughly explained later in this chapter). An example of this behavior is shown in next figure:

3. Design of Antennas

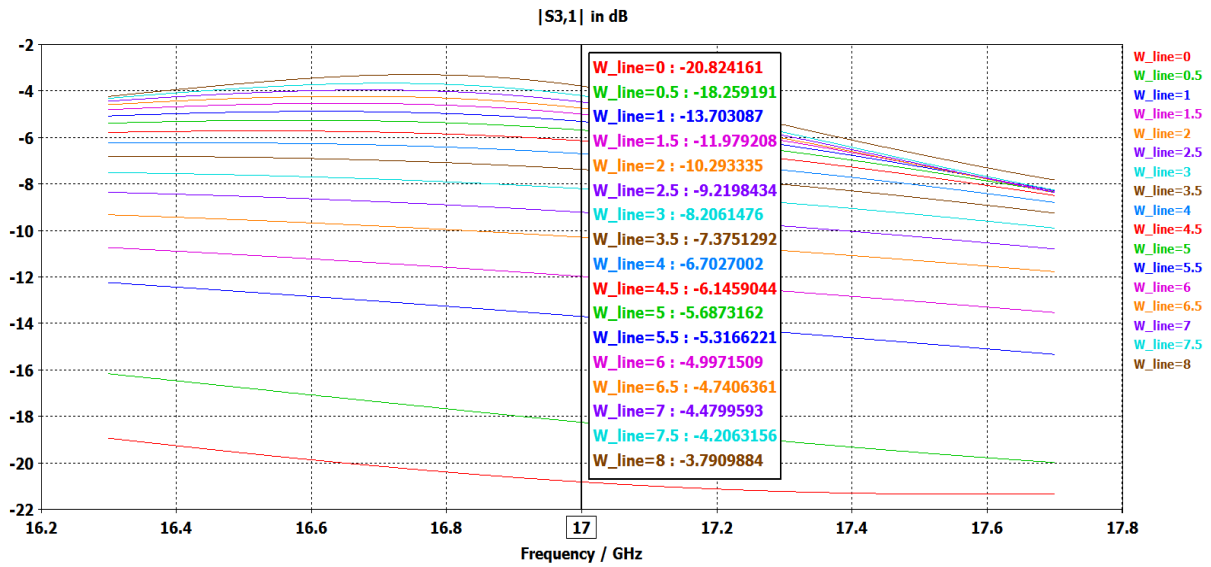


Figure 3-6: Coupling factor of a coupling line with length 4.55 mm, as a function of its width at central working frequency (17 GHz)

However, the problem with this distribution function is to obtain the lower coupling coefficients corresponding to the first elements of the array. With the proposed coupling structure, the lowest coupling factor is achieved by placing a via in the SIW without coupling line; which will transfer the power to the double patch structure. Considering the smallest rivet available at E.P.S. of external diameter $d=0.6$ mm. and the initial substrate configuration, the lowest possible coupling obtained is **-13.3 dB**, which is very far from the required one. Although other configurations were tried combining different heights of the substrates, it was impossible to reach the desired values as it is shown in the following table:

Via's diameter (mm.)	0.6				0.8				1.2			
	TLY-5A		Air		TLY-5A		Air		TLY-5A		Air	
Substrate's Thickness (mm.)	1	2	1.6	2.4	1	2	1.6	2.4	1	2	1.6	2.4
Coupling factor (dB)	-13.3	-15.558	-18.001	-19.389	-11.04	-13.185	-15.174	-16.438	-7.696	-9.5	-10.704	-11.867

Table 3-3: Coupling factors for single via element with different substrate configurations

So, implementing a Taylor feeding distribution is not a realistic option for this type of antenna. Instead, it has been proposed a uniform distribution, whose coupling coefficients are lower and granted achievable results with the chosen substrate's configuration. The coupling coefficients of the uniform distribution are exposed in the following table:

3. Design of Antennas

Element (k)	Feeding Function (F_k)	Coupling Coefficient S_k (dB)
1	1	-12.1289
2	1	-11.8544
3	1	-11.5614
4	1	-11.2472
5	1	-10.9084
6	1	-10.5410
7	1	-10.1395
8	1	-9.6972
9	1	-9.2046
10	1	-8.6490
11	1	-8.0117
12	1	-7.2644
13	1	-6.3614
14	1	-5.2199
15	1	-3.6671
16	1	-1.2272

Table 3-4: Amplitude and coupling coefficients for a linear array of 16 elements with uniform distribution and 2% power loss

Once all these features have been set, the next steps of the design of the linear array consist of characterizing the coupling lines, and also developing an analysis model to optimize the structure and compensate the coupling effects among the different elements.

3.5.2 Coupling Lines Design

The design of coupling lines is a crucial step, as it is particularly important to transfer with precision the power needed for each radiant element. Moreover, in end-feed arrays (fed from one extreme) this duty is especially difficult, as unexpected behavior in one element's coupling affects very negatively the following elements of the array.

3.5.2.1 3-port analysis model

One very important feature of the linear array is the possibility of make independent the design of the feeding structure (composed of the coupling lines in the SIW) from the radiant elements (double patch structure).

This is particularly useful, as each coupling line can be characterized and its coupling factor 'measured' through a port which will connect the SIW with the patch structure. In Figure 3-7 it can be seen how the individual design of the coupling lines has been made, presenting a section of conventional waveguide equivalent to the SIW design.

3. Design of Antennas

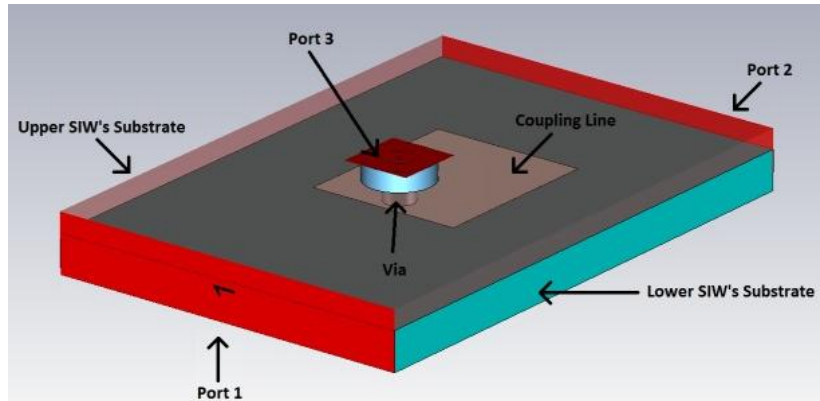


Figure 3-7: Example of a coupling line section in conventional waveguide with 3-port model

It consists on a double substrate layer of length λ_g and width a (all dimensions from Table 3-1), and a thin layer of metal between them where the coupling line is located. This conductor layer belongs to the lower metallic plane of the upper substrate, while the upper metallic layer of the lower substrate has been completely removed. Finally, a metallic cylinder forms the via which transfers power from the coupling line to the upper patch structure.

The distance of this cylinder to the edge of the coupling line must be big enough to enable proper soldering in the fabrication process. It has been tested how the position of the via inside the coupling line affects the coupling factor of the element. The results suggested placing the via the closest possible to the beginning of the coupling line, considering that the metallic via is centered in the substrate section and the coupling line extends to its end given the safety soldering distance from the edge.

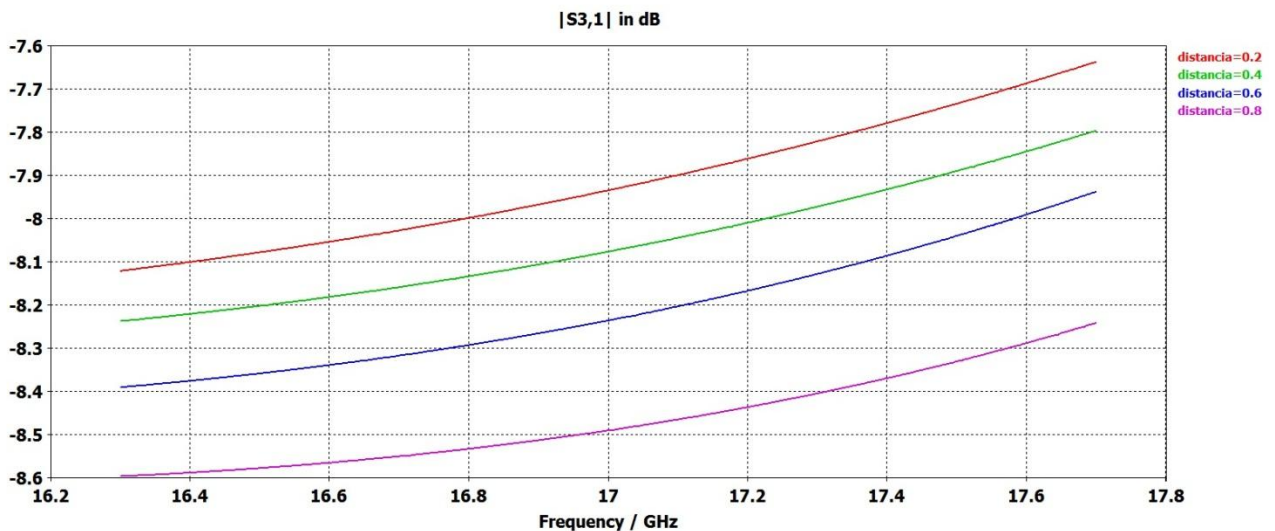


Figure 3-8: Coupled power as a function of the distance of the via from the line's edge

When the structure is drawn, the ports are placed. Considering the example coupling element from Figure 3-7 (which represents the k -th element of the linear array), **port 1** is placed as the input port that feeds the k -th element, and **port 2** as the output port which will transfer the progressive wave to the following element of the array. Finally, **port 3** is located above the via and it is surrounded by a vacuum hollow which simulates a coaxial structure. This structure models very faithfully the coupling factor of the line inside the SIW, and enables precise measurement of the power absorbed by the coupling line of the k -th element.

3. Design of Antennas

The value of the characteristic impedance of port 3 is very important. For general purposes, this impedance is set at a value of 48Ω , very close to the nominal 50Ω used for many radio frequency elements. As it influences significantly the coupling behavior of the structure, it is mandatory to maintain this value for every coupling line, independently of its via's diameter; and also for the upper patch structure.

Once the structure is drawn, the final step is to simulate the modeled coupling line. According to the calculated coupling values for each element summarized in Table 3-4, the dimensions of the line are adjusted in order to obtain at port 3 the desired power level. This adjustment does not need to be very thin, as it will be seen later that the coupling effect of the adjacent elements disturbs the coupling factor of each element. It would be a waste of time to try to get the exact power level of Table 3-4, as later on it will be completely modified.

It is important to note that all these designs of individual elements are made in a conventional waveguide structure. The main reason to do this is that simulation time is much lower in comparison to the same structure in SIW. CST software requires more time to evaluate and calculate fields in designs with multiple objects, and the results from simulations of the structure in SIW and waveguide are almost the same. Furthermore, the first three coupling lines consist of discs of different radius; elements from 4 to 15 are rectangular coupling lines and the last element has a special design which will be described later this chapter.

Element (k)	Theoretical Coupling Coeff. S_k (dB)	Obtained Coupling Coeff. S_k at 17 GHz (dB)	Coupling Line's Length (mm.)	Coupling Line's Width (mm.)
1	-12.1289	-11.884	0.56 (<i>disc</i>)	0.56 (<i>disc</i>)
2	-11.8544	-11.553	0.625 (<i>disc</i>)	0.625 (<i>disc</i>)
3	-11.5614	-11.269	0.65 (<i>disc</i>)	0.65 (<i>disc</i>)
4	-11.2472	-11.096	1.2	1.1
5	-10.9084	-10.54	1.35	1.3
6	-10.5410	-10.353	1.35	1.45
7	-10.1395	-9.892	1.6	1.7
8	-9.6972	-9.421	2.2	2.3
9	-9.2046	-8.889	2.9	3
10	-8.6490	-8.438	3.3	3
11	-8.0117	-7.745	3.65	4
12	-7.2644	-6.921	3.95	4
13	-6.3614	-7.016	4	6.5
14	-5.2199	-4.996	4.25	6
15	-3.6671	-3.443	4.4	8.5
16	-1.2272	-1.968	4.55	8.63

Table 3-5: Obtained amplitude for the coupling coefficients and line's dimensions for each element

It can be seen from Table 3-5 that the obtained results are a little higher than the expected ones. This overestimation has been done on purpose, considering that the coupling effect of the near elements in the array will decrease the power coupled by each element. This effect and countermeasures will be explained in later subsections of this chapter.

3. Design of Antennas

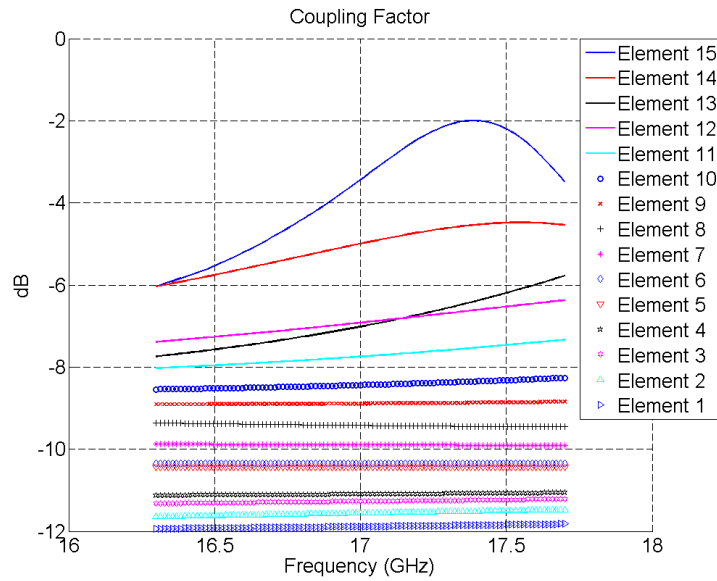


Figure 3-9: Coupling factor after individual design of each element

3.5.2.2 Progressive wave feeding

End-feeding antennas like the one designed in this CFP are based on the principle of progressive wave feeding for its radiating elements. Since the waveguide is fed from a given extreme, the wave propagates along the structure and provides power to the elements. Each line couples a certain amount of the signal's total power, depending on its dimensions. For this reason, for the following elements it should be taken into account that, every time the signal has passed through an element, the remaining power is lower than before. Therefore, the coupling lines will increase their dimensions as they gradually need to couple more of the remaining power.

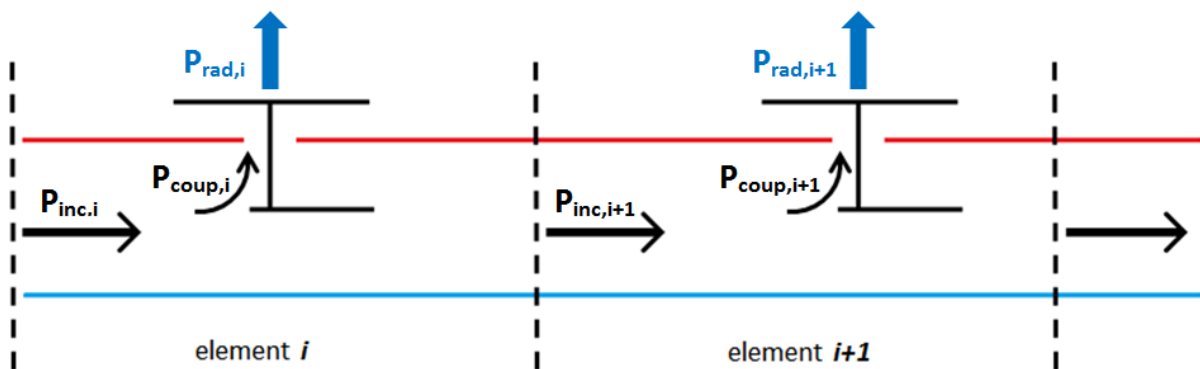


Figure 3-10: Progressive wave propagating along the SIW feeding array

As the reflection of each individual element is very good, it is considered that there is no reflection at the entrance of each element. Therefore, the available power at element $i+1$ is the power at the entrance of element i minus the power coupled by element i .

3. Design of Antennas

3.5.3 Different Linear Array Approaches

After each individual coupling line is characterized, the next step is to form the 16 element array with all of them. The design of each element has been done in substrate sections of length λ_g , to ease the procedure. However, when forming the complete array, the distance between the different elements is important to set the final characteristics of the antenna. Concerning this matter, there are two common methods to follow: set the elements at a distance of λ_g or at a distance of $3\lambda_g/4$. The formula for calculating the direction of the array maximum is presented as follows:

$$\alpha + k \cdot d \cdot \cos \theta_0 = 0 \quad (3.6)$$

Where α is the element-to-element phase shift in the excitation currents, k the propagation constant in vacuum, d the distance between elements and θ_0 is the value of θ for which the array factor is maximum.

If the elements are placed at λ_g and the phase difference α between them is 0° or 360° , theoretically the antenna will aim at broadside, i.e. the direction of maximum propagation is at $\theta_0 = 90^\circ$. On the other hand, if the radiant elements are separated $3\lambda_g/4$ from each other, a better reflection of the whole antenna is obtained, although there will be a deviation of several degrees in the direction of maximum propagation.

Both options have been studied, but the results from the simulation of the linear array with distance λ_g were far below the acceptable levels of reflection, as the reflection of each individual element is added in phase to the total. For this reason it was decided to continue the design with a distance between elements of $3\lambda_g/4$.

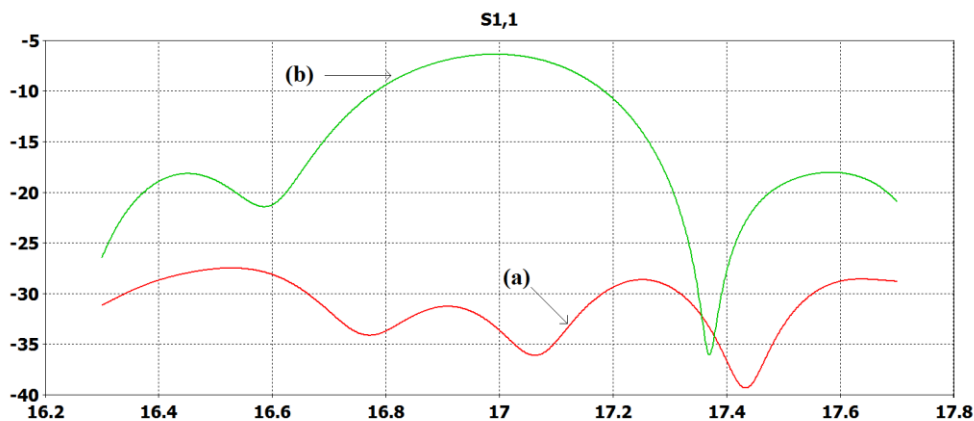


Figure 3-11: S_{11} parameter comparison for approximately (a) $d = 3\lambda_g/4$ and (b) $d = \lambda_g$

Once this decision is taken and starting from the 16 elements individually designed, two different linear arrays were proposed in the next stage of the CFP: an array with **optimized reflection** and another one with **constant phase difference** between each element. In both cases the linear array is fed with a conventional waveguide port of length $3\lambda_g/4$. The procedure followed for each linear array is very similar, although the optimized reflection case requires one additional step before forming the array with 16 elements. The steps to adjust the coupling coefficients which have been taken are the following:

3. Design of Antennas

- 0) Optimization of the reflection coefficient through coupling compensation between two by two elements. This step will be explained with more detail in the following subsection of this chapter. (*This step is just for the array with optimized reflection*)
- 1) Junction of the 16 elements in the array, forming a structure with 17 ports (port 1 for the input and the rest for each one of the radiant elements).

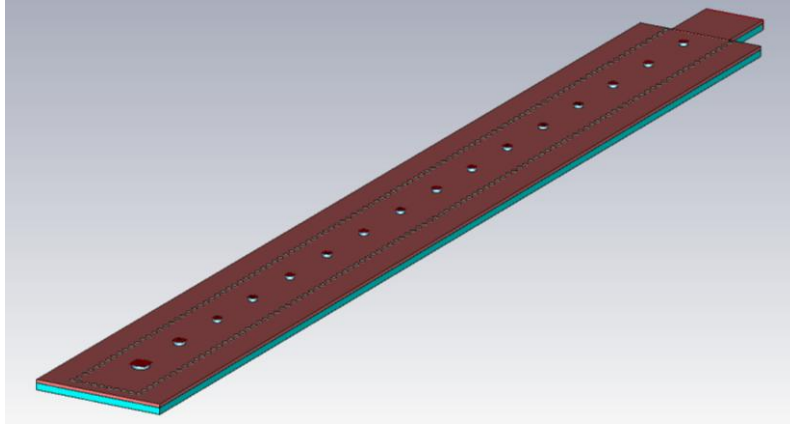


Figure 3-12: Feeding array structure in SIW with 17 ports, fed by a conventional waveguide port

- 2) Once the array is formed, it is simulated in CST Microwave Studio.
- 3) As now it is possible to access to the coupling factor of each element (both amplitude and phase) in ports 2 to 17, the results are compared with the desired ones. For the array with optimized reflection, the amplitude value in each port is compared with the desired one for the uniform distribution. For the constant phase shift array, the obtained phase in each port is studied and the phase difference in adjacent elements is compared with the initial value of 270° or -90° .
- 4) Adjustments are applied to the dimensions of the coupling lines and the distance between elements. Changes in the dimensions mainly vary the amplitude of the coupling coefficient, while a change in the distance modifies significantly the phase of the element.
- 5) Steps 2-5 are repeated until the linear array is completely adjusted.

3.5.4 Coupling model: S_{11} Optimization two-by-two

As it has been described in the previous subsection, before joining all the individual elements in the optimized reflection array, a coupling model has been applied.

From the works described in the literature and other projects previously carried out in RFCAS, it has been ascertained that the adjacent elements disturb the amplitude and phase of the coupling coefficient. For this reason it is necessary to adjust slightly the dimensions of each line and the separation inter-elements. By applying this method, a compensation of the internal mutual effects of the SIW is made.

3. Design of Antennas

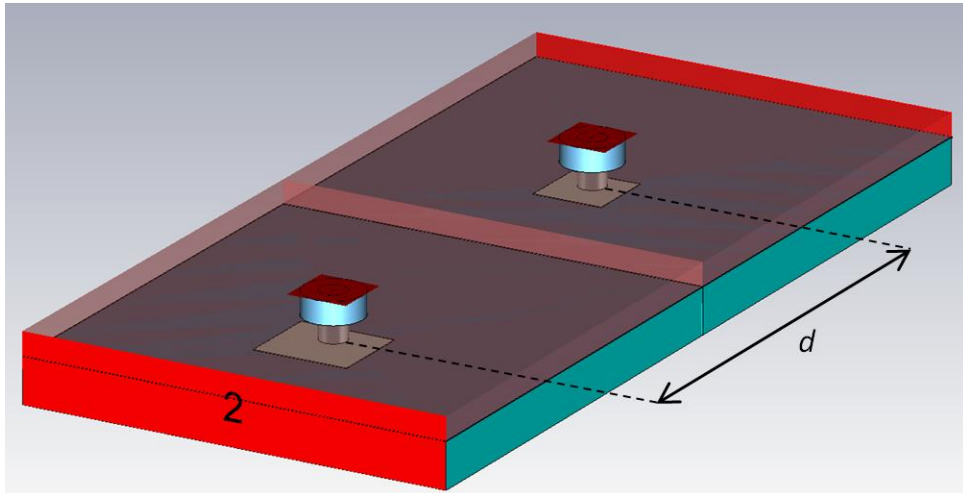


Figure 3-13: Example of two adjacent coupling line sections when applying compensation model

The procedure consists of analyzing sections of two consecutive coupling lines. When placed together, the coupling coefficient's amplitude and phase seen in the ports connected with the double stacked patch changes significantly from the one obtained in the individual design. Under the influence of element i , the following element $i+1$ is modified. Both the dimensions of the coupling line and the distance between vias' centers are adjusted so the right coupling coefficient is achieved again in element $i+1$, leaving element i untouched. Once the desired coupling coefficient is obtained for element $i+1$ after the modifications, the process is repeated for element $i+2$, and so on.

During the application of this coupling method it was proved that, in general, the amplitude of the coefficient was lower than the original. Due to this, all the coupling coefficients have been slightly oversized in prevision of similar effects at the time of forming the SIW feeding array. The following table shows how the dimensions of the coupling lines have been changed and the added/subtracted difference from the original $3\lambda_{gSIW}/4$ between elements.

Element (k)	Individual Design			Optimization two-by-two		
	Line's Length (mm.)	Line's Width (mm.)	Extra Distance (mm.)	Line's Length (mm.)	Line's Width (mm.)	Extra Distance (mm.)
1	0.56 (disc)	0.56 (disc)	-	0.56 (disc)	0.56 (disc)	-
2	0.625 (disc)	0.625 (disc)	0	0.56 (disc)	0.56 (disc)	0.24
3	0.65 (disc)	0.65 (disc)	0	0.585 (disc)	0.585 (disc)	0.28
4	1.2	1.1	0	1.15	1.15	0.06
5	1.35	1.3	0	1.2	1.2	0.2
6	1.35	1.45	0	1.3	1.4	0.18
7	1.6	1.7	0	1.55	1.55	0.88
8	2.2	2.3	0	1.85	2.1	0.12
9	2.9	3	0	2.9	2.8	0.25
10	3.3	3	0	3.6	3.3	0.35
11	3.65	4	0	3.9	4.3	0.4
12	3.95	4	0	4.1	4.95	0.43
13	4	6.5	0	4.45	7.5	0.44
14	4.25	6	0	4.55	8.63	-0.1
15	4.4	8.5	0	4.55	8.63	0.5
16	-	-	0	-	-	1

Table 3-6: Comparison of the line's dimensions before and after the reflection optimization process

3. Design of Antennas

3.5.5 S_{11} Optimization vs. Constant Phase Difference Feeding Arrays

After the design of the coupling lines and the application of the optimization two-by-two to compensate the internal mutual effects in the SIW, the feeding array is formed. As it has been explained before, now the coupling coefficients seen in the coaxial port of each element can be monitored and modified to get the wanted values.

However, at this point the amplitude of the coupling coefficients cannot be compared with the values of Table 3-5. Since all the elements must couple the same absolute power for the uniform distribution, the coupling coefficient for each element is:

$$P_{rad} = 10 \cdot \log_{10} \left(\frac{1}{M} \right) \quad (3.7)$$

For $M = 16$, the number of elements in the linear array, for each element it is obtained a power level of $P_{rad} = -12.04 \text{ dB}$. With this value and the phase difference of 270° , the arrays are adjusted. Bearing in mind that later the patch structure has to be added to the feeding array, the optimization of this stage is not extremely accurate. Additional coupling effects will be introduced with the radiating elements, and further adjustment will be needed.

Despite not being very precise in the obtaining of the coefficients' amplitude, the values for the fifteenth and especially sixteenth element were far beyond acceptance. For the last element it was impossible to get anything better than -18.5 dB . Due to this, a change in the design was made, ending the linear array in a short-circuit instead of an output port. With this new configuration, the coupling coefficients for each element change, as there is no power loss. Moreover, the last element of the array needed to be redesigned. This element was designed all together with the patch structure, so it will be explained later this chapter.

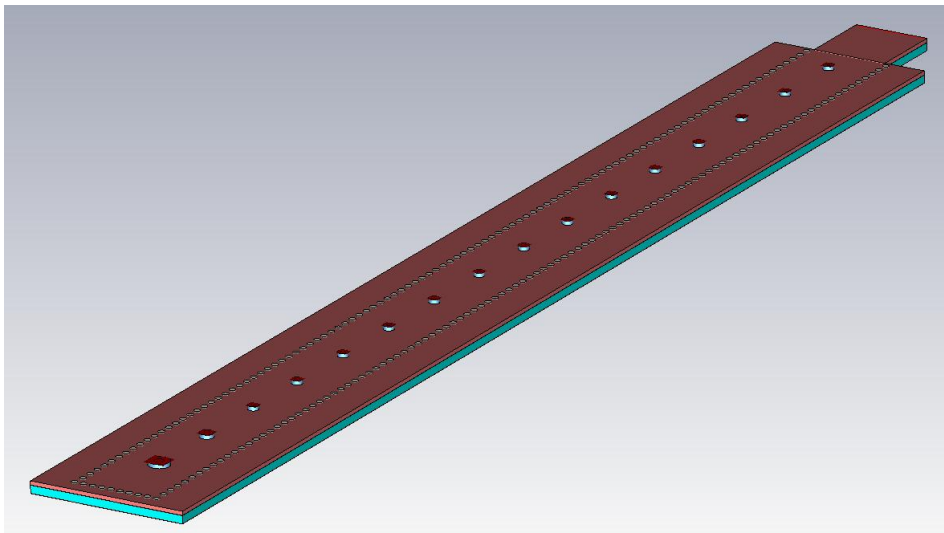


Figure 3-14: SIW feeding array ended in short-circuit, fed by conventional waveguide port

In the following tables the amplitude of the coupling coefficients and the phase difference are summarized, for the best performance and both feeding arrays ended in a short. In addition, the new coupling coefficients are presented:

3. Design of Antennas

Element (k)	Feeding Function (F _k)	Coupling Coefficient S _k (dB)
1	1	-12.0411
2	1	-11.7609
3	1	-11.4612
4	1	-11.1394
5	1	-10.7918
6	1	-10.4139
7	1	-10.0000
8	1	-9.5424
9	1	-9.0308
10	1	-8.4509
11	1	-7.7815
12	1	-6.9897
13	1	-6.0205
14	1	-4.7712
15	1	-3.0102
16	1	0

Table 3-7: Amplitude and coupling coefficients for a linear array of 16 elements with uniform distribution with no power loss

Element (k)	S ₁₁ Optimization		Constant Phase Difference	
	Coupling Coeff. S _k (dB)	Inter-element (k,k+1) phase difference (°)	Coupling Coeff. S _k (dB)	Inter-element (k,k+1) phase difference (°)
1	-12.259	-	-11.778	-
2	-12.167	-83.62	-12.009	-92.89
3	-12.158	-81.28	-12.072	-89.86
4	-12.276	-84.9	-11.879	-93.43
5	-12.181	-83.16	-12.201	-92.66
6	-12.116	-77.82	-12.003	-93.66
7	-12.356	-81.39	-12.406	-91.03
8	-12.203	-77.34	-11.916	-89.09
9	-12.24	-70.81	-12.113	-94.24
10	-12.152	-75.45	-12.188	88.11
11	-12.248	-77.07	-11.776	-93.87
12	-12.248	-72.68	-12.774	-86.75
13	-12.303	-72.26	-11.559	-88.24
14	-12.04	-67.45	-12.463	-94.36
15	-14.143	-80.99	-14.804	-93.4
16	-16.235	-110.52	-17.841	-82.34

Table 3-8: Amplitude and phase difference of the coupling coefficients, for S₁₁ optimization and constant phase difference SIW feeding arrays

From the results above, it can be seen the difficulty to obtain the appropriate values for the last element. This fact is more notorious in the amplitude of the coupling coefficient for the case of constant phase difference. Due to this another key decision was taken, and the design of the linear array from this point focuses on the **optimization of the antenna's reflection**.

Taking into account that the phase difference between elements should be constant in order to obtain a reasonable radiation pattern, from the phase differences of Table 3-8 a mean value is calculated. Thus, the mean phase difference is $\Delta\phi \approx -80^\circ$, a value which will be later used for the adjustment of the complete antenna.

3. Design of Antennas

3.6 Design of Unitary Element

For this CFP, a patch structure is proposed for the unitary radiating element of the linear array. It is an interesting option as both the feeding array and the radiating structure can be manufactured in printed circuit technology.

If a single patch is designed, there is an approximation expression to the radius of the patch, as described in [14]:

$$r = \frac{F}{\left\{ 1 + \frac{2t}{\pi \epsilon_r F} \left[\ln \left(\frac{\pi F}{2t} \right) + 1.7726 \right] \right\}^{\frac{1}{2}}} \quad (3.8)$$

$$F = \frac{8.791 \cdot 10^9}{f \sqrt{\epsilon_r}} \quad (3.9)$$

An important feature to be taken into account is the thickness of the substrate used. Whereas thicker substrates provide better radiation efficiency, it also contributes to higher levels of surface wave, which lead to higher losses.

Unfortunately, a single patch has a very limited bandwidth response. In the best of cases it is achieved a 4% of the bandwidth for the working frequency range of this CFP. Therefore, the structure was changed to a double stacked patch as found in [15]. With this new configuration, the approximation equation (3.8) does not provide the appropriate patch dimensions, so it is only a basis to start the work with.

For the designs of the double patch structure, the only requirement needed is good a reflection value, which is set at -20 dB. In the design, there are different via diameters connecting the coupling lines with the inferior patch. Therefore, a different design is needed for each size and all must fulfill the reflection requirements. Moreover, the double patch structure is designed as a one-port element. This port consists of the same coaxial previously explained in subsection 3.5.2.1, with a characteristic impedance of 48Ω.

In a preliminary stage of the radiating element design, it was used software Maxwell Ansoft Ensemble. It was useful for establishing approximate dimensions of the patches, but the scheme needed to be refined in CST Microwave Studio as there are some features that are approximated in Maxwell Ansoft Ensemble and require more detailed calculation. These include the method of calculation and the use of a finite ground plane which can characterize the behavior of the structure.

Once the design is taken to CST Microwave Studio, the most laborious task has been to find a patch's impedance similar to the one of the coaxial port, in order to achieve good matching. This impedance is modified by the relative location of the via in the patch. As it is particularly ineffective to try to obtain the patch's impedance, the procedure consisted of experimentally adjust the via's placement until the reflection is good enough. Due to impedance requirements, the via had to be placed out of the circumference of the patch, so an extra stretch and a soldering ring are required to connect the patch with the via.

3. Design of Antennas

After the optimization of the parameters of both structures, the obtained reflection response and the parameters' values are the following:

Param. Struc.	Inferior Patch Radius (mm.)	Superior Patch Radius (mm.)	Distance from Patch Center (mm.)	Soldering Ring Radius (mm.)	Extra Stretch (mm.)
Structure 1	2.86	3.235	3.5	0.58	0.7
Structure 2	2.86	3.25	3.55	0.65	0.58

Table 3-9: Summary table of patch structure parameters

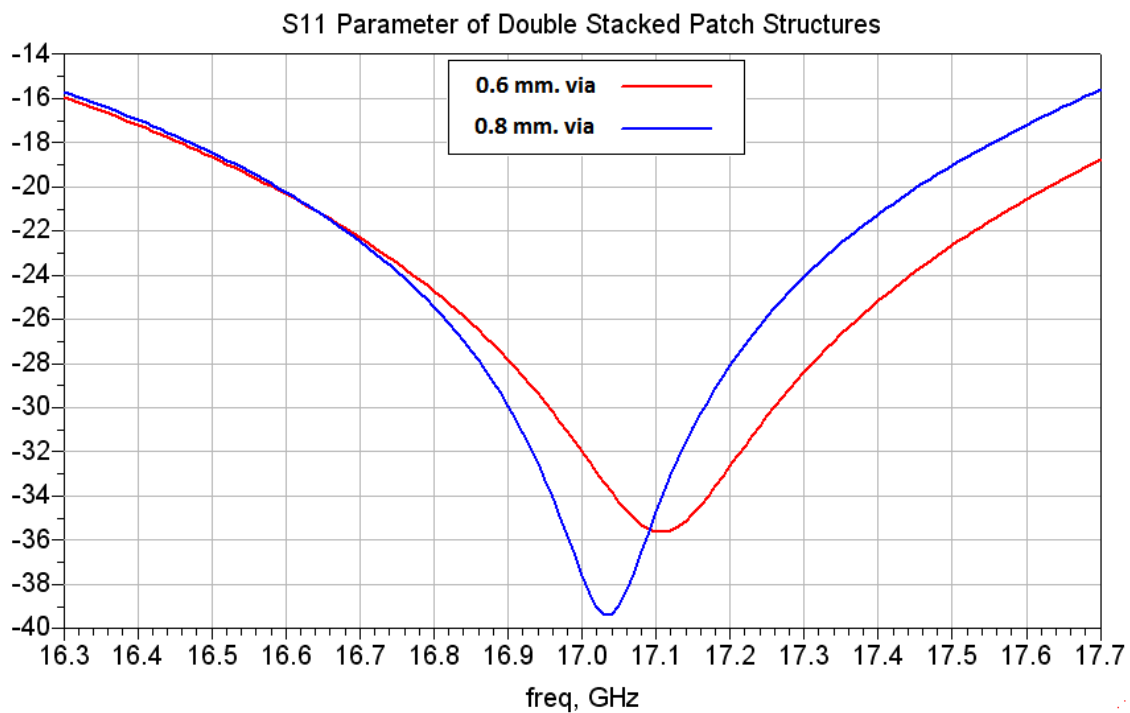


Figure 3-15: Reflection coefficient of the two patch structures designed

3.6.1 Design and Fabrication of the 16th Element

As it has been mentioned before, the last element has a special design as the linear array ends in a short-circuit. Its main feature is that it is optimized in reflection, so that the remaining power from the other 15 elements is fully seized. For this matter, it will be sought a reflection value below -20 dB in the whole frequency band of work.

It will be shown later this chapter that, apart from the internal mutual effects of the coupling lines, the radiating elements have a very strong disturbance effect on the coupled power of each element. For this reason it did not make too much sense to separately design the coupling and the patch structure, so for the last element all the effects are simultaneously taken into account and both parts are designed together.

3. Design of Antennas

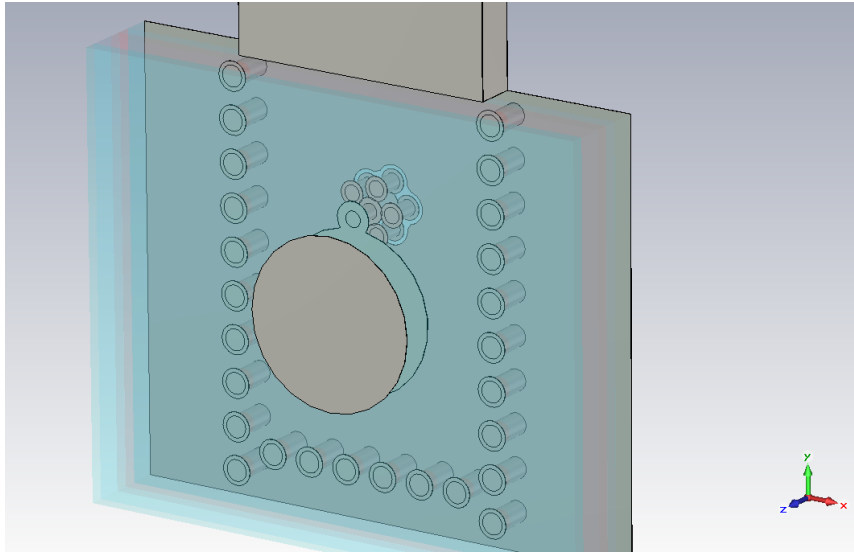


Figure 3-16: Design in CST Microwave Studio of the 16th element, with the bottom patch plane hidden

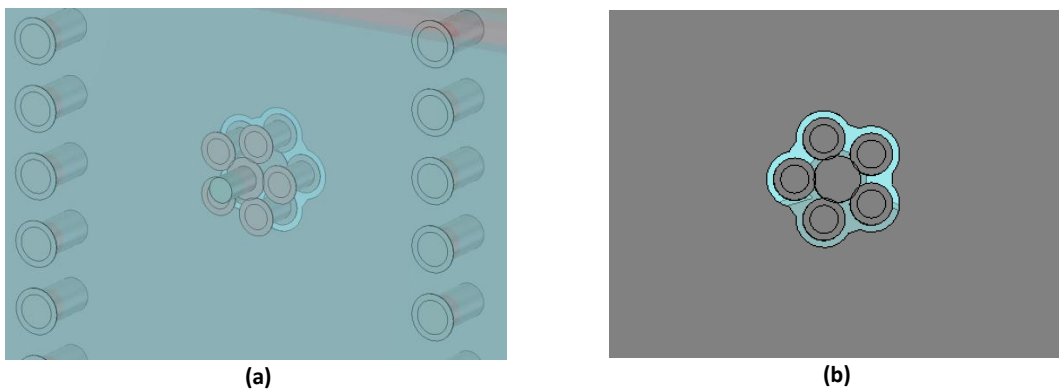


Figure 3-17: Detail of the coupling element (a) and bottom view in the ground plane (b)

Apart from the reflection constraint of the element, the main limiting factor has been to make it manufacturable in the laboratory of printed circuits at EPS. It was important to take into account not only the available material such as rivets, substrates, etc; but also the technological limitations to fabricate pieces or to have a high degree of precision.

The element consists of two differentiated parts: the coupling element and the double stacked patch structure. The coupling structure which substitutes the coupling lines of the other elements was originally a metallic cylinder, as it has been done in other works [13]. This structure is designed in the lower substrate of the SIW (TLY-5A of 1 mm.), in order to facilitate the construction and maintain the continuity and homogeneity of the SIW. However, it was not possible to fabricate such a small metal piece, so an alternative design with rivets is proposed.

Five rivets are placed equally spaced in a circumference, with two metallic discs centered in the same imaginary circumference, one on top and one on the bottom of the substrate. These two discs are there to keep the appearance and the electromagnetic characteristics of a cylinder. Drills are performed in the substrate and the rivets are inserted. Although it has been proved by simulations that continuity between the rivets' heads and the central metallic disc is not very important, they have been soldered to contribute to stability.

3. Design of Antennas

In the ground plane of the SIW, an emptying of the substrate's copper is made to avoid short-circuit. Small changes in the emptying induce to significant changes in the reflection response, and the closer the rivets are to the edge of the emptying, the better the reflection of the set. This is a critical design feature, and it has been taken to the manufacturing machine's limits of precision and usable tool (0.15 mm. of diameter).

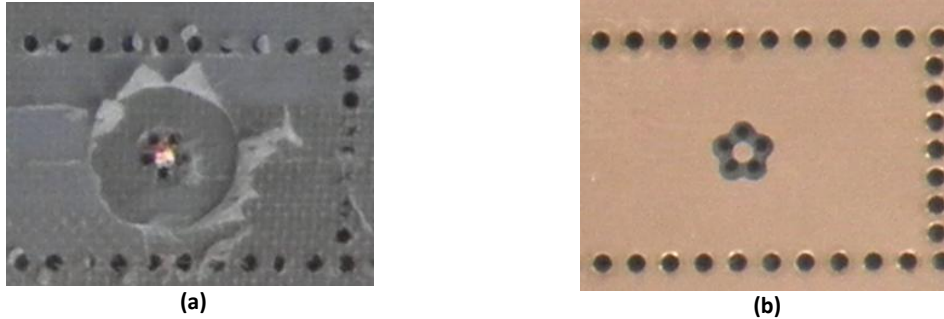


Figure 3-18: Top (a) and bottom (b) view of the 16th element in the prototype, before the insertion of the rivets

For the coupling via it has been used a regular rivet of 0.6 mm. of diameter, the same of the other elements. The via is placed and soldered upon the upper metallic disc. The double stacked patch structure is designed at the same, optimizing in this case the radius of the upper and the lower patch, and the radius of the soldering ring that connects the coupling via with the lower patch.

Last but not least, the distance from the whole element to the ending short-circuit is also optimized. Approximately the distance to the short-circuit should be $\lambda_{gSIW}/2$, so that the reflected wave at the short-circuit will have constructive interference with the travelling wave in the direction of propagation of the linear array. In the summary tables, this value has been considered between the center of the coupling via and the center of the vias at the short, so it is higher than the expected one.

3.6.2 Simulation Results

The S_{11} parameter in dB and Smith chart for the final optimization of the 16th element is presented as follows:

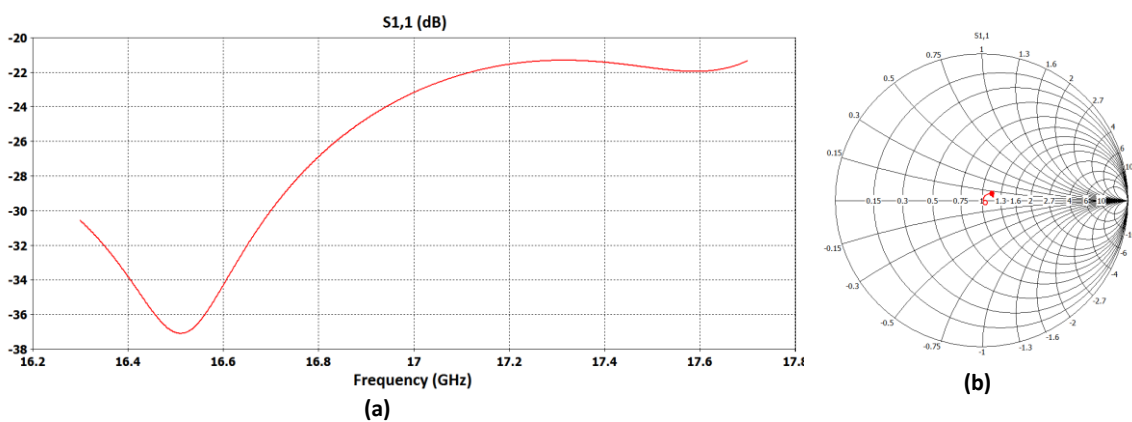


Figure 3-19: S_{11} parameter of the 16th element in dB (a) and in its Smith chart (b)

From the results of the simulations, the desired specifications are fulfilled in the whole frequency range. Therefore, a better behavior of the linear array is expected in comparison to the previous configuration with two ports.

3. Design of Antennas

3.7 Linear Array Implementation

When the design of the SIW feeding array and the double stacked patch structure are completed, they are put together to form the linear array. Although both parts have been optimized in reflection, when arranged together several mutual coupling effects appear and degrade the amplitude and phase of the coupling coefficients, as well as the reflection response of the antenna.

From this point till the end of the linear array's adjustment, the radiation pattern of the antenna will be checked to observe the effect of the changes applied. The obtained radiation pattern will be compared with the theoretical one, given a uniform distribution and a constant phase difference of $\Delta\varphi = -80^\circ$ between elements. The simulation of the linear array right after the junction of the feeding array and the patch structure, with the parameters of the individual design, gave the following results:

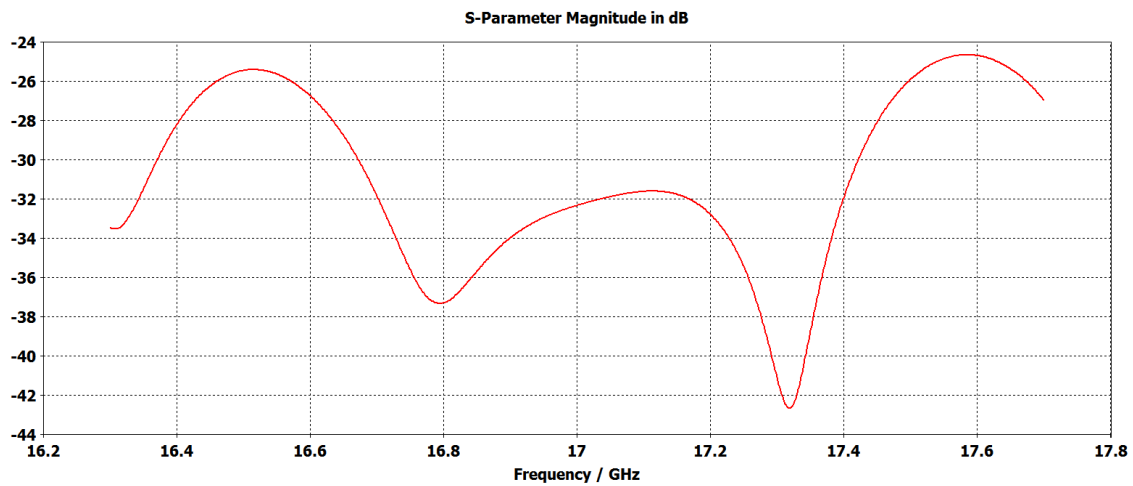


Figure 3-20: Reflection of the linear array with the feeding array joined with the patch structure

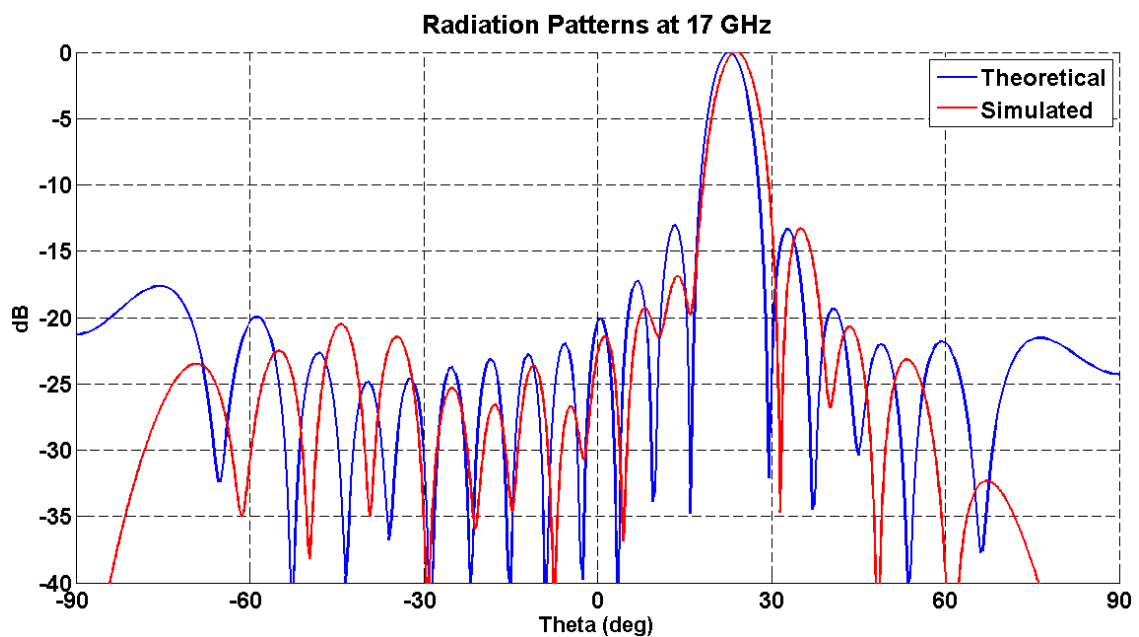


Figure 3-21: Theoretical versus simulated radiation pattern at 17 GHz

3. Design of Antennas

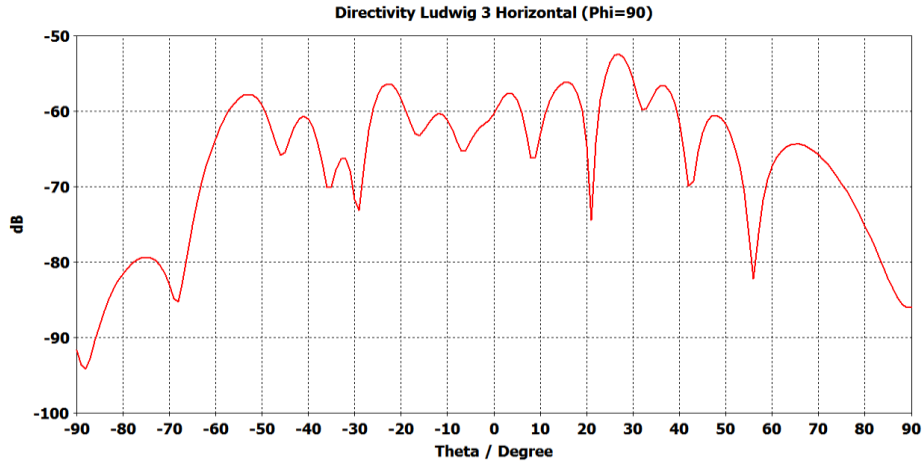


Figure 3-22: Cross-polar component of the linear array at 17 GHz for plane $\phi = 90^\circ$

From the results of Figure 3-21 it is clear that the simulated radiation pattern is not similar to the theoretical one. The most relevant mismatch is the null level of the secondary lobes, which prevents a clear definition of the main lobe. Therefore, adjustments need to be made. A compensation model consisting of studying the electric near-field radiated by the upper patches will be applied.

3.7.1 Radiated Electric Near-Field Compensation Model

In the previous subsection it was stated that the obtained radiation pattern from simulation was very different from the theoretical one. This is due to the disturbing effect of the adjacent elements, which alter the coupling coefficient of them. In order to compensate the mutual effects of all the elements in the linear array, a coupling model is proposed which not only compensates the effect of the external radiating elements, but also the mutual coupling effects inside the SIW. This model is based on [13], where a direct relation between the radiated electric field and the radiated power in each element is found:

$$|F_k|^2 = \frac{|E_k|^2}{\sum_{i=1}^{16} |E_i|^2} \cdot P_{abs} \quad (3.10)$$

$$P_{abs} = 1 - |S_{11}|^2 \quad (3.11)$$

Where P_{abs} is the total power given to the antenna and $\sum_{i=1}^{16} |E_i|^2$ is proportional to the total radiated power. From equations (3.10) and (3.11) and after normalization, the feeding coefficient is directly characterized by the radiated electric near-field.

This field is evaluated in CST Microwave Studio and separated in E_x , E_y and E_z . Taking y axis the direction of propagation of the progressive wave, the current in the upper patch is mainly oriented in y direction. Particularizing in the center of the superior patch of each element, the radiated electric field is characterized by component E_y . Through this component of the electric field, it is possible to calculate the amplitude and phase of the radiated electric field.

The radiated electric near-field is characterized using an electric field monitor in CST Microwave Studio, which can evaluate the field in the cutting plane XY perpendicular to the

3. Design of Antennas

direction of radiation. This plane has to be placed close enough to the upper patch in order to characterize well the obtained coefficient; in this case it is located at 0.5 mm. from the surface of the upper patch.

With the results obtained from each simulation, changes are made to the dimensions of the different coupling lines and the inter-element distance; so the coefficients of the radiated near-field resemble to theoretical ones of $|F_k|_{dB} = -12.04$ dB and $\Delta\varphi = -80^\circ$. As it will be shown later, the results match very well the expected ones. Differently as it happened during the stage of the individual design of the coupling lines, most of the times increasing the dimensions result in higher coupled power. However, when it is needed very fine adjustment this is not always true. Concerning the phase difference between elements, an increase in the distance causes the phase difference to increase, and the opposite effect if the distance is decreased.

Nevertheless, the disadvantage of this method is that it is iterative and simultaneous simulations cannot be performed. From the results obtained of one simulation, adjustments are made to go on with the matching process of the coupling coefficients. Therefore, a lot of time has been invested in this task, given that simulations of the complete antenna could last up to three hours.

3.7.2 Simulation Results

In order to complete the antenna, a feeding transition is needed. The following exposed results belong to the linear array with the designed feeding transition, which will be described in the next chapter. After applying the previously mentioned compensating model, there have been important changes in the coupling line's dimensions and the distance between elements, in order to match the radiation pattern to the theoretical one. These changes are summarized in the following table:

Element (k)	Linear Array Initial Design			Linear Array with Compensation Model		
	Line's Width (mm.)	Line's Length (mm.)	Inter-element Distance (mm.)	Line's Width (mm.)	Line's Length (mm.)	Inter-element Distance (mm.)
1	0.55(rad.)	0.55(rad.)	-	0.55(rad.)	0.55(rad.)	-
2	0.55(rad.)	0.55(rad.)	0.24	0.595(rad.)	0.595(rad.)	0.4
3	0.585(rad.)	0.585(rad.)	0.2	0.66(rad.)	0.66(rad.)	0.03
4	1.15	1.15	0.06	1.3	1.2	0.4
5	1.2	1.2	0.2	1.3	1.3	0.22
6	1.5	1.3	0.18	1.45	1.35	0.31
7	1.55	1.55	0.17	1.55	1.5	0.16
8	2.1	1.8	0.12	1.95	1.6	0.23
9	2.8	2.8	0.25	1.8	1.5	0.22
10	3.35	3.6	0.35	2.85	2.2	0.23
11	4.2	3.8	0.4	2.4	2.05	0.2
12	5	4.15	0.42	4.5	3.1	0
13	7.4	4.25	0.44	5.5	3.35	-0.05
14	8.5	4.55	-0.1	8.55	4.4	-0.9
15	8.63	4.55	0.5	8.55	4.55	1.2
16	-	-	0.7	-	-	0.9

Table 3-10: Comparison of different parameters of the linear array, before and after applying the radiated electric near-field compensation model

3. Design of Antennas

The reflection of the linear array and the radiation patterns with the new configuration of Table 3-10 obtained are the following.

3.7.2.1 S_{11} Parameter

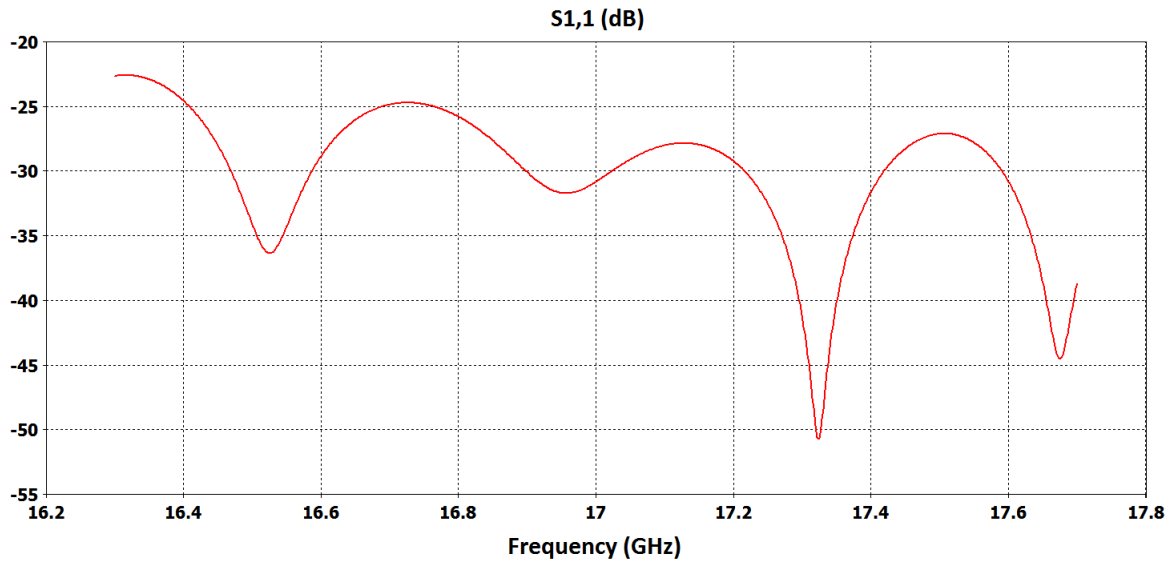


Figure 3-23: S_{11} parameter (in dB) of the linear array antenna

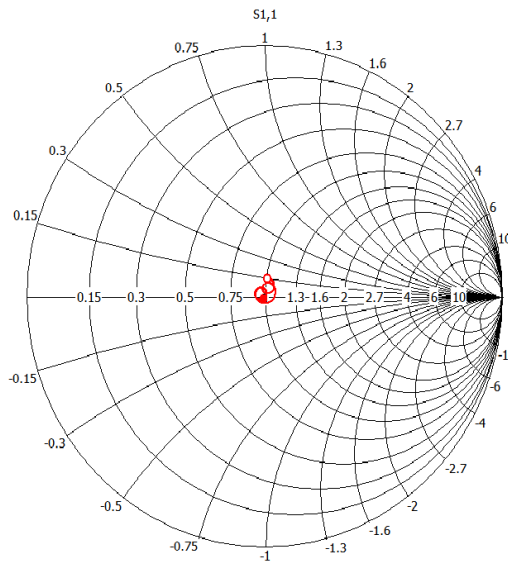


Figure 3-24: S_{11} parameter (in Smith chart) of the linear array antenna

From the results obtained, it can be seen that the reflection is below -22 dB in the whole frequency working band. Therefore, the initial constraints of a S_{11} parameter below -20 dB are fulfilled.

3. Design of Antennas

3.7.2.2 Radiation Pattern

As the radiated field is linearly polarized, the most interesting cutting planes for studying the radiation pattern are the vertical one at $\phi = 90^\circ$ for the co-polar component, and the horizontal one for the cross-polar component. For the previously mentioned cutting plane and in 3D, the co-polar and cross-polar components for different frequencies are presented as follows:

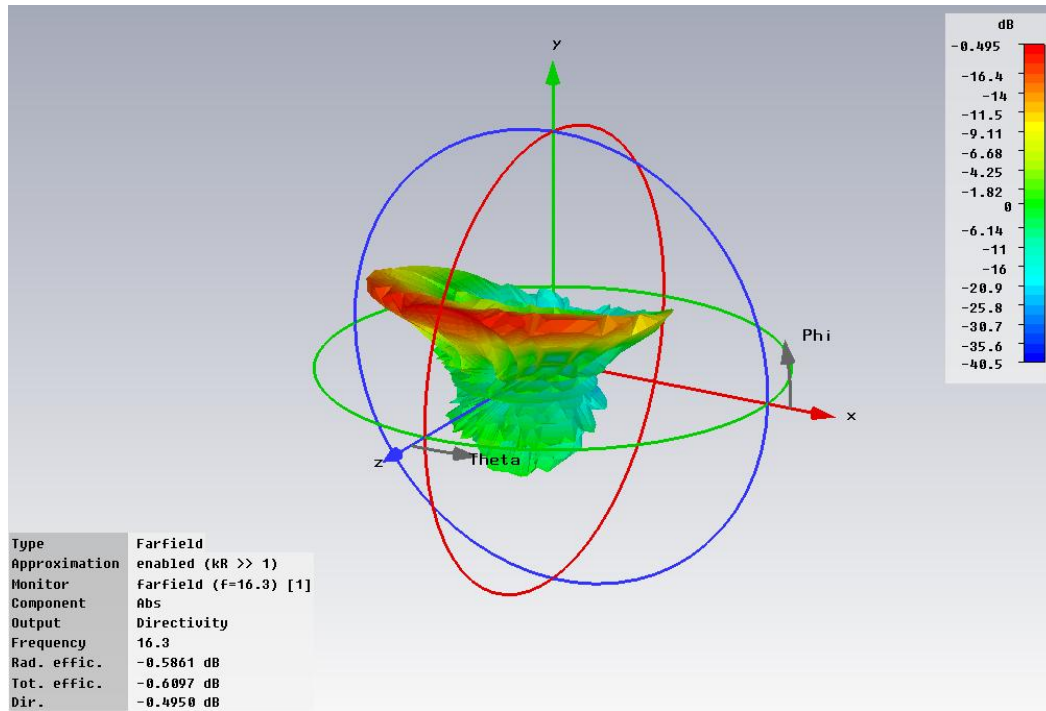


Figure 3-25: 3D radiation pattern at 16.3 GHz

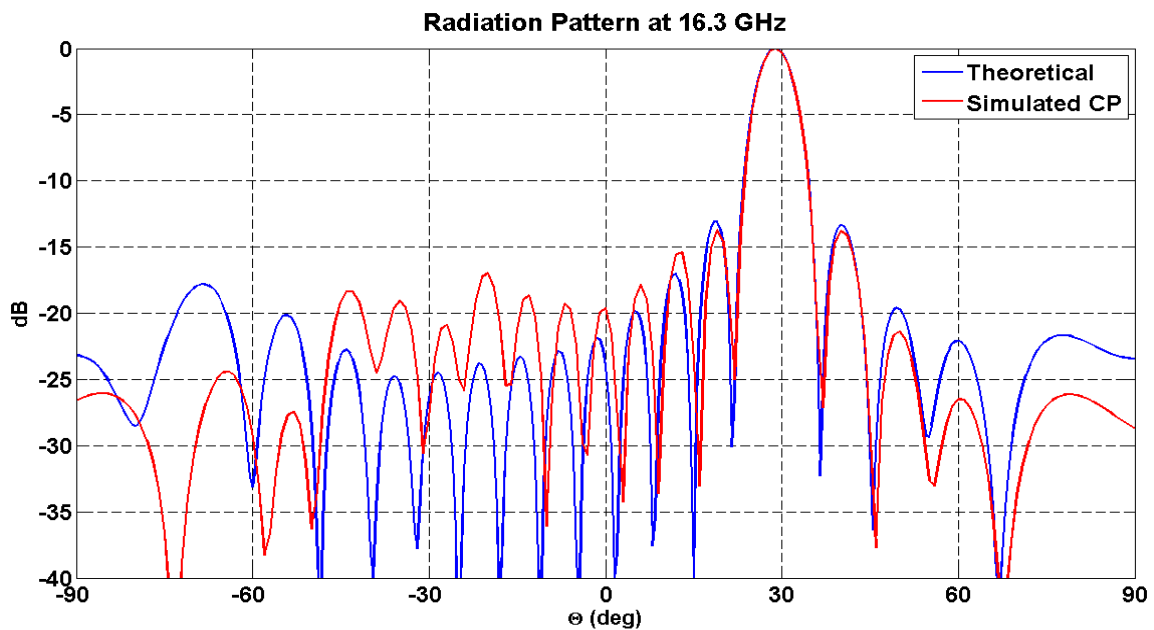


Figure 3-26: Simulated co-polar component of the radiation pattern at 16.3 GHz vs. the theoretical one

3. Design of Antennas

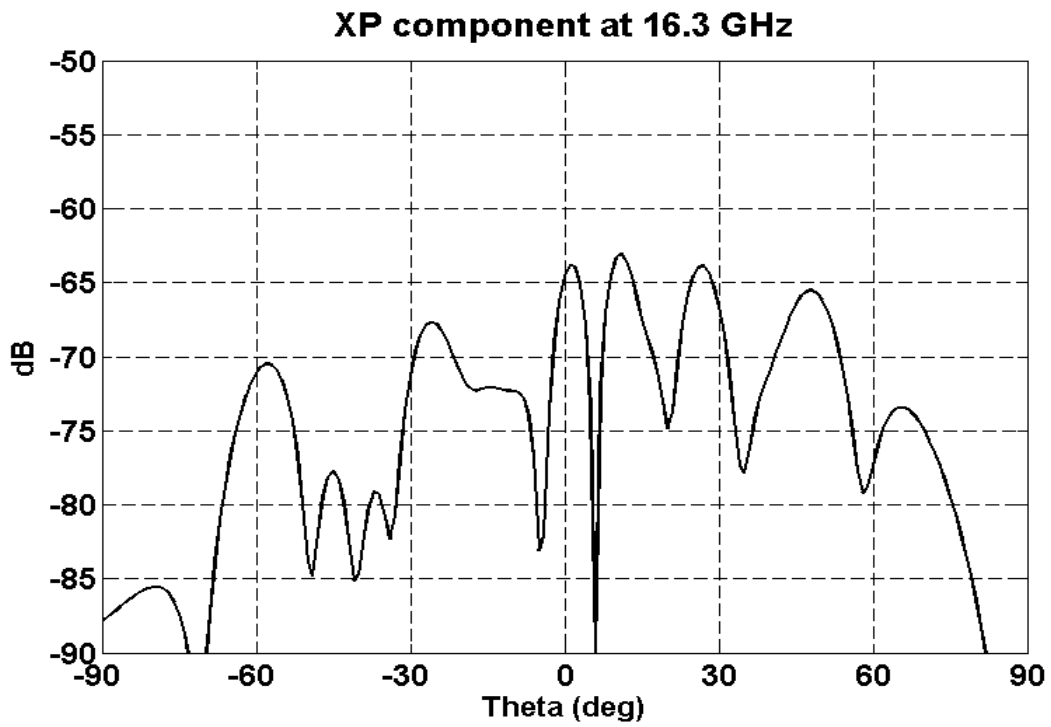


Figure 3-27: Cross-polar component of the radiation pattern at 16.3 GHz

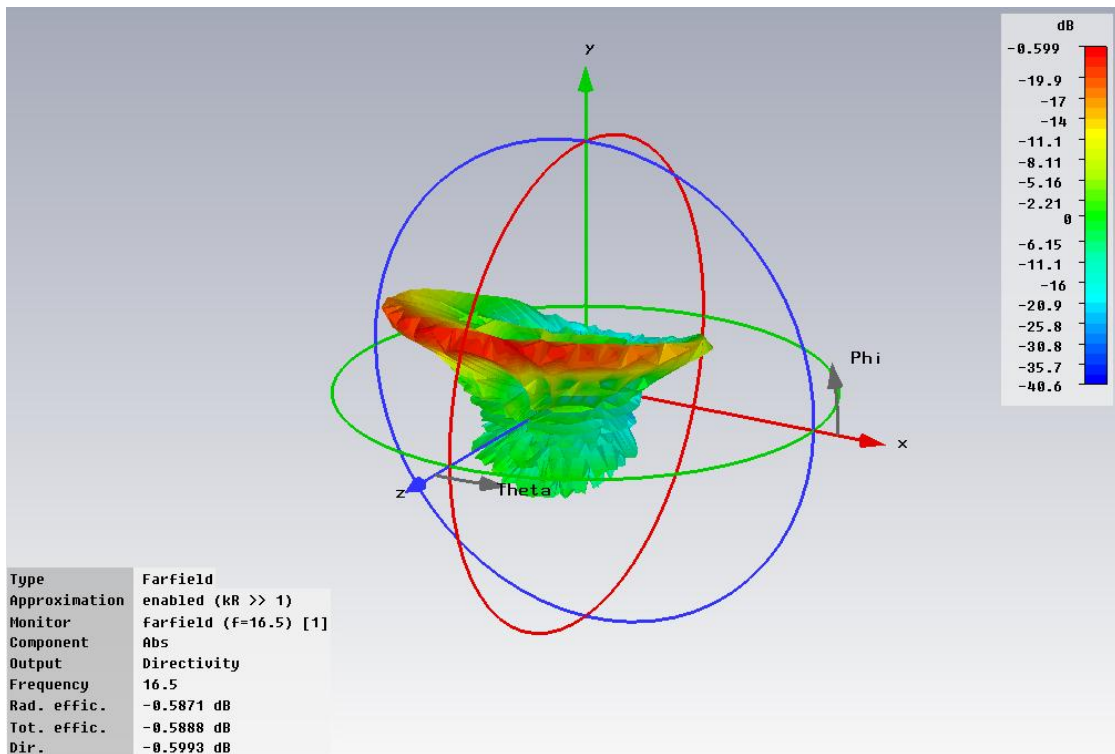


Figure 3-28: 3D radiation pattern at 16.5 GHz

3. Design of Antennas

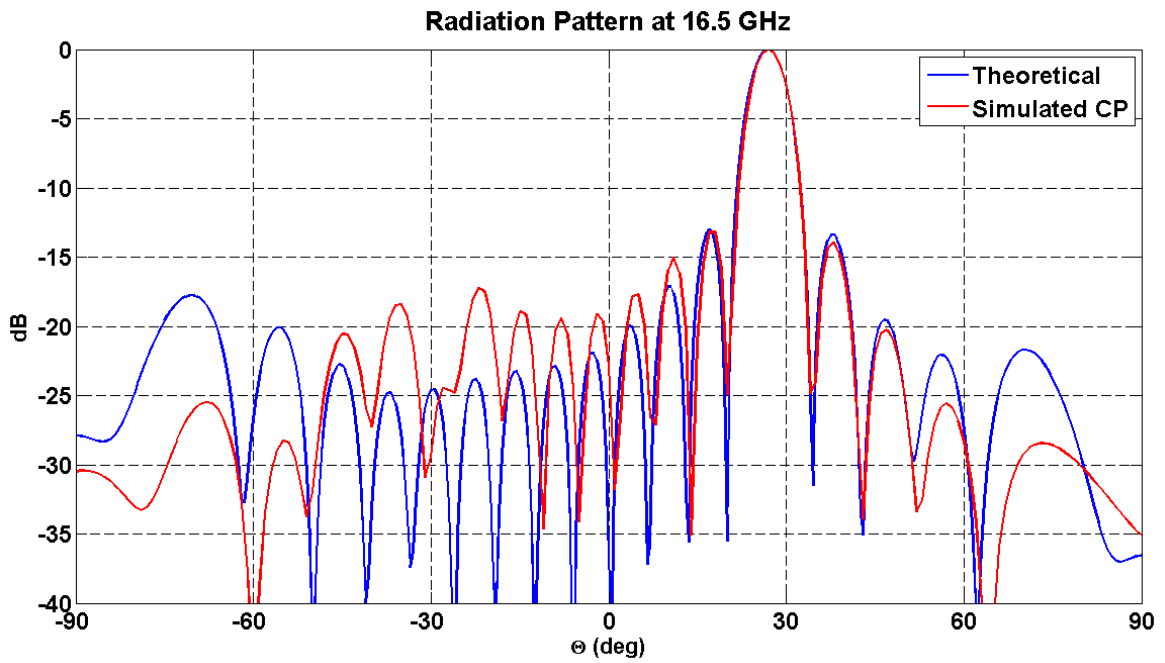


Figure 3-29: Simulated co-polar component of the radiation pattern at 16.5 GHz vs. the theoretical one

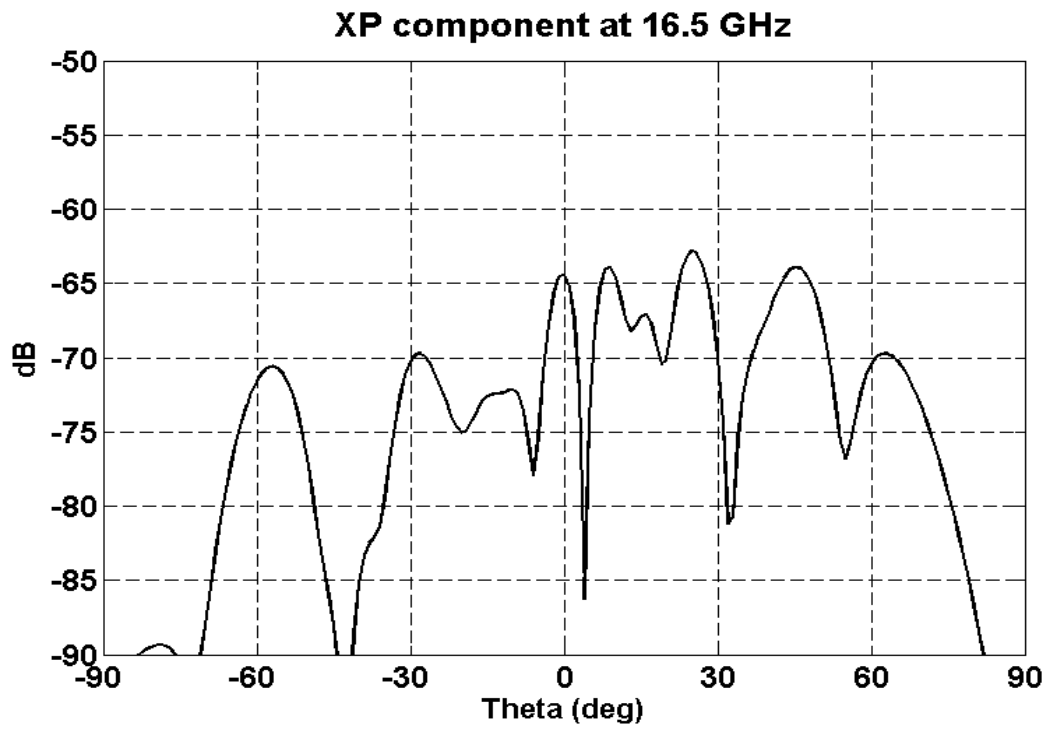


Figure 3-30: Cross-polar component of the radiation pattern at 16.5 GHz

3. Design of Antennas

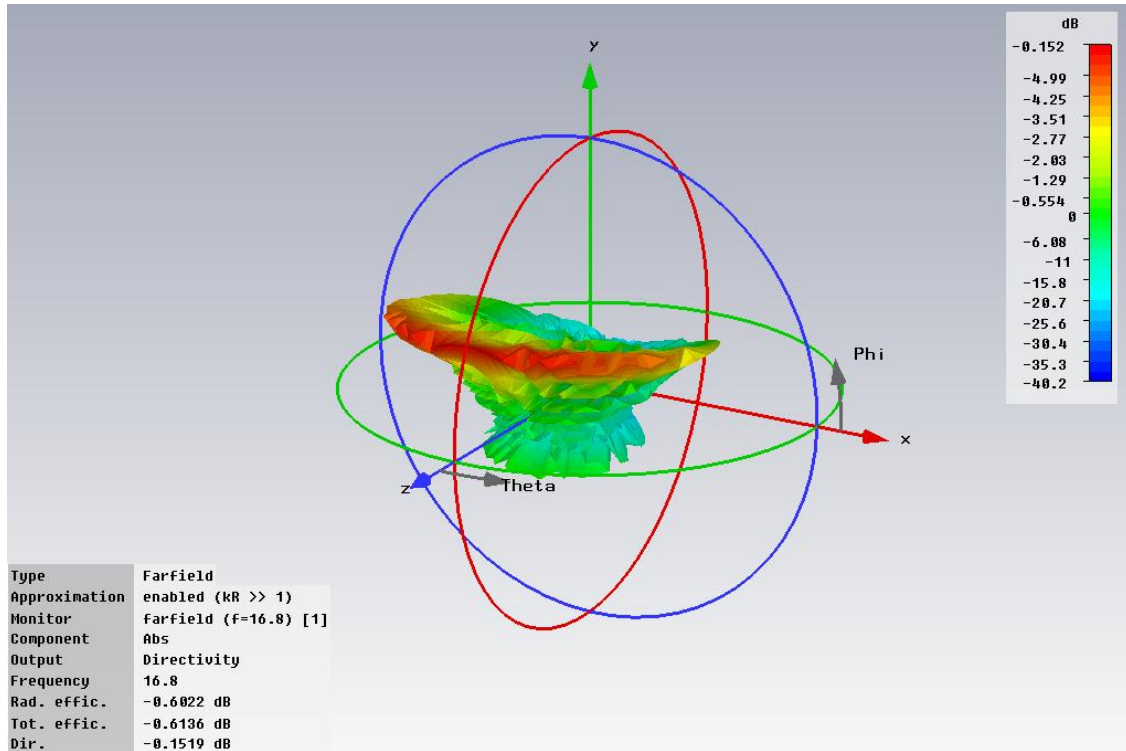


Figure 3-31: 3D radiation pattern at 16.8 GHz

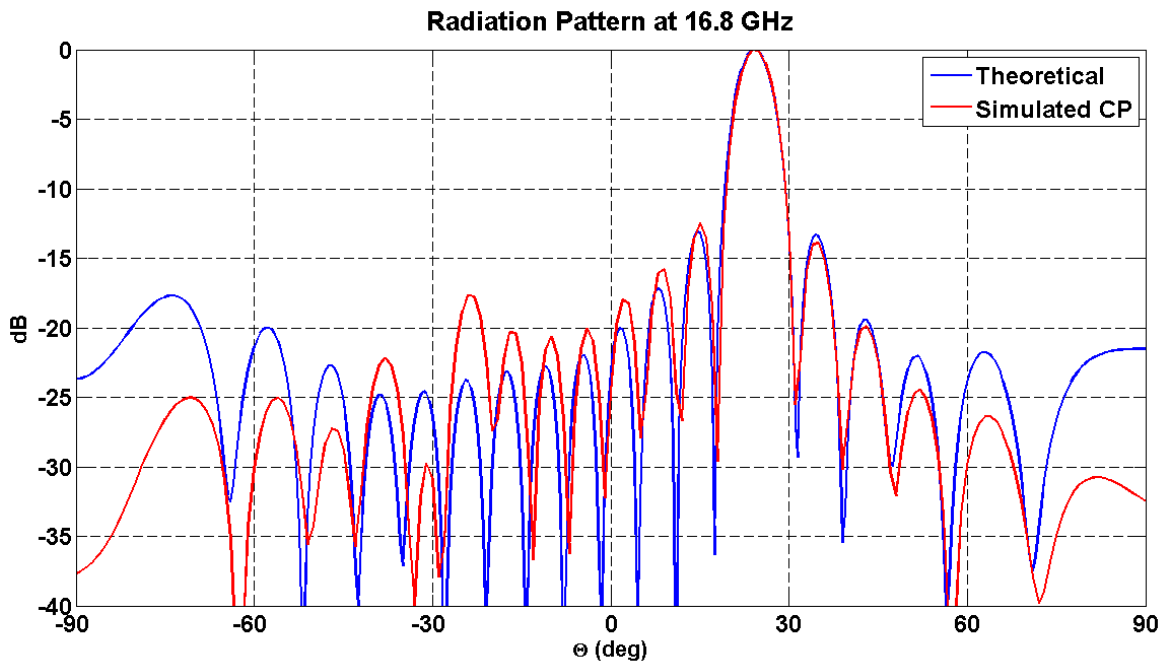


Figure 3-32: Simulated co-polar component of the radiation pattern at 16.8 GHz vs. the theoretical one

3. Design of Antennas

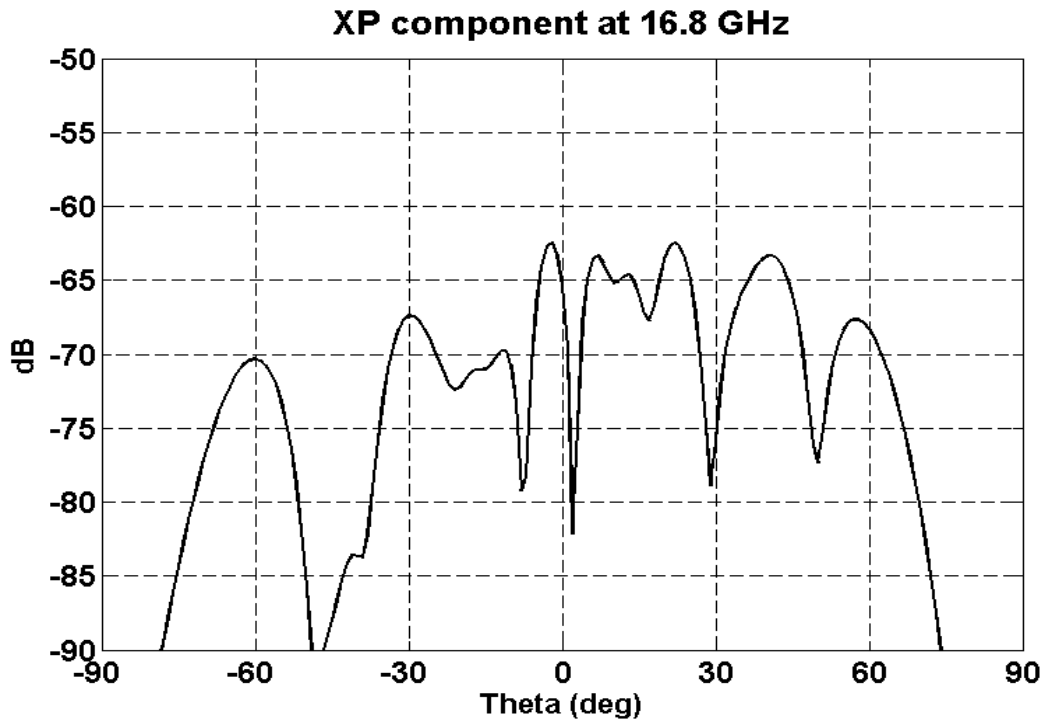


Figure 3-33: Cross-polar component of the radiation pattern at 16.8 GHz

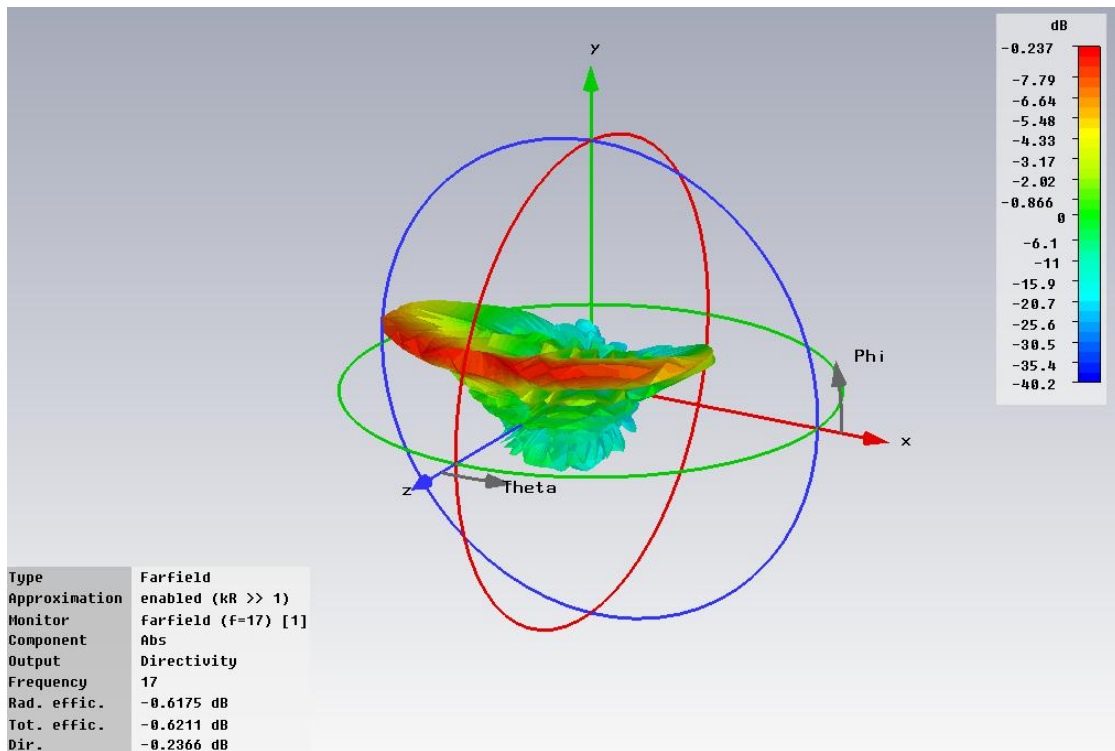


Figure 3-34: 3D radiation pattern at 17 GHz

3. Design of Antennas

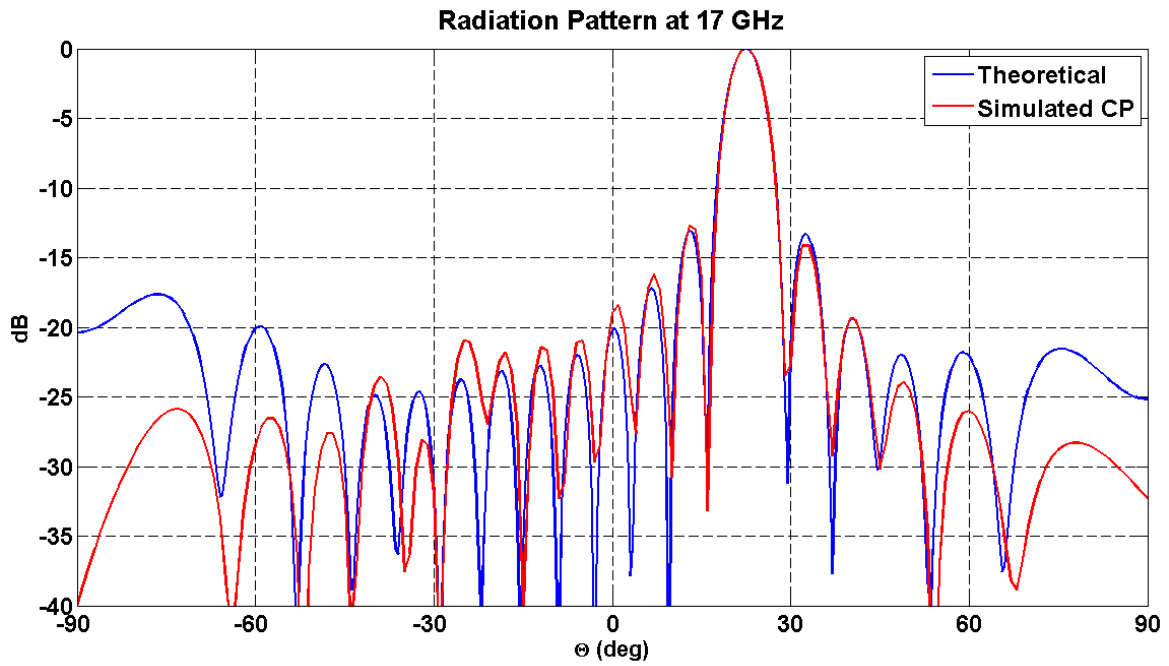


Figure 3-35: Simulated co-polar component of the radiation pattern at 17 GHz vs. the theoretical one

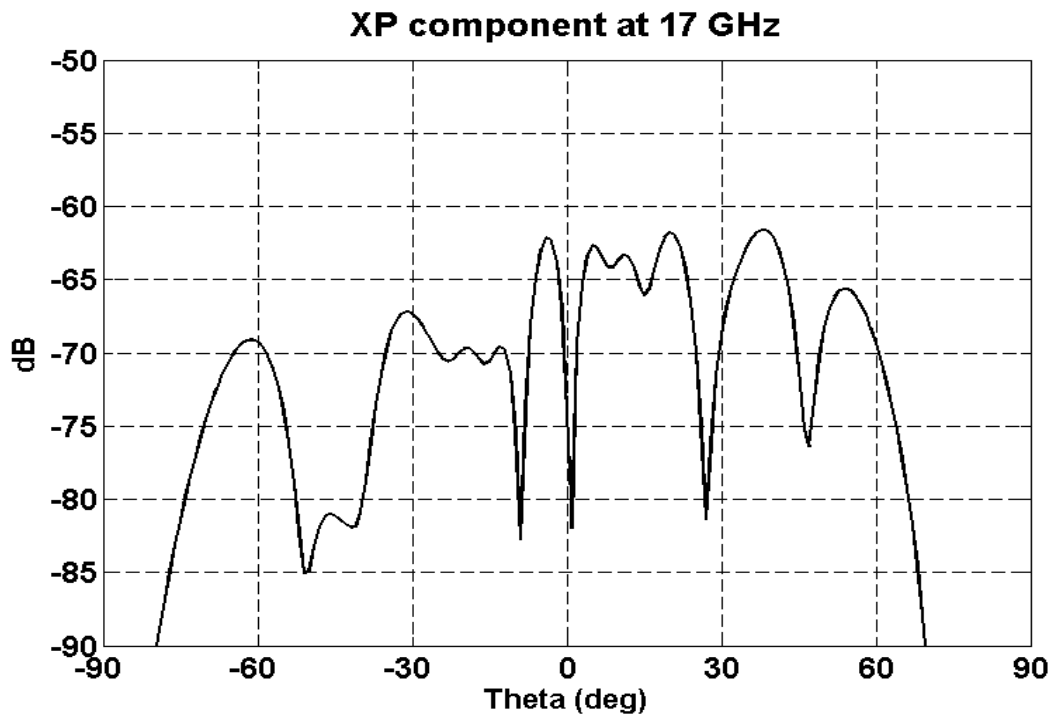


Figure 3-36: Cross-polar component of the radiation pattern at 17 GHz

3. Design of Antennas

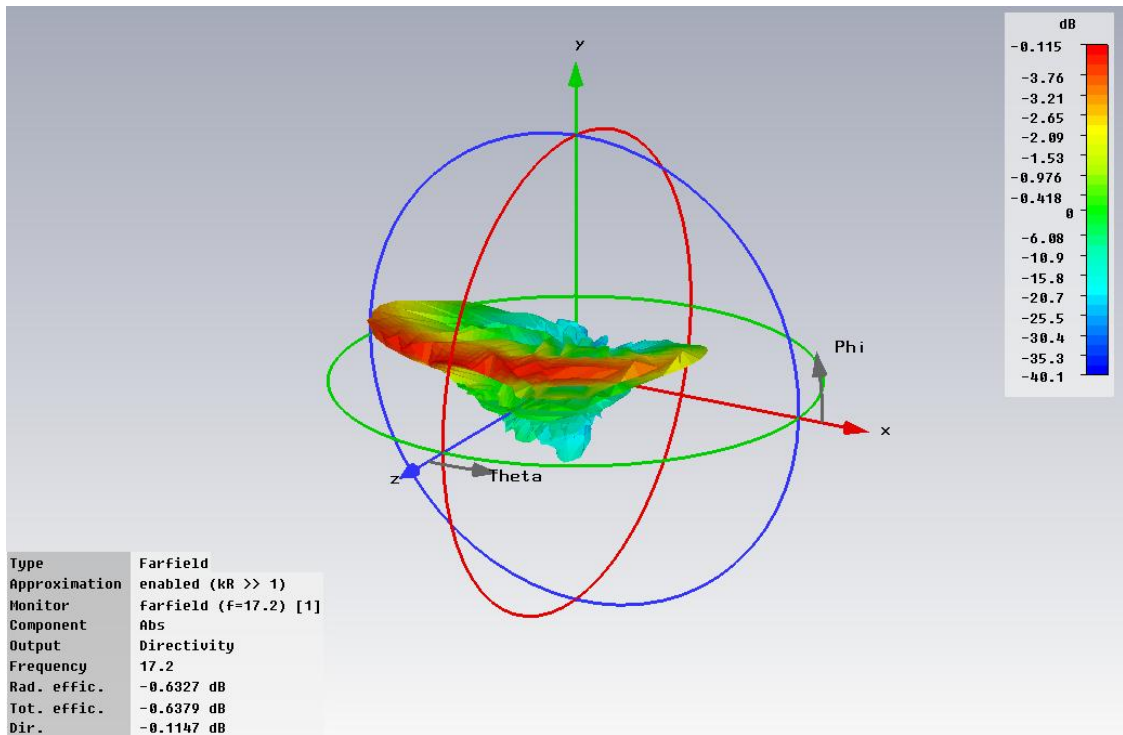


Figure 3-37: 3D radiation pattern at 17.2 GHz

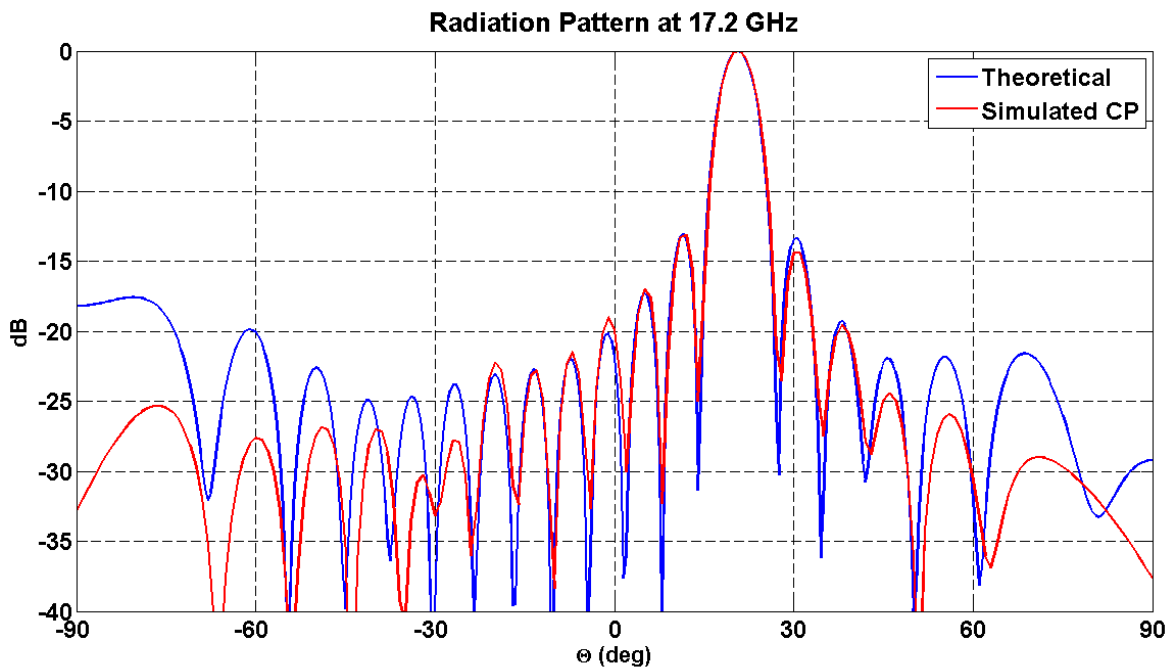


Figure 3-38: Simulated co-polar component of the radiation pattern at 17.2 GHz vs. the theoretical one

3. Design of Antennas

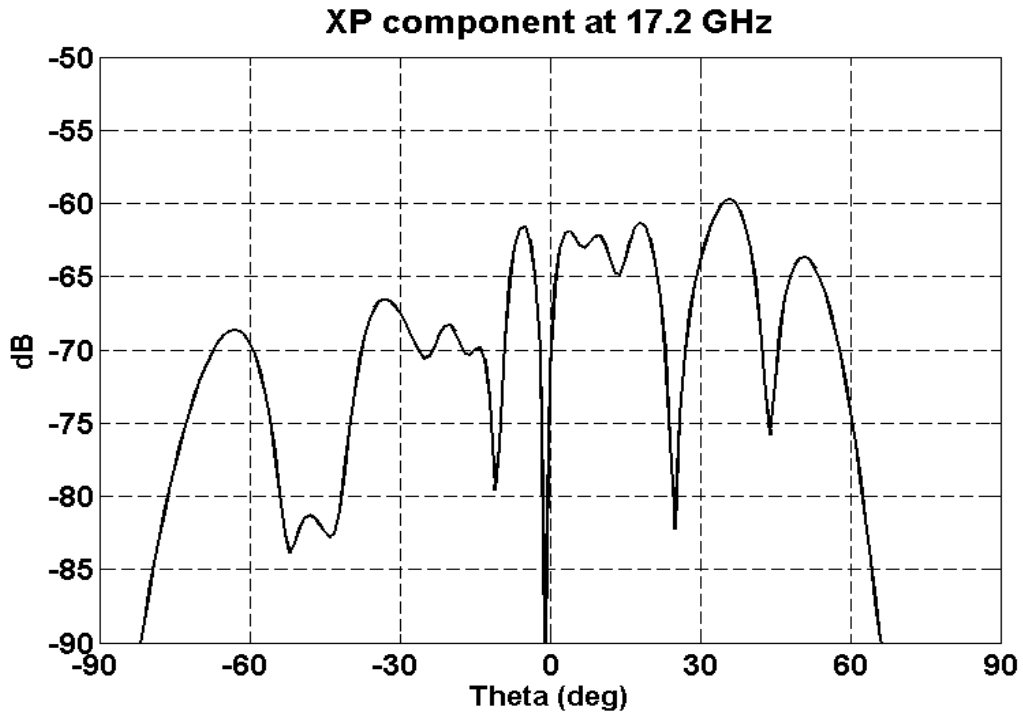


Figure 3-39: Cross-polar component of the radiation pattern at 17.2 GHz

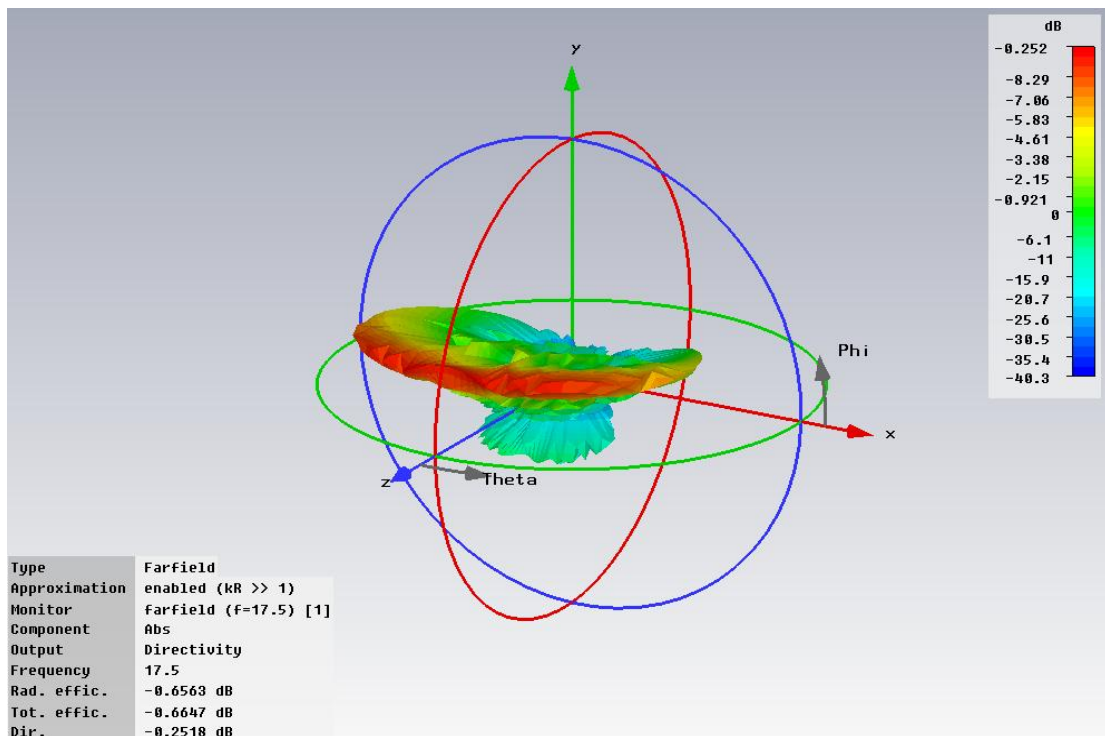


Figure 3-40: 3D radiation pattern at 17.5 GHz

3. Design of Antennas

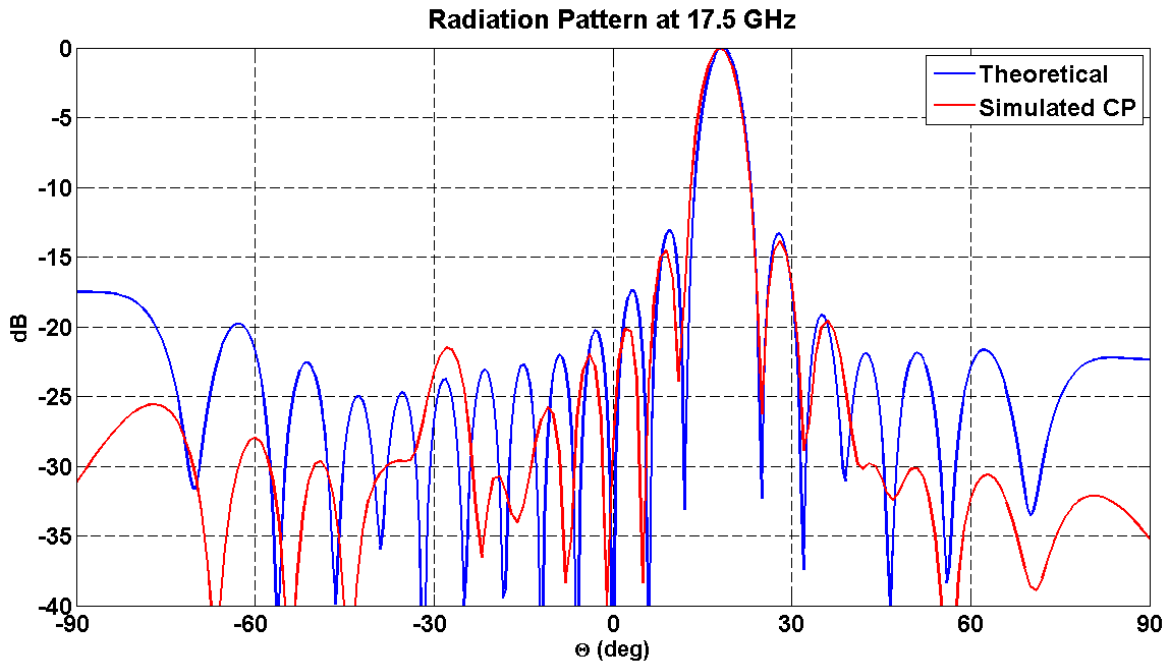


Figure 3-41: Simulated co-polar component of the radiation pattern at 17.5 GHz vs. the theoretical one

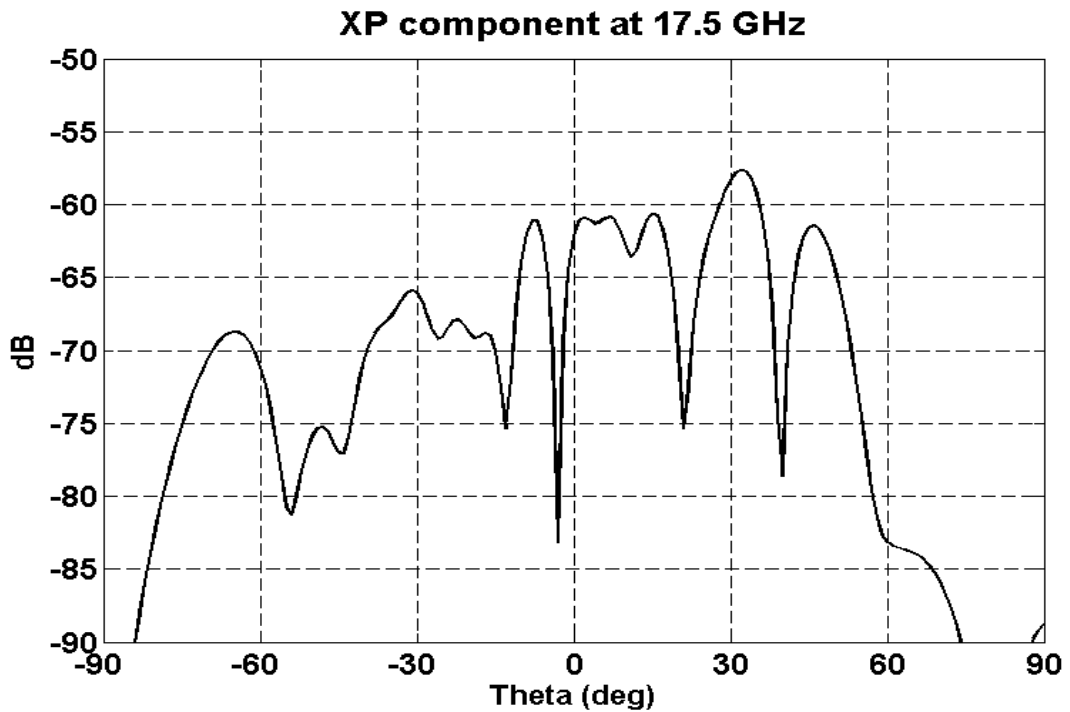


Figure 3-42: Cross-polar component of the radiation pattern at 17.5 GHz

3. Design of Antennas

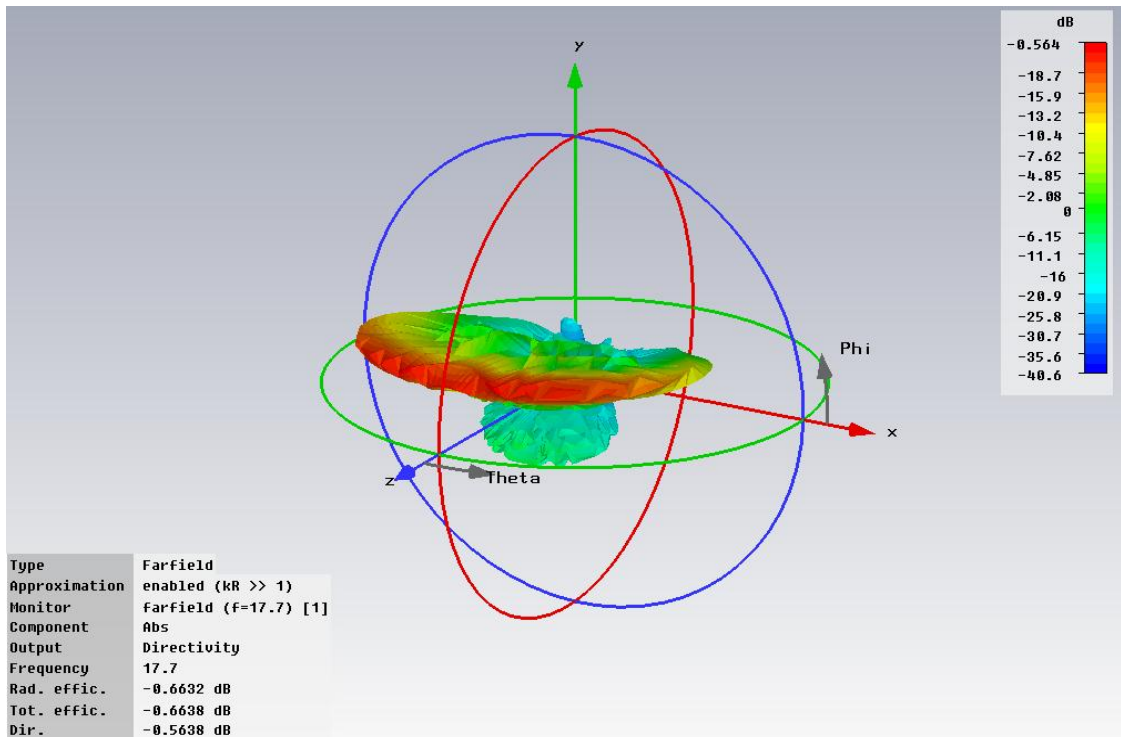


Figure 3-43: 3D radiation pattern at 17.7 GHz

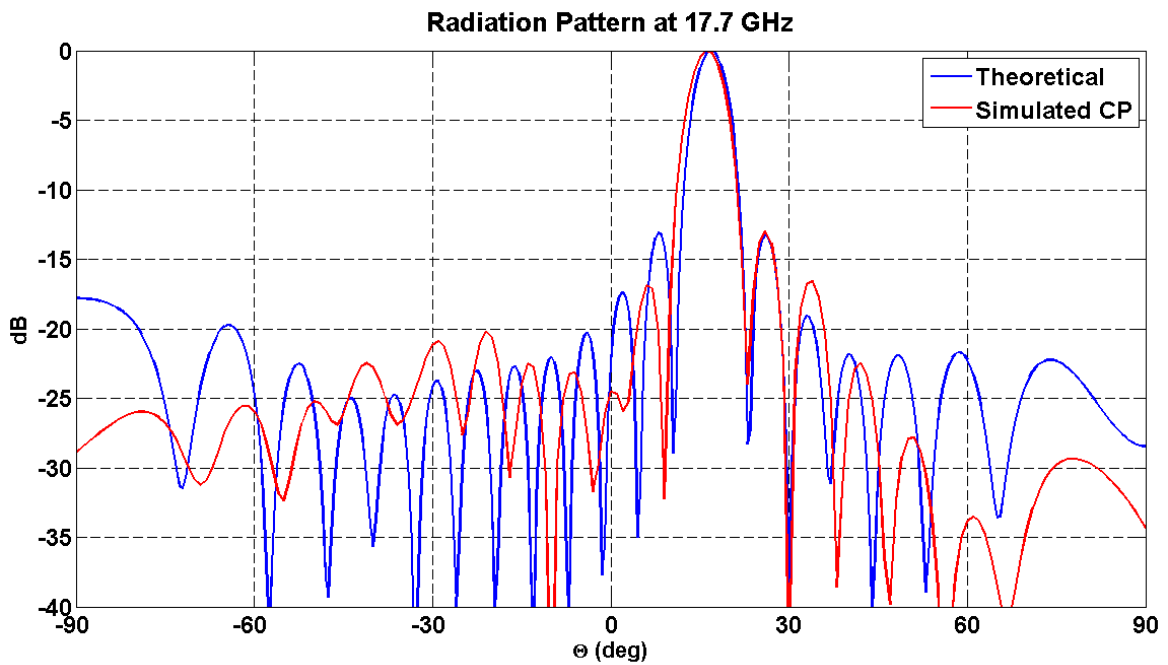


Figure 3-44: Simulated co-polar component of the radiation pattern at 17.5 GHz vs. the theoretical one

3. Design of Antennas

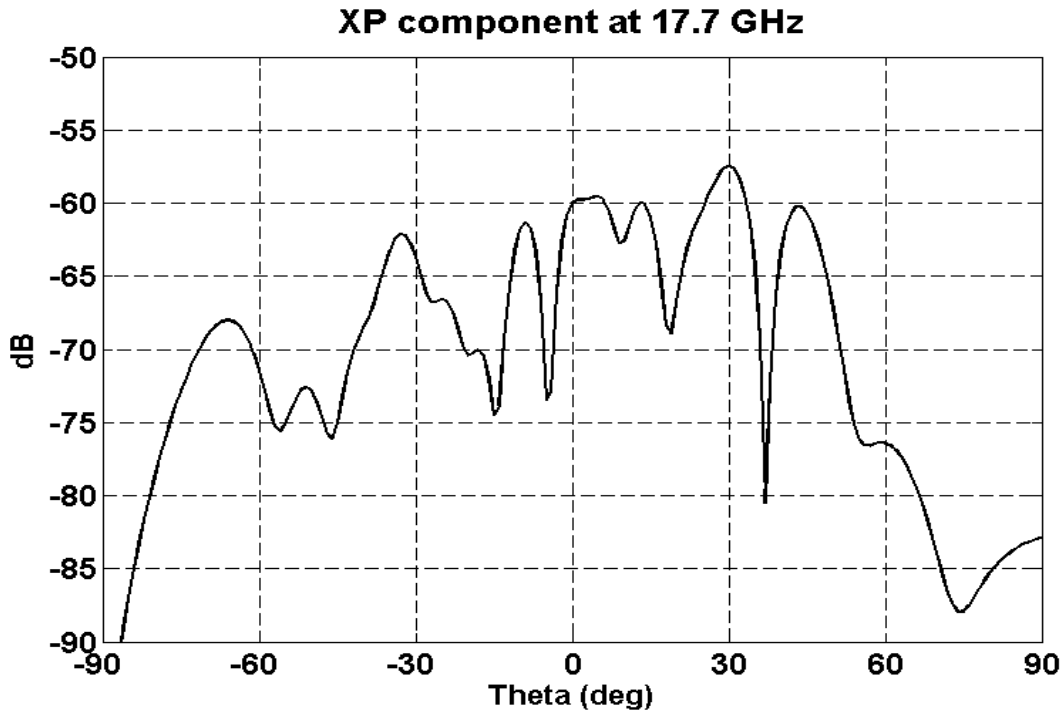


Figure 3-45: Cross-polar component of the radiation pattern at 17.7 GHz

3.7.2.3 Gain

Previously, the radiation patterns have been presented as normalized directivity. Now, the different gain values for several samples of the frequency working range are exposed as follows:

Freq. (GHz)	16.3	16.5	16.8	17	17.2	17.5	17.7
Gain (dB)	17.576	17.709	17.835	17.886	17.913	17.808	17.558

Table 3-11: Maximum gain values of the radiation at different frequencies

3.7.3 Conclusions

From the simulations' results, some conclusions can be drawn from the different radiation patterns and the behavior at different frequencies.

In first place, the results of the radiation patterns show a great resemblance between the theoretical radiation pattern and the finally obtained one. The application of the near-field compensation model has proved to be very accurate, from the results of the coupling coefficients summarized in Table 3-13. This has led to almost equal radiation patterns, achieving SLL of -12.7 dB versus the -13 dB given by the theoretical radiation pattern.

Secondly, a deviation in the main lobe direction of propagation is observed as the frequency monitor is varied. From equation (2.24), it can be seen that array factor behaves as a function of frequency (through k). Due to this, the phase of the array factor varies, and

3. Design of Antennas

consequently the direction of propagation. As the design has been optimized for the central frequency of 17 GHz, a slight loss in directivity and gain appears for other frequencies. Obviously, this also affects the level of the secondary lobes and the nulls found close to the main lobe. However, it can be seen that the SLL are good enough and this variation is not relevant.

Furthermore, the antenna has a very good linear polarization. The difference between the co-polar and the cross-polar components is highly notable, with values below -55 dB all over the frequency range.

Finally, the reflection of the antenna is still at acceptable values after the junction of the linear array and the proposed transition.

Elem. (k)	F _k	S _k (dB)	Via Diam. (mm.)	Dist. (mm.)	Line's Width (mm.)	Line's Length (mm.)	Distance (mm.)	Inf. Patch (mm.)	Sup. Patch (mm.)	Sold. Ring (mm.)	L_strech (mm.)	Coupling (dB)	Δφ (°)
1	1	-12.0411	0.6	0.25	0.55(rad.)	0.55(rad.)	-	2.86	3.235	0.58	0.6	-10,9092	-
2	1	-11.7609	0.6	0.25	0.55(rad.)	0.55(rad.)	0.24	2.86	3.235	0.58	0.6	-13,6302	94,70
3	1	-11.4612	0.6	0.25	0.585(rad.)	0.585(rad.)	0.2	2.86	3.235	0.58	0.6	-12,8679	79,32
4	1	-11.1394	0.6	0.25	1.15	1.15	0.06	2.86	3.235	0.58	0.6	-12,4386	90,09
5	1	-10.7918	0.6	0.25	1.2	1.2	0.2	2.86	3.235	0.58	0.6	-12,6603	86,25
6	1	-10.4139	0.6	0.25	1.5	1.3	0.18	2.86	3.235	0.58	0.6	-12,0712	86,02
7	1	-10.0000	0.6	0.25	1.55	1.55	0.17	2.86	3.235	0.58	0.6	-11,8755	82,21
8	1	-9.5424	0.6	0.25	2.1	1.8	0.12	2.86	3.235	0.58	0.6	-11,1847	81,60
9	1	-9.0308	0.6	0.25	2.8	2.8	0.25	2.86	3.235	0.58	0.6	-9,82305	74.81
10	1	-8.4509	0.6	0.25	3.35	3.6	0.35	2.86	3.235	0.58	0.6	-9,15063	76,48
11	1	-7.7815	0.6	0.25	4.2	3.8	0.4	2.86	3.235	0.58	0.6	-11,0026	80,23
12	1	-6.9897	0.6	0.25	5	4.15	0.42	2.86	3.235	0.58	0.6	-11,4847	83,04
13	1	-6.0205	0.6	0.25	7.4	4.25	0.44	2.86	3.235	0.58	0.6	-13,5612	84.62
14	1	-4.7712	0.6	0.25	8.5	4.55	-0.1	2.86	3.235	0.58	0.6	-12,4866	76,15
15	1	-3.0102	0.8	0.25	8.63	4.55	0.5	2.86	3.25	0.65	0.6	-15,0389	115,60
16	1	0	0.6	-	-	-	0.7	3.05	3.2	0.645	0	-28,1070	18,16

Table 3-12: Summary table of the parameters of the initial linear array

Elem. (k)	F _k	S _k (dB)	Via Diam. (mm.)	Dist. (mm.)	Line's Width (mm.)	Line's Length (mm.)	Distance (mm.)	Inf. Patch (mm.)	Sup. Patch (mm.)	Sold. Ring (mm.)	L_strech (mm.)	Coupling (dB)	Δφ (°)
1	1	-12.0411	0.6	0.25	0.55(rad.)	0.55(rad.)	-	2.86	3.235	0.58	0.6	-10.9708	82.83
2	1	-11.7609	0.6	0.25	0.595(rad.)	0.595(rad.)	0.4	2.86	3.235	0.58	0.6	-12.2857	78.10
3	1	-11.4612	0.6	0.25	0.66(rad.)	0.66(rad.)	0.03	2.86	3.235	0.58	0.6	-12.0250	82.22
4	1	-11.1394	0.6	0.25	1.3	1.2	0.4	2.86	3.235	0.58	0.6	-12.1766	77.62
5	1	-10.7918	0.6	0.25	1.3	1.3	0.22	2.86	3.235	0.58	0.6	-12.1683	81.22
6	1	-10.4139	0.6	0.25	1.45	1.35	0.31	2.86	3.235	0.58	0.6	-12.1186	81.12
7	1	-10.0000	0.6	0.25	1.55	1.5	0.16	2.86	3.235	0.58	0.6	-12.0625	76.53
8	1	-9.5424	0.6	0.25	1.95	1.6	0.23	2.86	3.235	0.58	0.6	-12.0235	87.42
9	1	-9.0308	0.6	0.25	1.8	1.5	0.22	2.86	3.235	0.58	0.6	-12.0754	69.68
10	1	-8.4509	0.6	0.25	2.85	2.2	0.23	2.86	3.235	0.58	0.6	-12.1463	87.04
11	1	-7.7815	0.6	0.25	2.4	2.05	0.2	2.86	3.235	0.58	0.6	-11.9788	71.44
12	1	-6.9897	0.6	0.25	4.5	3.1	0	2.86	3.235	0.58	0.6	-12.1147	89.60
13	1	-6.0205	0.6	0.25	5.5	3.35	-0.05	2.86	3.235	0.58	0.6	-12.1111	66.42
14	1	-4.7712	0.6	0.25	8.55	4.4	-0.9	2.86	3.235	0.58	0.6	-12.0329	86.23
15	1	-3.0102	0.8	0.25	8.55	4.55	1.2	2.86	3.25	0.65	0.6	-12.1185	76.92
16	1	0	0.6	-	-	-	0.9	3.05	3.2	0.645	0	-12.4248	82.83

Table 3-13: Summary table of the parameters of the final linear array, after applying the near-field compensating model

4 DESIGN OF TRANSITIONS

4.1 Introduction

In this chapter it is described the designed transition for the linear array antenna. Printed circuit technology enables different feeding techniques, for coaxial connectors either vertically or horizontally positioned. However, some of these configurations are not recommended for the working frequency band or the available manufacturing technology at EPS printed circuit laboratory.

After a brief analysis of some possible transition designs with their advantages and drawbacks, a thorough explanation of the transition implemented will be made and the presentation of the obtained results.

4.2 Printed Circuit Feeding Transitions

Regarding the possible transitions that can be implemented, there are two main groups: vertical SMA connector and horizontal SMA connector. This type of connector is chosen because the measurements made at EPS with the network analyzer require standard coaxial cables.

4.2.1 Vertical SMA Connector

This kind of transition apparently provides a simple and effective solution to the feeding of a SIW circuit. The inner conductor of the connector can be directly inserted in the dielectric of the SIW as mentioned in 2.6.1 or through a microstrip line which matched the connector's impedance to the SIW input impedance.

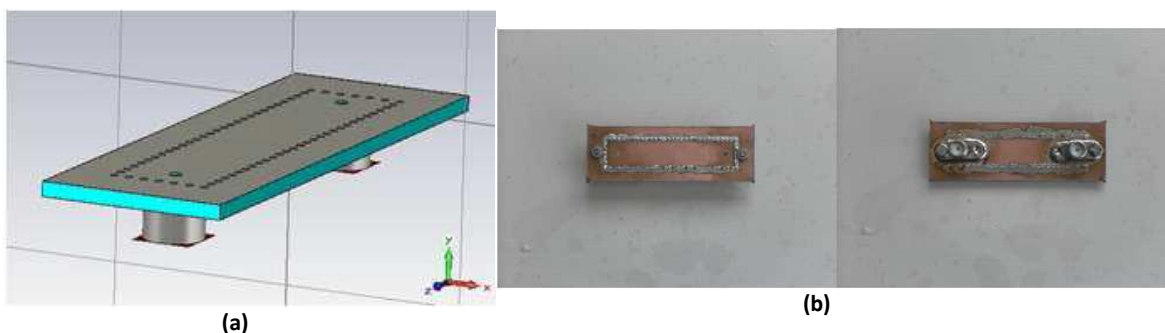


Figure 4-1: Design in CST (a) and prototype fabricated (b) of a vertical SMA transition to SIW back-to-back

Despite obtaining hopeful results concerning the reflection of the transition, manufacturing limitations prevented from developing a feeding system with stable behavior. The main problem found during the manufacturing process was the difficulty to adjust with

4. Design of Transitions

precision the length of the inner connector. Either in the case of direct feeding in the SIW or by a microstrip line, it is very difficult to manually file the inner conductor to the desired length. Working at 17 GHz means that differences of a tenth of millimeter in the inner conductor cause severe variations in the reflection response, up to 5 dB. Given the available material at the printed circuit laboratory, it was impossible to ensure that the prototypes would have the same dimensions as the designs in CST Microwave Studio. From the study made in [16], it can be seen that if good results are sought this type of transition is not the appropriate one.

In addition to the precision difficulty, if there is a microstrip line another problem could appear. If the line is long enough, the transmission is severely degraded due to electromagnetic radiation. As the structure lacks of electromagnetic isolation, the microstrip line radiates with a significant efficiency, resulting in ineligious transmission losses.

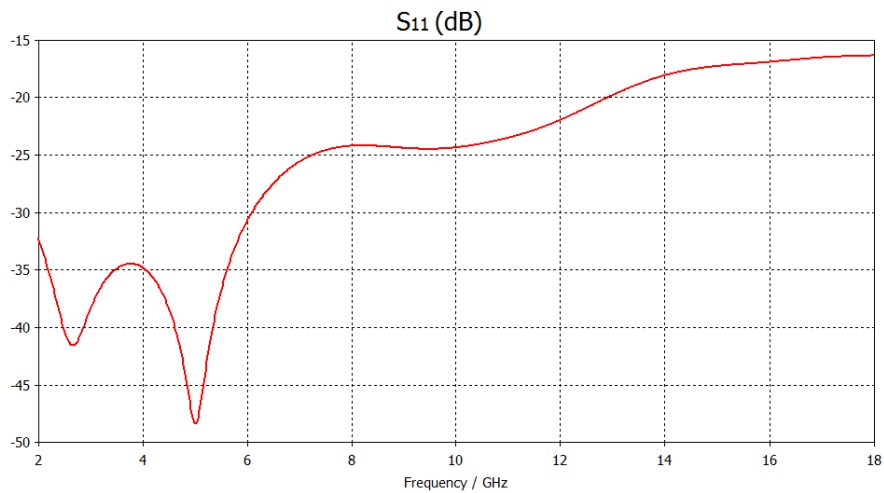


Figure 4-2: S_{11} parameter response of a SMA coaxial connector with a microstrip line

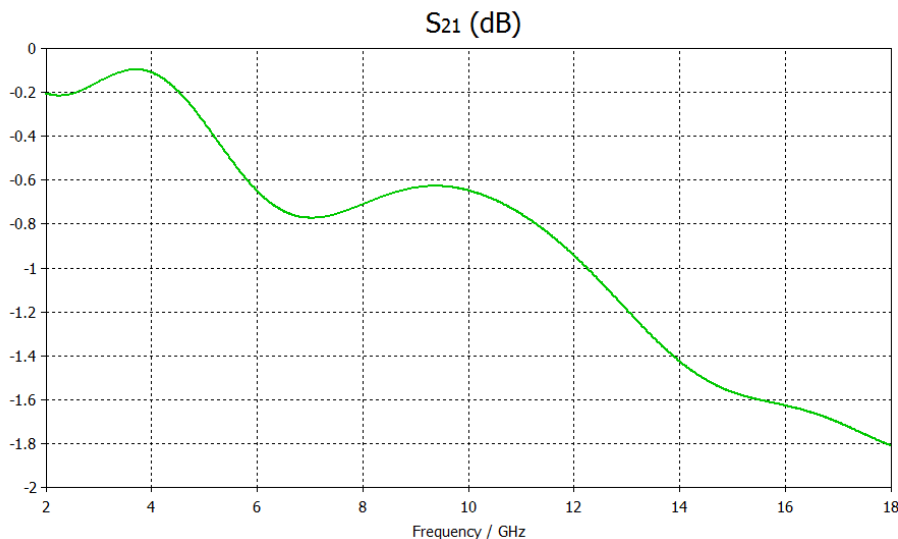


Figure 4-3: S_{21} parameter response of a SMA coaxial connector with a microstrip line

As it can be seen in Figure 4-2 and Figure 4-3, for a regular SMA coaxial connector and frequencies lower than 8 GHz the matching is almost perfect. Nevertheless, for higher frequencies the connector's behavior worsens.

4. Design of Transitions

4.2.2 Horizontal SMA Connector

Placing a horizontal connector avoids the disadvantages of the imprecise filing of the inner conductor of the coaxial. Unfortunately, the transmitted signal must reach the SIW through a microstrip line, so the radiation problem shows up again. Moreover, this fact is aggravated by the radiation of the bare inner conductor.

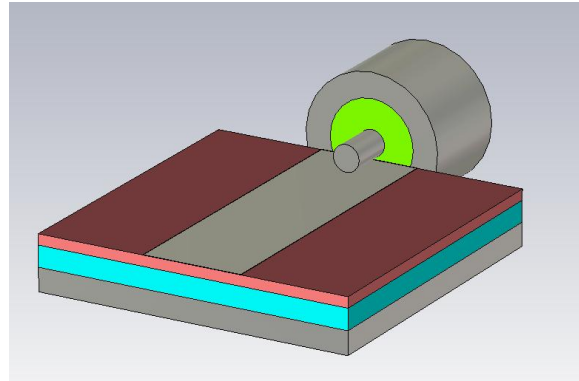


Figure 4-4: Horizontal SMA coaxial connector and microstrip line

Given that the horizontal connector is the most reasonable option of the two, it seems necessary to provide some kind of electromagnetic isolation to confine the signal and reduce losses associated to the radiation. For this reason, a metallic cover has been designed to enclose the connector.

4.3 Proposed Transition

4.3.1 General Features

The final design of the transition is based on the model proposed by [17]. It consists of two metallic pieces, one covering the inner conductor and the microstrip line and the other for fixing the connector and enabling screwing of the other piece to the linear array structure.

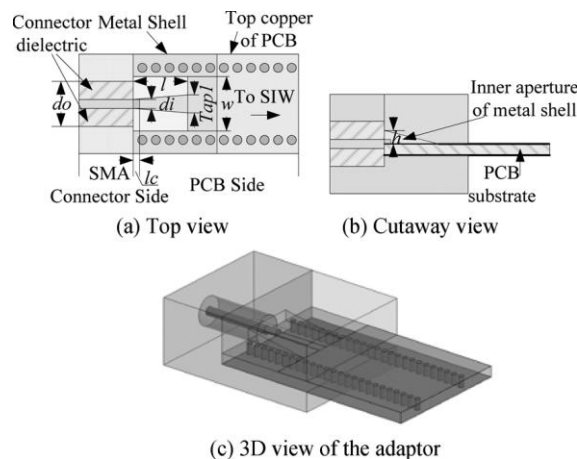


Figure 4-5: Scheme of the coaxial-microstrip-SIW transition proposed in [17]

4. Design of Transitions

The inner conductor of the coaxial connector is placed over a microstrip line, which feeds a section of SIW before reaching the linear array. Finally, the vias that form the lateral walls of the SIW are extended to the end of the dielectric (included the microstrip section), in order to favor the signal confinement inside the dielectric. All the parameters involved in the metallic pieces, the microstrip line and the SIW section have been optimized to provide the best results in reflection terms.

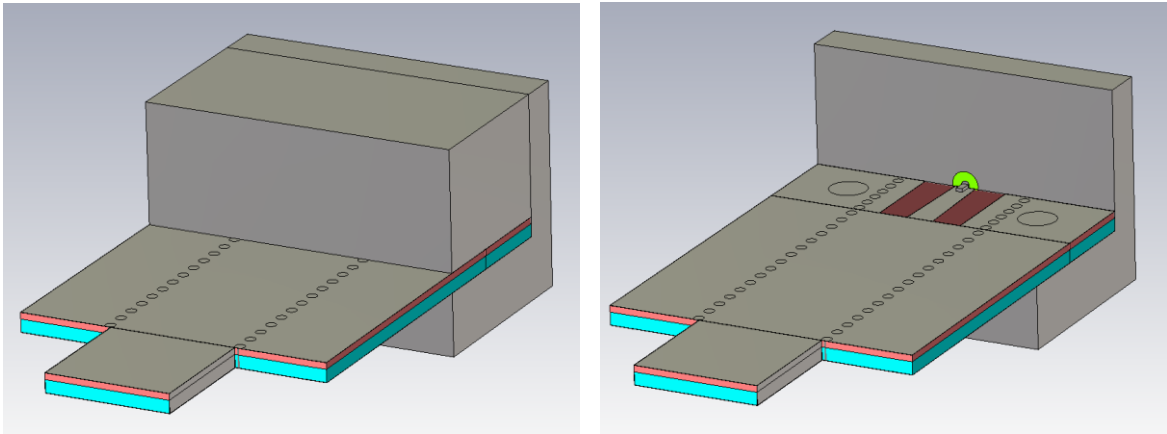


Figure 4-6: Design of the proposed transition in CST Microwave Studio, with and without the upper piece

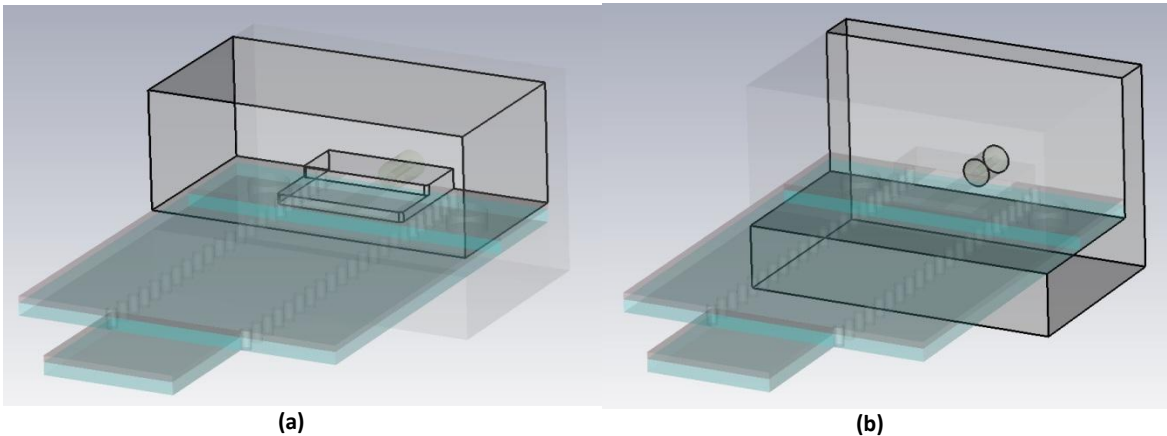


Figure 4-7: View of the two metallic pieces of the proposed transition: upper cover (a) and connector fixer (b)

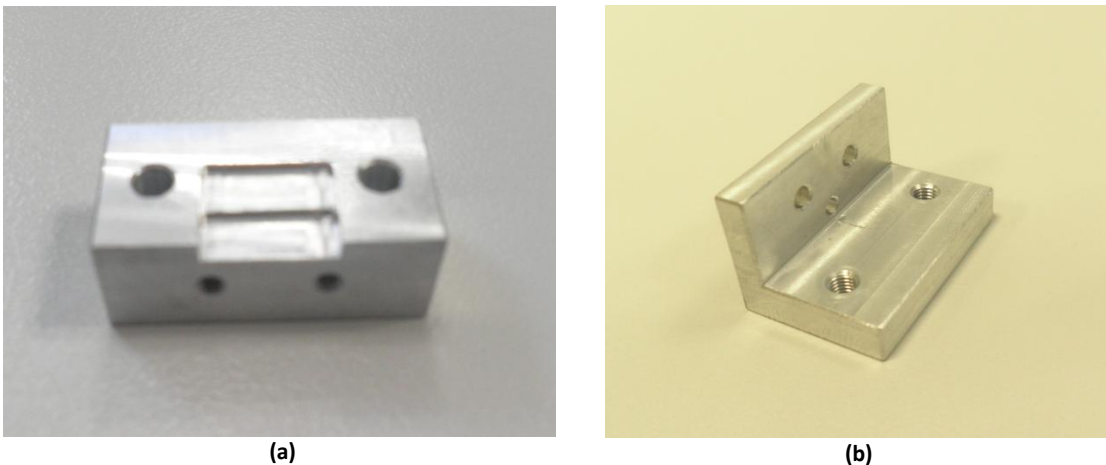


Figure 4-8: Manufactured transition pieces, insulating box (a) and connector fixer (b)

4. Design of Transitions

Both pieces have been manufactured externally to EPS, and for the fixer piece with 'L' form, two different models are available for two different connectors [18] and [19]. The reason for making the design for two different connectors is economical, as one of them is considerably cheaper than the other one. The upper piece (a in Figure 4-7) has an emptying in the area above the microstrip line, made in two steps to soften the impact of the signal propagation.

The function of the microstrip line is to match the connector's impedance to the input impedance of the SIW. There is an area where the copper of the substrate has been removed, to form the microstrip line, but kept to continue with the SIW structure from the linear array. The microstrip is tapered to make a smooth transition from the inner conductor, but being careful about not causing a short-circuit with the metal of the fixer piece.

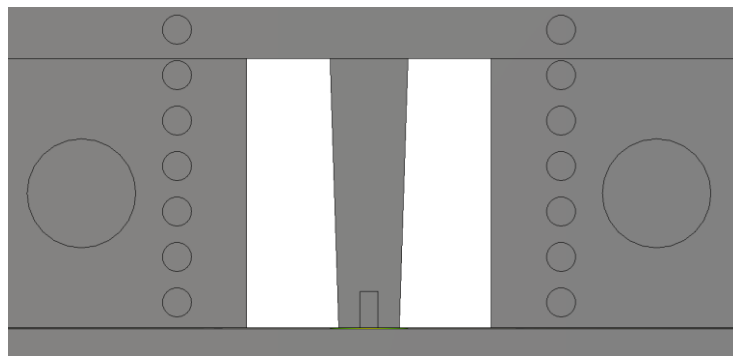


Figure 4-9: Detail of the tapered microstrip line, with an emptying around it and the extension of the SIW's vias

Detailed plans of each metallic piece and the transition section, with all the concerning parameters, can be consulted in appendix E.

4.3.2 Simulation Results

The reflection coefficient in dB and in Smith chart and the transmission coefficient for both connectors are presented as follows:

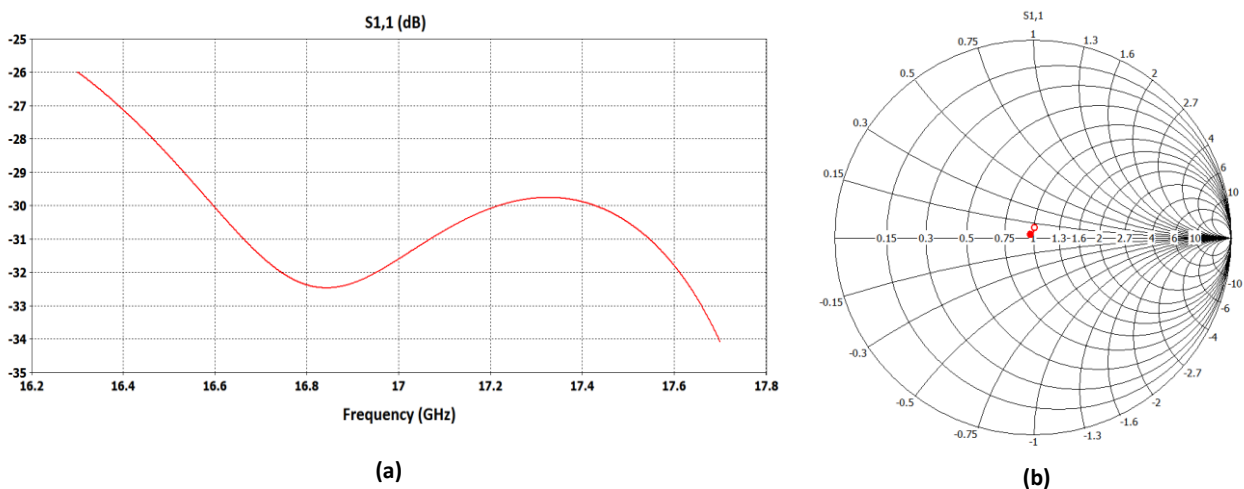


Figure 4-10: Reflection coefficient in dB (a) and in Smith chart (b) for the transition with connector [18]

4. Design of Transitions

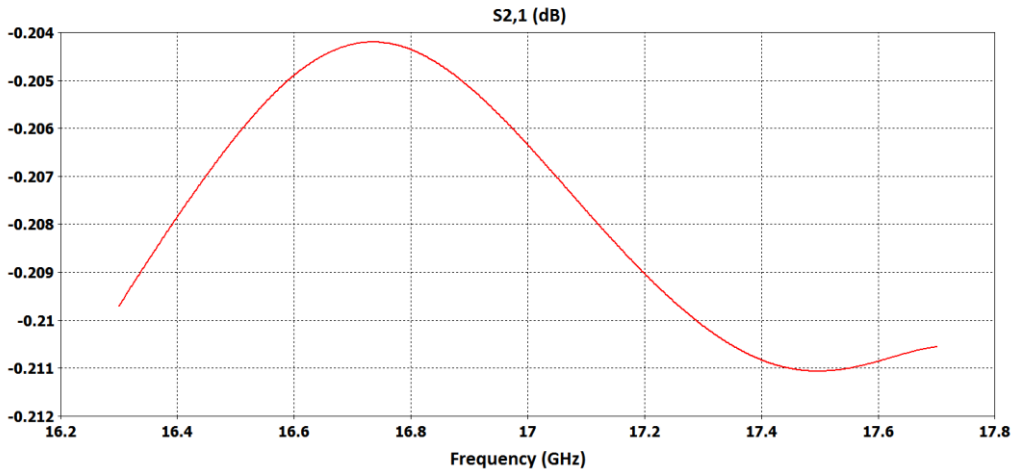


Figure 4-11: Transmission coefficient in dB for the transition with connector [18]

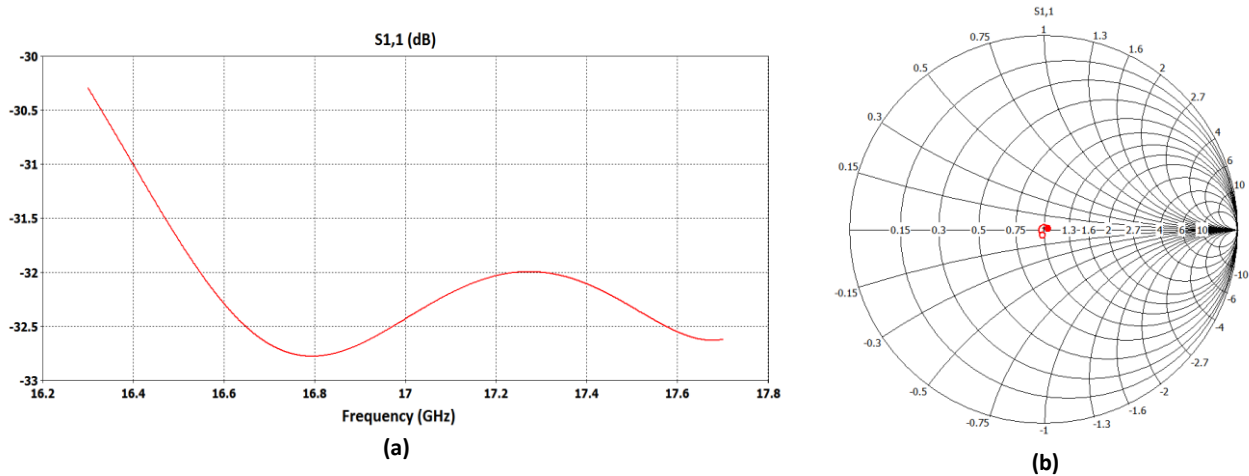


Figure 4-12: Reflection coefficient in dB (a) and in Smith chart (b) for the transition with connector [19]

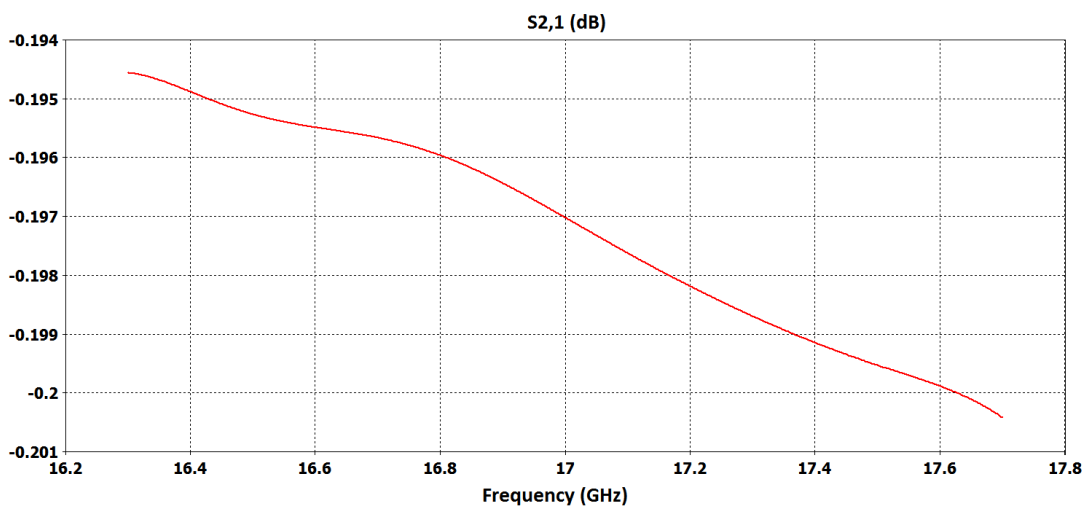


Figure 4-13: Transmission coefficient in dB for the transition with connector [19]

As it can be seen, both connectors have very good levels of matching. The most relevant feature is that both are integrated with the same upper metallic piece, and microstrip

4. Design of Transitions

and SIW section have the same measures; with the only exception of the fixer piece which is necessarily different. With these results, it is guaranteed that the linear array will have an acceptable reflection which will not degrade the behavior characterized in the previous chapter.

In relation to the electromagnetic radiation of the transition, the radiation patterns of the structure at 17 GHz for both connectors are the following ones:

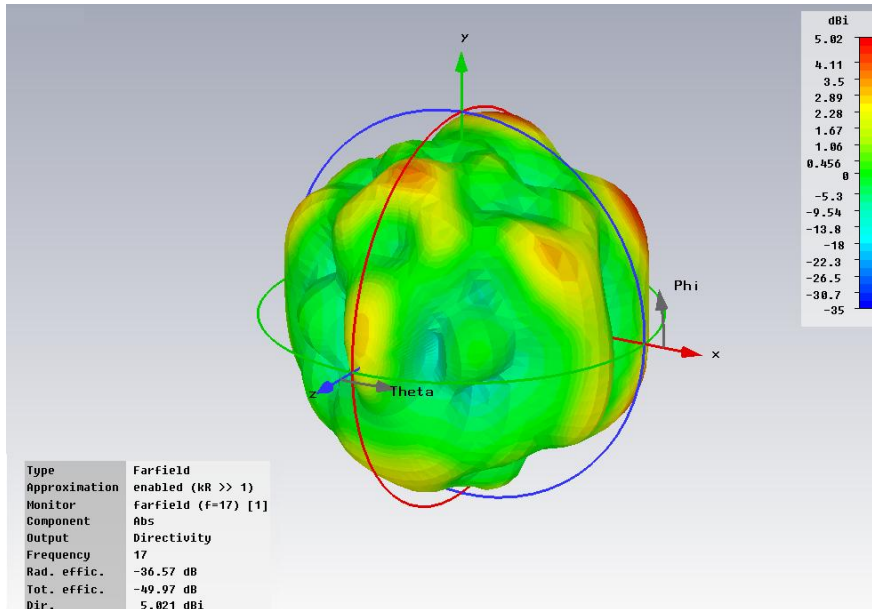


Figure 4-14: Radiation pattern in 3D at 17 GHz for the connector [18]

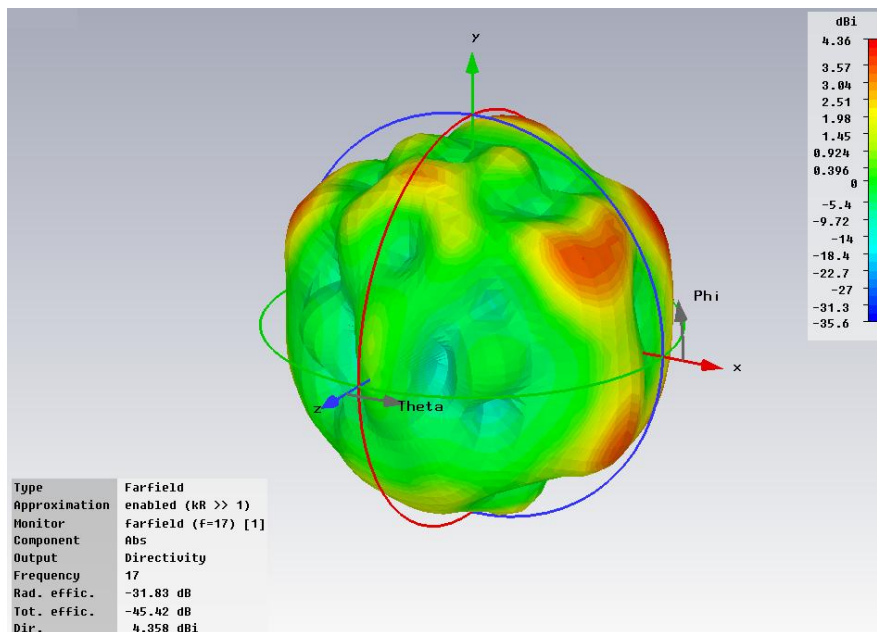


Figure 4-15: Radiation pattern in 3D at 17 GHz for the connector [19]

From the results obtained from the simulations, the radiation efficiency is almost negligible, reaching levels below -31 dB for both connectors. Apart from reducing the losses associated to radiation, this will be very beneficial as the radiation pattern of the linear array will not be disturbed by unwanted radiation from the transition.

5 INTEGRATION AND RESULTS

5.1 Proposed Transition

In this chapter, the union process of the designed linear array and transition takes place. Once this is done, the results from the simulations after applying the near-field compensation coupling model are presented. Afterwards, the process of manufacturing and assembly of the prototype of the linear array antenna is described, followed by the results of the measurements. Finally, the simulated and measured results will be analyzed and compared.

5.2 Union of the Linear Array Antenna

In chapters 3 and 4, the design processes of the linear array and the transition have been described. As it has been mentioned before, although the individual designs were well matched, at the time of their junction the result is degraded. The optimization process which provides the results exposed in chapter 3 has focused on the adjustment of the radiation pattern of the antenna, trying to obtain the most similar radiation pattern to the theoretical one.

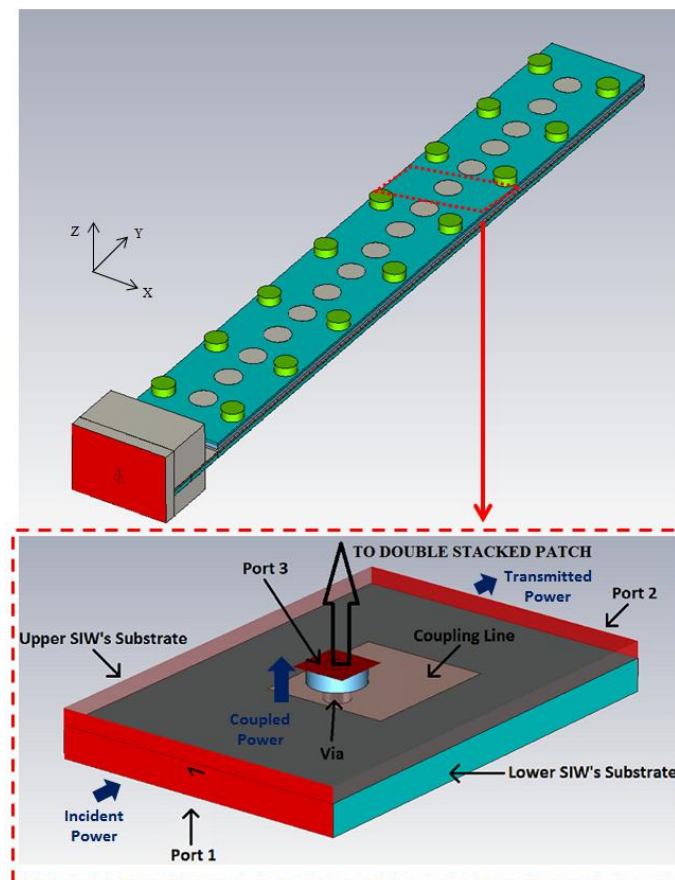


Figure 5-1: Linear array antenna with the designed transition, and a detail of coupling line section

5. Integration and Results

For this matter, the compensation coupling model explained in 3.7.1 has been used. From the extracted electric near-field, adjustments in the dimensions of the coupling lines and inter-element distance are made. The final goal is trying to improve the radiation pattern shown in Figure 3-21 in both co-polar and cross-polar to make it more alike the theoretical one, while maintaining good enough levels of matching in the whole structure. Reached this point, not only the close radiating elements disturb the coupling coefficient of each element; but also the transition deteriorates the radiation pattern of the linear array. Moreover, bearing in mind the later construction of the prototype, several mounting screws have been placed to fix the double patch structure to the feeding SIW array and enable later measurement of the antenna in an anechoic chamber.

5.3 Manufacturing of the Prototype

In order to check the results obtained from the simulations of the design, a prototype of the linear array antenna has been manufactured. The prototype has been fully fabricated at the laboratory of printed circuits of EPS, with the exception of the metallic transition pieces described in 4.3.1. The manufacturing process consisted of the following stages:

- 1) Construction of the all the different layers involved in the linear array antenna.
- 2) Mounting of the upper SIW substrate with the lower patch layer.
- 3) Assembly of the SIW.
- 4) Mounting and soldering of the connector and the transition pieces.
- 5) Final assembly of the double stacked patch structure.

A more detailed description of the steps needed to obtain the files required for the printed circuit manufacturing machine can be found in appendix C.

5.3.1 Construction of all Layers

The first step is to manufacture the different layers which integrate the antenna. With the substrates described in 3.2, the layers have been fabricated in the LKPF machine; with the exception of the ROHACELL layer which has been manually cut and drilled.

There had been some problems concerning the construction of the upper patch layer and the upper SIW layer. For the first one, the difficulty is related to the stiffness of the material. As it is Teflon-based and very thin, it is very flexible and the printed circuit machine had problems to appropriately remove the copper. Regarding the upper SIW layer, the main difficulty has been to match with precision the elements of the top and bottom of the layer. The machine has to perform an emptying in the top to avoid short-circuit with the coupling via, and to etch in the bottom to make the coupling lines. A drill is required to connect both planes, and it needs to be placed in the appropriate location to meet the design's requirements. A poor correspondence between both planes will result in a misalignment, which would considerably degrade the antenna's performance.

5. Integration and Results

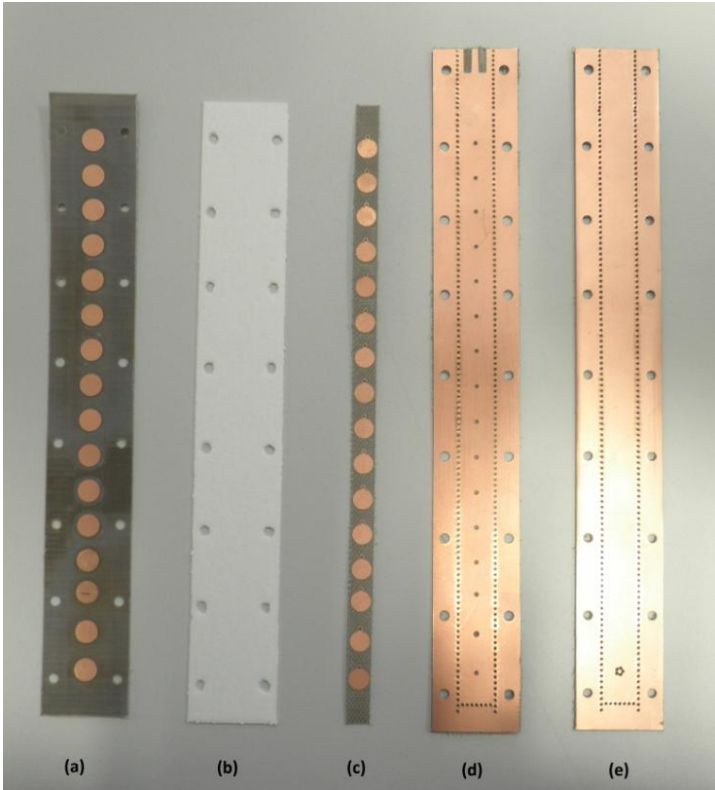


Figure 5-2: Top view of all the layers: upper patch (a), ROHACELL (b), lower patch (c), upper SIW (d) and bottom of lower SIW (e)

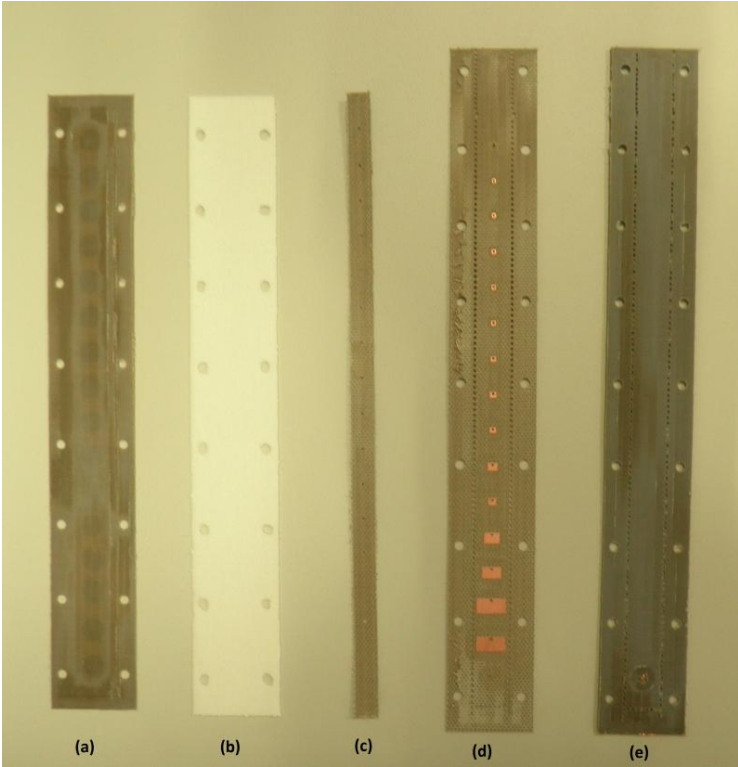


Figure 5-3: Bottom view of all the layers: upper patch (a), ROHACELL (b), lower patch (c), upper SIW (d) and top of lower SIW (e)

5. Integration and Results

5.3.2 Mounting of the Upper SIW and Lower Patch Layers

The first assembly step to be done is connecting the upper SIW layer with the lower patch layer by means of the coupling vias; so the coupling lines are connected with the patch structure.

The lower patch layer has been fabricated narrower than the rest of layers. This has been done for mounting limitations, in order to have access to the drills of both layers of the SIW and enable the later riveting. However, if the SIW were mounted in first place, there will be no access to the coupling lines and it would be impossible to insert and rivet the coupling via.

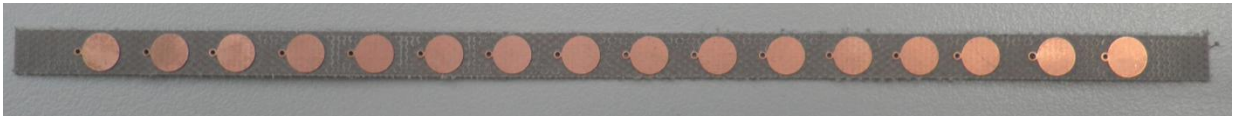
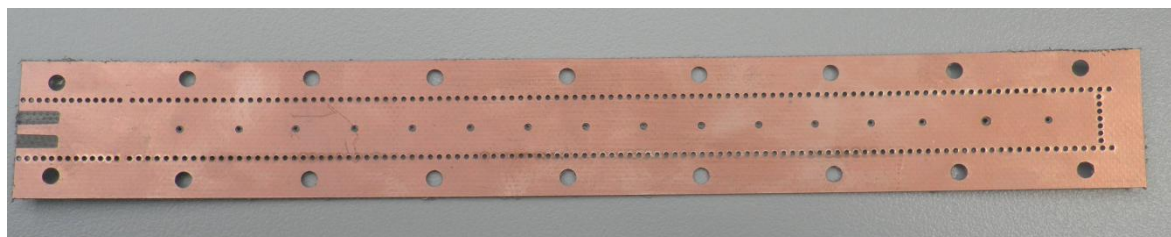


Figure 5-4: Top view of the lower patch layer

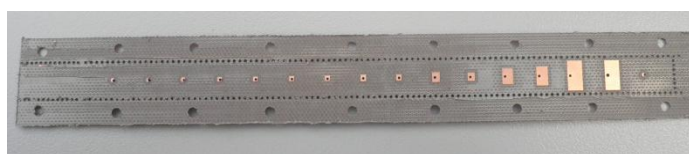


Figure 5-5: Detailed view of the lower patches of the 14th, 15th and 16th elements (from left to right), which include the three different patch structures designed

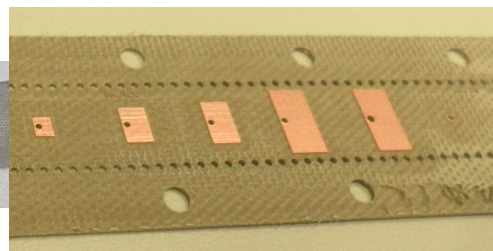
The head of the rivet has been placed in the side of the coupling line, as it occupies less space than the crushed ball. It is important that the layers of the SIW are as stuck as possible, so the dielectric constant of the structure can be maintained.



(a)



(b)



(c)

Figure 5-6: Top view of the upper SIW layer (a), bottom view with the coupling lines (b) and detail of the coupling lines from 11th to 16th element

5. Integration and Results

After the riveting is done, it is necessary to solder both extremes of the coupling via; with extra care in trying to make the soldering tin flow through the hollow rivet to benefit continuity. As these elements are very small, the soldering was made with the aid of a microscope.

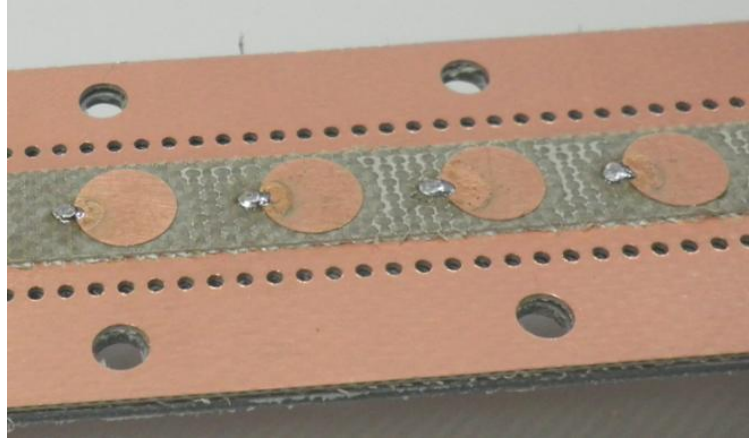
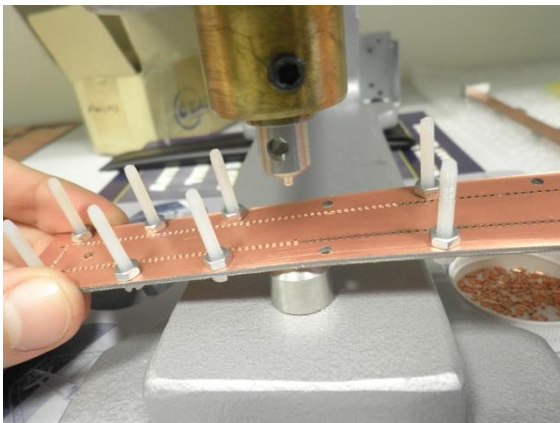


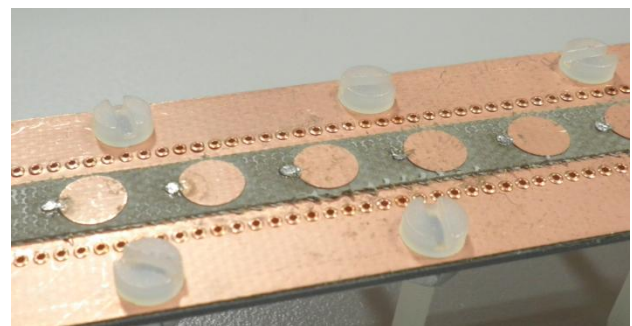
Figure 5-7: Mounted and soldered patches to the coupling vias

5.3.3 Assembly of the SIW

Once the lower patch layer is joined to the upper SIW layer, the assembly of the SIW feeding array may begin. For this stage it is necessary to insert rivets in the holes performed through both layers, and after this process is completed the whole pack is soldered to guarantee metallic continuity. Teflon screws provide pressure to avoid unwilling air gaps during the mounting process and contribute to uniformity.



(a)



(b)

Figure 5-8: Riveting process (a) and SIW completely riveted before soldering (b)

5. Integration and Results

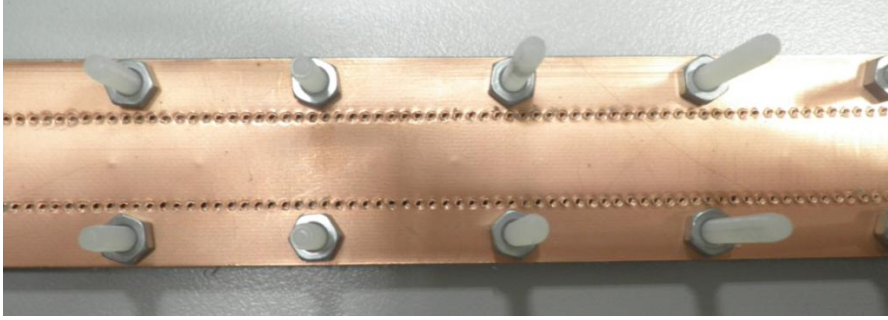


Figure 5-9: Bottom view of the riveted SIW

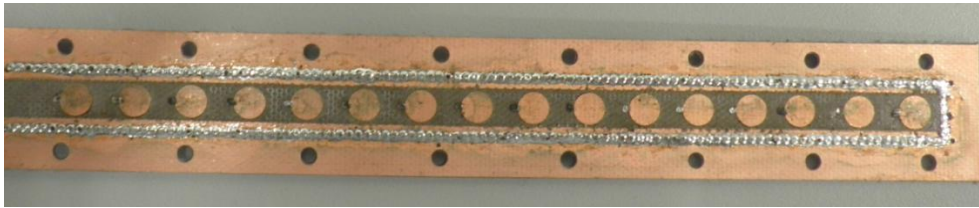


Figure 5-10: Top view of mounted and soldered SIW

5.3.4 Mounting of Connector and Transition

Right after soldering the SIW, the metallic transition pieces and the connector are mounted in the antenna. As the microstrip and transition section are included in the upper SIW layer, it is only necessary to screw the pieces and solder the inner conductor of the connector to the microstrip line.



Figure 5-11: Mounted and soldered connector in the SIW

5. Integration and Results

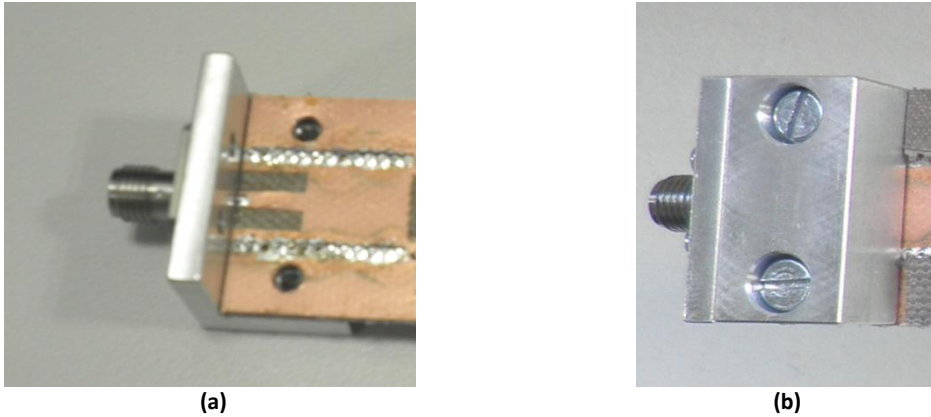


Figure 5-12: Soldered connector (a) and fully mounted transition (b)

5.3.5 Final Assembly of the Patch Structure

Finally, the last step is to join the remaining layers of ROHACELL and the upper patches to the rest of the antenna. The structure is fixed with Teflon screws to avoid electromagnetic interference (although they have already been included in the design's simulations), emphasizing in applying the maximum possible pressure to correctly join all layers.

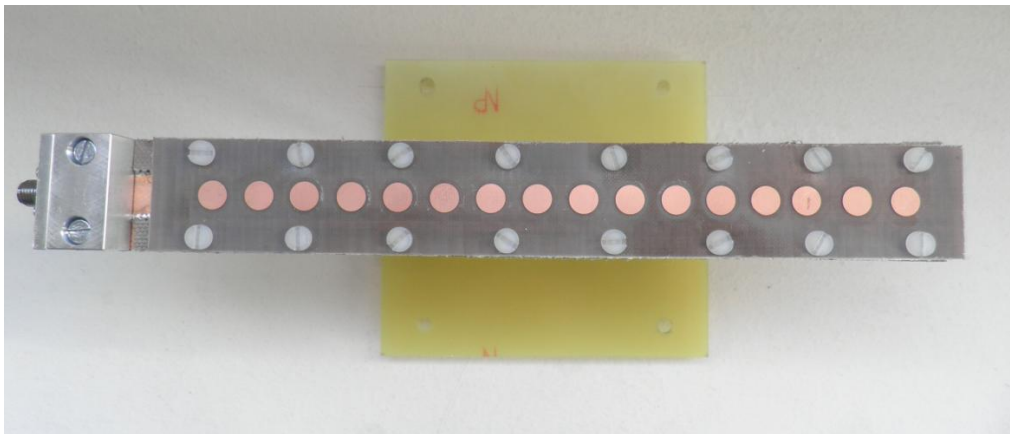


Figure 5-13: Antenna completely assembled with fiber glass piece for later measurement in anechoic chamber

5.4 Prototype's Measurements

With the prototype fabricated, measurements have been made to compare with the results obtained from simulations. It has been characterized the reflection of the antenna with a network analyzer at EPS, and external measurements of the radiation pattern directivity and gain have been carried out in an anechoic chamber.

5.4.1 S_{11} Parameter

For the measurements of the S_{11} parameter, a network analyzer [20] and one coaxial cable [21] has been used. The antenna's S_{11} parameter has been measured for a wider band

5. Integration and Results

than the working one, in order to better analyze the antenna's behavior. The results extracted from the network analyzer are the following ones:

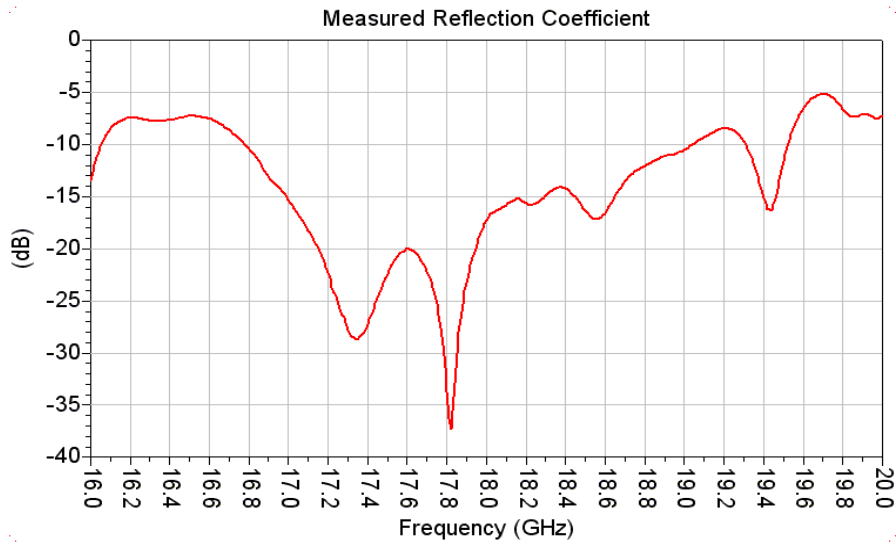


Figure 5-14: Measured S_{11} parameter (in dB)

As it can be seen, the results for the lower band (16.3 – 16.9 GHz) do not correspond with the expected ones. Although certain degree of worsening is expected when comparing the results from simulations versus the prototype's measurements, it is clear that the curve's behavior is not the same in both cases. These results will be analyzed and explained in the conclusions subsection of this chapter.

5.4.2 Radiation Patterns

The radiation pattern of the linear array antenna has been measured for several frequencies, in both co-polar and cross-polar components. The obtained results are the following:

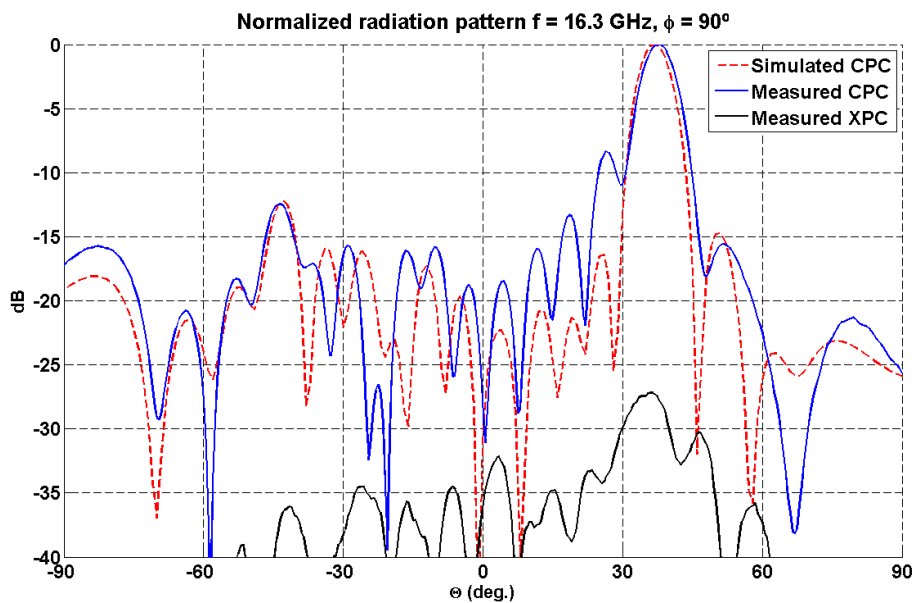


Figure 5-15: Measured co-polar and cross-polar components versus the air gap co-polar component at 16.3 GHz

5. Integration and Results

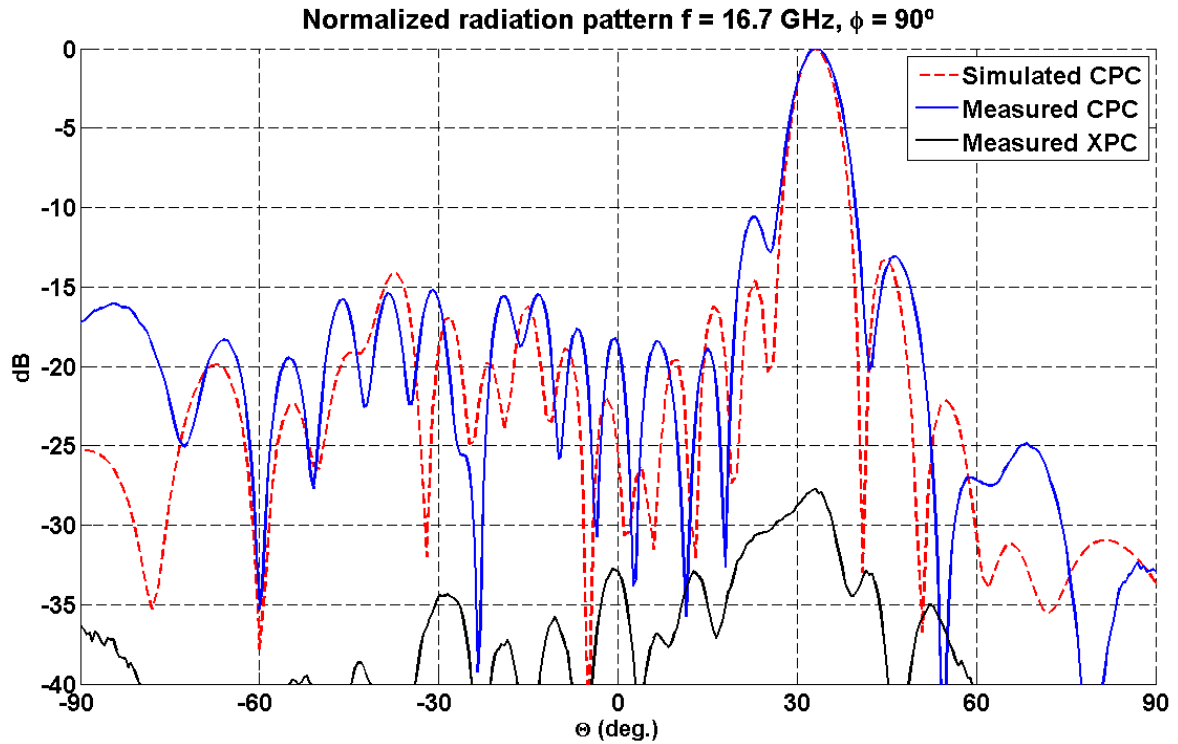


Figure 5-16: Measured co-polar and cross-polar components versus the air gap co-polar component at 16.7 GHz

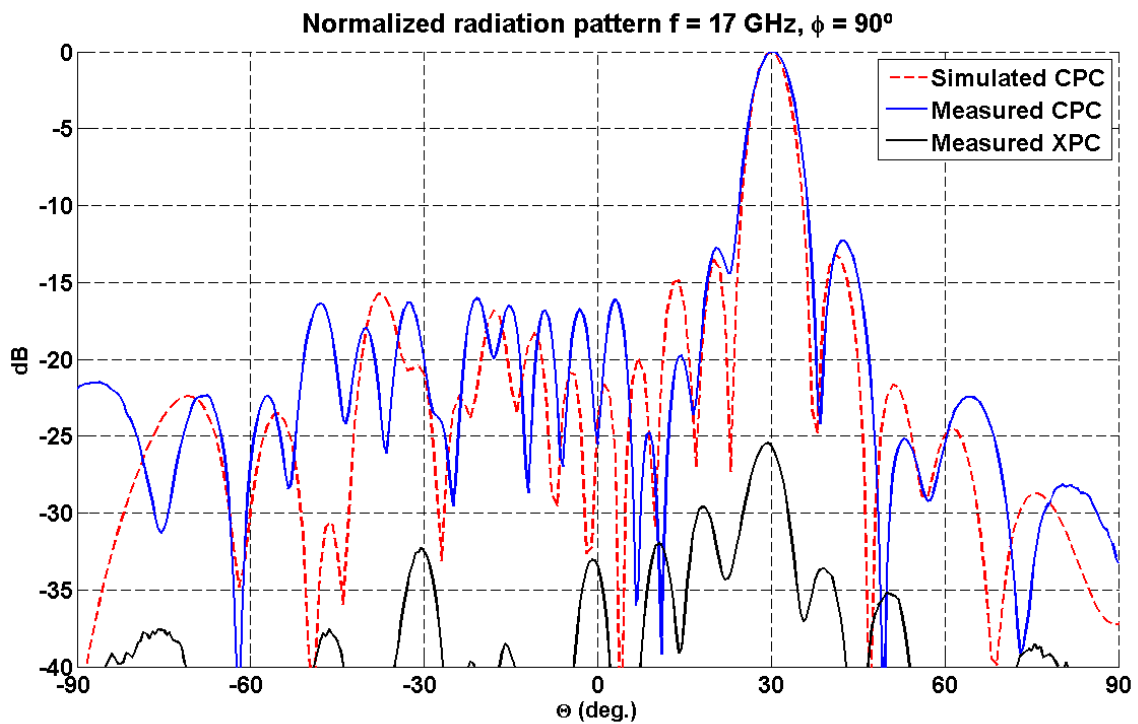


Figure 5-17: Measured co-polar and cross-polar components versus the air gap co-polar component at 17 GHz

5. Integration and Results

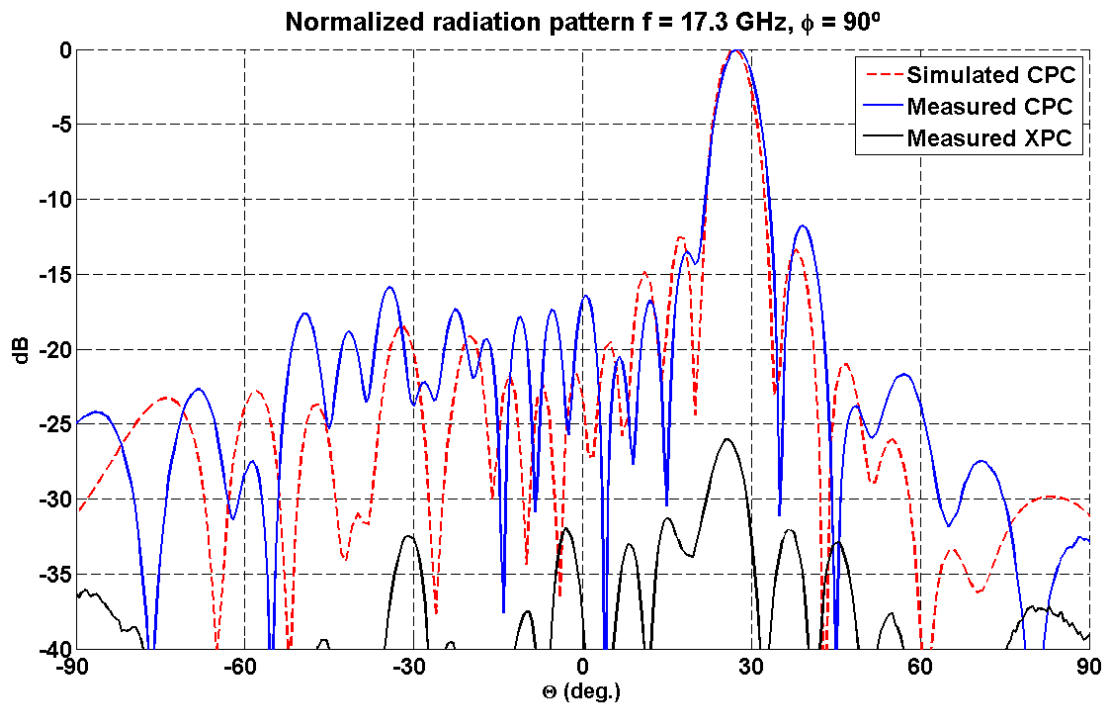


Figure 5-18: Measured co-polar and cross-polar components versus the air gap co-polar component at 17.3 GHz

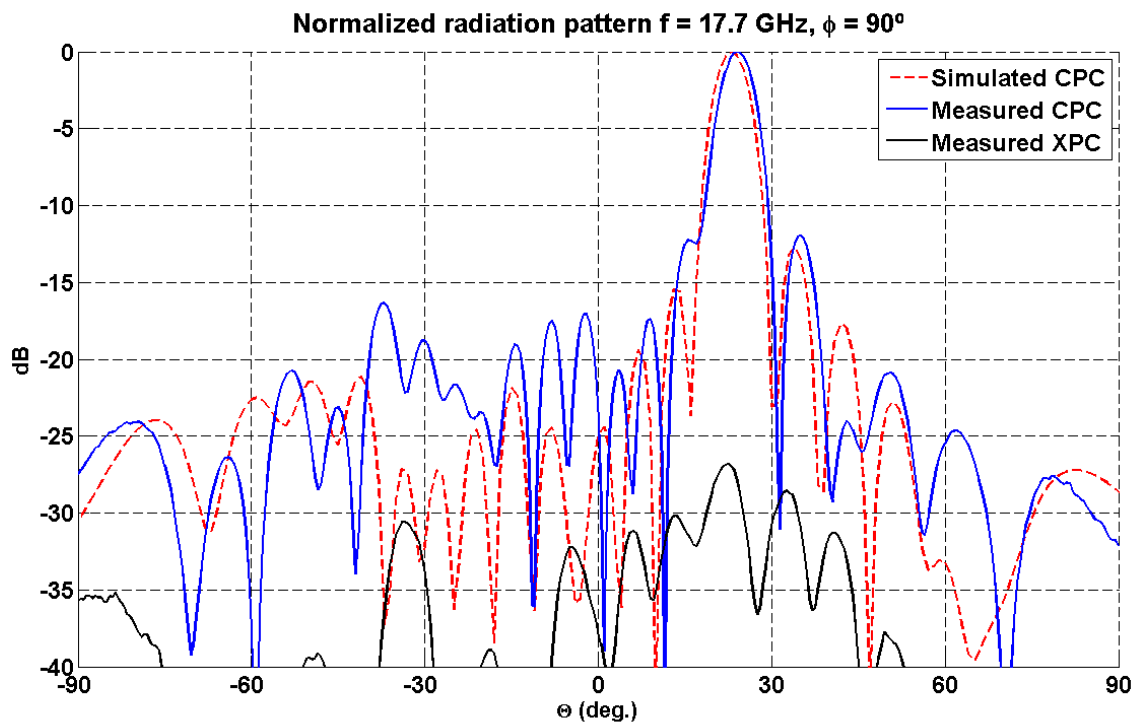


Figure 5-19: Measured co-polar and cross-polar components versus the air gap co-polar component at 17.7 GHz

5. Integration and Results

5.5 Comparison and Results

Once the results from simulations and measurements are collected, it is time to compare and analyze them.

5.5.1 S_{11} Parameter

Regarding the antenna's reflection, important differences can be found between the simulation results and the prototype's measurements. At first glance, a clear deterioration in the reflection response can be observed for the lower frequency band (16.3 – 16.9 GHz). The levels are much higher than in the rest of the band, which is fair well characterized with values below -15 dB from 17 to 17.7 GHz.

However, the wide band measurement provides some additional information of the prototype's response. Rather than a deterioration in the reflection, a deviation in the frequency band has happened. The good reflection response is extended till 18.6 GHz, which is out of the design frequency range. This indicates that the curve has moved to higher frequencies, and the part in the lower band does not belong to a frequency range where the antenna has been characterized.

The most reasonable explanation for this phenomenon is that fabrication errors have modified the expected behavior of the antenna. As the manufacturing process of the SIW is handmade, it is very likely that air gaps have been inserted between the layers. Just considering the SIW, the additional air between the substrate's layers has caused a change in the dielectric constant of the structure, which is lower than de designed one. Due to this, the wavelength of the SIW has changed. Taking into account that the SIW's wavelength is a parameter used in the inter-element distance, changes in its value has led to unexpected results.

Furthermore, the 16th element has a very delicate design where manufacturing errors are even more likely to have happened. Any difference with the original design may have caused an increase in the reflection coefficient and a worse general behavior of the whole linear array.

5.5.2 Radiation Pattern

In relation to the radiation pattern, the same deviation noted before appears. Regarding the radiation pattern at the central frequency of 17 GHz, the main lobe maximum direction gain has moved from 22° to 30°. The reason for this is apparently the same as before. This deviation has influenced negatively in the directivity of the antenna, resulting in a gain loss at all frequencies; but especially in the lower band (16.3 – 16.9 GHz) due to the high reflection values observed in Figure 5-14.

Considering the reflection values over 17 GHz, rather than a general worsening of the antenna's performance the operating bandwidth has moved in frequency. Regarding a bandwidth of 1.4 GHz of the original design, in Figure 5-14 the reflection is below -15 dB in almost all the frequency band between 17 GHz and 18.4 GHz.

5. Integration and Results

5.5.3 Linear Array Antenna with Uniform Air Gap

In 5.5.1 it was stated that the variations observed in the measured results may have been caused by air insertion during the manufacturing process. The head and the crushing of the rivets lead to not uniform surfaces, which prevent from ideal assembly. Moreover, the soldering tin makes some parts thicker than the designed ones. Additional simulations have been carried out to try to justify this behavior.

The two main features which are analyzed are the reflection's response of the antenna in the band from 16 to 20 GHz, and the aiming deviation of the main lobe at all frequencies in comparison with the simulation results. Air gaps will be added in different parts of the linear array in order to change its response to a more 'realistic' one.

Different uncertainties have been incorporated to the ultimate design simulated. Air gaps have been added between the two layers of the SIW, between the connector and the substrate and between the upper piece of the transition and the SIW upper side. The most relevant observed effect has been the air gap between the two layers of the SIW. Whereas the air insertion in the other areas previously mentioned has not caused significant changes in the reflection curve or radiation pattern, an air gap in this place plays an important role.

In mean terms, an air gap of 0.08 mm. along the whole substrate displaces the main lobe maximum to 30° at the central frequency of 17 GHz, which is the deviation value obtained from the measurements of the prototype. Once the main lobe maximum direction is set, the reflection obtained for that value is the following one:

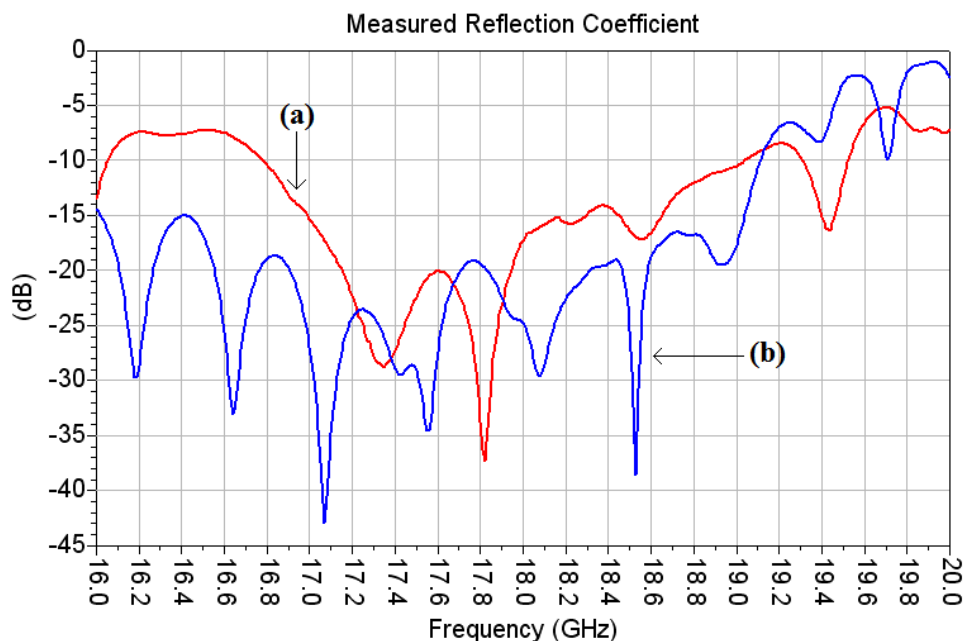


Figure 5-20: Measured reflection coefficient (a) versus reflection response of the linear array with air gap (b)

In comparison to the measured reflection, the monotony of the curve follows fair well the behavior of Figure 5-14; despite the lower band S_{11} parameter values are not as high as in the measurements.

5. Integration and Results

5.5.4 Efficiency

Finally, the efficiency of the manufactured prototype is characterized. The efficiency of the measured antenna is the relation between the maximum gain obtained from the measurements and from the simulations of the antenna with the air gap.

Freq. (GHz)	16.3	16.7	17	17.3	17.7	18
Gain (dB)	13.607	13.954	14.543	15.096	15.835	15.20

Table 5-1: Measured maximum gain

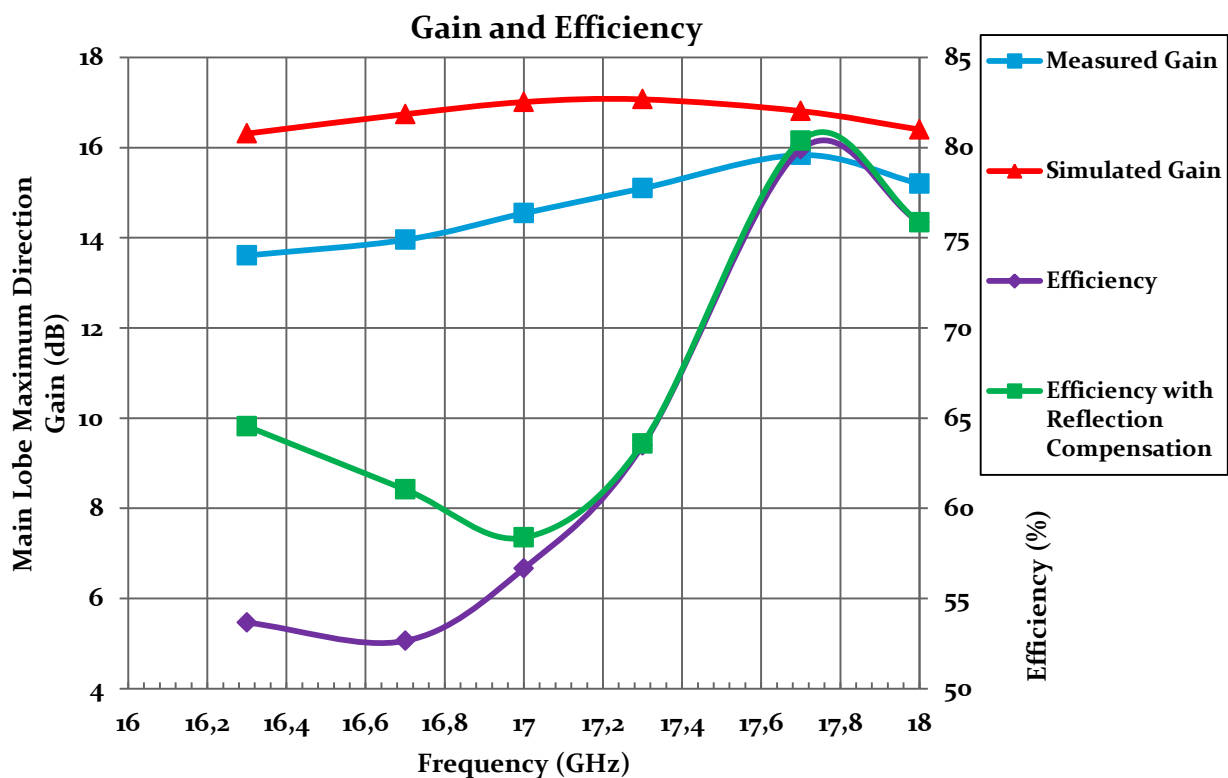


Table 5-2: Measured and simulated gain and efficiency of the antenna

Apparently, the efficiency of the antenna is not so good in the working frequency band. If the values of maximum simulated and measured gain are strictly taken, the efficiency is low for the first part of the band. However, if the deviation due to the air gap is considered and the S_{11} parameter is supposed to be better (as for the mean value in the 17 – 18.4 GHz band); the difference between both gains is narrowed.

As a conclusion, if the air gap introduced during the manufacturing process could be controlled; the antenna's efficiency would be higher in the desired working frequency band.

6 CONCLUSIONS AND FUTURE WORK

6.1 Introduction

In this chapter a summary of the work carried out is presented, with some conclusions extracted from the obtained results and the personal experience of the CFP. Then, some future work lines are proposed.

6.2 Conclusions

In this CFP a linear array over SIW with linear polarization has been proposed, consisting of 16 elements which follow a uniform distribution. For the radiating elements, a double stacked patch structure has been designed. The linear array ends in a short-circuit and it is optimized in reflection. The SIW feeding array and the patch structure have been designed independently.

The SIW feeding array has been designed over a combination of substrates TLY-5A ($\epsilon_r=2.17$) for the lower layer and RF-35 ($\epsilon_r=3.5$) for the upper one. Along the SIW, a progressive wave propagates and feed the 16 radiating elements. Between both layers, a series of coupling lines are placed longitudinally the direction of propagation of the progressive wave. These lines couple power from the progressive wave and transfer it to the double patch structure by the means of metallic vias. The size of the coupling lines varies depending on the required feeding coefficient for each element. The elements are separated approximately $3\lambda_{gSIW}/4$ from each other, in order to optimize the reflection of the array. To accomplish this feature, an optimization two-by-two is made in order to compensate the internal mutual effects inside the SIW.

For the double stacked patch structure, the same substrates TLY-5A and RF-35 are used, although in different thickness. Between them, a layer of ROHACELL is placed to provide mechanical support to the structure. The different patches have been also optimized in reflection.

For both the SIW feeding array and the patch structure, the design has been made taking into account its later construction at the laboratory of printed circuits at EPS. This fact imposes several restrictions to the dimension of several elements, but the manufacturing of a prototype is an important milestone in order to compare the realizability of the project. Once both parts have been designed, the linear array is formed. The global set presents very good levels of reflection, although a real feeding system is still pending to be incorporated to the design.

A SMA-microstrip-SIW transition is proposed to feed the linear array. Moreover, two metallic pieces have been manufactured to provide electromagnetic insulation and prevent the power loss due to unexpected radiation. In comparison to other transitions designed, the proposed one has fair good levels of reflection and efficiently transmits the power to the SIW.

6. Conclusions and Future Work

When the transition is integrated with the linear array, a compensation model is proposed to adjust the radiation pattern to the theoretical one. This model analyzes the radiated electric near-field in the center of each patch and at a very close distance. From the field extracted, a relation is found between the field components and the coupling coefficient of the element. Modifying the coupling lines and the distance between them, a very similar radiation pattern to the theoretical one is obtained. The key point of this method is that all the coupling effects are compensated, the internal inside the SIW and the external of the radiating elements. From the final results, this coupling model has proved to be extremely useful and effective to adjust the radiation pattern, while maintaining the reflection of the whole set below the required specifications.

A linear array with an aiming of 22.5° and maximum gain of 17.88 dBi at 17 GHz is obtained by simulations. A -3 dB beamwidth of 5.9° and SLL of 12.7 dB are obtained. The reflection coefficient is below -20 dB in the whole working frequency band.

Finally, a prototype has been manufactured to check the validity of the results and the fabrication possibilities at EPS. The fabrication has been conditioned by the technological limitations of the machinery and the material availability. The handmade procedure has introduced several uncertainties in the prototype, which have modified the expected behavior of the antenna worsening the features. Furthermore, as the antenna is a multilayer structure, the probability of making mistakes during the manufacturing process is increased and good results are more difficult to achieve.

The prototype's measurements have given an aiming of 30° at 17 GHz with a maximum gain of 16 dBi. A 6% reflection bandwidth and an efficiency of 56.6 % are obtained.

However, in comparison to other works done at EPS, the obtained results are fairly acceptable, given the already known circumstances. As a conclusion, if a higher quality system is wanted, the available resources at EPS are not enough to guarantee the best achievable performance; due to the difficulty of reliable and precise manufacturing. The high frequency range of work leads to very sensitive designs where very small changes considerably vary the linear array's performance. The difference between the expected results and the extracted from the prototype's measurements has been partially justified by the air insertion in the structure during the manufacturing process. Additional simulations prove that the deviations in the radiation pattern and the reflection curve have been caused by this fact.

6.3 Future Work

As a short term future working line, the external fabrication of the linear array designed in this CFP is proposed. In order to fulfill this task, some modifications should be done in the design. This is due to the differences between the manufacturing methods used at the workshop in EPS and the ones used in the industry. According to the constraints imposed by the manufacturers, changes in the design may need to be done.

In a long term line, considering the results of this CFP good enough, these could be the base of the design of a 2D planar array. Taking advantage of the high directivity antennas designed with this technology, integration in a wider context of planar arrays is very interesting.

6. Conclusions and Future Work

On one hand, finishing some unclosed investigation paths of this CFP could lead to different works. This would include the design of the linear array and later optimization for a phase difference between elements of 270° , following the same method described in this CFP.

On the other hand, an approach to a linear array with a separation between elements around λ_{gSIW} could be tried. This disposition could enable designs with circular polarization and two-port antennas.

If an acceptable design cannot be achieved with the changes proposed above, different substrates with fewer losses and different dielectric constants could be used. This would lead to completely different designs and antennas with different characteristics to the studied in this CFP.

Finally, for any design implemented, it is important to consider the possible external fabrication of the prototype. The manufacturers may force the designer to meet more strictly their requirements in some areas, but they may also impose fewer limitations to others.

REFERENCES

- [1] J. L. Masa-Campos and J. A. Ruiz-Cruz, *Antenas y Circuitos de Alta Frecuencia*, Asignatura de máster impartida en la Escuela Politécnica Superior de la Universidad Autónoma de Madrid, 2009.
- [2] W. L. Stutzman and G. A. Thiele, *Antenna Theory and Design*, John Wiley & Sons, Inc, 1998.
- [3] M. Ferrando-Bataller and A. Valero-Nogueira, *Antenas*, Asignatura impartida en la Universidad Politécnica de Valencia.
- [4] D. M. Pozar, *Microwave Engineering*, John Wiley & Sons, Inc., 2005.
- [5] D. K. Cheng, *Fundamentos de Electromagnetismo para Ingeniería*, Addison Wesley, 1997.
- [6] D. Deslandes and K. Wu, "Accurate Modeling, Wave Mechanisms, and Design Considerations of Substrate Integrated Waveguide," *IEEE Trans. Microwave Theory Tech*, vol. 54, pp. 2516-2526, June 2006.
- [7] L. Yan, W. Hong, G. Hua, J. Chen, K. Wu and T. Cui, "Simulation and experiment on SIW slot array antennas," *IEEE Microwave Wireless Compon. Lett.*, vol. 14, no. 9, pp. 446-448, Sept. 2004.
- [8] D. Deslandes and K. Wu, "Integrated Microstrip and Rectangular Waveguide in Planar Form," *IEEE Microwave and Wireless Components Letters*, vol. 11, pp. 68-70, Feb. 2001.
- [9] "TLY-5A Data sheet:," Available: <http://www.taconic-add.com/en/pdf/tly.pdf>.
- [10] "RF-35 Data sheet:," Available: <http://www.taconic-add.com/pdf/rf35.pdf>.
- [11] C. A. Balanis, *Advanced Engineering Electromagnetics*, John Wiley & Sons, Inc, 1989, pp. 394-414.
- [12] "Bungard's Rivets:," Available: http://www.bungard.de/ru/downloads/fav_ane1.pdf.
- [13] J. L. Masa-Campos, S. Klinger and M. Sierra-Pérez, "Parallel plate patch antenna with internal horizontal coupling lines and TENO mode excitation," *IEEE Transactions on Antennas and Propagation*, vol. 57, no. 7, p. 2185 – 2189, July 2009.
- [14] C. A. Balanis, *Antenna Theory: Analysis and Design*, John Wiley & Sons, Inc, 1997.
- [15] D. M. Pozar and D. H. Schaubert, *Microstrip Antennas*, John Wiley & Sons, Inc, 1995.
- [16] P. Sánchez-Olivares, *Diseño de array lineal plano con guía de alimentación en sustrato integrado para banda Ku*, PFC, Sept. 2011.

References

- [17] P. Chen and W. Hong, "A Multibeam Antenna Based on Substrate Integrated Waveguide Technology for MIMO Wireless Communications," *IEEE Transactions on Antennas and Propagation*, vol. 57, no. 9, pp. 1813-1821, June 2009.
- [18] "Huber-Suhner connector;," Available: http://www.hubersuhner.com.sg/es/mozilla/hs-sup-search-prod-rf-pan-2g?p_Query=23_SMA-50-0-94/199_NE&cls=09FB405D9D5FF3A6&query=&step=1&applied=1&selected=1&search=type&display=12&vt=14117&unit=si&listed=0&sort=asc&col=1&prm=88EF608A2AB4FA568896C59D2B3247D.
- [19] "Radiall Connector," Available: R125 496.100.
- [20] "Agilent E5071C ENA Network Analyzer," Available: <http://cp.literature.agilent.com/litweb/pdf/5989-5479EN.pdf>.
- [21] "Agilent 85131E Flexible Test Port Cable," Available: www.home.agilent.com.
- [22] "Acquired at Elate S.A. Circuitos Impresos," Available: <http://www.elatesa.com>.
- [23] "Bungard riveting machine," Available: www.bungard.de.
- [24] "JBC Soldering Station," Available: <http://www.jbctools.com/>.
- [25] "LPKF Printed Circuit Machine," Available: <http://www.lpkf.com/>.
- [26] "Software property of LPKF," Available: <http://www.lpkf.es/productos/creacion-rapidaprototipos->.

APPENDIXES

A. INTRODUCCIÓN

En este documento se describe el proyecto de ingeniería consistente en un array lineal de parches sobre guía de onda en sustrato integrado, que opera en la banda Ku (12.4 – 18 GHz).

A.1 Motivación

Con la emergencia de las nuevas tecnologías y sus continuas mejoras, es de vital importancia adaptar las estructuras y dispositivos existentes a ellas. Estas motivaciones vienen dadas por diversos factores, como el tamaño de las antenas, su coste, adaptabilidad al entorno, etc. Al final, el objetivo es proveer a los usuarios un servicio de calidad y una comunicación lo más amplia posible, por lo que es necesario buscar y desarrollar nuevas soluciones.

Para muchas aplicaciones, antenas de un solo elemento son incapaces de cumplir los requerimientos de ganancia o del diagrama de radiación. Combinando varios de estos elementos unitarios en arrays, es posible obtener nuevas soluciones a partir del efecto combinado de las antenas unitarias.

Finalmente, la tecnología de circuitos impresos cada día está adquiriendo más importancia, pues permite fabricar antenas de alta ganancia con costes más bajos y menores dimensiones en relación a la tecnología convencional.

A.2 Objetivos

El objetivo de este proyecto es diseñar y caracterizar un array lineal implementada en tecnología de circuitos impresos para la banda Ku. Los objetivos concretos de este proyecto son los siguientes:

1. Diseño de los elementos radiantes con optimización de reflexión, formados por líneas de acoplo y parches, y su posterior caracterización.
2. Diseño del array lineal sobre guía en sustrato integrado (SIW), implementando los elementos mencionados anteriormente.
3. Diseño y caracterización de transiciones que puedan alimentar eficientemente la antena, y al mismo tiempo mantener buenos niveles de adaptación con la antena.
4. Integración del array lineal y las transiciones diseñadas para su posterior construcción y medida.

A.3 Estructura del Documento

Este documento está estructurado de la siguiente manera:

- **Capítulo 1: Introducción**
Este capítulo presenta la motivación, objetivos y estructura de este documento.
- **Capítulo 2: Estado del Arte**
En este capítulo se expone el estado del arte de los arrays de antenas, tecnologías de circuitos impresos y SIW, entre otras.
- **Capítulo 3: Diseño de Antenas**
Hay tres partes diferenciadas en este capítulo
 - Diseño del array en SIW y las líneas de acoplo que alimentan los parches.
 - Diseño de los elementos radiantes unitarios.
 - Diseño de antenas con una determinada directividad y polarización lineal.
- **Capítulo 4: Diseño de Transiciones**
Diferentes transiciones de alimentación son descritas en este capítulo, teniendo en cuenta que deben ser realizables y ofrecer buenos niveles de adaptación.
- **Capítulo 5 Integración y Resultados**
En este capítulo se expone la combinación de los arrays lineales y las transiciones, así como la fabricación de la antena y los resultados de las medidas.
- **Capítulo 6: Conclusiones y Trabajo Futuro**
El capítulo final resume los logros obtenidos en el proyecto, presenta los resultados obtenidos del diseño y el proceso de fabricación; y por último sugiere posibles mejoras y líneas de trabajo futuro.

B. CONCLUSIONES

B.1 Introducción

En este capítulo se presenta un resumen del trabajo llevado a cabo, con las conclusiones extraídas de los resultados obtenidos y la experiencia personal de este Proyecto Fin de Carrera (PFC). Finalmente, se proponen algunas líneas de trabajo futuro.

B.2 Conclusiones

En este PFC un array lineal sobre SIW con polarización lineal ha sido propuesto, formado por 16 elementos con una distribución uniforme. Para los elementos radiantes, una estructura de doble parche ha sido diseñada. El array lineal termina en un cortocircuito y ha sido optimizado en reflexión. El array en SIW de alimentación y la estructura de doble parche han sido diseñadas independientemente.

El array en SIW de alimentación ha sido diseñado con una combinación de substratos TLY-5A ($\epsilon_r=2.17$) para la capa inferior y RF-35 ($\epsilon_r=3.5$) para la superior. A lo largo de la SIW, una onda progresiva se propaga y alimenta los 16 elementos radiantes. Entre ambas capas, una serie de líneas de acoplo están colocadas longitudinalmente a la dirección de propagación de la onda progresiva. Estas líneas acoplan potencia de la onda progresiva y la transfieren a la estructura de doble parche a través de vías metálicas. El tamaño de las líneas de acoplo varía dependiendo del coeficiente de acoplo requerido en cada elemento. Los elementos están separados aproximadamente $3\lambda_{gSIW}/4$ uno del otro, para poder optimizar la reflexión del array. Para realizar esta tarea, una optimización dos a dos es llevada a cabo para compensar los efectos de acoplo mutuos que ocurren dentro de la SIW.

Para la estructura de doble parche, los mismos substratos TLY-5A y RF-35 han sido utilizados, aunque con distintos espesores. Entre ellos se sitúa una capa de ROHACELL para proporcionar soporte mecánico a la estructura. Los distintos parches también han sido optimizados en reflexión.

Tanto para el array en SIW como para la estructura de parches, el diseño se ha realizado teniendo en cuenta la posterior construcción en el laboratorio de circuitos impresos de la EPS. Debido a esto se imponen restricciones a las dimensiones de los elementos en el diseño, pero la fabricación del prototipo es una etapa fundamental para poder valorar la viabilidad del proyecto. Una vez que ambas partes se han diseñado, el array lineal está completamente formado. El conjunto global presenta muy buenos niveles de reflexión, aunque aún debe incorporarse un sistema de alimentación real.

Para alimentar el array lineal se propone una transición SMA-microstrip-SIW. Además, dos piezas metálicas han sido fabricadas para proporcionar aislamiento electromagnético e impedir pérdidas de potencia asociadas a radiación imprevista. En comparación con otras transiciones diseñadas, la propuesta de este PFC tiene buenos niveles de adaptación y transmite eficientemente potencia a la SIW.

Cuando la transición se integra con el array lineal, se ha desarrollado un modelo de compensación para ajustar el diagrama de radiación al teórico. El modelo analiza el campo eléctrico cercano radiado en el centro de cada parche, a una distancia muy cercana de la superficie. A partir del campo cercano extraído, se obtiene una relación entre las componentes de campo y los coeficientes de acoplo en cada elemento. Modificando las líneas de acoplo y las distancia entre ellas, se acaba obteniendo un diagrama de radiación muy parecido al teórico. La característica principal de este método es que todos los efectos mutuos de acoplo son compensados, tanto los internos en la SIW como los externos de los elementos radiantes. A partir de los resultados finales, el modelo de acoplos ha resultado ser de gran utilidad y muy efectivo para ajustar el diagrama de radiación, a la vez que se han mantenido los niveles de reflexión por debajo de las especificaciones requeridas.

Por último, un prototipo ha sido fabricado para comprobar tanto la validez de los resultados como las posibilidades de fabricación de la EPS. El proceso de fabricación ha sido condicionado por las limitaciones tecnológicas de la maquinaria y la disponibilidad de material. El procedimiento manual de varias etapas ha introducido incertidumbres en el prototipo, las cuales han modificado el comportamiento de la antena empeorando sus características. Además, debido a que la antena es una estructura multicapa, la probabilidad de cometer errores durante el proceso construcción se incrementa y es más difícil obtener buenos resultados.

Sin embargo, en comparación con otros trabajos realizados en la EPS, los resultados obtenidos son bastante aceptables dadas las circunstancias conocidas. En conclusión, si se quiere un sistema de alta calidad, los recursos disponibles en la EPS nos son suficientes para garantizar las mejores prestaciones; debido a la dificultad para tener una fabricación fiable y precisa. La banda de altas frecuencias en la que se trabaja obliga a realizar diseños muy sensibles, donde pequeños cambios provocan variaciones considerables en el comportamiento del array lineal. Las diferencias entre los resultados esperados y los extraídos de las medidas del prototipo han sido parcialmente justificados por la inserción de aire en la estructura durante el proceso de construcción. Simulaciones adicionales han probado que las desviaciones en el diagrama de radiación y el coeficiente de reflexión han sido causadas por este hecho.

B.3 Trabajo Futuro

Como línea de trabajo futuro a corto plazo, se propone la fabricación del array lineal por medios externos a la EPS. Para llevar a cabo esta tarea, se deben realizar algunas modificaciones en el diseño. Esto es debido a las diferencias en los procesos de fabricación de la EPS y la industria. De acuerdo a las restricciones impuestas por los fabricantes, deben aplicarse los cambios pertinentes.

A largo plazo y tomando como base todos los resultados de este PFC, se puede abordar el diseño de un array planar en 2D. Gracias a la alta directividad de las antenas diseñadas mediante esta tecnología, la integración en contextos más amplios de arrays planares resulta muy interesante.

Por una parte, terminar algunas de las líneas de investigación sin finalizar de este PFC puede derivar en distintos trabajos. Esto incluiría el diseño y optimización de un array lineal con diferencia de fase entre elementos de 270° , siguiendo el mismo procedimiento que el descrito en este PFC.

Appendix

Por otra parte se podría intentar un diseño de array lineal donde los elementos estuviesen separados alrededor de λ_{gSIW} . Esta disposición podría permitir diseños con polarización circular o antenas de dos puertos.

Si no se pudiese conseguir un diseño aceptable con las propuestas mencionadas anteriormente, podrían usarse distintos sustratos con menores pérdidas y diferentes constantes dieléctricas. Esto daría lugar a diseños y antenas con diferentes características a las estudiadas en este PFC.

Por último, para cualquier diseño implementado, es importante considerar la opción de fabricar externamente el prototipo. Los fabricantes pueden forzar al diseñador a cumplir ciertos requerimientos en determinadas áreas, aunque pueden imponer menos limitaciones en otras.

C. MANUFACTURING OF PRINTED CIRCUITS

Throughout this document there are several references to the fabrication process of printed circuits. Its main characteristics are the low cost and simplicity, which make them perfect for developing a prototype with reasonable levels of effort and costs. There are different methods to manufacture printed circuit antennas: chemical and mechanical.

The chemical method consists of applying a mask where the printed circuit is drawn to the substrate. The slab is immersed in a solution of ferric chloride, which reacts with the copper and removes it from the areas where the mask was not applied.

On the contrary, the mechanical method uses a precision milling machine controlled by software. By the means of several tools, the copper is removed from the substrate. This method is cleaner and more secure than the chemical one, although a bit less precise. The printed circuit laboratory at EPS owns a milling machine from the series 'LPKF ProtoMat S100', so this has been the method used for the construction of the linear array antenna proposed in this CFP.

C.1 Material Used

For the manufacturing process, the following material has been used:

- Substrate TLY-5A of thickness 0.508 mm. and 1mm. [9]
- Substrate RF-35 of thickness 0.508 mm. [10]
- Substrate FR-4 of thickness 1.6 mm. [22]
- Riveting machine [23] and rivets [12] from BUNGARD
- Coaxial connectors [18] and [19]
- Soldering station [24]
- Milling machine 'LPKF ProtoMat S100' [25]
- Software 'CircuitCAM' and 'Board Master' [26]

C.2 Manufacturing Process

The different stages involved in the manufacturing of a printed circuit will be explained below; starting from the software design till the circuit is finished. Moreover, a description of the tools used by the milling machine and their main characteristics are also presented.

Appendixes

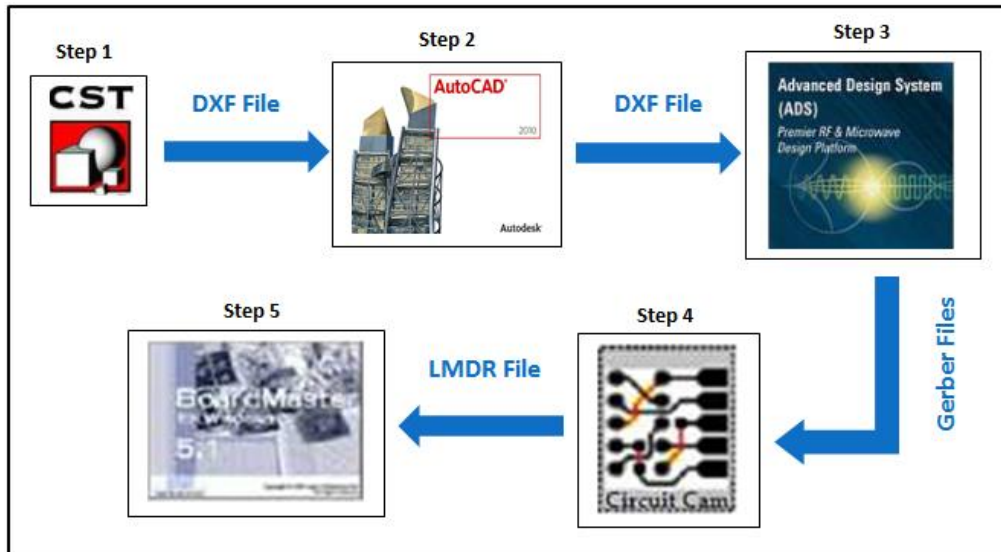
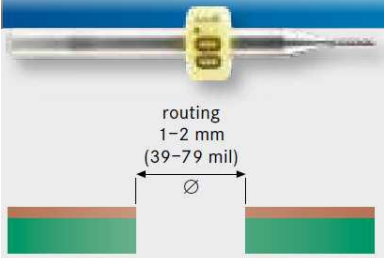
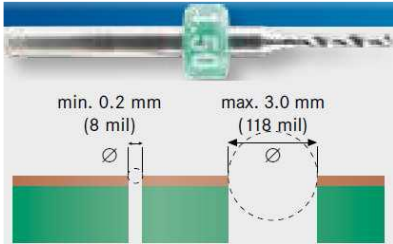


Figure C-1: Diagram of the software design process involved in the manufacturing of the prototype

- **Step 1:** Once the design is finished in CST Microwave Studio, for each layer that needs to be constructed, a DXF file is exported.
- **Step 2:** The exported DXF files are combined in software 'AutoCAD', where the different layers needed for the milling machine 'LPKF ProtoMat S100' are defined. These normally include: board outline layer, top layer, drill layer and bottom layer.
- **Step 3:** For producing printed circuits, it is necessary to obtain the Gerber file for each layer. These files are generated with Advanced Design System (ADS) from the files imported from AutoCAD.
- **Step 4:** With the Gerber files generated, it is time to use the specific software of the milling machine LKPF. From the Gerber files, software CircuitCam allows to select which tools will be used during the manufacturing process and how they will be applied to the substrate slab. The available tools for the milling machine are the following:

Universal Cutter	End Mill	End Mill RF
<p>0.2-0.5 mm (8-20 mil)</p>	<p>isolation 0.8-3.0 mm (31-118 mil)</p> <p>engraving 0.8-3.0 mm (31-118 mil)</p> <p>aluminum</p>	<p>0.15-0.4 mm (6-16 mil)</p>
It marks the circuit's contour and eliminates copper with precision	Removes copper with less precision. Useful for quick removal in big areas	The most precise tool for copper removal, specially indicated for RF circuits

Contour Router	Spiral Drill
 <p>routing 1-2 mm (39-79 mil)</p>	 <p>min. 0.2 mm (8 mil)</p> <p>max. 3.0 mm (118 mil)</p>
It cuts the board outline of the circuit in the slab	Drilling tool indicated for making precise drills of several diameters

- **Step 5:** After CircuitCam software exports a LMDR file, software Board Master uses the file to control the data flow between the computer and the milling machine.
- **Step 6:** Finally, the milling machine has to have indicated the different execution phases for printing each layer.

D. MEASUREMENTS WITH NETWORK ANALYZER

D.1 Material Used

A network analyzer is a device which can characterize the properties of electric networks, associated to reflection and transmission of signals through the scattering parameters (S parameters). Many properties can be expressed as a function of S parameters, such as gain, return losses, voltage standing wave ratio (VSWR) or reflection coefficient.

The available network analyzer at EPS is Agilent – Model E5071C [20]. It has two ports with a working frequency range from 9 KHz to 26 GHz.

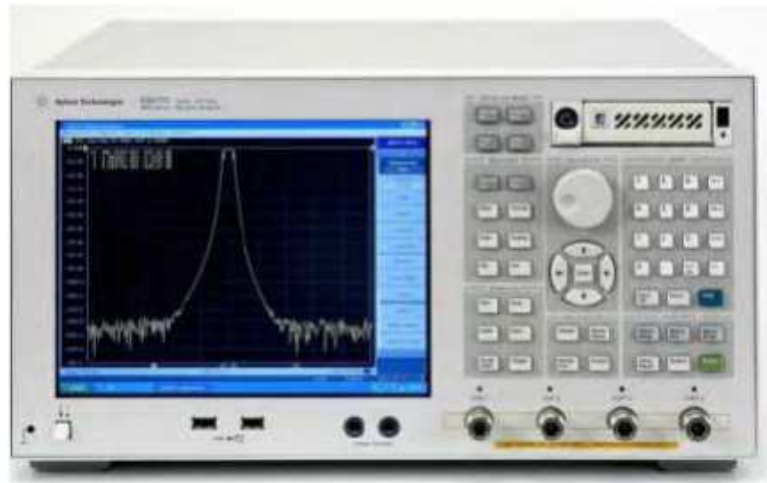


Figure D-1: Network analyzer E5071C property of EPS

D.2 Coaxial Cables

In order to measure the S parameters of a circuit with the vector network analyzer (VNA), one or two coaxial cables are required to connect the VNA with the circuit. The highest quality available cables at EPS are the set Agilent 3.5 mm. Flex F-M Test Port Cable [21], which are suitable for measurements from DC up to 26.5 GHz and have male connectors.



Figure D-2: Coaxial cables used for measurements with VNA, property of EPS

D.3 Calibration Kit

For an appropriate measurement of the S parameters in a microwave circuit, it is necessary to eliminate the inherent errors of the measurement cables, connectors, etc. For this reason, the VNA needs to be calibrated prior to measurements. With the calibration the VNA can subtract the previously mentioned systematic errors and give the real information of the circuit. Once the calibration is done, the S parameters at the input of the circuit can be obtained.

The procedure to calibrate the VNA consists of connecting at the end of the cable which will be used for measuring the circuit a series of terminations: an open circuit, a short-circuit and a load of 50Ω (the characteristic impedance of the circuit). The calibration kit available at EPS is the HP/Agilent 85052D 50 ohm 3.5 mm calibration kit 9GHz. Male and female connectors are available for each one of the three terminations.



Figure D-3: Content of the calibration kit 85052D de Agilent Technologies, property of EPS

Before the calibration starts, it is necessary to set the frequency range where the measurements will be made. The VNA's behavior varies depending on its operating frequency range, so it is important to calibrate it in the appropriate band. Furthermore, whereas in consecutive measurements it is not necessary; if the tested device is changed many times or the measurements are carried out in, for instance, different days; the VNA needs to be recalibrated.

E. PLANS

E.1 Transition SMA – Microstrip – SIW

- Top view:

Substrates:

- TLY-5A 0400 CH/CH: 1.016 mm. (lower layer)
- RF-35 0200 CH/CH: 0.508 mm. (upper layer)

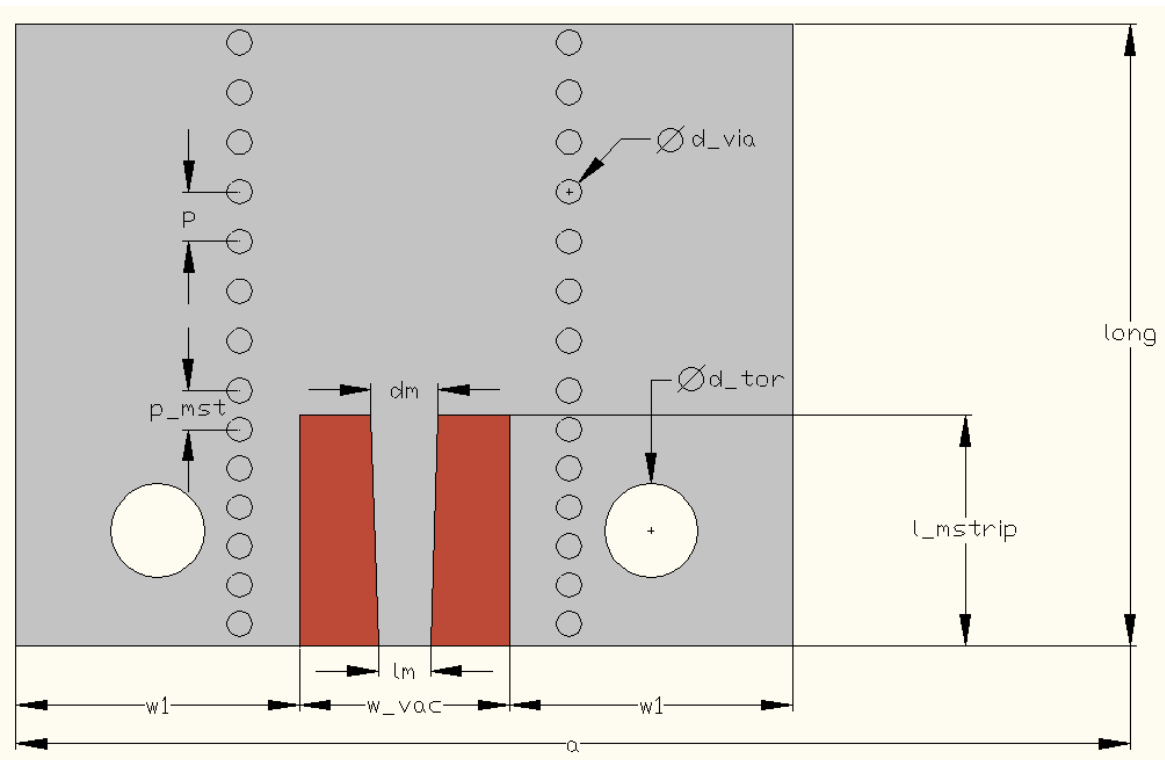


Figure E-1: Top view of the transition section with all the important concerning parameters

Parameter	Value (mm.)
long	18.15
l_{mstrip}	7.1
d_{via}	0.8
d_{tor}	3
p	1.6
p_{mst}	1.4
dm	2.15
l_m	7.1
a	25
$w1$	9.125
w_{vac}	2.54

Table E-1: Values of the parameters of the transition section

E.2 Connector Fixer Metallic Piece

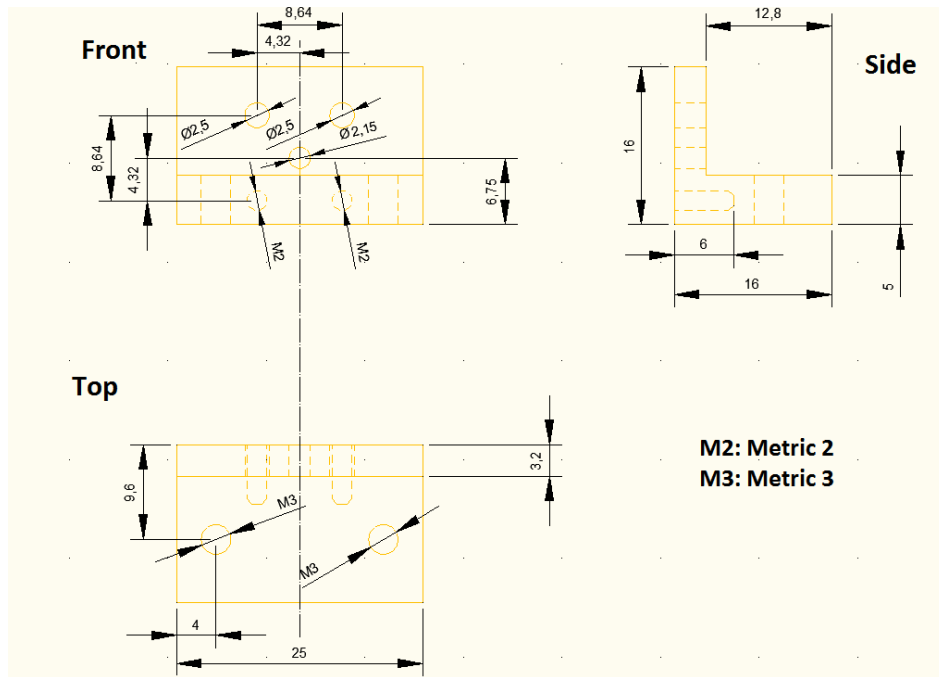


Figure E-2: Plans of the fixer metallic piece of the proposed transition

E.3 Upper Metallic Piece

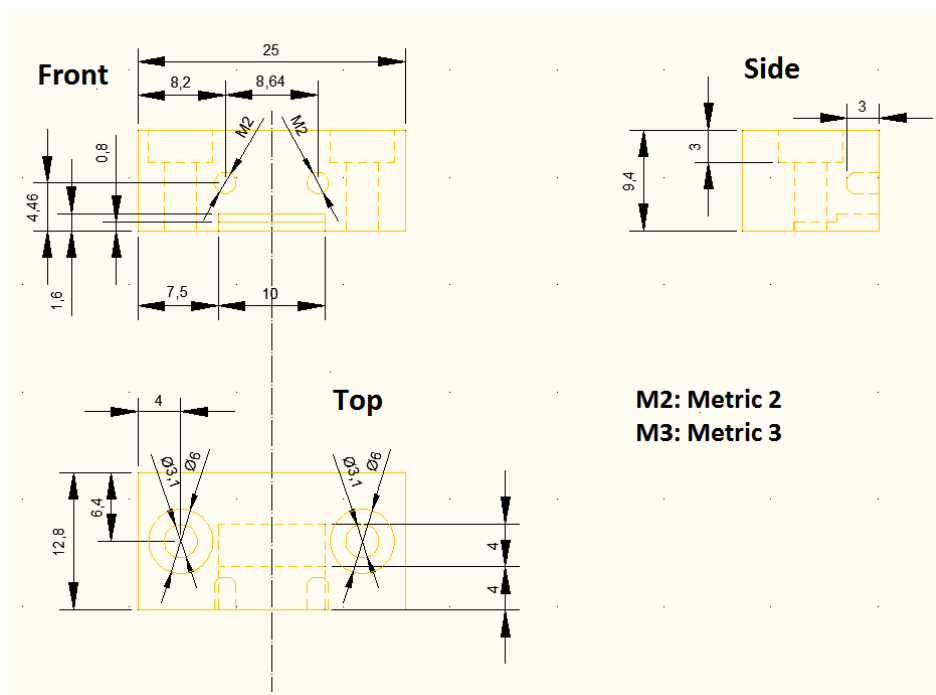


Figure E-3: Plans of the insulating metallic piece of the proposed transition

F. PUBLICATIONS

According to the results obtained from this CFP, two articles have been written to summarize and present the linear array antenna designed.

One article has been submitted to the XXVII National Symposium of International Union of Radio Science (URSI 2012) held in Elche. The article presents the designed linear array antenna and has been accepted and opts to the Young Scientists Award.

The second one has been submitted to IEEE Transactions on Antennas and Propagation, and it extends the mutual coupling model proposed and provides further calculations which had not been obtained prior to submitting the previous paper. This communication is pending of acceptance.

- 1) D. García-Valverde, J.L. Masa-Campos, "Linear Patch Array Over Substrate Integrated Waveguide For Ku Band", 27th Simposium Nacional URSI 2012, Elche (Spain), 12th -14th September 2012.
- 2) D. García-Valverde, J. L. Masa-Campos, P. Sánchez-Olivares, B. Taha-Ahmed, J. Córcoles.-Ortega, "Linear Patch Array Over Substrate Integrated Waveguide For Ku Band" *IEEE Transc. Antennas and Propag.*

Appendixes

Estimado autor,

Como Presidentes del Comité Científico del XXVII Simposium Nacional de la Unión Científica Internacional de Radio, URSI 2012, le comunicamos que su trabajo número 93 titulado Linear Patch Array Over Substrate Integrated Waveguide For Ku Band ha sido ACEPTADO para su publicación en URSI 2012.

URSI 2012 Elche Submission 93

Paper 93						
Title:	Linear Patch Array Over Substrate Integrated Waveguide For Ku Band					
Paper:	PDF					
Category:	Artículo íntegro en inglés (opta a premio URSI)					
Keywords:	Hybrid mode Coupling lines Substrate Integrated Waveguide (SIW) Double stacked patch					
Topics:	Antenas					
Abstract:	A Substrate Integrated Waveguide (SIW) 16-element linear array antenna is presented, with linear polarization (LP) for Ku band (16.3 GHz - 17.7 GHz) and uniform distribution. A double microstrip patch structure has been used as radiating elements. Coupling lines are placed inside the waveguide to couple power from the SIW to the radiating elements. The coupling lines are connected to the inferior patches by means of metallic vias. These lines need the propagation of a hybrid mode to function properly. An antenna prototype has been manufactured and measured. A 16 dBi gain with a 6% reflection bandwidth and 56.6% efficiency is obtained.					
Time:	Apr 13, 10:59 GMT					
Authors						
first name	last name	email	country	organization	Web site	corr
David	Garcia Valverde	david.garciav@estudiante.uam.es	Spain	Autonoma University of Madrid		✓
Jose Luis	Masa Campos	joseluis.masa@uam.es	Spain	Autonoma University of Madrid		✓

Premio para Jóvenes Científicos URSI 2012

La Unión Científica Internacional de Radio (URSI) concede un Premio para Jóvenes Científicos al mejor artículo presentado en el Simposium y tres Accésit (está previsto que los premios sean entregados durante la Cena de Gala). El Comité URSI 2012 y Comité Nacional Español URSI querrían destacar que los cuatro artículos premiados serán invitados a publicar versiones extendidas de sus artículos en **The Radio Science Bulletin**.

Condiciones para optar al premio:

- Según lo acordado en la asamblea URSI celebrada en Leganés (7 de septiembre 2011), aquellos autores que quieran optar al Premio Jóvenes Científicos URSI 2012 deberán enviar el trabajo completo en inglés.
- Ser menor de 35 años a fecha de 30 de septiembre de 2012.
- Ser el primer autor de un trabajo aceptado en el Simposium.
- El candidato al premio deberá exponer el trabajo en el Simposium.
- Solicitar la participación siguiendo las instrucciones correspondientes al envío de trabajos.

El jurado encargado de evaluar y seleccionar los artículos premiados estará compuesto por el siguiente comité internacional de expertos:

- Francisco Ares, Presidente Comité Nacional Español de URSI
- Germán Torregrosa Penalva, Co-Presidente del Comité Científico URSI 2012
- Cynthia Furse, Universidad de Utah, USA
- Giorgio Franceschetti, Universidad de Nápoles, Italia
- Giuliano Manara, Presidente Internacional de la Comisión B (Campos y Ondas)
- Kathleen Melde, Universidad de Arizona, USA
- Marco Luise, Presidente internacional de la Comisión C (Sistemas de Radio-Comunicación y Procesado de Señal)
- Sembiam R. Rengarajan, Presidente de la Comisión B (Campos y Ondas) de la USNC-URSI (United States National Committee for the International Union of Radio Science)
- W. Ross Stone, Editor, URSI Radio Science Bulletin, San Diego, USA
- Werner Wiesbeck, Universidad de Karlsruhe, Alemania

La selección de los artículos premiados tendrá en cuenta la evaluación recibida por los artículos durante el proceso de revisión del congreso (25% de la puntuación total), la evaluación realizada por el comité internacional de expertos (50% de la puntuación total), y la evaluación recibida por la presentación del artículo en el congreso (25% de la puntuación total).

Linear Patch Array Over Substrate Integrated Waveguide For Ku Band

Journal:	<i>Transactions on Antennas and Propagation</i>
Manuscript ID:	AP1207-0955
Proposed Manuscript Type:	Communication
Date Submitted by the Author:	06-Jul-2012
Complete List of Authors:	Garcia-Valverde, David; Autonoma University of Madrid, Electronic and Communication Technologies Masa-Campos, José Luis; Autonoma University of Madrid, Electronic and Communication Technologies Sánchez-Olivares, Pablo; Autonoma University of Madrid, Electronic and Communication Technologies Taha-Ahmed, Bazil; Autonoma University of Madrid, Electronic and Communication Technologies Córcoles, Juan; Universidad Autónoma de Madrid, Departamento de Tecnología Electrónica y de las Comunicaciones; Autonoma University of Madrid, Electronic and Communication Technologies; Universidad Politécnica de Madrid, Departamento de Electromagnetismo y Teoría de Circuitos
Key Words :	Antenna array mutual coupling, Antenna arrays, Antenna array feeds, Waveguide antennas

Linear Patch Array Over Substrate Integrated Waveguide For Ku Band

D. García-Valverde, J.L. Masa-Campos

david.garciav@estudiante.uam.es, joseluis.masa@uam.es

Group of Radio-Frequency, Circuits, Antennas and Systems (RFCAS)

Department of Electronic and Communication Technologies, Autonoma University of Madrid (U.A.M.)
28049 – Madrid, Spain

Abstract- A Substrate Integrated Waveguide (SIW) 16-element linear array antenna is presented, with linear polarization (LP) for Ku band (16.3 GHz – 17.7 GHz) and uniform distribution. A double microstrip patch structure has been used as radiating elements. Coupling lines are placed inside the waveguide to couple power from the SIW to the radiating elements. The coupling lines are connected to the inferior patches by means of metallic vias. These lines need the propagation of a hybrid mode to function properly. An antenna prototype has been manufactured and measured. A 16 dBi gain with a 6% reflection bandwidth and 56.6% efficiency is obtained.

Keywords- Hybrid mode, coupling lines, Substrate Integrated Waveguide (SIW), double stacked patch.

I. INTRODUCTION

Since the early 1990s, substrate integrated waveguide (SIW) has provided a useful alternative to conventional waveguide designs for millimeter and microwave circuits [1]-[2]. SIWs can be fabricated with a lower cost and weight than metallic waveguides, while maintaining the loss features of the last ones. Furthermore, from a mechanical point of view SIWs are more easily integrated in printed circuits designs such as microstrip lines, as they can be fabricated within the same substrate [1].

Patch antennas have a wide variety of applications, from mobile to satellite communications. Works on coupling lines with parallel plates and radial antenna had been proposed by the authors [3]-[4]. Nevertheless, this is the first time that coupling lines are integrated in a SIW structure; as before they have only been used in conventional waveguide designs.

It is necessary to introduce two dielectrics with different dielectric constant in the SIW, in order to generate a hybrid mode which will be explained later. Afterwards, the design process will be exposed, taking special interest in the independence of two procedures: design of the SIW feeding system with coupling lines and design of the radiating element. Once the principles of coupling lines are characterized, a linear array SIW LP antenna will be designed to compare and verify results.

II. THEORETICAL BACKGROUND

When a waveguide is filled with a uniform dielectric, the coupling line structure does not work as it should. With the introduction of two different dielectric constants, the propagated fundamental mode changes from a pure

TE₁₀ to a *Longitudinal Section Magnetic* (LSM) mode [5]. Now that the E_z field component is not null, the lines disposed longitudinally along the SIW couple more or less power as a function of its dimensions. The via couples the E_y field component of the regular TE₁₀ mode, and the lines couple the E_z field component generated by the LSM. The power is transmitted to a double patch structure by the vias. As a result of this, the cutoff frequency of the LSM mode is within the range given by ϵ_{r_1} and ϵ_{r_2} :

$$\frac{1}{2a\sqrt{\mu_2\epsilon_{r_2}}} \leq f_{c_{LSM10}} \leq \frac{1}{2a\sqrt{\mu_1\epsilon_{r_1}}} \quad (1)$$

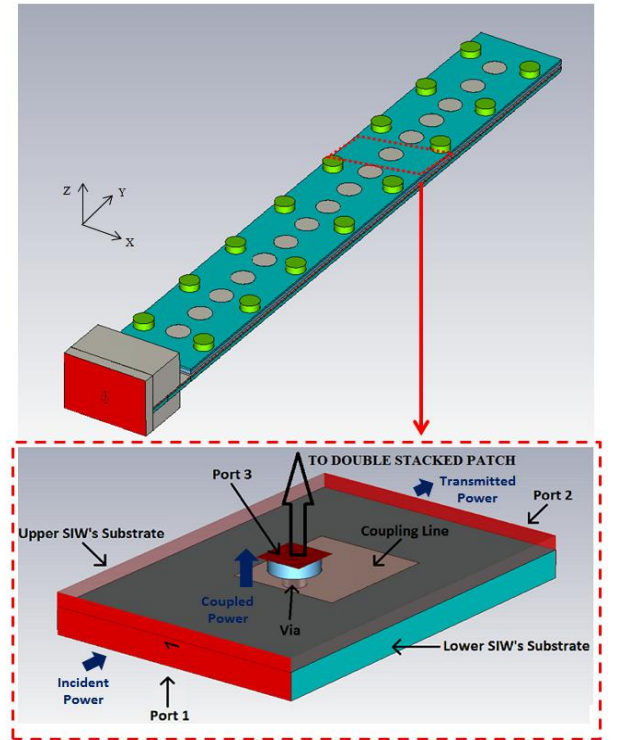


Fig. 1. General structure of the linear array and example of coupling line section in conventional waveguide

III. DESIGN OF LINEAR ARRAY

A. Antenna Structure

A 16-element LP SIW linear array antenna with double stacked patch structure is proposed. It is fed by a progressive wave which propagates along the SIW and it is coupled by the coupling lines; following a uniform distribution. The SIW is composed of two substrate layers, which include a microstrip-SIW transition. A double

stacked patch structure for the radiating elements [6] is connected to the SIW through vias of 0.6 mm. and 0.8 mm. of diameter. As there are vias' sizes, a different patch structure needs to be designed for each case. From the coaxial port defined in Fig. 2, the patch structure is designed as a 1-port circuit fed by a coaxial port with the same characteristic impedance (48 Ω) until the dimensions are optimized for -20 dB in the whole frequency band.

B. Coupling Lines and 3-Port Model

As the feeding system in the SIW is connected through vias to the radiating elements, a coaxial port can be considered at the end of via as it is shown in Fig. 1 (port 3). Thanks to this, it is possible to measure the coupling coefficient required for the distribution function in this port. Thus, the design stages of the feeding SIW array and the patch structure can be made independent. Each coupling line can be designed individually, with an input port (port 1), an output port (port 2) and the previously mentioned coaxial port.

The coupling lines are composed of a rectangular or cylindrical patch and a metallic via. The distance from the via to the edge of the line is optimized to couple as much power as possible, whereas the diameter of the via is limited to 0.6 mm. or 0.8 mm. due to availability and manufacturing restrictions. By analyzing the amplitude and phase of the coefficient at port 3, the dimensions of the coupling line can be adjusted to meet the requirements of the chosen distribution function. However, the coupled power varies with port's 3 impedance, so any further designs have to maintain the same value. The amplitude of the coupling coefficients of each element have been calculated from 0.

$$|S_k|^2 = \frac{F_k^2(x_k)}{\sum_{i=1}^M F_i^2(x_i) - \sum_{i=1}^{k-1} F_i^2(x_i)} \quad (2)$$

Where M is the number of elements in the linear array, F the feeding amplitude function, x the coupling element placement and t the uncoupled residual power ($t = 0$ in this case).

TABLE I

COUPLING COEFFICIENT AMPLITUDE AND DIMENSIONS OF COUPLING LINES

Index	Theoretical S_k (dB)	Designed S_k (dB)	Length (mm.)	Width (mm.)
1	-12.1289	-11.884	0.56 (disc)	0.56 (disc)
2	-11.8544	-11.553	0.63 (disc)	0.63 (disc)
3	-11.5614	-11.269	0.65 (disc)	0.65 (disc)
4	-11.2472	-11.096	1.2	1.1
5	-10.9084	-10.54	1.35	1.3
6	-10.5410	-10.353	1.35	1.45
7	-10.1395	-9.892	1.6	1.7
8	-9.6972	-9.421	2.2	2.3
9	-9.2046	-8.889	2.9	3
10	-8.6490	-8.438	3.3	3
11	-8.0117	-7.745	3.65	4
12	-7.2644	-6.921	3.95	4
13	-6.3614	-7.016	4	6.5
14	-5.2199	-4.996	4.25	6
15	-3.6671	-3.443	4.4	8.5

Table I summarizes the theoretical coupling coefficients at design frequency 17 GHz, the obtained ones after individual design of the elements and the coupling line's dimensions. Elements 1-14 use a via of 0.6 mm of diameter, and the 15th element a via of 0.8 mm of diameter.

As the linear array antenna ends in a short-circuit, the 16th element has a different configuration. This element requires good reflection in order to not waste any of remaining power that reaches it. On the contrary to the rest of elements, this element has been designed integrated with the double patch structure; so the whole element could be appropriately optimized in reflection. Fig. 2 shows the coupling coefficient of each element as a function of frequency.

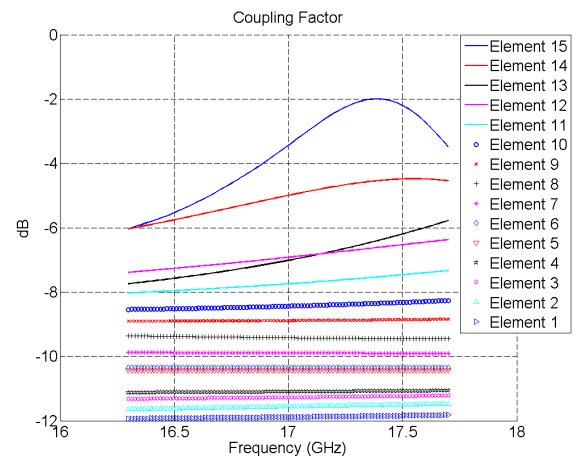


Fig. 2. Coupled power for each coupling line

C. Feeding SIW Array

Once all the elements are characterized, the feeding SIW array is formed. It was considered to have an inter-element separation of λ_{gSIW} (wavelength of the SIW) for a broadside aiming, or $3\lambda_{gSIW}/4$ which introduces a beamtilt. From simulations it was stated that placing the elements at a distance λ_{gSIW} did not provide good enough levels of reflection, as the reflection of each individual element is added in phase to the total. Therefore, the elements are placed at approximately $3\lambda_{gSIW}/4$ one from each other.

When arranged all together, each coupling line suffers from internal mutual coupling. In order to compensate this behavior, a compensation two-by-two is applied to optimize the reflection. In this stage, the line dimensions and the distance between coupling vias are slightly modified to optimize S_{11} parameter.

D. Linear Array and Coupling Model

A 16 element travelling wave LP linear array antenna is formed by the combination of the SIW feeding system and the double patch structure. The mutual coupling model established is based on [3]. There is a direct relation between radiated power and radiated electric field, so consequently the coupling coefficients are related with the electric field as follows:

$$|F_k|^2 = \frac{|E_k|^2}{\sum_{i=1}^{16} |E_i|^2} P_{abs} \quad (3)$$

$$P_{abs} = 1 - |S_{11}|^2 \quad (4)$$

Where P_{abs} is the total power given to the antenna and $\sum_{i=1}^{16} |E_i|^2$ is proportional to the total radiated power. From equations (3) and (4), after normalization, the feeding coefficient is directly characterized by the radiated electric near-field. This field is evaluated in CST Microwave Studio and separated in E_x , E_y and E_z . Taking y axis the direction of propagation of the progressive wave and particularizing in the center of the superior patch of each element, the radiated electric field is characterized by component E_y . The near-field is measured at a close distance of the upper patch (0.5 mm.). Since all elements should couple the same absolute power for the uniform distribution 0, the coupling coefficient calculated from the near-field must be compared with:

$$|F_k|_{dB} = 10 \log_{10} \left(\frac{1}{M} \right) \quad (5)$$

From (5) and $M=16$, it is obtained $|F_k|_{dB} = -12.04$ dB for each element. Comparing this value with the calculated from the extracted near-field, the dimensions of the coupling lines and the inter-element's separation are adjusted to reach the desired values. The most important feature of this compensation model is that it takes into account the coupling effect of both the radiating elements and the coupling lines inside the SIW.

TABLE II: COUPLING COEFFICIENT AMPLITUDE AND DIMENSIONS OF COUPLING LINES BEFORE AND AFTER APPLYING THE COMPENSATION MODEL

Index	S_k without compensation model (dB)	S_k with compensation model (dB)	Length (mm.)	Width (mm.)
1	-10,913	-10,971	0.55 (disc)	0.55 (disc)
2	-13,639	-12,286	0.60 (disc)	0.60 (disc)
3	-12,867	-12,025	0.66 (disc)	0.66 (disc)
4	-12,439	-12,177	1.2	1.3
5	-12,660	-12,168	1.3	1.3
6	-12,072	-12,119	1.35	1.45
7	-11,876	-12,063	1.5	1.55
8	-11,186	-12,024	1.6	1.95
9	-9,823	-12,075	1.5	1.8
10	-9,149	-12,146	2.2	2.85
11	-11,001	-11,979	2.05	2.4
12	-11,482	-12,115	3.1	4.5
13	-13,561	-12,111	3.35	5.5
14	-12,480	-12,033	4.4	8.55
15	-15,049	-12,119	4.3	8.55
	-28,024	-12,425	-	-

Table II summarizes the coupling coefficients, before and after applying the compensation model; and the dimensions of the coupling lines after the final adjustment are presented. This illustrates how the elements were modified to meet the requirements, and compare them with the results in Table I.

IV. SIMULATED RESULTS

The entire matched and adjusted SIW structure is simulated in software CST Microwave Studio. The

characterization of the SIW has been done according to [7]. To comply these constraints and minimize leakage losses in the operating frequency, $d=0.8$ mm. and $p=1.6$ mm. are chosen. Fig. 3 shows the reflection coefficient of the antenna with all the additional accessories required for later measurement, in comparison to the reflection of the SIW feeding array for λ_{gSIW} and $3\lambda_{gSIW}/4$. The initial requirement of -15 dB in the whole band is satisfied.

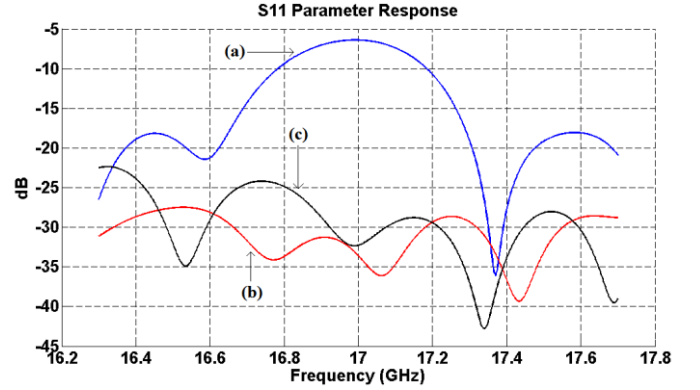


Fig. 3. SIW feeding array reflection coefficient for a distance of approximately (a) λ_g , (b) $3\lambda_g/4$ and (c) antenna's reflection

In Fig. 4, the simulated radiation patterns of the linear array, with and without applying the compensation model, are presented versus the theoretical one. Due to separating the elements approximately $3\lambda_g/4$ one from each other, the main lobe of the theoretical radiation pattern is deviated 22° from broadside. Comparing the results before and after applying the compensation model, with the final adjustment the simulated SLL (-12.7 dB) is almost matched to the theoretical one (-13 dB). There is also an accentuation of the secondary lobe's nulls in comparison to the linear array before the model is applied. Furthermore, the deviation of 2° from the direction of maximum radiation is also corrected with the application of the coupling model.

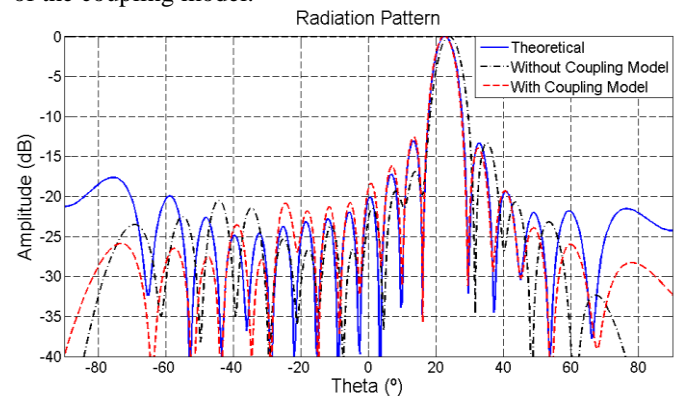


Fig. 4. Theoretical and simulated radiation patterns with compensation model and without it, at 17 GHz

V. EXPERIMENTAL RESULTS

A prototype has been manufactured by standard PCB process with TLY-5A TACONIC substrate ($\epsilon_r = 2.17$, $\tan \delta = 0.0011$, thickness = 1 and 0.508 mm.) and RF-35 TACONIC ($\epsilon_r = 3.5$, $\tan \delta = 0.0029$, thickness = 0.508 mm.). In Fig. 5 it can be shown the SMA-microstrip-SIW horizontal transition that has been designed [8].

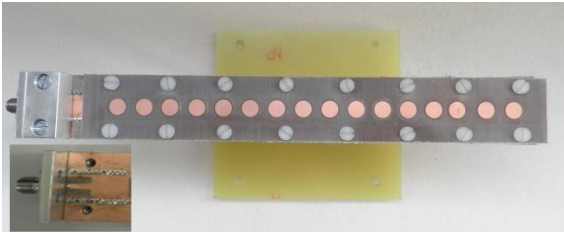


Fig. 5. Manufactured 16-element SIW LP linear array antenna prototype, with horizontal transition detail in bottom image

The reflection measurements are exposed in Fig. 6. The differences between simulated and measured S_{11} parameter are due to manufacturing process. A deviation in frequency of the whole function can be observed. The radiation pattern is presented in Fig. 7, and the same deviation is present, as the main lobe maximum direction has varied from 22° to 30° at 17 GHz.

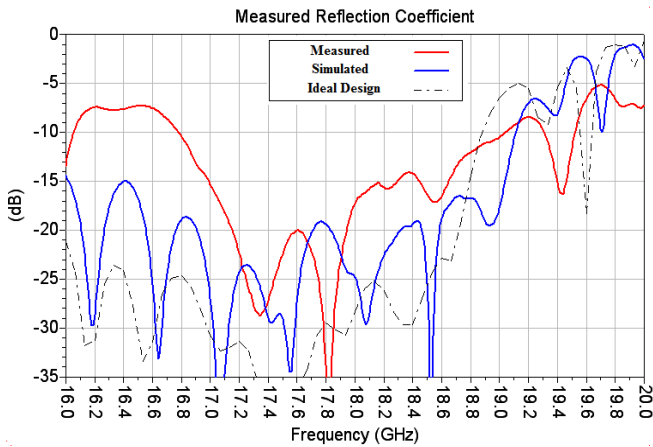


Fig. 6. Prototype's measured reflection coefficient versus simulated reflection coefficient with air gap and ideal design

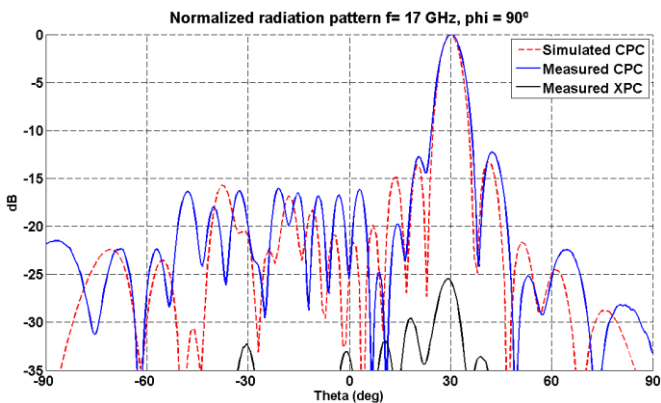


Fig. 7. Prototype's measured radiation pattern versus simulated at 17 GHz

It has been proved by simulations that these deviations have been caused by the introduction of air inside the SIW during the manufacturing process. Thus, the effective dielectric constant of the SIW is modified, and consequently the wavelength of the structure changes. As this value has been taken into account in many design features, its modification affects the expected frequency behavior of the linear array antenna. In mean terms, a gap of 0.08 mm. of air between both substrates produces such variation in the main lobe direction of propagation and also characterizes fair well the measured reflection response. However, the effect of the gap on the secondary lobes is not relevant, although there is a slight widening of 0.5° in the main lobe. The array's reflection

response is displaced approximately 1 GHz, and a 6% reflection bandwidth (-15 dB criteria) is obtained. The average gain reduction in the lower band (16.3 - 16.9 GHz), due to the high reflection values caused by the manufacturing process, is estimated in 0.7 dB. In Fig. 8 the simulated and measured gain and the antenna's efficiency are presented.

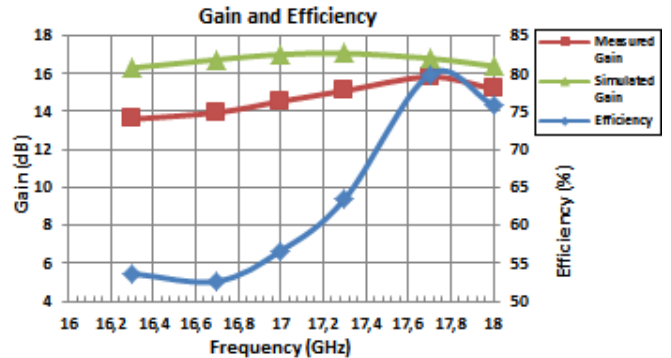


Fig. 8. Simulated and measured gain and efficiency

CONCLUSIONS

In this paper a SIW linear array antenna with double stacked patch has been presented. A compensation model, which takes into account the effects inside and outside the SIW, has been applied with very satisfactory results. A -12.7 dB SLL and 17.31 dBi peak gain at 22° from broadside at the design frequency have been achieved by simulations. The measured linear array has suffered a band deviation due to air insertion, resulting in a displacement of the reflection response and the main lobe maximum direction. Due to the high difficulty for precise manufacturing, the results obtained from the prototype's measurement are acceptable.

ACKNOWLEDGEMENT

This work is supported by Madrid Regional Government and the Autonoma University of Madrid, Ref. CCG10-UAM/TIC-5754.

REFERENCES

- [1] D. Deslandes, and K. Wu, "Integrated microstrip and rectangular waveguide in planar form," *IEEE Microwave Wireless Compon.*, vol. 11, no. 2, pp. 68 – 70, Feb. 2001.
- [2] K. Sakakibara, Y. Kimura, A. Akiyama, J. Hirokawa, M. Ando, N. Goto, "Alternating phase-fed waveguide slot arrays with a single-layer multiple-way power divider," *IEE Proc. Microw. Antennas Propag.*, vol. 144, no.6, pp.425-430, Dic. 1997.
- [3] J. L. Masa-Campos, S. Klinger, M. Sierra-Pérez, "Parallel plate patch antenna with internal horizontal coupling lines and TE_{N0} mode excitation", *IEEE Transactions on Antennas and Propagation*, vol. 57, no.7, pp. 2185 – 2189, Julio 2009.
- [4] J.L. Masa-Campos, M. Sierra-Pérez, "Linearly Polarized Radial Line Patch Antenna with Internal Rectangular Coupling Patches", *Microwave and Optical Technology Letters*, vol.46, no. 4, Aug. 2005
- [5] C. A. Balanis, "Advanced Engineering Electromagnetics", John Wiley & Sons 1989.
- [6] D. M. Pozar and D. H. Schaubert, "Microstrip Antennas", IEE Press, 1995
- [7] D. Deslandes and K. Wu, "Accurate modeling, wave mechanisms, and design considerations of a substrate integrated waveguide," *IEEE Trans. Microw. Theory Tech.*, vol. 54, no. 6, pp. 2516–2526, Jun. 2006.
- [8] P. Sanchez-Olivares and J.L. Masa Campos, "Slot radiator with tuning vias for circularly polarized SIW linear array", Accepted for 6th European Conference of Antennas and Propagation 26-30 Mar. 2012, Prague.

Linear Patch Array Over Substrate Integrated Waveguide For Ku Band

D. García-Valverde, J. L. Masa-Campos, P. Sánchez-Olivares, B. Taha-Ahmed, J. Córcoles-Ortega

Abstract- A Linearly Polarized Patch Array and direct probe feed over SIW network (LP-PASIW) for Ku band (16.3 GHz – 17.7 GHz) is presented. A double stacked microstrip patch structure has been used as radiating elements. Internal SIW coupling patches are placed inside the SIW to obtain the desired radiation pattern. The internal coupling and external radiating patches are connected by means of copper vias. A mutual coupling model is also proposed to adjust the radiation and reflection properties of the array. An antenna prototype has been manufactured and measured with satisfactory results. 16 dBi peak gain and 80 % efficiency values, as well as a 10% reflection bandwidth are achieved.

Index Terms – Hybrid LSM^y mode, internal coupling patches, Substrate Integrated Waveguide (SIW), double stacked patch, mutual coupling model.

INTRODUCTION

Since the early 1990s, substrate integrated waveguides (SIW) have provided a useful alternative to conventional waveguide designs for millimeter and microwave circuits, due to their lower cost and weight properties, as well as easy integration with the transceiver, while maintaining the loss features. Mainly, slot applications have been presented over SIW for both linear and circular polarization. The slot length, jointly with the SIW, is used to obtain the desired radiation pattern. Resonant arrays over SIW in mm-wave band of aperture coupled patches have also been presented to use the narrower beam-width patch response in the array side lobe levels. In all previous cases, a strong dependency between the radiating element and the feeding network limits the designer versatility.

In this communication, a linearly polarized patch array over an entire SIW feeding network (LP-PASIW) is presented for the first time with direct probe patch feeding. Internal coupling patches inside a multilayer structure are used to feed the radiating external patches as authors showed in previous works for parallel plate and radial waveguides. Feeding and radiating element networks can be separately treated. The proposed antenna is a proof of concept for a future higher gain structure to operate in a satellite and radio-location systems at 16.3 to 17.7 GHz frequency range. The design principles and mutual coupling effects will be exposed in Section II. Simulated and measured results of a 16 elements LP-PASIW prototype will be discussed in Sections III and IV. Finally, conclusions are drawn in Section V.

Manuscript received July 6, 2012. This work was supported by Madrid Regional Government and the Autonomia University of Madrid, Ref. CCG10-UAM/TIC-5754.

D. García-Valverde, J.L. Masa-Campos, P. Sánchez-Olivares, J. Córcoles-Ortega, B. Taha-Ahmed are with group of Radio-Frequency: Circuits, Antennas and Systems (RFCAS), Department of Electronic and Communication Technologies, Autonomia University of Madrid (U.A.M.), 28049 – Madrid, Spain (e-mail: david.garciav@estudiante.uam.es, joseluis.masa@uam.es).

LINEAR ARRAY DESIGN

Antenna Structure

The proposed LP-PASIW is composed of a 16-element linear array of double stacked circular patches (Fig. 9) fed by a SIW. The patch feeding is achieved by means of rectangular coupling patches placed inside the SIW and connected to the external radiating patches with vias. The travelling wave propagated inside the SIW is coupled to the external patches by means of the internal coupling patches, with dimensions according to the required uniform amplitude array distribution 0-0. The whole array is manufactured in a multilayer PCB with Fig. 9d layer structure and the following data:

- SIW: TACONIC TLY5A substrate with dielectric constant $\epsilon_{r2} = 2.17$, loss tangent $tg\delta_1 = 0.0012$, thickness $b_1 = 1$ mm, and TACONIC RF35 substrate with dielectric constant $\epsilon_{r2} = 3.5$, loss tangent $tg\delta_2 = 0.0029$ and thickness $b_2 = 0.5$ mm, where the internal SIW coupling patches are printed. To minimize leakage losses 0-0, copper vias of diameter $d_{siw} = 0.8$ mm and center separation $p_{siw} = 1.6$ mm are connecting the upper and bottom copper layers of both substrates to define the SIW. The SIW width is set to $a_{siw} = 10.6$ mm according to the central frequency (17 GHz). Likewise, copper vias of diameter $d_{via} = 0.6$ mm are implemented to connect the internal SIW coupling patches and the external lower radiating patches.
- DOUBLE STACKED RADIATING PATCH: TACONIC RF35 substrate with thickness $b_2 = 0.5$ mm for the lower patches of radius 2.86 mm, ROHACELL 51 HF substrate of dielectric constant $\epsilon_{r3} = 1.05$, loss tangent $tg\delta_3 = 0.004$, thickness $b_3 = 1$ mm between the two stacked patches, and TACONIC TLY5A substrate with thickness $b_2 = 0.5$ mm for printing the upper patches of radius 3.24 mm.

SIW Theoretical Background

The SIW is equivalent to a conventional waveguide of width $a_{eq} = 10.1$ mm (Fig. 9b), filled with the same dielectrics of Fig. 9d (0). The two dielectrics inside the waveguide (with different dielectric constants, ϵ_{r1} and ϵ_{r2}) modifies the pure TE_{10} fundamental mode (for $x'y'z'$ waveguide axis in Fig. 9) propagated in a uniformly filled waveguide into a hybrid *Longitudinal Section Magnetic* (LSM^y) mode. In this case, an E_z field component appears besides the E_y field of the pure TE_{10} mode. The wave propagated inside the waveguide is then coupled to the external double stacked patches by means of two mechanisms: copper vias introduced in the SIW with length $b_2 = 0.5$ mm due to E_y field; and printed patches inside the SIW (dimensions W and L in Fig. 9b), due to the E_z field generated by the LSM^y mode. According to the cut-off frequency of the fundamental mode (LSM_{10}^y) in the equivalent

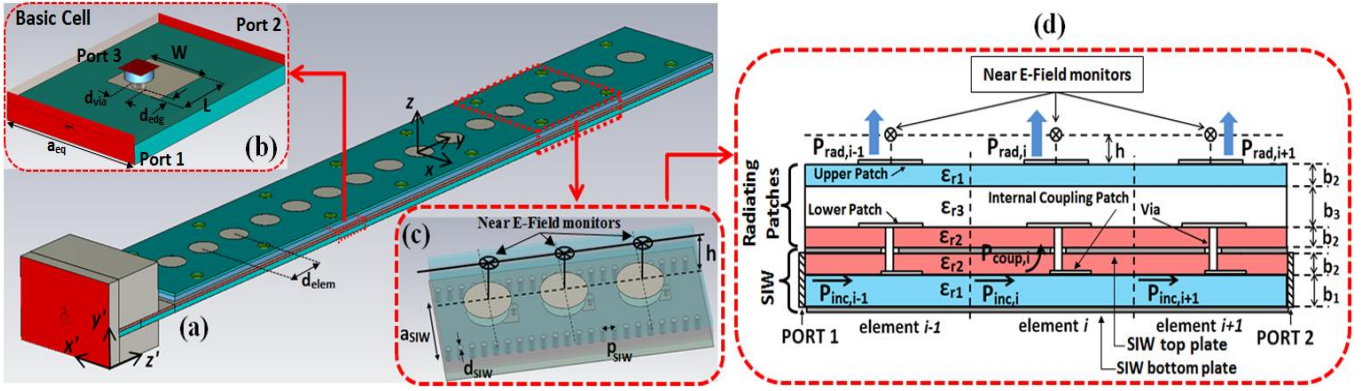


Fig. 9. 16 element LP-PASIW structure: (a) Array 3D view, (b) basic cell model with internal coupling patch, (c) three elements structure for mutual coupling model with near E-field monitors, and (d) multilayer scheme.

conventional waveguide is 9.42 GHz, and the effective dielectric constant of the multilayer substrate inside the SIW is $\epsilon_{\text{reff}} = 2.49$.

Basic Cell Model for SIW Array Design

One of the advantages of PASIW antennas is the independency between the feeding network and the radiating patch design. The SIW feeding is firstly designed with a basic cell model (Fig. 9b) composed of a single internal coupling patch in conventional waveguide ($a_{\text{eq}} = 10.1$ mm). In the commercial software CST Microwave Studio, input (port 1) and output (port 2) waveguide ports are defined, as well as a coaxial port set to 50 Ω (double stacked patch impedance) to simulate the radiating patch joint (port 3). The amplitude of the coupling coefficient of the i th-element C_i in the M elements' linear array ($M = 16$ in this case) is defined as

$$|C_i| = \frac{P_{\text{rad},i}}{P_{\text{inc},i}} = \frac{|F_i|^2}{\sum_{j=1}^M |F_j|^2 - \sum_{j=1}^{i-1} |F_j|^2} \quad (1)$$

where $P_{\text{inc},i}$ is the incident power to the internal coupling patch and $P_{\text{rad},i}$ is the radiated power by the i -th external stacked patch, t the ending non-radiated power in the array and F_i the desired normalized feeding distribution. In this design uniform amplitude distribution has been specified. The assumption of no losses in radiating patches has been considered ($P_{\text{rad},i} = P_{\text{coup},i}$, with $P_{\text{coup},i}$ the coupled power to the radiating patch). This coupling coefficient can be directly checked in the basic cell simulation model of Fig. 9b with the amplitude of the S_{31} scattering parameter.

In Section II.A it was indicated that, the internal SIW coupling structures are composed of a rectangular or circular patch and a copper via of $b_2 = 0.5$ mm length. The distance from the via to the edge of the coupling patches ($d_{\text{edg}} = 0.25$ mm) is optimized to maximize the coupled power, whereas the via diameter is limited to $d_{\text{via}} = 0.6$ mm due to manufacturing restrictions. By analyzing the calculated amplitude of the coupling coefficients C_i in (1), the dimensions of the internal coupling patches can be adjusted to meet the requirements of the desired feeding distribution F_i 0-0. In this preliminary design stage no mutual coupling is considered.

Separately, the double stacked radiating patch structure is designed under the criteria of a -20 dB reflection coefficient peak value in the whole frequency band. Likewise, in order to increase the antenna efficiency the non-radiated power has been set to $t = 0$. Therefore the last array element is designed

as a matched load with a different configuration. As Fig. 10 shows, the internal coupling structure of the last element is designed jointly with the double stacked patch and also with an ending short-circuit wall of copper vias. The separation between the short-circuit and the internal coupling structure is $d_{\text{sc}} = 9$ mm. The internal coupling structure consists of a central via of $b_2 = 0.5$ mm length in the ϵ_{r2} SIW substrate, and five vias of $b_1 = 1$ mm length which are arranged in a pentagon on a printed "clover" shape in both sides of the ϵ_{r1} SIW substrate. The characteristic dimensions of the "clover" are $d_1 = 0.5$ mm and $d_2 = 1.35$ mm. All the involved copper via diameters in this last element are 0.6 mm.

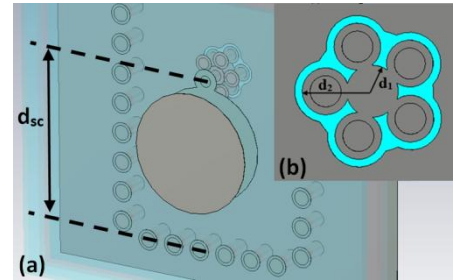


Fig. 10. 16th element of the LP-PASIW: (a) 3D view, and (b) SIW bottom plate detail

In order to reduce the internal reflection in the SIW, the array element separation has been theoretically fixed to $d_{\text{elem}} = 3\lambda_{g\text{SIW}}/4 = 10$ mm $= 0.57\lambda_0$ ($\lambda_{g\text{SIW}}$ is the wavelength in the SIW and λ_0 the air wavelength, both at 17 GHz). In 0 it was shown that this separation leads to a reflection cancellation two by two elements inside the waveguide. As a consequence, the feeding phase difference between adjacent array elements is -90° , which generates a 26° array beamtilt.

Mutual Coupling Model

The preliminary dimensions of the internal coupling patches can be obtained applying the basic cell model in section II.C. Nevertheless, a mutual coupling model has been applied in the array design and compared with the previously published multiport method in 0 for SIW slot antennas. The proposed model is based on the three element scheme in Fig. 9c and Fig. 9d, although, as in basic cell model, the equivalent conventional waveguide has been used to reduce time simulation. Input (port 1) and output (port 2) waveguide ports are defined in CST Microwave Studio. Likewise, three near E-field monitors in front of the center of each radiating stacked patch are also considered ($h = 0.5$ mm, with h the vertical separation between the radiating upper patch center and the near E-field monitor). Based on this structure, the size

of the internal coupling patch of the central i th-element (in Fig. 9d) is modified from the obtained initial values with the basic cell model, to take into account the mutual coupling of the $i-1$ th and $i+1$ th adjacent elements.. This resizing is achieved by comparing the simulated result of the near E-field monitor and the amplitude of the desired feeding distribution $|F_i|$.

Likewise, the element separation d_{elem} is also slightly modified to compensate the mutual coupling effects in the theoretical reflection cancelation detailed in Section II.C. Therefore, the S_{11} scattering parameter of the three elements Fig. 9d structure is minimized as a function of d_{elem} . The average new optimize element separation is $d_{elem} = 10.45$ mm, which modifies the main lobe beamtilt to 22.5° .

The mutual compensation method is iteratively applied in groups of three elements in the whole linear array. The resulting dimensions and distances from the proposed model are quite similar to the obtained ones by applying 0 to the three patches structure of Fig. 9d (originally was implemented with two slots). Nevertheless, the time simulation for the proposed two ports and E-filed monitor model is significantly shorter than in the six ports structure of 0. Nevertheless, while in the proposed model the simulation provides a direct result of the obtained feeding amplitude and phase including mutual coupling, 0 model requires a scattering matrix post-processing to analyze the coupling coefficient of the i th-element.

LP-PASIW SIMULATED RESULTS

The entire LP-PASIW has been simulated in CST Microwave Studio with the preliminary internal coupling patch sizes from the basic cell model, as well as with the final optimized dimensions after applying the proposed mutual coupling model. Table I summarizes the simulated results of the normalized feeding amplitude in dB ($|F_i^{sim}|_{dB}$) in both cases (obtained with near E-field monitors), which must be compared with the theoretical amplitude for $M = 16$ elements and uniform distribution ($|F_i|_{dB} = 12.04$ dB, $\forall i$). Likewise, the preliminary and final dimensions of the internal coupling patches are shown. Elements 1 to 3 are implemented with a circular disc instead of a rectangular patch, and final element 16 was previously described in Fig. 10 and Section II.C.

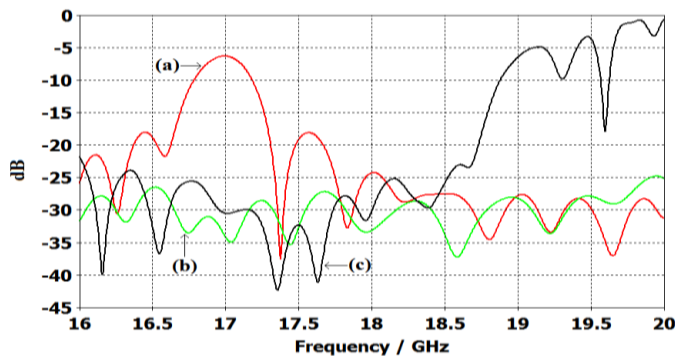


Fig. 11. SIW feeding network and LP-PASIW simulated reflection coefficient: (a) $d_{elem} = \lambda_{gsiw}$, (b) $d_{elem} = 3\lambda_{gsiw}/4$, and (c) LP-PASIW with mutual coupling model

Fig. 3 shows a comparative graph of the simulated reflection coefficient of the SIW feeding network with ideal

50Ω loads (instead of the double stacked patches) in two situations: a) element separation $d_{elem} = \lambda_{gsiw}$, and b) $d_{elem} = 3\lambda_{gsiw}/4$. Likewise, the simulated reflection of the final LP-PASIW structure is also included (Fig. 3c). The reflection compensation is clearly observed at the design frequency (17 GHz), as well as the bandwidth LP-PASIW reduction in high frequencies compared with the alone SIW feeding network, due to the limited double stacked patch bandwidth response.

TABLE I

LP-PASIW SIMULATION RESULTS OF NORMALIZED FEEDING AMPLITUDE AND DIMENSIONS OF INTERNAL COUPLING PATCHES WITH BASIC CELL AND MUTUAL COUPLING MODELS

Elem.	Basic Cell Model			Mutual Coupling model		
	$ F_i^{sim} _{dB}$	L (mm)	W (mm)	$ F_i^{sim} _{dB}$	L (mm)	W (mm)
1	-10.91	0.56^{*1}		-10.97	0.55^{*1}	
2	-13.64	0.63^{*1}		-12.29	0.60^{*1}	
3	-12.87	0.65^{*1}		-12.03	0.66^{*1}	
4	-12.44	1.2	1.2	-12.17	1.2	1.3
5	-12.66	1.35	1.35	-12.16	1.3	1.3
6	-12.07	1.35	1.35	-12.11	1.35	1.45
7	-11.88	1.6	1.6	-12.06	1.5	1.55
8	-11.19	2.2	2.2	-12.02	1.6	1.95
9	-9.82	2.9	2.9	-12.07	1.5	1.8
10	-9.15	3.3	3.3	-12.14	2.2	2.85
11	-11.00	3.65	3.65	-11.97	2.05	2.4
12	-11.48	3.95	3.95	-12.11	3.1	4.5
13	-13.56	4	4	-12.11	3.35	5.5
14	-12.48	4.25	4.25	-12.03	4.4	8.55
15	-15.05	4.4	4.4	-12.11	4.3	8.55
16	-28.02	$^{-*2}$		-12.42	$^{-*2}$	

*1: Disc radius, *2: Last array element in Fig.2

In Fig. 12, the simulated radiation patterns of the LP-PASIW with basic cell and mutual coupling model are presented versus the theoretical one. The expected theoretical 22.5° main lobe beamtilt, as well as the side lobe level are correctly predicted with the mutual coupling model. Nevertheless, the basic cell model presents a 2° deviation error in the main lobe beamtilt, a side lobe asymmetry and a certain effect of null filling.

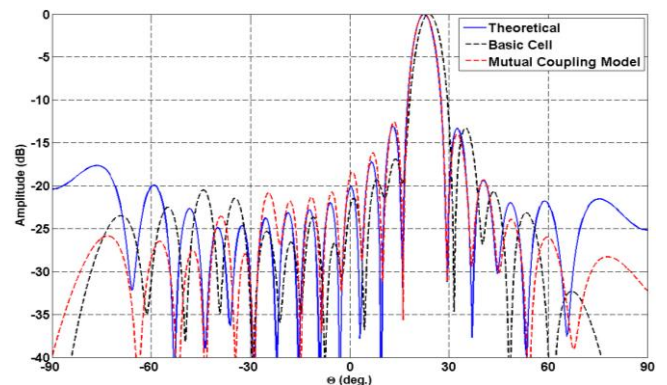


Fig. 12. Theoretical and simulated normalized radiation patterns with basic cell and mutual coupling models at 17 GHz ($\phi = 90^\circ$, for xyz axis in Fig.1)

EXPERIMENTAL RESULTS

An on-home prototype of the 16 elements LP-PASIW has been manufactured by standard PCB process (Fig. 5). All the vias are implemented with special manual PCB rivets. The substrate multilayer stacking is achieved both with plastic screws and via rivets. A SMA-microstrip-SIW horizontal transition has also been included 0.

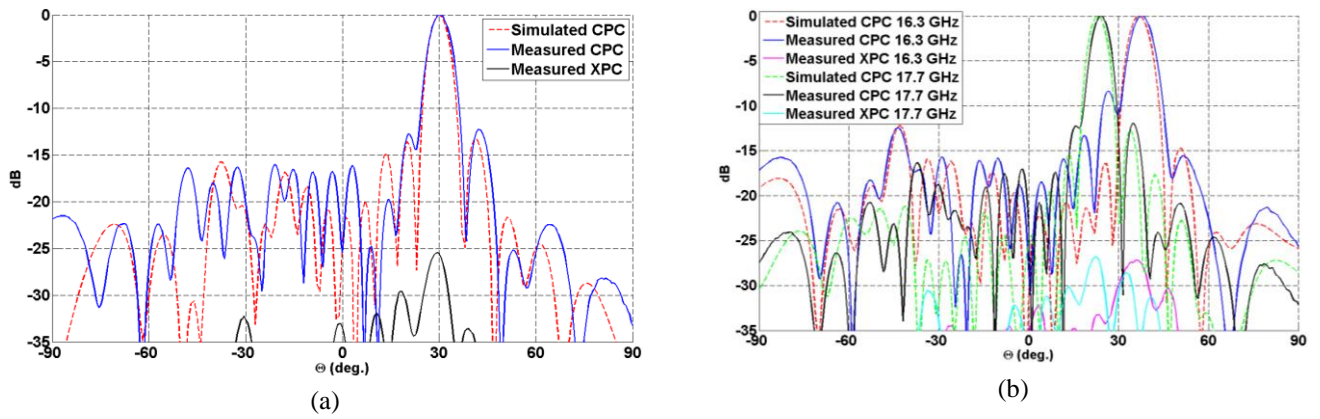


Fig. 13. Prototype measured versus simulated (with 0.08 mm uniform air gap in SIW) radiation pattern at $\phi = 90^\circ$ plane:(a) 17 GHz, (b) 16.3 GHz and 17.7 GHz

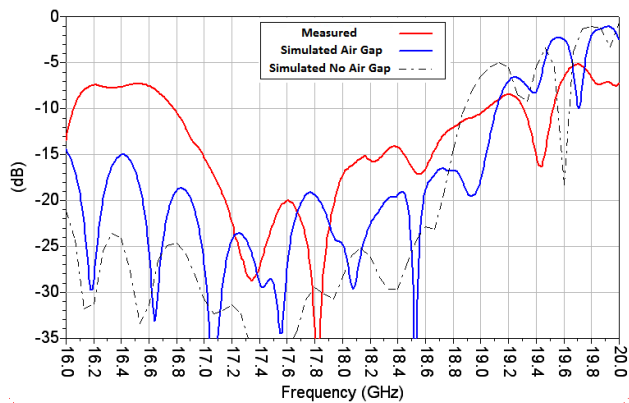


Fig. 14. Prototype measured versus simulated (with and without 0.08 mm uniform air gap in SIW) reflection coefficient.

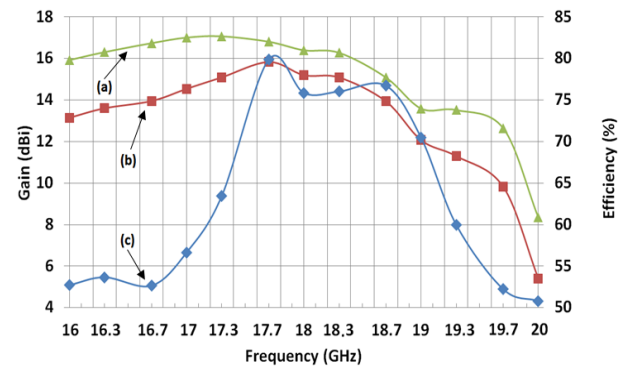


Fig. 15. Antenna gain and efficiency at the main lobe angle: (a) Simulated gain, (b) measured gain, and (c) efficiency

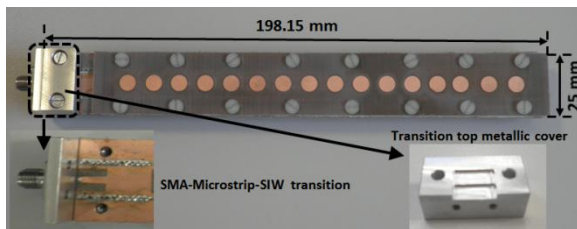


Fig. 16. Homemade manufactured 16-element LP-PASIW prototype

The measured radiation pattern is presented in Fig. 13, with the typical band response of a progressive wave design. Good vertical polarization purity is obtained. A 0.5° main lobe widening and a beamtilt displacement from 22.5° to 30° are observed at 17 GHz. This effect is due to the appearance of a non-uniform air gap layer in between the SIW substrates during the manual stacking process. Thus, the SIW effective dielectric constant ϵ_{eff} is modified. In order to verify this effect a 0.08 mm thickness uniform gap has been introduced in the antenna simulation. As Fig. 13a shows the beamtilt and main lobe widening are correctly predicted, although not completely for the sidelobe response. The measured prototype gain and efficiency at the main lobe angle are shown in Fig. 15. A peak gain value of 16 dBi and 80 % efficiency is observed at 17.7 GHz. As reflection coefficient measurement in Fig. 14 confirms, 0.8 GHz upper frequencies displacement and reflection deterioration in lower band are detected, mainly due to the manufacturing tolerance errors of the on-home procedure. The antenna gain behavior is also affected for this reason. Nevertheless a 10% reflection (-15 dB

criteria) and efficiency bandwidth ($> 70\%$ criteria) is obtained.

CONCLUSIONS

In this communication a linearly polarized double stacked patch linear array over SIW has been firstly presented as a probe of concept. The array design process is quite flexible due to the independency between the feeding SIW network and radiating elements parameters. A mutual coupling model has been considered to design the internal SIW coupling patches with satisfactory results. Peak gain and efficiency values of 16 dBi and 80 % at 17.7 GHz have been achieved, with a 10 % bandwidth. Nevertheless, the on-home manufacturing process generates a deterioration of the antenna performance in reflection and radiation properties. In future research scopes an external PCB fabrication, as well as a high gain 2D array will be developed based on this communication results.

REFERENCES

- [1] D. Deslandes, and K. Wu, "Integrated microstrip and rectangular waveguide in planar form," *IEEE Microwave Wireless Compon.*, vol. 11, no. 2, pp. 68 – 70, Feb. 2001.
- [2] L. Yan, W. Hong, G. Hua, J. Chen, K. Wu and T. J. Cui, "Simulation and experiment on SIW slot array antennas," *IEEE Microwave Wireless Compon. Lett.*, Vol. 14, No. 9, pp. 446-448, Sept. 2004.
- [3] P. Chen, W. Hong, Z. Kuai, and J. Xu, "A substrate integrated waveguide circularly polarized slot radiator and its linear array," *IEEE Antennas and Wireless Propag. Letters*, Vol. 8, pp. 120 – 123, 2009.
- [4] W.M Abdel-Wahab, S. Safavi-Naeini, and D. Busuioc, "Low cost 60 GHz millimeter-wave microstrip patch antenna array using low-loss

- planar feeding scheme," *Proc. IEEE Antennas Propag. Int. Symp., APS-URSI 2011*, pp. 508 – 511.
- [5] J. L. Masa-Campos, S. Klinger, M. Sierra-Pérez, "Parallel plate patch antenna with internal horizontal coupling lines and TE_{N0} mode excitation", *IEEE Trans. on Antennas and Propag.*, vol. 57, no.7, pp. 2185 – 2189, Jul. 2009.
- [6] J. L. Masa-Campos, M. Sierra-Pérez, "Linearly Polarized Radial Line Patch Antenna with Internal Rectangular Coupling Patches", *IEEE Trans. on Antennas and Propag.*, vol. 59, no.8, pp. 3049 – 3052, Aug. 2011.
- [7] D. M. Pozar and D. H. Schaubert, "Microstrip Antennas", *IEE Press*, 1995.
- [8] D. Deslandes and K. Wu, "Accurate modeling, wave mechanisms, and design considerations of a substrate integrated waveguide," *IEEE Trans. Microw. Theory Tech.*, vol. 54, no. 6, pp. 2516–2526, Jun. 2006.
- [9] C. A. Balanis, "Advanced Engineering Electromagnetics", John Wiley & Sons 1989, pp. 394 – 414.
- [10] J. L. Masa-Campos and M. Sierra-Pérez, "Radial-line planar antenna with microstrip-feed coupling lines", *Microwave and Optical Technology Letters*, vol. 46, no. 4, pp. 305-311, Aug. 2005.
- [11] P. Chen and W. Hong, "A Multibeam Antenna Based on Substrate Integrated Waveguide Technology for MIMO Wireless Communications," *IEEE Transactions on Antennas and Propagation*, vol. 57, no. 9, pp. 1813-1821, June 2009.

G. PRESUPUESTO

1. Ejecución Material

- Compra de ordenador personal (Software incluido)..... 2.000 €
- Alquiler de impresora láser durante 6 meses 50 €
- Material de oficina 150 €
- Material de fabricación de prototipos
 - Conectores 30 €
 - Substrato de circuitos impresos..... 450 €
- Alquiler de máquina fresadora durante 1 mes 4.800 €
- Herramienta remachadora y remaches 455 €
- Medidas con el analizador de redes durante 3 h 180 €
- Medidas en cámara anecoica h durante 4 h 472 €

Total de ejecución material 8.587 €

2. Gastos generales

- 16 % sobre Ejecución Material 1.373,92 €

3. Beneficio Industrial

- 6 % sobre Ejecución Material 515,22 €

4. Honorarios Proyecto

- 1500 horas a 15 € / h 22.500 €

5. Material fungible

- Gastos de impresión..... 200 €
- Encuadernación..... 5 €

6. Subtotal del presupuesto

- Subtotal Presupuesto 33.181,14 €

7. I.V.A. aplicable

- 18% Subtotal Presupuesto 5.972,61 €

8. Total presupuesto

- Total Presupuesto 39.153,75 €

Madrid, Junio de 2012

El Ingeniero Jefe de Proyecto

Fdo.: David García Valverde

Ingeniero Superior de Telecomunicación

H. PLIEGO DE CONDICIONES

Este documento contiene las condiciones legales que guiarán la realización, en este proyecto, de un array lineal de parches sobre guía de substrato integrado para banda Ku. En lo que sigue, se supondrá que el proyecto ha sido encargado por una empresa cliente a una empresa consultora con la finalidad de realizar dicho sistema. Dicha empresa ha debido desarrollar una línea de investigación con objeto de elaborar el proyecto. Esta línea de investigación, junto con el posterior desarrollo de los programas está amparada por las condiciones particulares del siguiente pliego.

Supuesto que la utilización industrial de los métodos recogidos en el presente proyecto ha sido decidida por parte de la empresa cliente o de otras, la obra a realizar se regulará por las siguientes:

Condiciones generales

1. La modalidad de contratación será el concurso. La adjudicación se hará, por tanto, a la proposición más favorable sin atender exclusivamente al valor económico, dependiendo de las mayores garantías ofrecidas. La empresa que somete el proyecto a concurso se reserva el derecho a declararlo desierto.

2. El montaje y mecanización completa de los equipos que intervengan será realizado totalmente por la empresa licitadora.

3. En la oferta, se hará constar el precio total por el que se compromete a realizar la obra y el tanto por ciento de baja que supone este precio en relación con un importe límite si este se hubiera fijado.

4. La obra se realizará bajo la dirección técnica de un Ingeniero Superior de Telecomunicación, auxiliado por el número de Ingenieros Técnicos y Programadores que se estime preciso para el desarrollo de la misma.

5. Aparte del Ingeniero Director, el contratista tendrá derecho a contratar al resto del personal, pudiendo ceder esta prerrogativa a favor del Ingeniero Director, quien no estará obligado a aceptarla.

6. El contratista tiene derecho a sacar copias a su costa de los planos, pliego de condiciones y presupuestos. El Ingeniero autor del proyecto autorizará con su firma las copias solicitadas por el contratista después de confrontarlas.

7. Se abonará al contratista la obra que realmente ejecute con sujeción al proyecto que sirvió de base para la contratación, a las modificaciones autorizadas por la superioridad o a las órdenes que con arreglo a sus facultades le hayan comunicado por escrito al Ingeniero Director de obras siempre que dicha obra se haya ajustado a los preceptos de los pliegos de condiciones, con arreglo a los cuales, se harán las modificaciones y la valoración de las diversas unidades sin que el importe total pueda exceder de los presupuestos aprobados. Por consiguiente, el número de unidades que se consignan en el proyecto o en el presupuesto, no podrá servirle de fundamento para entablar reclamaciones de ninguna clase, salvo en los casos de rescisión.

8. Tanto en las certificaciones de obras como en la liquidación final, se abonarán los trabajos realizados por el contratista a los precios de ejecución material que figuran en el presupuesto para cada unidad de la obra.

9. Si excepcionalmente se hubiera ejecutado algún trabajo que no se ajustase a las condiciones de la contrata pero que sin embargo es admisible a juicio del Ingeniero Director de obras, se dará conocimiento a la Dirección, proponiendo a la vez la rebaja de precios que el Ingeniero estime justa y si la Dirección resolviera aceptar la obra, quedará el contratista obligado a conformarse con la rebaja acordada.

10. Cuando se juzgue necesario emplear materiales o ejecutar obras que no figuren en el presupuesto de la contrata, se evaluará su importe a los precios asignados a otras obras o materiales análogos si los hubiere y cuando no, se discutirán entre el Ingeniero Director y el contratista, sometiéndolos a la aprobación de la Dirección. Los nuevos precios convenidos por uno u otro procedimiento, se sujetarán siempre al establecido en el punto anterior.

11. Cuando el contratista, con autorización del Ingeniero Director de obras, emplee materiales de calidad más elevada o de mayores dimensiones de lo estipulado en el proyecto, o sustituya una clase de fabricación por otra que tenga asignado mayor precio o ejecute con mayores dimensiones cualquier otra parte de las obras, o en general, introduzca en ellas cualquier modificación que sea beneficiosa a juicio del Ingeniero Director de obras, no tendrá derecho sin embargo, sino a lo que le correspondería si hubiera realizado la obra con estricta sujeción a lo proyectado y contratado.

12. Las cantidades calculadas para obras accesorias, aunque figuren por partida alzada en el presupuesto final (general), no serán abonadas sino a los precios de la contrata, según las condiciones de la misma y los proyectos particulares que para ellas se formen, o en su defecto, por lo que resulte de su medición final.

13. El contratista queda obligado a abonar al Ingeniero autor del proyecto y director de obras así como a los Ingenieros Técnicos, el importe de sus respectivos honorarios facultativos por formación del proyecto, dirección técnica y administración en su caso, con arreglo a las tarifas y honorarios vigentes.

14. Concluida la ejecución de la obra, será reconocida por el Ingeniero Director que a tal efecto designe la empresa.

15. La garantía definitiva será del 4% del presupuesto y la provisional del 2%.

16. La forma de pago será por certificaciones mensuales de la obra ejecutada, de acuerdo con los precios del presupuesto, deducida la baja si la hubiera.

17. La fecha de comienzo de las obras será a partir de los 15 días naturales del replanteo oficial de las mismas y la definitiva, al año de haber ejecutado la provisional, procediéndose si no existe reclamación alguna, a la reclamación de la fianza.

18. Si el contratista al efectuar el replanteo, observase algún error en el proyecto, deberá comunicarlo en el plazo de quince días al Ingeniero Director de obras, pues transcurrido ese plazo será responsable de la exactitud del proyecto.

19. El contratista está obligado a designar una persona responsable que se entenderá con el Ingeniero Director de obras, o con el delegado que éste designe, para todo relacionado con ella. Al ser el Ingeniero Director de obras el que interpreta el proyecto, el contratista deberá consultarle cualquier duda que surja en su realización.

20. Durante la realización de la obra, se girarán visitas de inspección por personal facultativo de la empresa cliente, para hacer las comprobaciones que se crean oportunas. Es obligación del contratista, la conservación de la obra ya ejecutada hasta la recepción de la misma, por lo que el deterioro parcial o total de ella, aunque sea por agentes atmosféricos u otras causas, deberá ser reparado o reconstruido por su cuenta.

21. El contratista, deberá realizar la obra en el plazo mencionado a partir de la fecha del contrato, incurriendo en multa, por retraso de la ejecución siempre que éste no sea debido a causas de fuerza mayor. A la terminación de la obra, se hará una recepción provisional previo reconocimiento y examen por la dirección técnica, el depositario de efectos, el interventor y el jefe de servicio o un representante, estampando su conformidad el contratista.

22. Hecha la recepción provisional, se certificará al contratista el resto de la obra, reservándose la administración el importe de los gastos de conservación de la misma hasta su recepción definitiva y la fianza durante el tiempo señalado como plazo de garantía. La recepción definitiva se hará en las mismas condiciones que la provisional, extendiéndose el acta correspondiente. El Director Técnico propondrá a la Junta Económica la devolución de la fianza al contratista de acuerdo con las condiciones económicas legales establecidas.

23. Las tarifas para la determinación de honorarios, reguladas por orden de la Presidencia del Gobierno el 19 de Octubre de 1961, se aplicarán sobre el denominado en la actualidad "Presupuesto de Ejecución de Contrata" y anteriormente llamado "Presupuesto de Ejecución Material" que hoy designa otro concepto.

Condiciones particulares

La empresa consultora, que ha desarrollado el presente proyecto, lo entregará a la empresa cliente bajo las condiciones generales ya formuladas, debiendo añadirse las siguientes condiciones particulares:

1. La propiedad intelectual de los procesos descritos y analizados en el presente trabajo, pertenece por entero a la empresa consultora representada por el Ingeniero Director del Proyecto.

2. La empresa consultora se reserva el derecho a la utilización total o parcial de los resultados de la investigación realizada para desarrollar el siguiente proyecto, bien para su publicación o bien para su uso en trabajos o proyectos posteriores, para la misma empresa cliente o para otra.

3. Cualquier tipo de reproducción aparte de las reseñadas en las condiciones generales, bien sea para uso particular de la empresa cliente, o para cualquier otra aplicación, contará con autorización expresa y por escrito del Ingeniero Director del Proyecto, que actuará en representación de la empresa consultora.

Appendixes

4. En la autorización se ha de hacer constar la aplicación a que se destinan sus reproducciones así como su cantidad.

5. En todas las reproducciones se indicará su procedencia, explicitando el nombre del proyecto, nombre del Ingeniero Director y de la empresa consultora.

6. Si el proyecto pasa la etapa de desarrollo, cualquier modificación que se realice sobre él, deberá ser notificada al Ingeniero Director del Proyecto y a criterio de éste, la empresa consultora decidirá aceptar o no la modificación propuesta.

7. Si la modificación se acepta, la empresa consultora se hará responsable al mismo nivel que el proyecto inicial del que resulta el añadirla.

8. Si la modificación no es aceptada, por el contrario, la empresa consultora declinará toda responsabilidad que se derive de la aplicación o influencia de la misma.

9. Si la empresa cliente decide desarrollar industrialmente uno o varios productos en los que resulte parcial o totalmente aplicable el estudio de este proyecto, deberá comunicarlo a la empresa consultora.

10. La empresa consultora no se responsabiliza de los efectos laterales que se puedan producir en el momento en que se utilice la herramienta objeto del presente proyecto para la realización de otras aplicaciones.

11. La empresa consultora tendrá prioridad respecto a otras en la elaboración de los proyectos auxiliares que fuese necesario desarrollar para dicha aplicación industrial, siempre que no haga explícita renuncia a este hecho. En este caso, deberá autorizar expresamente los proyectos presentados por otros.

12. El Ingeniero Director del presente proyecto, será el responsable de la dirección de la aplicación industrial siempre que la empresa consultora lo estime oportuno. En caso contrario, la persona designada deberá contar con la autorización del mismo, quien delegará en él las responsabilidades que ostente.